NASA CR-135215

AUGMENTOR EMISSIONS REDUCTION TECHNOLOGY PROGRAM

Final Report

by

W.C. Colley
M.J. Kenworthy
D.W. Bahr

GENERAL ELECTRIC COMPANY

Prepared For

National Aeronautics and Space Administration

NASA Lewis Research Center
Contract NAS3-19737

1. Report No.	2. Government Accession No.	3. Recipient's Catalog No.
NASA CR-135215		

4. Title and Subtitle	5. Report Date
Augmentor Emissions Reduction Technology Program Final Report	November 1977
	6. Performing Organization Code
7. Author(s)	8. Performing Organization Report No.
W.C. Colley, M.J. Kenworthy, and D.W. Bahr	R77AEG593
9. Performing Organization Name and Address	10. Work Unit No.
General Electric Company Aircraft Engine Group Cincinnati, Ohio 45215	11. Contract or Grant No.
	NAS3-19737
12. Sponsoring Agency Name and Address	13. Type of Report and Period Covered
National Aeronautics and Space Administration Washington, D.C. 20546	Contractor Report
	14. Sponsoring Agency Code

15. Supplementary Notes

Project Manager: James S. Fear, NASA-Lewis Research Center, Cleveland, Ohio 44135

16. Abstract

This experimental program investigated techniques and developed technology to reduce pollutant emissions from duct-burner-type augmentors for use on advanced supersonic cruise aircraft. Twelve test configurations, representing variations of two duct-burner design concepts, were tested in a rectangular sector test rig at inlet temperature and pressure conditions corresponding to takeoff, transonic climb, and supersonic cruise flight conditions. Both design concepts used piloted flameholders to stabilize combustion of lean, premixed fuel/air mixtures. The concepts differed in the flameholder type used. High combustion efficiency (97%) and low levels of NO_x emissions (1.19 g/kg fuel) were achieved. The detailed measurements suggested the direction that future development efforts should take to obtain further reductions in emission levels and associated improvements in combustion efficiency over an increased range of temperature rise conditions.

17. Key Words (Suggested by Author(s))	18. Distribution Statement
Augmentor Combustion Duct Burner Emissions Turbofan	Unclassified - Unlimited

19. Security Classif. (of this report)	20. Security Classif. (of this page)	21. No. of Pages	22. Price*
Unclassified	Unclassified	161	

* For sale by the National Technical Information Service, Springfield, Virginia 22151

TABLE OF CONTENTS

TABLE OF CONTENTS (Cont'd)

LIST OF ILLUSTRATIONS

LIST OF ILLUSTRATIONS (Continued)

LIST OF ILLUSTRATIONS (Continued)

LIST OF ILLUSTRATIONS (Continued)

LIST OF ILLUSTRATIONS (Concluded)

LIST OF TABLES

LIST OF TABLES (Concluded)

1.0 SUMMARY

An experimental program was conducted to investigate techniques and develop technology to reduce emissions from duct burner-type augmentors suitable for use on an advanced supersonic cruise aircraft. The tests were performed in a rectangular sector test rig, 194 mm high and 432 mm wide, at inlet temperature and pressure conditions simulating true flight conditions. Twelve test configurations were screened for emissions characteristics, and detailed data were taken on selected configurations at test conditions corresponding to takeoff, transonic climb, and supersonic cruise.

The basic approach used for the duct burner designs was a staged system. The first stage was a stable pilot, using conservative swirl cup technology derived from turbine engine main combustors. The second, or main, stage consisted of flameholder arrays downstream of the pilot stage. The basic technology for defining workable staged combustion configurations with reasonable performance came from extensive duct burner experimental investigations on similar configurations directed toward military applications that had been conducted at General Electric in prior years. To minimize the oxides of nitrogen (NO_x) emissions level, which had not been an object of the previous duct burner investigations, most of the fuel was burned in the main stage as a lean, premixed stream. Two types of main stage flameholder arrays were used. The first type consisted of circumferential V-gutter flameholders similar to those of turbojet afterburners. The second type consisted of swept radial flameholders patterned after those developed for main combustors in the NASA/CE Experimental Clean Combustor Program.

The most attractive configuration identified in this program featured the use of a swept radial flameholder array extending both inward and outward from a central annular pilot. With this configuration, the best overall mission performance was obtained at all operating conditions. At the supersonic cruise operating conditions, with the main stage air uniformly carbureted for optimum emissions performance, a NO_x emission index of 1.19, and a combustion efficiency of 97% were measured compared with the program goals of 99% combustion efficiency and 1.0 g/kg fuel for NO_x. It was determined from individual gas samples that much of the combustion inefficiency was due to quenching near the film-cooled liners. If future development efforts are successful in eliminating this wall quenching, overall combustion efficiency levels above the 99% measured in the central part of the stream should be achievable. At these 99% efficiency conditions for the central part of the stream, NO_x emission index levels of 1.10 at takeoff and 1.17 at supersonic cruise were measured, closely approaching the program goals.

While the best emissions performance at supersonic cruise was obtained at a fuel/air ratio of 0.0324, a supersonic cruise fuel/air ratio of 0.020 is indicated for optimum mission specific fuel consumption and capability of achieving the required wide fuel/air ratio operating range from takeoff to cruise. At the 0.020 fuel/air ratio, emissions performance was degraded.

Staging techniques to maintain optimum fuel/air ratios locally in the stream were investigated, with only limited success. These techniques included carburetion of the main-stage air on only one side of the pilot, sometimes coupled with axial displacement of the uncarbureted flameholders. At a supersonic cruise fuel/air ratio of 0.020, a combustion efficiency of 94% and a NO_x emission index of 1.3 were measured.

Variations in fuel injection techniques produced only moderate effects on emissions performance. These variations included two different axial injection stations, alternative atomizing techniques including high pressure air atomization, and vapor fuel injection.

Future development work on duct burners should include efforts to reduce combustion-driven resonance, which was present in all configurations at the highest fuel/air ratios. Efforts to minimize wall quenching and efforts to increase performance with fuel staging for wide fuel/air ratio capability should also be included.

2.0 INTRODUCTION

The purpose of this program was to investigate techniques and develop technology to reduce the pollutant emissions levels of duct burner-type augmentors suitable for use on an advanced supersonic cruise aircraft. This effort focused on reducing emissions of NO_x, carbon monoxide (CO), unburned hydrocarbons (HC), and smoke at all flight conditions, with particular emphasis on reduction of these emissions during supersonic cruise at high altitude. These reductions in pollutant emissions were to be accomplished with minimum and acceptable sacrifices in duct burner performance requirements such as combustion efficiency, total pressure loss, and altitude relight capability. Performance and pollutant emissions goals were defined for three flight conditions: supersonic cruise, takeoff, and transonic climb, as shown in Table I. These goals emphasized high combustion efficiency and extremely low NO_x emission.

Duct burners must achieve good performance levels at severe burning conditions. The burner inlet air temperatures are generally low, comparable to those of main combustors at idle conditions. These temperatures are much lower than those of main combustors at full power and are also lower than those of afterburners. At the same time, duct burners generally must operate in a minimum passage height in order to minimize the overall engine diameter and, hence, the aircraft drag. This latter consideration results in flow reference Mach numbers through the burner that are higher than those in main combustors. While more combustion length is available than in main combustors, the achievement of extremely high combustion efficiencies is nevertheless difficult because of the adverse operating conditions of duct burners.

Previous duct burner development work did not emphasize the attainment of low NO_x emission levels. High combustion efficiency, however, has always been an important objective in development work. Combustion efficiency is frequently optimized by providing nearly stoichiometric fuel/air ratios in the burning zone. The resultant high flame temperatures do not result in lowest NO_x formation. To approach the low NO_x goals of this program, the combustion must take place at lean conditions where the flame temperatures are low. The achievement of high combustion efficiency at these lean conditions is very difficult. Thus, although high combustion efficiency can be achieved in duct burners, the simultaneous achievement of high combustion efficiency and low NO_x emission levels was the primary challenge in this development test investigation.

In recent years, duct burner designs have involved some sort of axial staging of the combustion process. The staging process helps achieve good performance in minimum passage heights. For the past seven years, the staged duct burner development work at General Electric has concentrated on concepts utilizing a pilot burner for the first stage with flameholder arrays for the second (main) stage. The experimental investigations have included many variations on the exact features. For the pilot burner, these variations included airflow fraction, fuel/air ratio, length, and specific swirl cup and

Table I. Program Goals.

Flight Condition	Supersonic Cruise	Sea Level Takeoff	Transonic Climb
Emission Index, g/kg fuel			
Oxides of Nitrogen (NO_x)	1.0	1.0	---
Carbon Monoxide (CO	30	---	---
Total Hydrocarbons (HC)	2.5	---	---
Combustion Efficiency, %	99	99	99
SAE Smoke Number	15	15	15
Total Pressure Loss (Including heat addition loss) (Percent of inlet total pressure)	6.5	---	---

dilution air introduction features. For the main stage flameholder arrays, these variations included flameholder width, spacing, and slope, as well as the effect of arrays on only one or both sides of the pilot compared with arrays on both sides, including the effect of axial stagger of the flameholders between the two sides. This work was directed toward achieving satisfactory operating characteristics for military engines, including combustion efficiency at hig' fuel/air ratios, but did not include any development to reduce NO_x emission levels. Thus, this work provided a sound basis for selecting, for this emissions reduction program, configurations known to be operable and to have reasonable characteristics for lightoff and combustion efficiency at high fuel/air ratios. This background also provided guidance in optimizing combustion efficiency at the lean conditions known to be important for achieving low NO_x.

Recent NASA-sponsored work on the development of low emissions for main combustors conducted at General Electric under the Experimental Clean Combustor Program, Contract NAS3-18551 (Reference 1), has identified that combustion of a second stage can be achieved with very low NO_x levels. The general approach to achieve these low NO_x levels is to burn most of the fuel in a very lean, relatively premixed state. Thus, this low NO_x technology from main combustor investigations, together with the extensive duct burner experience, provided the background for the selection of configurations to be tested in this duct burner emissions reduction program.

In this experimental program, variations on two different flameholding approaches were investigated, both of which were coupled with a first-stage pilot. One concept involved circumferential flameholders similar to those commonly used in afterburners. The other concept used sloped radial flameholders similar to those recently investigated for main combustors under Contract NAS3-18551. Both design concepts were suitable for the envelope and operating conditions of a baseline engine designed to cruise at Mach 2.4 and 16.7 km altitude. Screening tests on 12 configurations were conducted, with more detailed measurements made on selected configurations. All tests were conducted in a rectangular sector test vehicle simulating a portion of a full annular burner and utilizing true inlet air temperature and pressure conditions.

3.0 DUCT BURNER TEST CONFIGURATIONS

3.1 Design Requirements

For the purpose of defining geometry features and cycle conditions for this investigation, a baseline duct-burning turbofan engine was selected. This engine, designated GE21, was designed for a supersonic cruise mission. Supersonic cruise was defined at Mach 2.4 and 16.74 km (54,900 feet) altitude on a standard day.

3.1.1 Baseline Engine Description

A schematic of the GE21 duct-burning turbofan engine and pod configuration is shown in Figure 1. Sea level static characteristics and key dimensions of this engine are listed in Table II.

The duct burner of the GE21 engine is used during takeoff, climb, and cruise. For study purposes, the engine has an advanced technology retractable chute-type noise suppressor in the duct stream only. At takeoff, the duct stream is limited to an average temperature of 1198 K to maintain suppressor metal temperatures within uncooled limits. The duct burner nozzle inlet temperature is limited to 1310 K at all other flight conditions. This temperature was selected to meet a study requirement thrust/drag ratio of 1.2 and to minimize the nozzle cooling requirements.

Engine cycle parameters pertaining to the duct burner are listed in Table III for four key operating conditions: sea level takeoff, transonic climb, supersonic cruise, and altitude relight. The tests conducted in this program were based on these conditions.

3.1.2 Temperature Rise Requirements

The maximum desired temperature rise of the baseline engine is 856 K, which occurs at the sea level takeoff operating condition. Since the fuel/air ratio is only 0.024, which is only 35% of the stoichiometric fuel/air ratio, efficient burning can best be accomplished by confining the combustion process to only a portion of the airstream. This permits the air not required for combustion to bypass the high pressure losses of the flame-holding region and mix in later, downstream of the duct burner, through low-pressure-loss apertures. In addition, the air bypassing the duct burner need not be diffused down to the low reference Mach numbers desired for stable, efficient, and low-pressure-loss burning; this results in a minimum total required passage height and permits the overall diameter of the engine to be sized for minimum aircraft drag.

FOLDOUT FRAME 1.

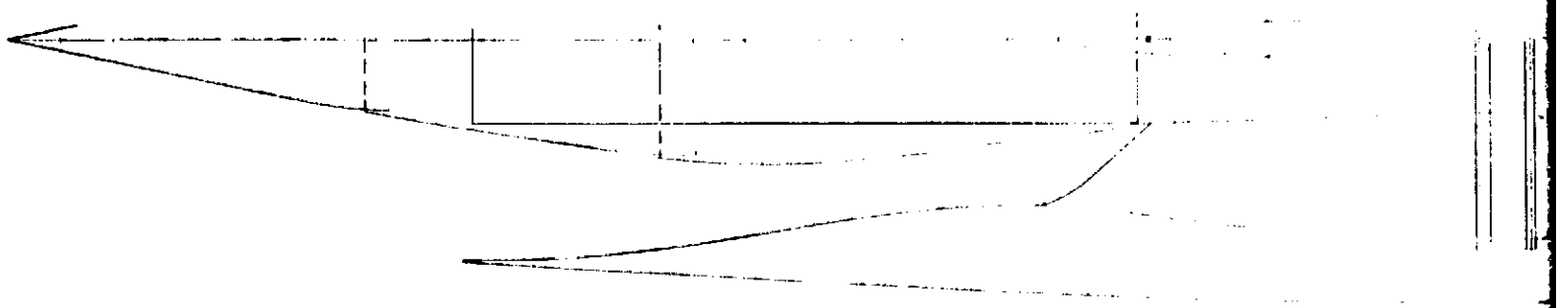

Figure 1. GE21/F2.4 Study P11 Baseline

FOLDOUT FRAME 2.

ORIGINAL PAGE IS
OF POOR QUALITY

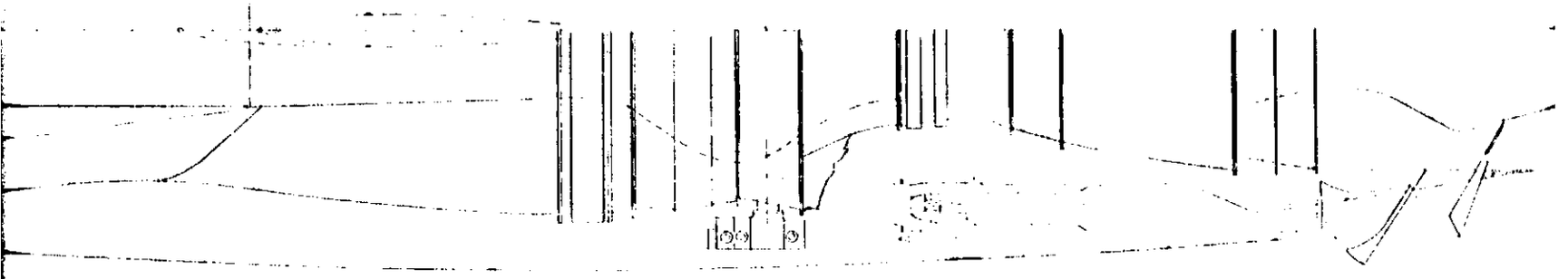

Figure 1. GE21/F2.4 Study P11 Baseline Duct Burning Turbofan Engine.

ORIGIN

FOLDOUT FRAME 2.

FOLDOUT FRAME 3.

ORIGINAL PAGE IS
OF POOR QUALITY

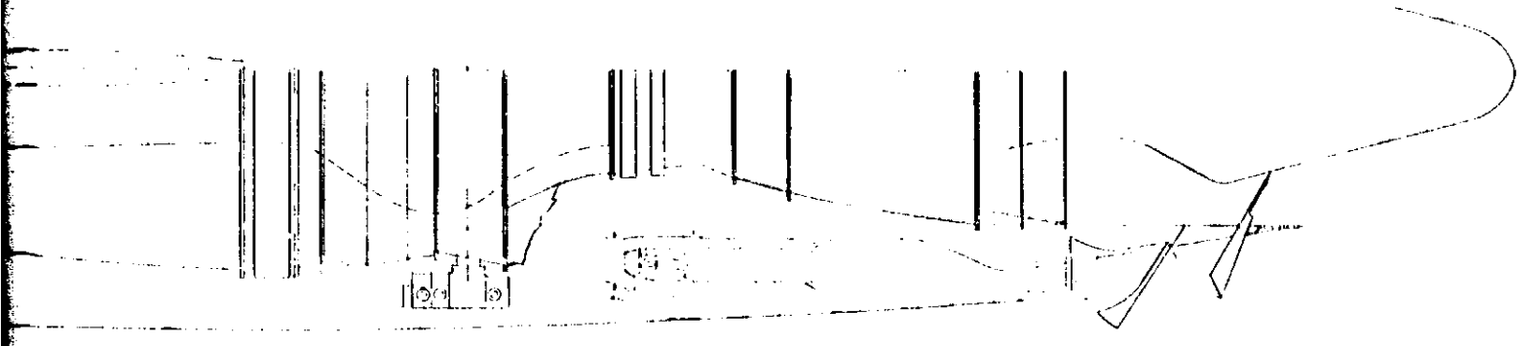

Study P11 Baseline Duct Burning Turbofan Engine.

ORIGINAL PAGE IS
OF POOR QUALITY

Table II. GE21/F2.4 Duct Burning Turbofan Engine Specifications.

Sea level static characteristics:	
Bypass Ratio	1.5
Inlet Airflow	431 kg/sec
Fan Pressure Ratio	4.0
Overall Pressure Ratio	22.5
Maximum Turbine Rotor Inlet Temperature	1810 K
Maximum Duct Exit Temperature	1310 K
Key dimensions:	
Inlet Flange Diameter (OD)	1800 mm
Maximum Diameter (OD)	2130 mm
Length, Front Face to Plug Nozzle Tip (Supersonic inlet not included)	5690 mm

Table III. Key Duct Burner Operating Conditions, GE21/F2.4 Study P11.

Flight Condition	Supersonic Cruise	Transonic Climb	Sea Level Takeoff	Altitude Relight
Flight Mach Number	2.4	1.0	0	0.95
Altitude, km	16.73	9.45	0	10.67
Fan Discharge Total Temperature, K	595	446	455	366
Fan Discharge Total Pressure, kPa	261	210	384	142
Fan Discharge Mach Number	0.41	0.41	0.41	0.41
Duct Burner Reference Mach Number	0.10	0.10	0.10	0.10
Duct Burner Exit Total Temperature, K	1283	1987	2014	533
Mixed Fan Stream Exit Temperature, K	949	1291	1311	450

At the supersonic cruise operating condition, the duct burner fuel/air ratio is only 39% of that required for takeoff. Modulation of the burner over such a range of fuel/air ratios requires fuel staging such that some part of the air that is carbureted at takeoff is not carbureted at cruise.

3.1.3 Envelope and Flow Requirements

The fan discharge Mach number of the baseline engine is 0.41, nearly constant at all flight conditions. Sufficient space is available to diffuse the fan duct stream to an average reference Mach number of 0.146. Approximately half of the duct stream is assumed to bypass the duct burner at a Mach number of 0.22. The internal duct burner reference Mach number is thus only 0.10, with an annulus height of approximately 180 mm.

The fan duct of the baseline engine extends from the fan discharge plane to the fan stream nozzle, the throat of which is located in the plane of the low pressure turbine. Some of this length is required for the fan discharge diffuser, and some is required for a mixing chamber to mix duct burner discharge gas with bypass air ahead of the nozzle. The remaining length available for the duct burner is approximately 850 mm.

3.2 Duct Burner Designs

Two duct burner design concepts were investigated in this program. Both concepts used a pilot burner stage plus main stage flameholder array. The two concepts differed principally in the design of the main stage flameholders. Concept 1, depicted in Figure 2, used circumferential flameholders derived from turbojet afterburner technology. Concept 2, depicted in Figure 3, used swept radial flameholders derived from the NASA/GE Experimental Clean Combustor Program. In each duct burner concept, the pilot burner operates with only a small percentage of the total air. Through its piloting action, this pilot burner provides stability for the main stage flameholders. From upstream fuel injectors, the main stage burner is supplied with carbureted air in a uniform premixed condition. The fuel/air ratio of the main stage is regulated so that combustion temperatures are high enough for CO and HC to be cleaned up in the relatively long 600-mm final burning section, yet low enough to avoid NO_x generation.

3.2.1 Duct Burner Concept 1

Duct burner Concept 1 consisted of an annular pilot stage located centrally in the duct, with circumferential main stage flameholders located both inside and outside of the pilot discharge annulus. This arrangement is illustrated in Figure 2.

The pilot stage burner was patterned after the main combustor designs evolved in the NASA/GE Experimental Clean Combustor Program (ECCP),

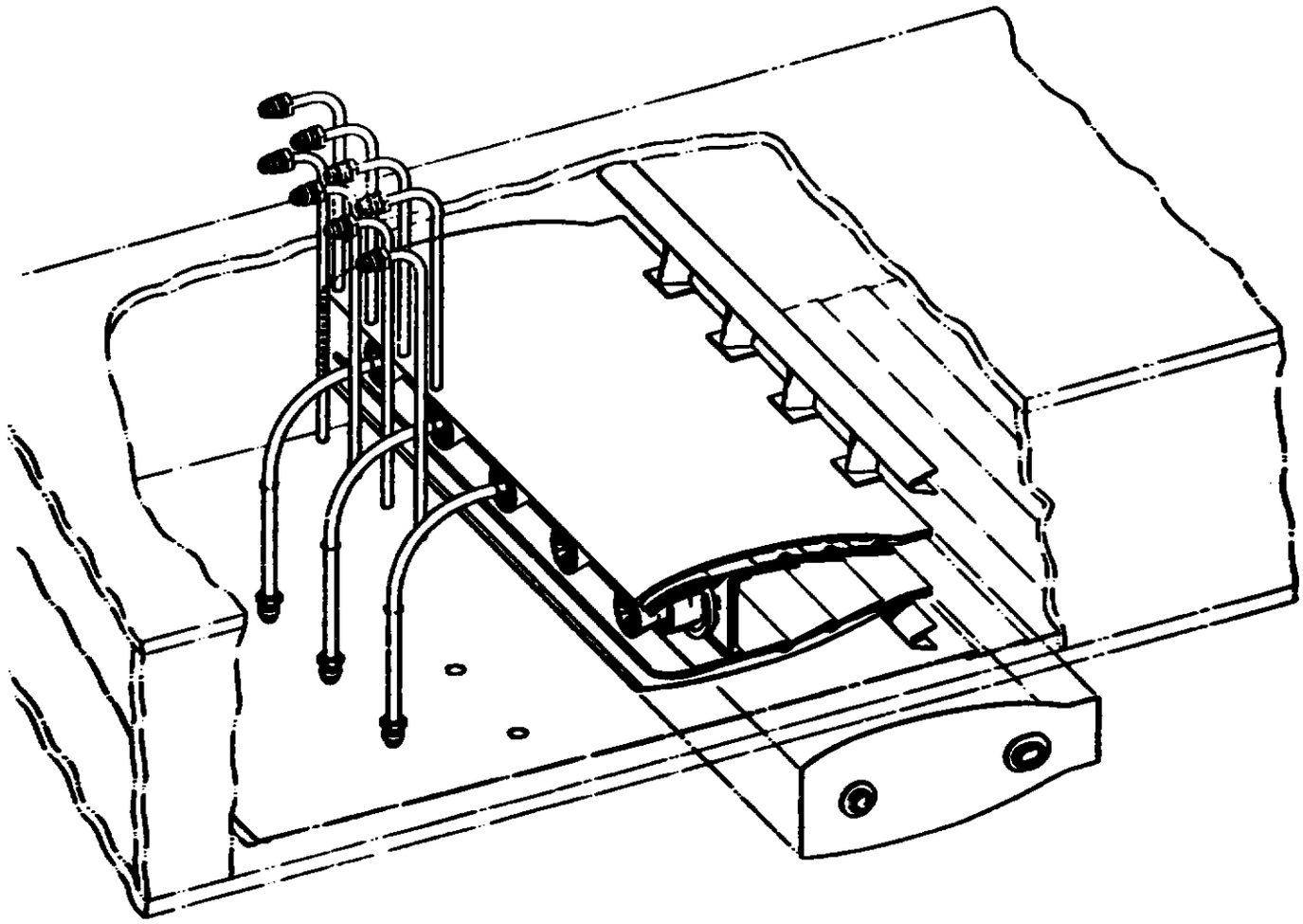

Figure 2. Duct Burner Concept 1, Augmentor Design Technology.

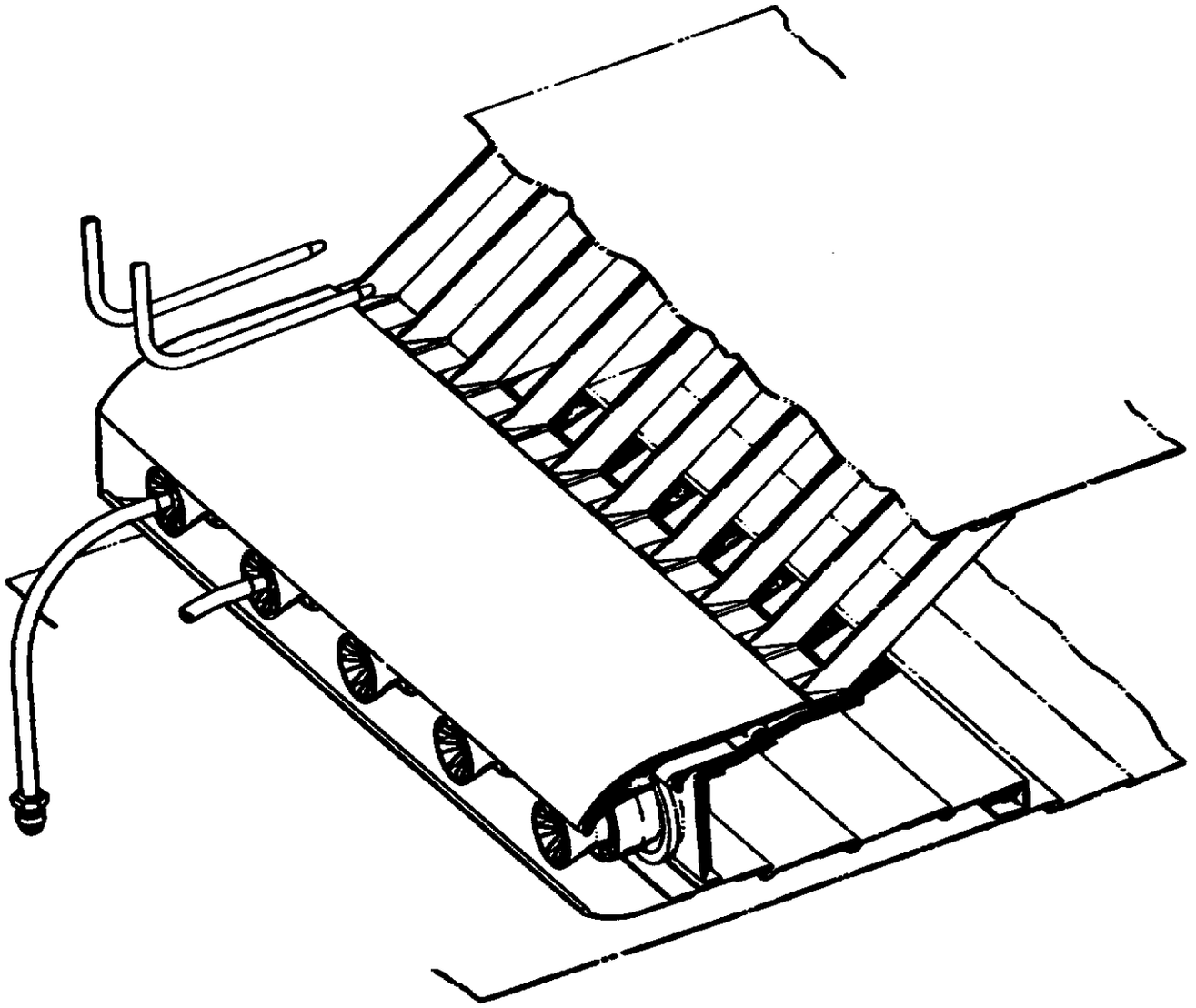

Figure 3. Duct Burner Concept 2, NASA ECCP Radial/Axial Staged Combustor Design Technology.

(References 1 and 2). The pilot burner used two-stage coaxial swirlers for each fuel nozzle, conservative stacked-ring cooling liners, and little or no dilution air.

The fuel nozzles were of the pressure-atomizing simplex type, fitted with a boattailed air shroud to prevent carbon buildup on the nozzle face. Except for the nozzle flow coefficient, this was the same nozzle design as that selected for the ECCP Phase III double annular combustor (Reference 1). Circumferential nozzle spacing was 76.2 mm.

The primary and secondary air swirler designs were identical to those of the outer dome of the ECCP Phase III double annular combustor (Reference 1). Each primary swirler had an effective metering area of 87 mm^2 and imparted a swirl of 37°. The primary swirler discharged through a venturi to prevent carbon deposition. Each secondary swirler had an effective flow area of 129 mm^2 and imparted a counterrotating swirl of 60°.

The swirlers discharged into barrels which were mounted in a dome protected by flat (rather than conical) splash plates. Dome height was 63.5 mm.

The pilot stage flame zone was contained by stacked-ring-type film cooled liners. Cooling air was metered into the plenum of each cooling slot by a circumferential row of small holes. Slot flow was smoothed by an overhanging lip. Panel length was 46 mm, and the pilot was three panels long. The design cooling flow was 4.8 $mg/(m^2 \cdot Pa \cdot s)$ at the supersonic cruise condition.

For the first duct burner test configuration, dilution air was introduced through a single row of holes in the first liner panel. Hole diameter was 4.8 mm.

The pilot stage was designed initially to accept 10% of the burner airflow under the liners at the flameholder plane, and to operate with a pilot fuel/air mass ratio of 0.03.

The piloted flameholder of duct burner Concept 1 used technology drawn from afterburner design experience: the ring V-gutter flameholder has been used effectively in the J47, J79, J93, and GE4 augmented turbojet engines. Two concentric circumferential flameholders were placed at the pilot burner discharge plane, connected to the pilot by short, slightly swept radial spokes in line with each pilot fuel nozzle. This arrangement is indicated in Figure 2.

A flameholder width of 19 mm was selected for the circumferential gutters based on previous successful experience in laboratory flame tunnel tests of piloted duct burner configurations. The radial spokes were 25 mm wide.

The pilot burner discharge annulus height was determined by gas dynamic calculations. It was assumed that 10% of the air emerged from the pilot, heated to 1522 K. The balance of the air at 595 K flowed through the flameholder gaps with a discharge coefficient of 0.94. The blockage was adjusted so that the total pressure loss was 3% after the air streams and wakes mixed to uniformity in the duct downstream without further heating, and with a reference Mach number of 0.1. This calculation predicted a total-to-static pressure drop of 5.6% at the pilot discharge plane, which was used to define the pilot flow metering area. The pilot discharge height appropriate for a passage height of 160 mm was 33 mm.

The design selected for the standard main stage fuel injectors was a radial splash plate spraybar, illustrated in Figure 4. The spraybar outside diameter was 6.3 mm. The fuel orifice, sized for a maximum pressure drop of 2 MPa, directed the fuel jet upstream against the downstream surface of the splash plate suspended 3.2 mm ahead of the spraybar. Atomization occurred first as the fuel sheet spread away from the point of impact of the jet on the plate, and then as the air stream sheared the fuel sheet away from the edge of the plate. In duct burner Concept 1, the spraybars contained one splash plate each and were located in the high velocity stream flowing around the widest part of the pilot cowl, in both the inner and outer passage. Circumferential spacing between spraybars was 43 mm.

3.2.2 Duct Burner Concept 2

Duct burner Concept 2 consisted of an annular pilot stage with swept radial main stage flameholders. In one configuration, the pilot stage was located against the inner wall of the duct, with the flameholders extending outward to the outer wall. This arrangement is illustrated in Figure 3. In other configurations, the pilot stage was centered in the duct, with the flameholders extending both inward and outward.

The pilot stage burners used in duct burner Concept 2 were similar to those used in Concept 1, described above. The fuel nozzles, primary and secondary swirlers, and domes were identical to those of Concept 1. The pilot cooling liners were somewhat different: the Concept 2 pilot liners were only two panels long, and the panel length was 53 mm. Dilution holes 6.3 mm in diameter were used in the first panel of some configurations. The Concept 2 pilots were designed initially to accept 10% of the burner airflow under the liners at the flameholder plane and to operate with a pilot stage fuel/air ratio of 0.03. These parameters were modified during the test program, as described below in Section 3.3.

The main stage of duct burner Concept 2 used swept radial flameholders patterned after the main stage of the radial-axial combustor configuration tested in the ECCP (Reference 2). In principle, the swept radial flameholder concept offers a greater length of flameholder edge and shorter flamespreading distances than does a circumferential flameholder array having the same effective blockage.

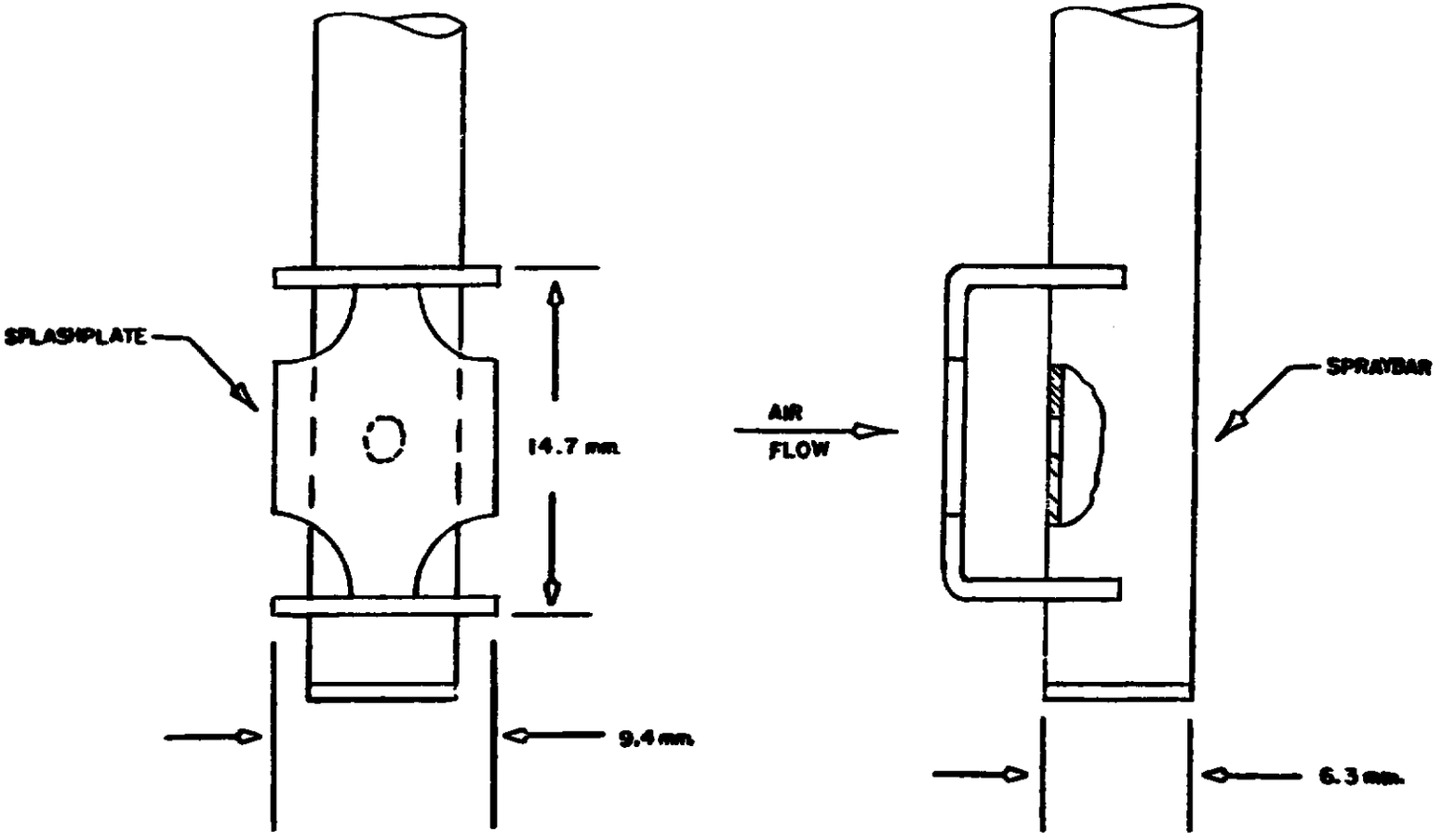

Figure 4. Standard Splashplate Spraybar Design.

A sweep angle of 60° and a semicircular gutter cross section were selected for the flameholder array. The number of flameholders was set at two per pilot fuel nozzle, i.e. the flameholder spacing was 38 mm, half the pilot nozzle spacing.

The appropriate flameholder blockage was calculated by a momentum balance across the mixing chamber downstream of the flameholder array. The nominal total pressure drop was 3% with a reference Mach number of 0.1, inlet temperature of 595 K, and the pilot stream (10% of total flow) heated to 1522 K. The discharge angle of the flow from the swept flameholder array was calculated by balancing axial and transverse momentum, assuming that the flameholder drag force acts normal to the flameholder edge. The discharge coefficient for the semicircular flameholders was assumed to be 1.0. From these calculations, a flameholder width of 24 mm was selected, with a pilot burner exit height of 51 mm for the one-sided configurations and 54 mm for the symmetric configurations, in the 160-mm duct height. The total-to-static pressure drop at the pilot discharge was calculated to be 5.4%.

Some configurations of duct burner Concept 2 used radial splash plate spraybars for main stage fuel injection, located in the high velocity stream flowing around the widest part of the pilot cowl. With a central pilot, these spraybars were identical to those used with Concept 1, described above. When the pilot was located against the inner wall of the duct, the spraybars extended from the outer wall only and contained two splash plates each, instead of one.

Variations of the standard fuel injector design were tested with Concept 2. These variations will be identified in the descriptions of the individual test configurations following.

3.3 Duct Burner Test Configurations

Twelve duct burner test configurations were defined for evaluation in an existing 194 by 432 mm rectangular sector test rig. Originally, the configurations were defined to be six variations each of the two duct burner concepts. Because of early hardware damage on Concept 1 and good emissions results from Concept 2, more configuration variations of Concept 2 than of Concept 1 were investigated. As it developed, three of the configurations represented variations of duct burner Concept 1; the remainder represented Concept 2. Only the burner region itself was simulated in the test rig. Neither the fan discharge diffuser nor the bypass air stream with its specific liner and downstream mixer region was part of the test models.

The test rig was equipped with upper and lower multijet-type cooling liners used in previous test programs. The nominal height under these liners was 160 mm The multijet liner design has film air injected through rows of discrete holes aimed parallel to the panel surface, without plenum or overhang. Each row had 1.9-mm holes spaced 2.5 mm on centers. Panel length was 38 mm.

The sector endwalls were protected by slave liners cooled by unheated auxiliary air downstream of the main stage flameholders. The standard endwall liner was a simple flat plate with a narrow backside passage for convection cooling. Some film protection was provided by rows of holes drilled perpendicularly through the plate and covered by baffles. Special endwall liners were used with Configurations 4 and 5.

Upstream of the main stage flameholders, the sector endwalls were protected by closing the pilot cowls and liners to form a box.

All duct burner configurations were mounted with the pilot burner dome splash plates in a common axial position, 760 mm from the tunnel exit.

The 12 test configurations are described below. Key features are summarized in Table IV.

3.3.1 Configuration 1

Configuration 1, shown in Figure 5, was the basic representation of duct burner Concept 1. Circumferential main stage flameholders were mounted symmetrically above and below the centrally mounted pilot, at the same axial station. The gap between each flameholder and the adjacent liner was maintained at 11 mm by a spring attached to the liner. Standoffs on the flameholder compressed the spring to compensate for expansion and stackup tolerance. The burning length from the main stage flameholders to the tunnel exit was approximately 600 mm.

Main stage fuel was injected from standard radial splash plate spraybars located 200 mm ahead of the flameholders. The nominal flow of the pilot spray nozzles was 2.1 g/s at 690 kPa pressure drop.

3.3.2 Configuration 2

Configuration 2, shown in Figure 6, represented duct burner Concept 2 with the pilot located against the inner wall of the duct. The burning length from the main stage flameholders to the tunnel exit varied from about 630 mm at the pilot discharge to 480 mm at the outer wall.

Main stage fuel was injected from standard splash plate spraybars located as shown. The pilot fuel nozzles were enlarged to 3.0 g/s at 690 kPa to relieve clogging problems experienced in testing Configuration 1.

3.3.3 Configuration 3

Configuration 3 represented the variation of duct burner Concept 2 using a central pilot with swept radial flameholders above and below. The upper (outer) flameholders were displaced downstream 150 mm from the lower flameholders, as shown in Figure 7. The purpose of this arrangement was to prevent

Table IV. Duct Burner Test Configurations.

Configuration Number	Flameholders	Secondary Spraybars	Pilot	Comments
1	Circumferential, same axial station.	Standard splash plate.	Concept 1 standard.	Basic Concept 1.
2	Swept radial, one side only.	↓	Concept 2 offset.	Assymmetric Concept 2.
3	Swept radial, axially staged.		Concept 2 standard	Axially staged Concept 2.
4	↓		↓	Alternate resonance-suppression sidewall liners
5		Airblast.		Evaluate effect of atomization.
6	Swept radial, same axial station.	Standard splash plate.	Concept 2 w/upstream snout extension, reduced flow swirlers.	Symmetric Concept 2
7	↓	Circumferential splash plate far upstream.	Reduced flow snout extension.	Improve pilot stability, reduce contribution of pilot emissions.
8		↓	Original snout extension.	Increase premix length.
9	Add connecting gutter at tip of one side only.	Vapor, far upstream.	Reduced flow snout extension.	Show ultimate benefit of prevaporization.
10	↓	Circumferential splash plate far upstream.	↓	Eliminate quenching of HC near liners.
11	Circumferential, axially staged.	Standard splash plate.	Concept 1 standard, repaired.	Further evaluation of circumferential flameholders.
12	Add liner covers.	↓	↓	Reduce early quenching by liner cooling air.

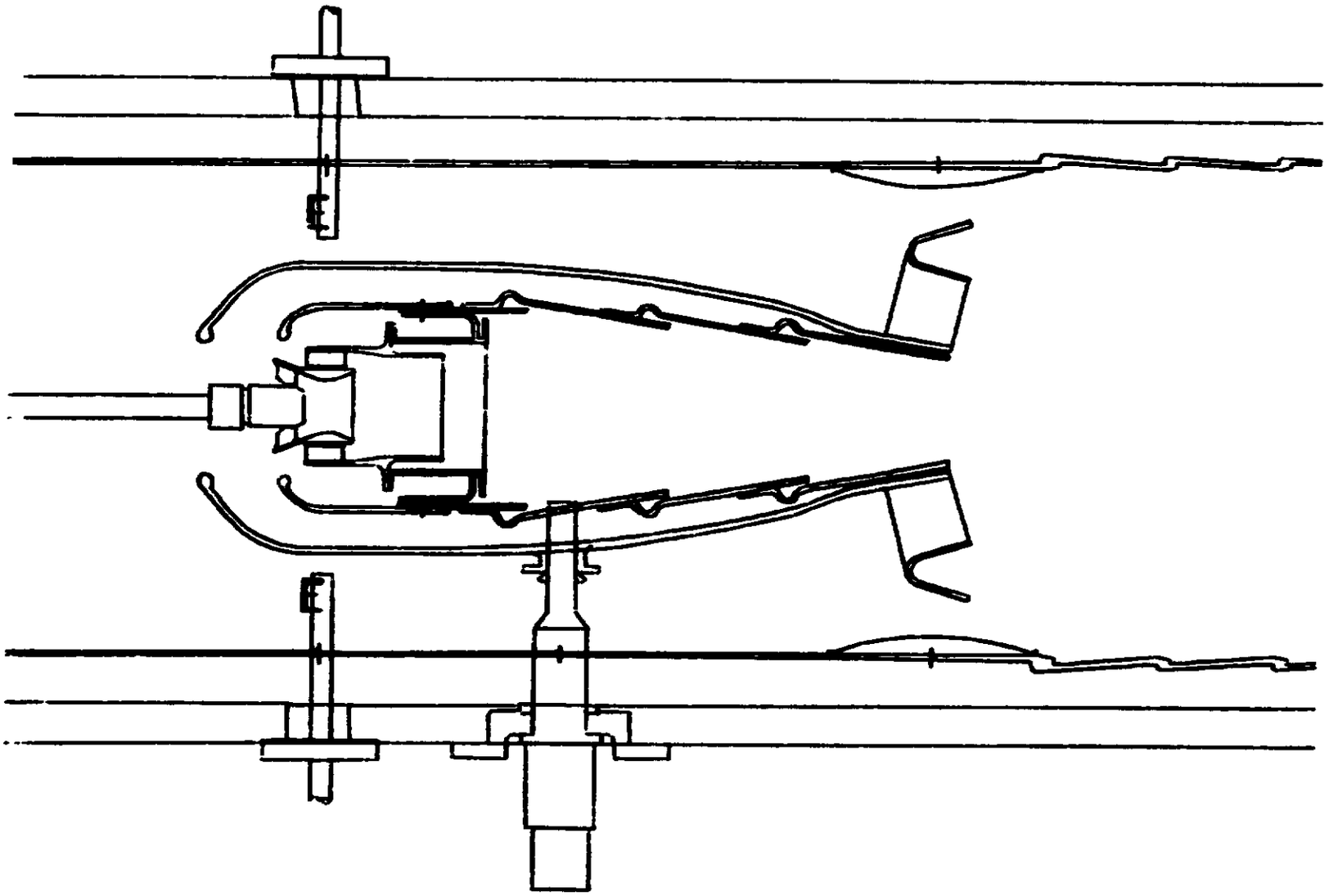

Figure 5. Configuration 1 Flowpath.

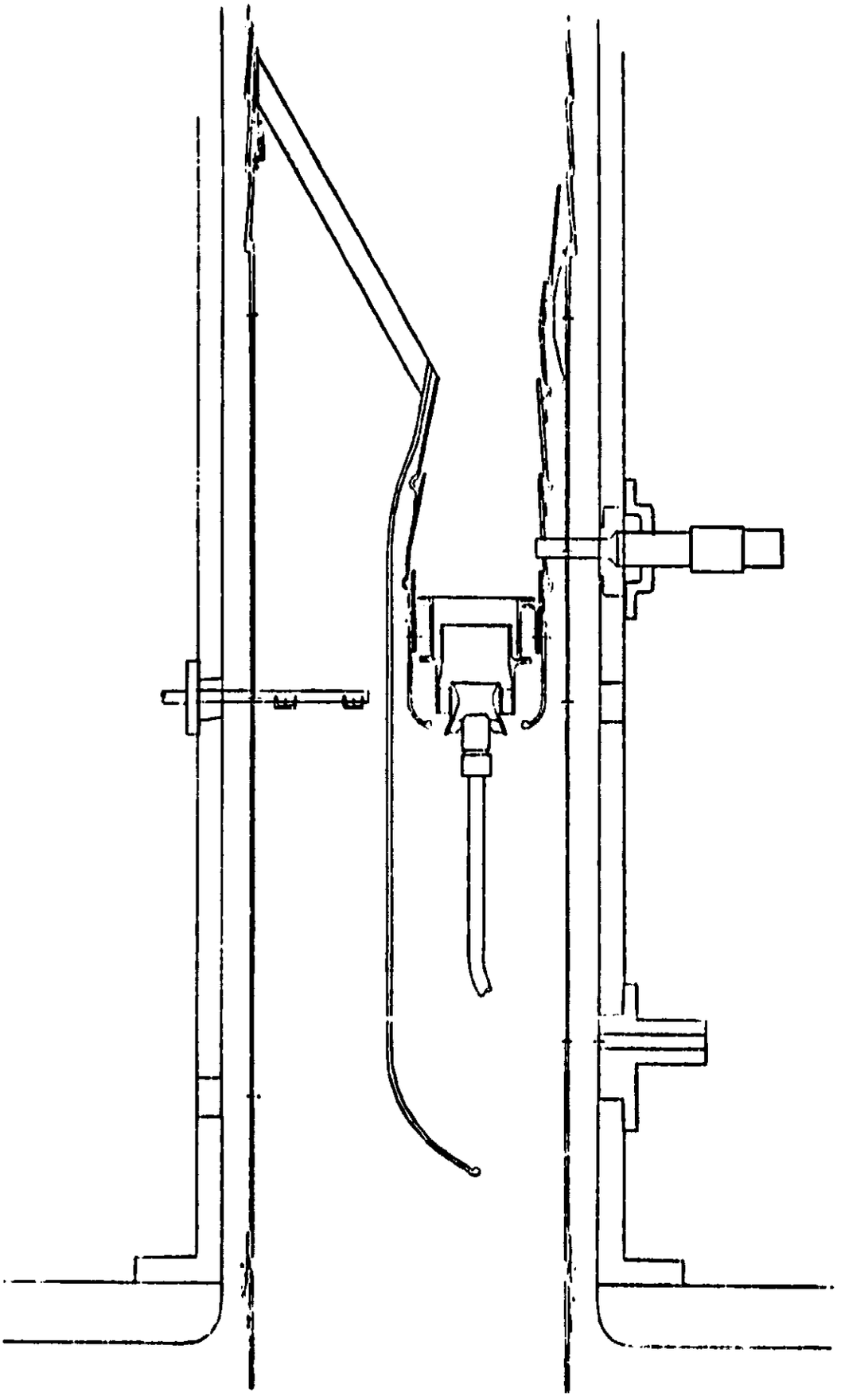

Figure 6. Configuration 2 Flowpath.

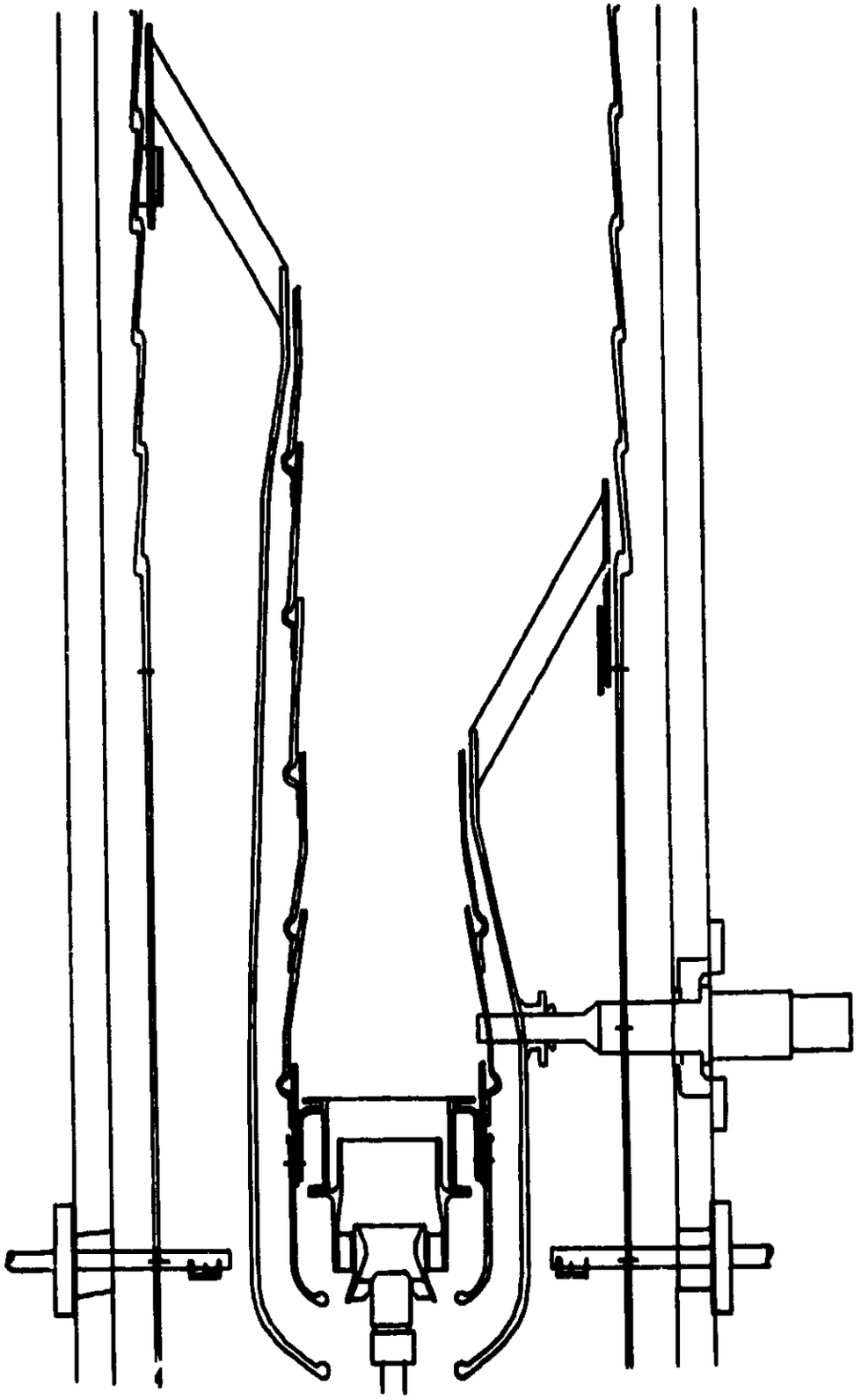

Figure 7. Configurations 3 and 4 Flowpath.

premature quenching of the combustion from the lower main stage flameholders by the mixing of uncarbureted air jets from the upper flameholders at the supersonic cruise operating condition, where only half the main stage is carbureted. The burning length for the lower flameholder array was about 600 mm.

Main stage fuel was injected from standard splash plate spraybars located as shown in Figure 7. The pilot fuel nozzles were enlarged to 3.7 g/s at 690 kPa in the process of repairing damage from previous testing.

Configuration 3, like Configurations 1 and 2, used simple sector endwall cooling liners consisting of a flat plate cooled by a strong backside flow of cold air, some of which bled through baffled holes for film protection.

3.3.4 Configuration 4

Configuration 4 was identical to Configuration 3 except for the sector endwall cooling liners. Configuration 4 was built up using alternate existing endwall liners with a longer spacing between the film baffles than for Configuration 3, 89 mm versus 38 mm, in an attempt to achieve improved resonance suppression. This particular liner had seemed to provide resonance suppression in a previous duct burner test program. However, with Configuration 4, only minor changes in resonance characteristics were encountered. After Configuration 5 was tested, the original endwall liners were reinstalled in the sector test rig.

3.3.5 Configuration 5

Configuration 5 (Figure 8) was derived from Configuration 4 by replacing the standard splash plate type main stage fuel spraybars with special air blast spraybars. The air blast spraybar consisted of two 6.35-mm OD tubes. The front tube carried fuel injected through two 0.635-mm orifices angled 45° aft. Unheated 650 kPa air was injected from two 1.32-mm orifices in the rear tube, angled 45° forward and aimed to impinge on the fuel jets.

3.3.6 Configuration 6

Configuration 6, illustrated in Figure 9, represented duct burner Concept 2 using a central pilot with swept radial main stage flameholders. Both the upper and lower flameholders were located at the same axial station, with a burning length of about 600 mm.

Main stage carburetion was provided by standard radial splash plate spraybars located 200 mm ahead of the flameholders.

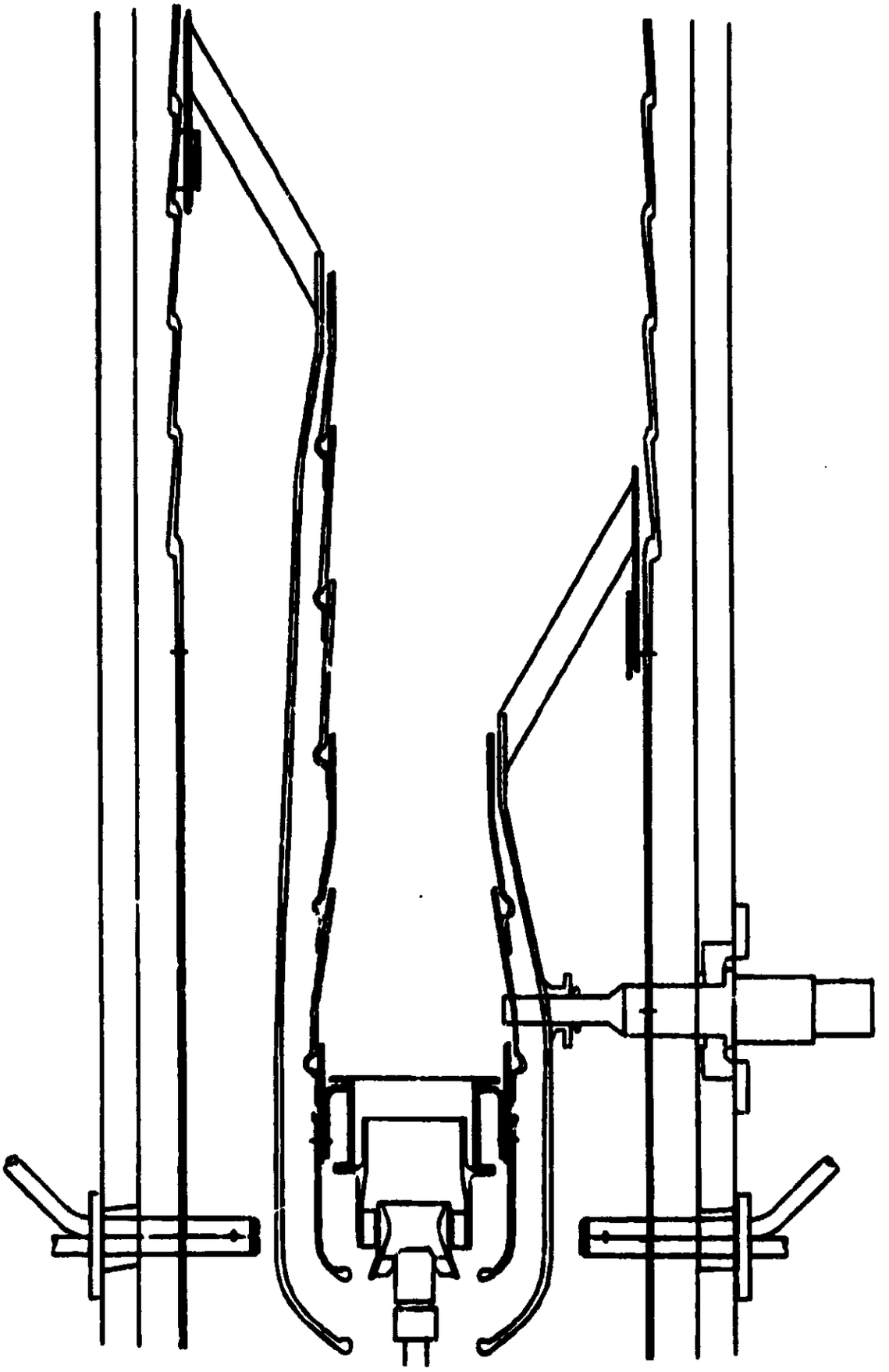

Figure 8. Configuration 5 Flowpath.

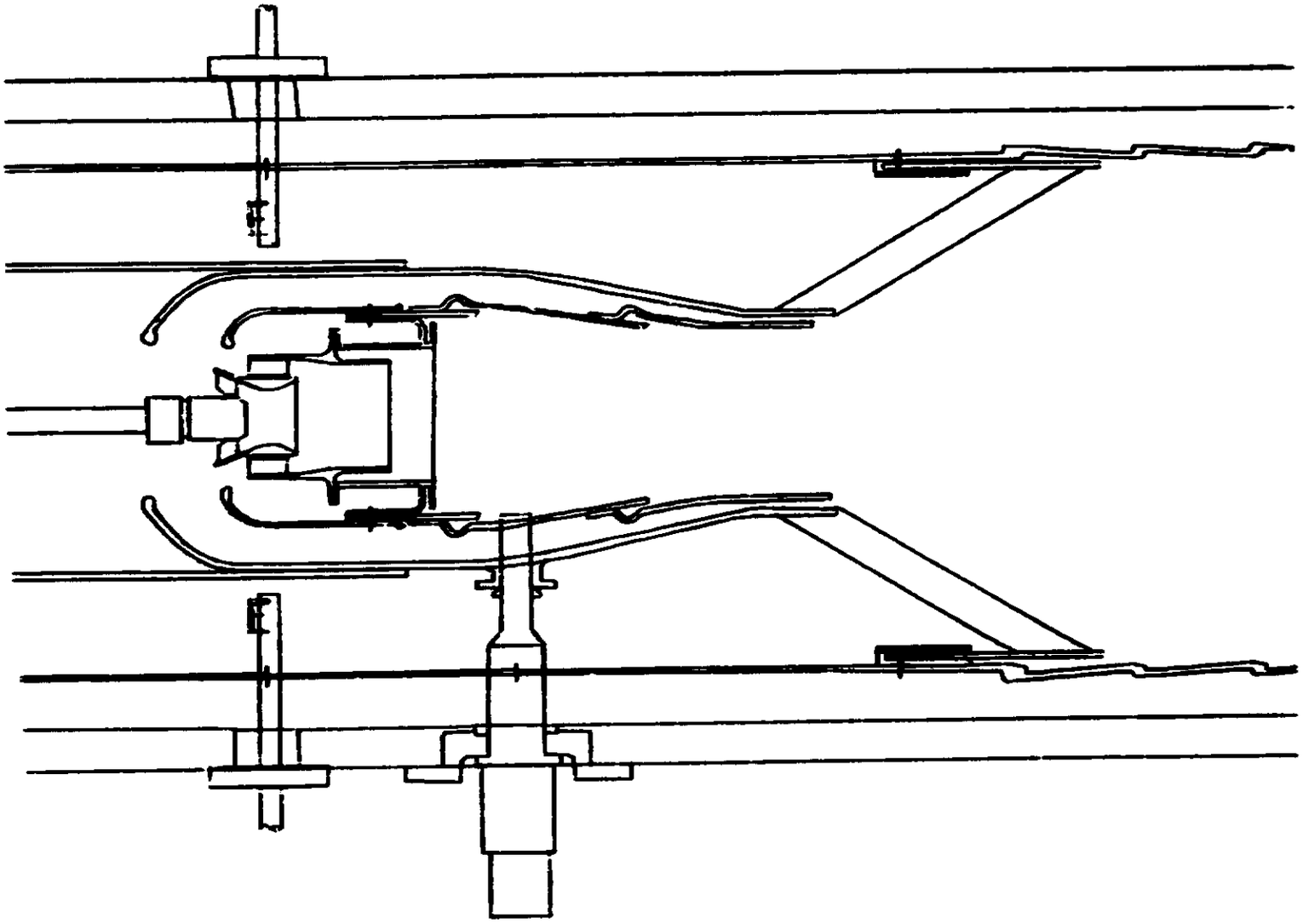

Figure 9. Configuration 6 Flowpath.

Configuration 6 was tested with an extension fitted to the pilot burner cowl. This extension moved the pilot air intake upstream to a point ahead of auxiliary fuel injectors located in the test rig inlet bellmouth. The cowl extension and upstream fuel injectors were used for derivatives of Configuration 6 but were not used in testing Configuration 6 itself. However, constriction of the main stage airflow past the upstream injectors increased the main stage air passage pressure drop, causing additional air to be diverted through the pilot.

The pilot was modified in an attempt to improve its stability and thereby reduce combustor resonance. All dilution holes were closed, and one-fourth of the secondary swirler passages were blocked. The net effect of the pilot modification and the pilot cowl extension was estimated to be a reduction in pilot airflow from 10% to 9% of the duct burner airflow under the liners at the flameholder station.

3.3.7 Configuration 7

Configuration 7 (Figure 10) was derived from Configuration 8 by adding a throttle plate to the pilot cowl air intake and removing the unused radial splash plate spraybars. The resulting configuration included a central pilot modified by closing all dilution holes and one-fourth of the secondary swirler passages, swept radial main stage flameholders at the same axial station, and a pilot cowl that extended upstream into the test rig inlet bellmouth where main stage fuel was injected from circumferential splash plate spraybars. Only the lower passage spraybar was used in testing Configuration 7.

The pilot intake throttle plate contained five 28.5-mm diameter holes. Its function was to balance the main stage air passage pressure drop caused by the circumferential spraybars, so that the pressure drop across the pilot liner would be in correct proportion to the pressure drop across the main stage flameholders. The pilot airflow was estimated to be 7% of the duct burner airflow under the liner at the flameholder station.

3.3.8 Configuration 8

Configuration 8 (Figure 11) was geometrically identical to Configuration 6. The difference between the two was the injector used for the main stage fuel. In Configuration 8, the main stage fuel was injected from circumferential splash plate spraybars located in the test rig inlet bellmouth 590 mm upstream from the flameholders. The spraybar configuration was linearly scaled from the standard splash plate spraybar design (Figure 4) to a spraybar diameter of 9.5 mm. The fuel orifices were spaced 29 mm apart along the bar. A pilot cowl extension was used, as shown in Figure 11, to prevent main stage fuel from entering the pilot and to provide high air velocity past the spraybars.

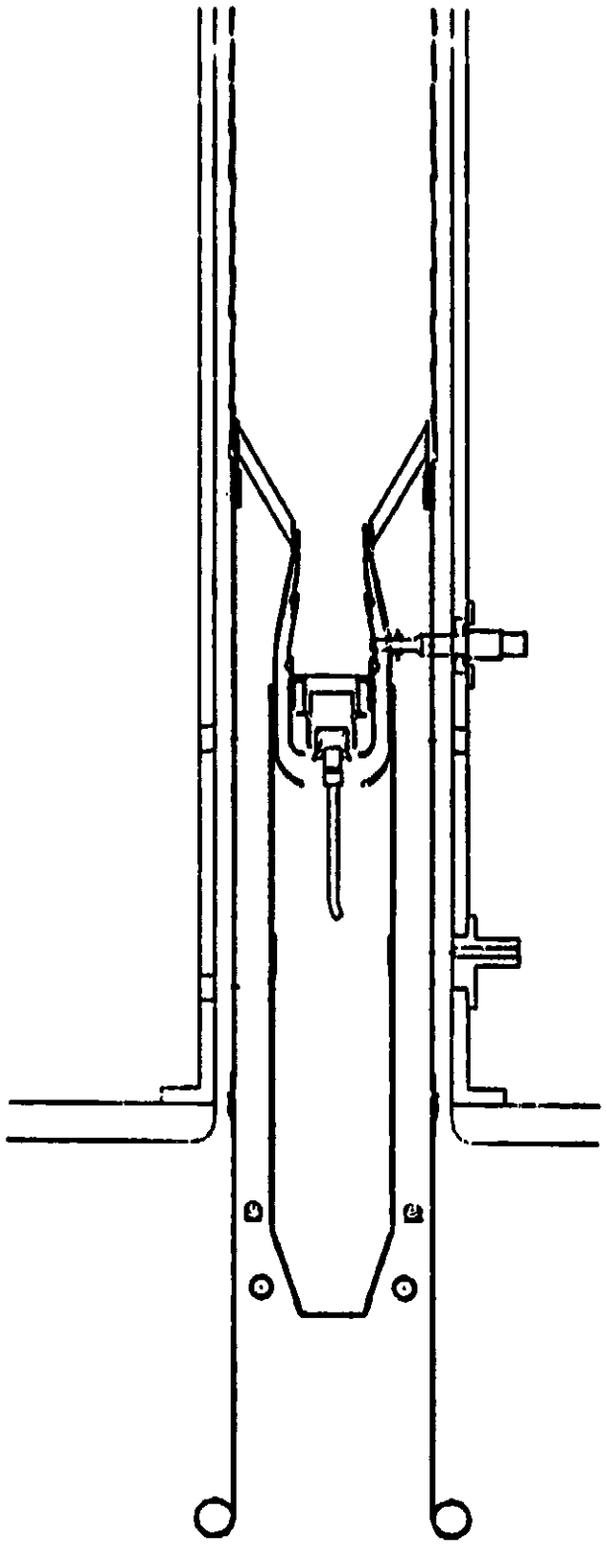

Figure 10. Configuration 7 Flowpath.

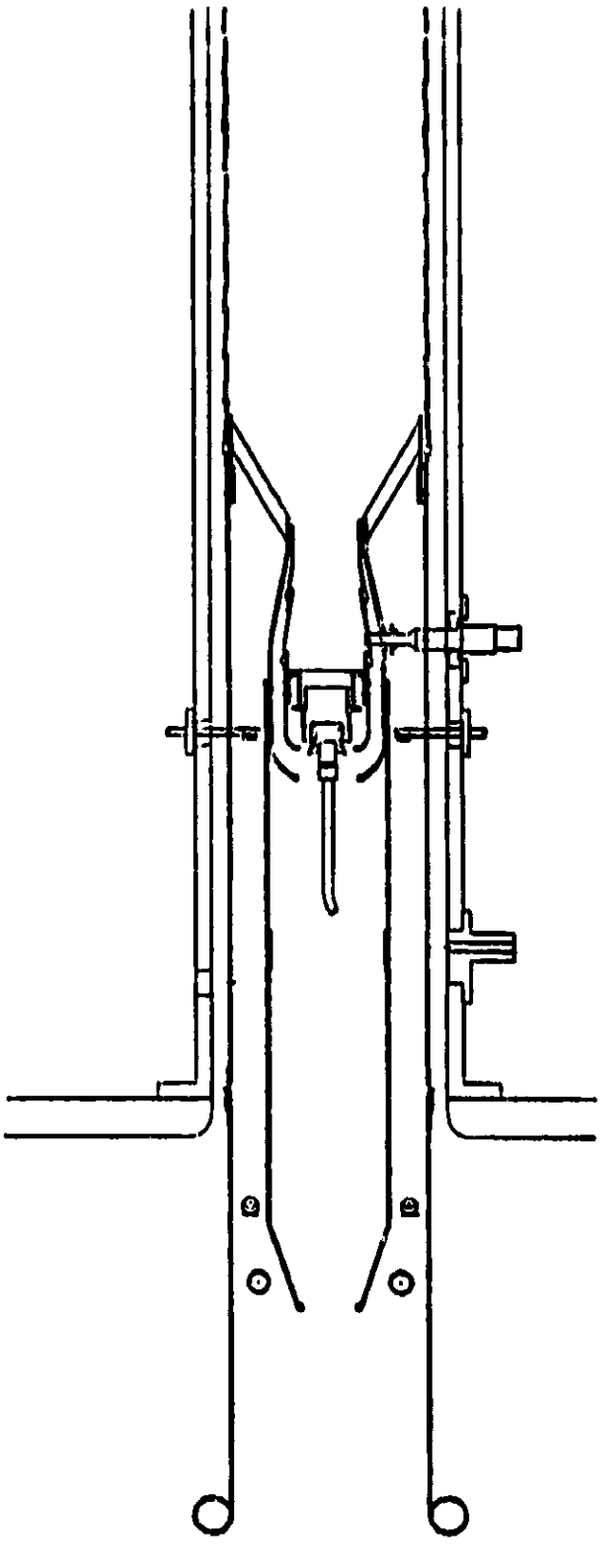

Figure 11. Configuration 8 Flowpath.

Vapor fuel spraybars located just ahead of the circumferential splash plate spraybars and standard radial spraybars located further downstream were installed during the testing of Configuration 8 but were not used.

3.3.9 Configuration 9

Configuration 9 (Figure 12) was geometrically identical to Configuration 10. For Configuration 9, the fuel was heated to 590 K, a temperature calculated to fully vaporize the fuel at burner pressure, and injected from one (the lower) or both of the circumferential vapor spraybars located in the test rig inlet bellmouth. Each spraybar contained two rows of 1.3-mm orifices spaced 13 mm apart, directing fuel jets normal to the airflow. The circumferential splash plate spraybars used for liquid fuel were retained just downstream of the vapor fuel spraybars but were not used.

3.3.10 Configuration 10

Configuration 10 was derived from Configuration 7 by adding a narrow (6-mm wide) crossfire gutter at the downstream end of the upper swept radial flameholders, next to the liner, as shown in Figure 13. The intent of this modification was to promote the burning of a streak of raw fuel previously observed near the liners.

Configuration 10 thus included a central pilot, modified by closing all dilution holes and one-fourth of the secondary swirler passages, and equipped with an extended cowl with a throttle plate at the intake, and Concept 2 swept radial flameholders at the same axial station, the upper one of which was equipped with a crossfire gutter next to the liner. Main stage fuel was injected either from the upper circumferential splash plate spraybar only, or from both upper and lower spraybars equally, at different test points.

3.3.11 Configuration 11

Configuration 11, illustrated in Figure 14, represented duct burner Concept 1 with a central pilot stage and circumferential main stage flameholders. The upper flameholder was displaced 180 mm downstream from the lower flameholder, with the upper pilot cowl and liner extended accordingly. Upper liner cooling slots ahead of the flameholder were covered. The upper flameholder was hung from the upper liner by hooks of a length to maintain the flameholder-to-liner gap at 11 mm. The lower flameholder-to-liner gap was 9 mm, maintained by a spring and standoff arrangement similar to Configuration 1. Burning length from the lower main stage flameholder to the tunnel exit was about 600 mm.

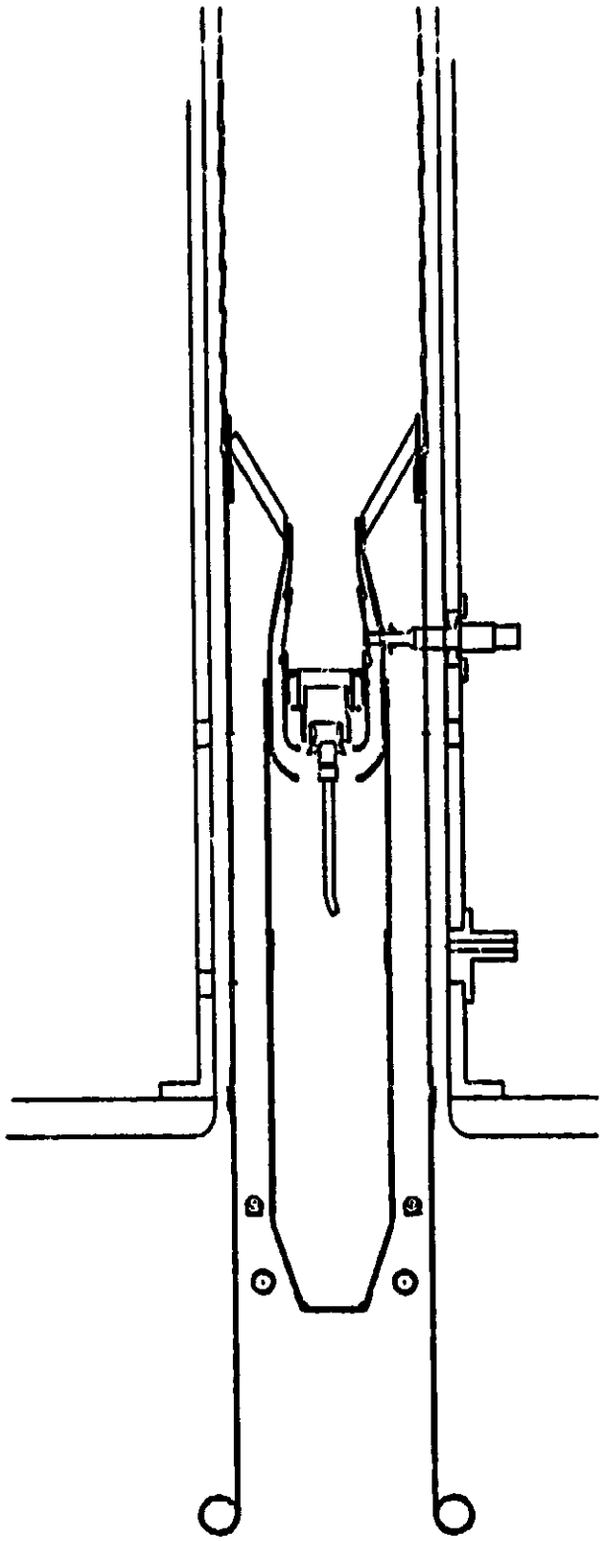

Figure 12. Configuration 9 Flowpath.

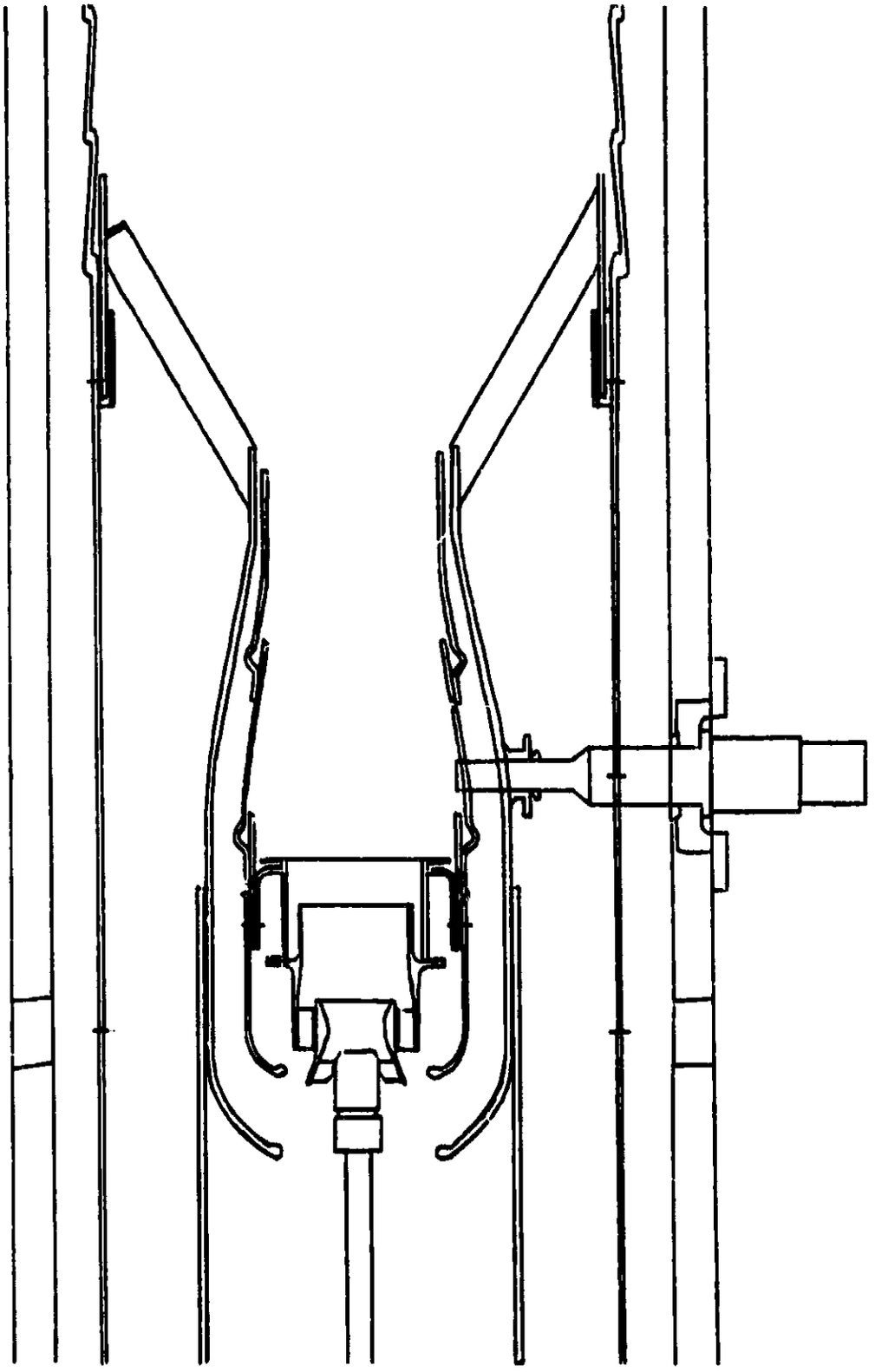

Figure 13. Configuration 10 Flowpath.

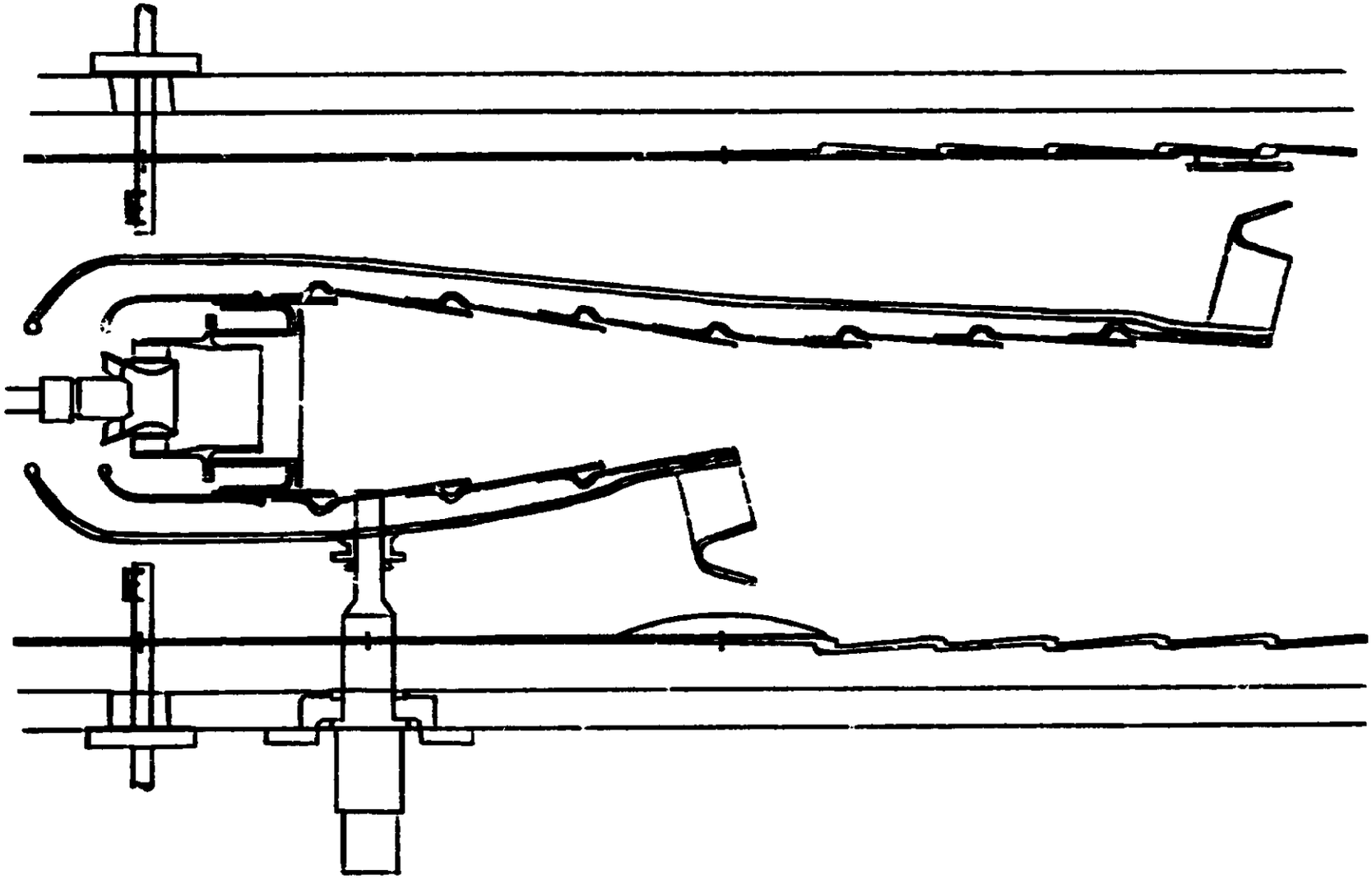

Figure 14. Configuration 11 Flowpath.

The pilot cowl was not fitted with an upstream extension. The pilot dilution holes were closed, but all secondary swirler passages were left open.

Main stage fuel was injected from standard splash plate spraybars located as shown in Figure 14.

3.3.12 Configuration 12

Configuration 12 (Figure 15) was derived from Configuration 11 by adding a splitter plate to delay the mixing of lower liner cooling air with burning gases from the lower main stage flameholder. Configuration 12 thus represented duct burner Concept 1 with a central pilot and circumferential main stage flameholders, the upper of which was displaced 180 mm downstream from the lower. Main stage fuel was injected from standard splash plate spraybars located abreast of the pilot swirlers.

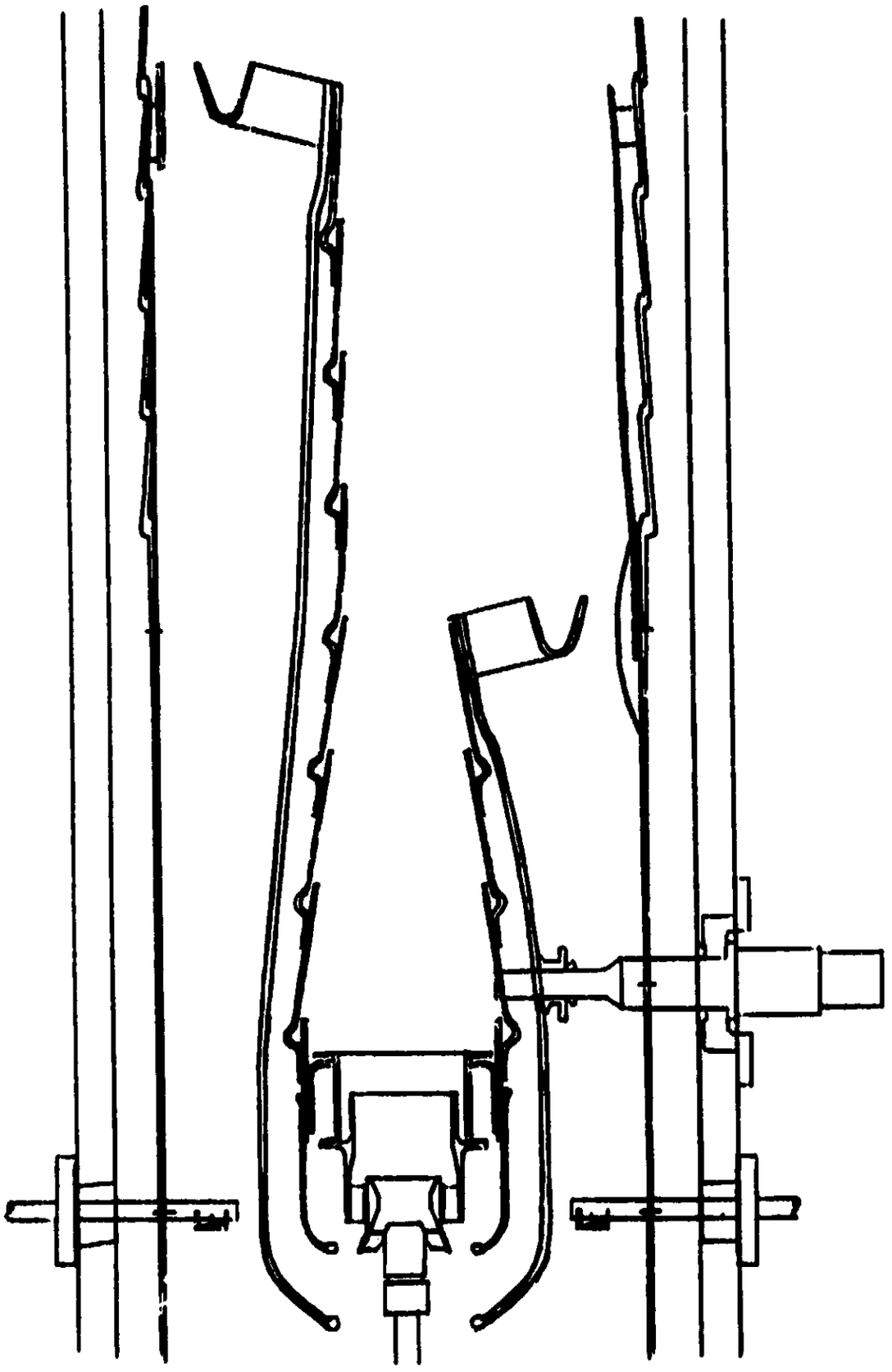

Figure 15. Configuration 12 Flowpath.

4.0 TEST FACILITIES AND EQUIPMENT

4.1 Pressure Sector Test Rig

The duct burner test configurations were evaluated in a rectangular sector test rig. The rectangular duct (duct burner housing) had a 194- by 432-mm cross section and housed the inlet bellmouth, the cooling liners, and the duct burner assembly. The duct was enclosed in an 860-mm diameter pressure vessel designed to permit test operation up to 310 kPa gage pressure. The enclosing vessel was fabricated in three pieces to facilitate assembly of the duct and service leadouts for instrumentation, fuel systems, cooling air, etc. An adapter plate was utilized at the inlet section of the test rig to provide attachment to the test cell air supply. The inlet bellmouth extended forward of the adapter plate into the air supply pipe. The rig exhaust section, including a water quench section, was designed for attachment to the test cell exhaust ducting. A sketch of the assembled pressure tank is shown in Figure 16.

The pressurizing tank completely encapsulated the duct burner housing and all of its service requirements, such as thermocouples, fuel injection manifolds, igniter components, gas sampling traversing probes, and slave cooling air systems. To prevent damage in the event of a leak from a fuel line or manifold, the pressurized space between the augmentor duct and the pressure vessel was purged with steam. A baffle was placed at the exhaust plane of the augmentor duct to limit recirculation of exhaust gases into the purged cavity. The fuel lines leading through the inlet adapter plate to the injectors located in the inlet bellmouth were double-walled conduit, with the space between walls steam-purged and vented into the pressurized space downstream. Provisions were made in the design for sealed access ports through the forward section of the pressure vessel for all required electrical, gas, and liquid service lines. Additionally, a sealed traversing rod was provided to allow traversing of the combined total pressure and gas sampling probes across the burner exit plane.

The test rig was mounted on two dollies. The forward section of the pressurizing tank, the front adapter plate, and the duct burner housing assembly initially were mounted in the forward dolly. All burner service connections were checked for leaks, electrical continuity, etc. before the second section, mounted on the aft dolly, was installed.

4.2 Services

Air was supplied to the test rig compressed and heated to conditions fully representative of the baseline engine fan discharge air stream. Compression was accomplished by centrifugal compressors with water-cooled aftercoolers. Heating was done after compression in a nonvitiating heat exchanger. Temperature control was accomplished by bypassing the heater with part of the airflow, which was mixed with heated air before being metered to the test rig. Air humidity was not controlled.

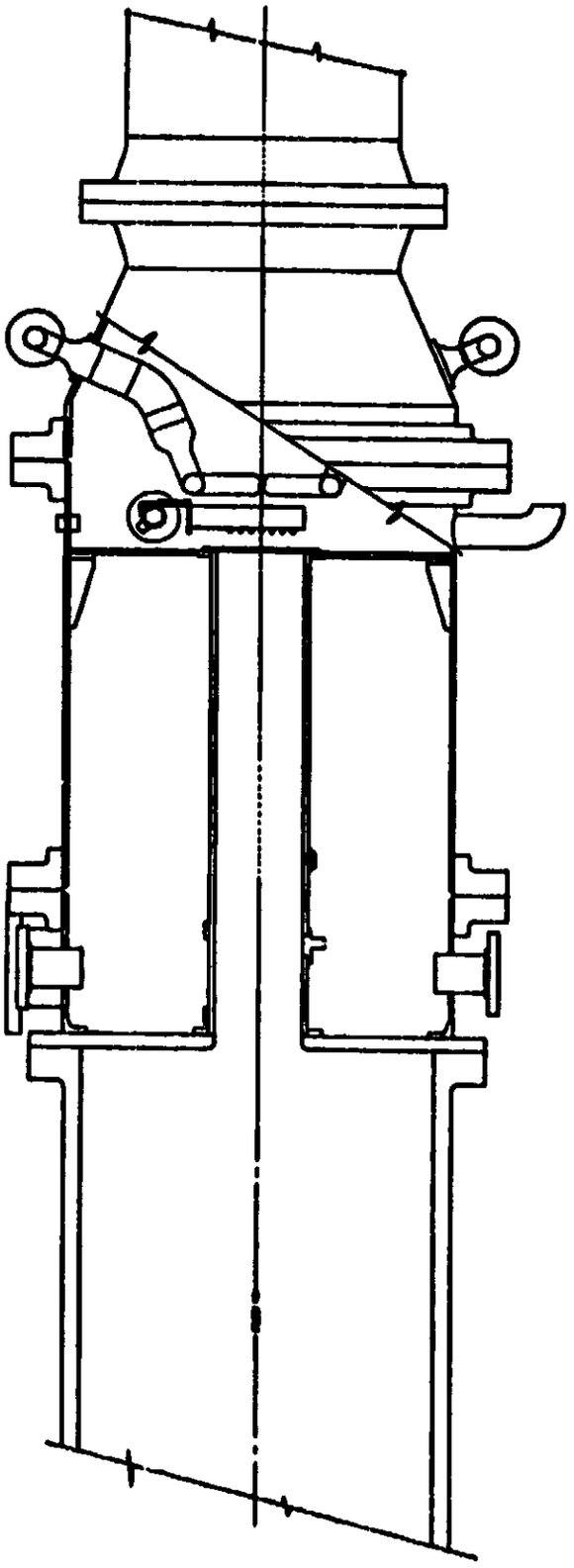

Figure 16. Pressure Sector Test Rig.

Unheated auxiliary air was used for cooling the sector end wall liners. The airflow to the two liners was regulated at 2.86 kg/s per megapascal of test pressure. Of this, about 38% was bled into the burner as film air, and the rest was dumped from the aft end of the panels into the exhaust chamber. Auxiliary air was also used for protection of the dynamic pressure transducers.

JP-5 fuel from bulk storage was pressurized by a positive-displacement pump, then distributed to the various fuel manifolds through a system of control valves and redundant flowmeters. The fuel system is shown schematically in Figure 17. Nitrogen was used to purge residual fuel from the lines and manifolds after system shutdown to avoid coking of spraybars and nozzles.

For one configuration (Configuration 9), the fuel heater shown schematically in Figure 17 was used to vaporize the main stage fuel. For this configuration, all main stage fuel was drawn from only one of the two main stage fuel systems. Initial heating was done in a steam heat exchanger. Final heating was done in an air heat exchanger by an unvitiated hot auxiliary air supply. The fuel was maintained at supercritical pressure in the heater, then flashed to vapor across a throttle valve downstream. The vapor fuel was piped directly to the vapor fuel injectors, one of which could be turned off by a gate valve when necessary.

City water supplied from high pressure centrifugal pumps was used to quench the combustion gases at the burner exit and also to cool the burner exit survey rakes and the dynamic pressure gages.

The quenched exhaust gases passed into the exhaust ducting through a butterfly valve ("blast gate") used to regulate the test rig pressure. From the exhaust ducting, the gases were released to the atmosphere through a silencer.

Steam for purging dead spaces within the pressure vessel, for heating fuel, and for tracing gas sample lines was supplied saturated at 1.0 MPa pressure.

Ignition energy was supplied from an aircraft engine type of capacitor-discharge ignition exciter.

4.3 Instrumentation

The various airflows were metered by ASME standard thin-plate orifice flowmeters. The heated test air was measured downstream of the temperature and flow control valves using a 177.17-mm orifice in a 603-mm ID pipe. The auxiliary airflow to the sector end wall liners was measured by a 51.16-mm orifice in a 102-mm pipe. Airflows were calculated from the measured pressure drops across these orifices using the procedures of Reference 3.

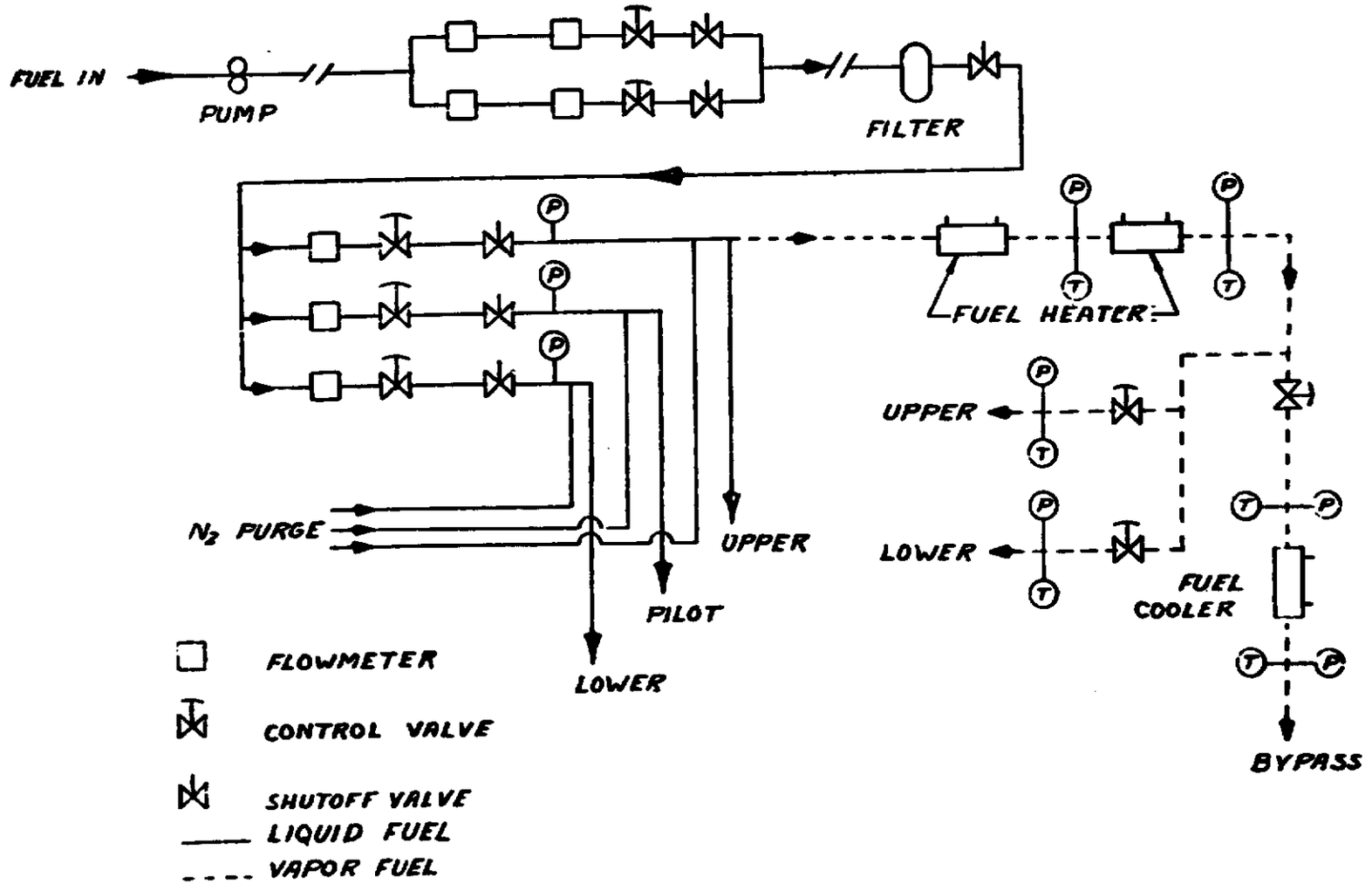

Figure 17. Fuel System Schematic.

Fuel flows were measured by turbine-type flowmeters, calibrated within six months by time and weight methods using the same fuel type as used in the test. The measured flows were corrected for variations in fuel specific gravity. Flowmeter speed was measured by an electromagnetic pickup, which produced an electrical signal with a frequency proportional to meter speed.

Temperatures were measured with metal-sheathed chromel-alumel thermocouples. Sheath diameter was, typically, 1.6-mm. For measuring gas temperatures, the sheaths were sealed over the thermocouple junctions to protect them. For measuring structure temperatures, the sheaths were stripped back for a short distance and the thermocouple wires spotwelded directly to the metal surface. Thermocouple signals were referenced to a single controlled-temperature bath, and the calibration and zero signals were processed through the same bath. The alloy-to-copper junctions were made in a stabilized thermal sink, and the output of the low-level switch was processed through the same sink and then referenced to the controlled reference temperature before going to the low level amplifier and analog-to-digital converter.

Time-averaged pressures were measured by electrical transducers connected to the test rig through scanning valves. Gas stream total pressures were measured by simple impact tubes aimed against the expected flow direction. Static pressures were measured by tubes attached to small holes drilled perpendicularly through the duct wall.

Axial measurement stations were designated by their distance in centimeters from the front edge of the inlet bellmouth.

The duct burner inlet total pressure and temperature were measured by two rakes located in the inlet bellmouth. Each rake spanned the 160-mm radial height of the duct, and contained four total pressure tubes separated by three thermocouples.

The pilot fuel nozzle pressure drop was defined as the pressure difference between the fuel pressure in the line outside the pressure vessel and the average stream total pressure at the augmentor exit plane. The main stage fuel injector pressure drop was taken as the difference between fuel line pressure and average augmentor inlet total pressure.

Test air humidity was measured by an on-line mositure monitor which provided a continuous indication of the dew point of an air sample drawn from the supply ducting ahead of the test rig. This meter was used for Configurations 7, 9, 10, 11, and 12. For other configurations, the air humidity was assumed to be 3.57 g/kg for data reduction purposes.

Dynamic pressure was measured at up to four locations in the sector test rig by piezoelectric crystal transducers (Kulites). The transducer installation is illustrated in Figure 18. The installed package consisted of an adapter section, a cooling unit, an enclosure, an infinite line, and the transducer. The adapter section, from the point of entry into the augmentor chamber to the face of the transducer, was the same for all units. The

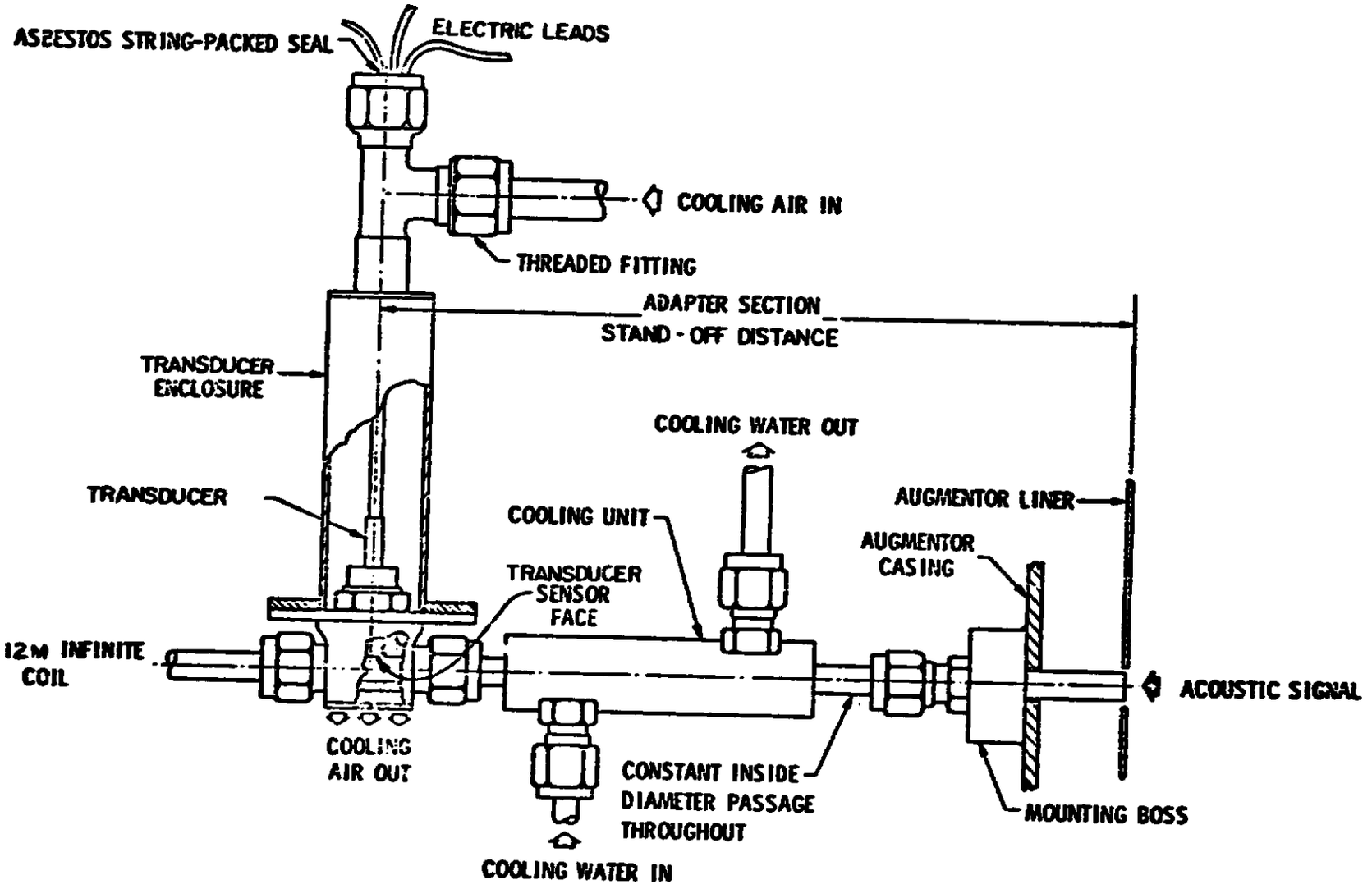

Figure 18. Dynamic Pressure Probe Installation.

constant standoff distance was necessary to synchronize phasing, i.e., the phase change through each standoff tube was constant provided the air temperature was the same in each tube. The standoff tube separated the transducer from the hot combustion chamber, and the cooling unit prevented overheating of the air through which the dynamic pressure signal passed between the combustion chamber and the face of the transducer. Since the transducers were located within the steam-purged cavity, air passing through the enclosure further cooled the temperature-sensitive crystal. The enclosure provided protection from external shocks and handling. The 12-meter infinite coil allowed attenuation of all dynamic pressure signals and was sealed to backpressure the signal passage. The transducer's electrical signals were displayed on oscilloscopes and recorded on magnetic tape.

The four dynamic pressure sensing points were:

1. Inside pilot cowl, on sector endwall, adjacent to the pilot swirlers.

2. Inside pilot liner, on sector endwall, 50 mm downstream of pilot dome.

3. Upper main stage liner, 368 mm from exit, 89 mm off sector centerline.

4. Sector endwall liner, 137 mm from exit.

Configurations 1 and 2 contained only points 1 and 4. In Configurations 4 and 5, the sensing tube at point 4 did not penetrate the endwall liner.

The duct burner exhaust gas composition and total pressures were measured using two exhaust gas sampling rakes, each containing seven sampling elements and attached to a common traversing bar. The two rakes were traversed across the long dimension of the duct exit, and measurements were taken at the discrete locations shown in Figure 19. All performance data were based on measurements in the proximity of the center of the exit cross section, and thus there was reasonable assurance that the performance measurements were free of effects from the sector endwalls.

The exhaust gas sampling probes were double-jacketed to provide steam heating of the sampling lines and water cooling of the probe housing. The sampling lines were steam-heated to maintain gas sample temperatures high enough to avoid condensation of hydrocarbons prior to analysis. An illustration of the sample probe construction is shown in Figure 20.

The sample line from each rake element was routed to a heated valve box containing manually-operated valves by which each element could be connected to the gas analyzers individually, or several elements could be manifolded together for analysis. The valves also permitted the sample lines to be shut off for total pressure measurement, or routed to the smoke measurement console.

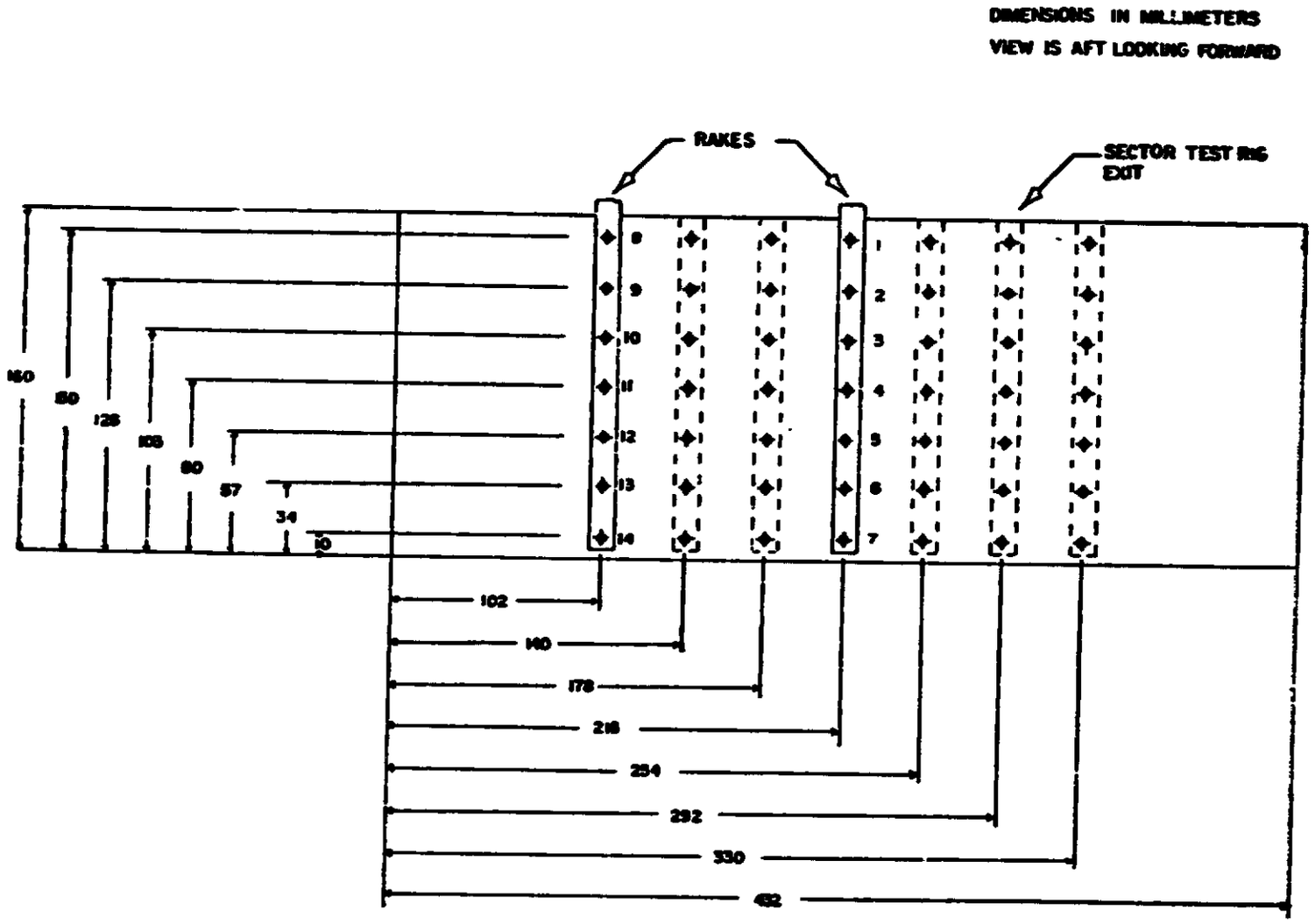

Figure 19. Exhaust Stream Gas Sample Element Locations.

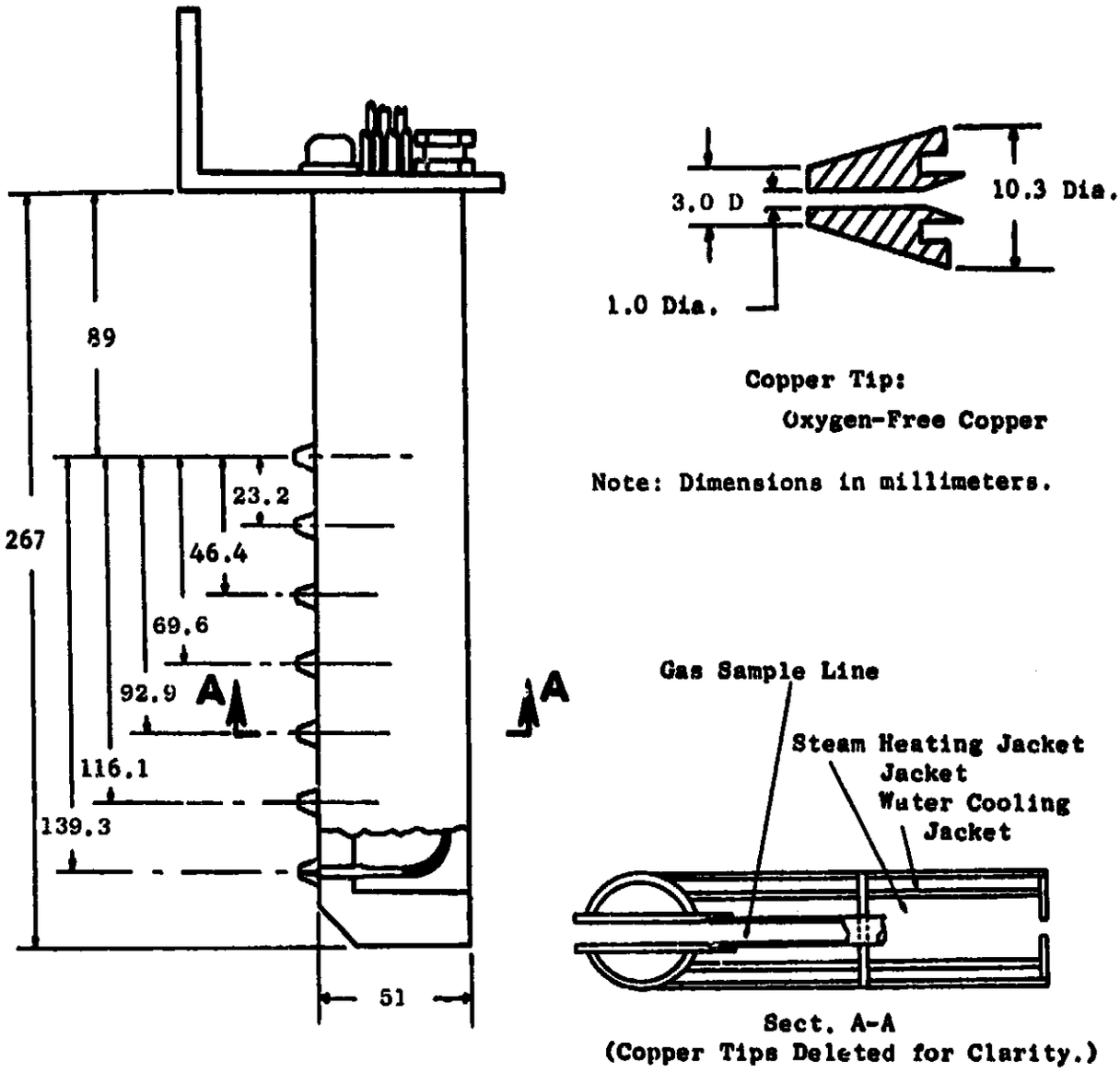

Figure 20. Duct Burner Exhaust Gas Sampling Rake.

The exhaust gas emissions data were obtained with an on-line gas analysis system. With this system, exhaust gas streams were continuously processed and the CO_2, CO, HC, smoke, NO, and NO_2 concentrations calculated. A flow diagram of the system is shown in Figure 21. The four basic instruments for measuring gaseous emissions concentrations in this on-line system were a flame ionization detector (FID) for measurements of the total HC concentrations, two nondispersive infrared (NDIR) analyzers for measurements of the CO and CO_2, and a heated chemiluminescence analyzer for measuring NO and NO_2.

The flame ionization detector was designed specifically for determining the total HC concentrations in gas turbine engine exhaust gases. It consisted of a heated inlet sample line, an ionization analyzer module, and an electrometer amplifier module.

The nondispersive infrared (NDIR) analyzers used a double-beam optical system to measure the differential absorption of infrared energy. An ice-bath water trap was installed upstream of the analyzers to provide dry samples for analysis. The two analyzers used had different reference absorption cells, one for CO reference and the other for CO_2 reference.

In the chemiluminescence analyzer, the NO in the sample gas was measured directly. The internal temperature of the analyzer flowpaths was controlled at about 328 K to prevent moisture condensation within the system. The measurement of the total NO_x concentration of the exhaust gas was accomplished by use of a thermal converter. This is a device that reduces NO_2 in the gas sample to NO and oxygen as a result of heating the sample to a prescribed temperature for a given period of time. When the sample leaving the converter is passed through the NO analyzer, a reading is obtained that is equal to the NO_x concentration (the sum of the newly-formed NO plus the NO present in the original stream).

None of the foregoing gas analyzers measured quantitatively without being calibrated. There is no electrical calibration signal that can be used to simulate an actual reading, such as millivolt simulation for temperature in the case of thermocouples. The standard General Electric analyzer calibration procedures were used throughout the program. These calibration procedures involved the use of calibration gases having nominal concentrations of CO, NO, NO_2 and propane in nitrogen and oxhgen mixtures which were obtained from an appropriate vendor. The vendor prepared the mixture of the gases by the use of partial pressures or gravimetrically and then analyzed the gas in the bottle. The precision of the calibration procedure was obtained by requiring the supplier to guarantee that all of the constituents in the bottle were within five percent of the nominal value specified and that the accuracy of the analyses met the following criteria:

Constituent Concentration Range	Analysis Accuracy
10 - 15%	± 2% Relative
50 ppm - 10%	± 3% Relative
10 ppm - 50 ppm	± 5% Relative

FOLDOUT FRAME 1.

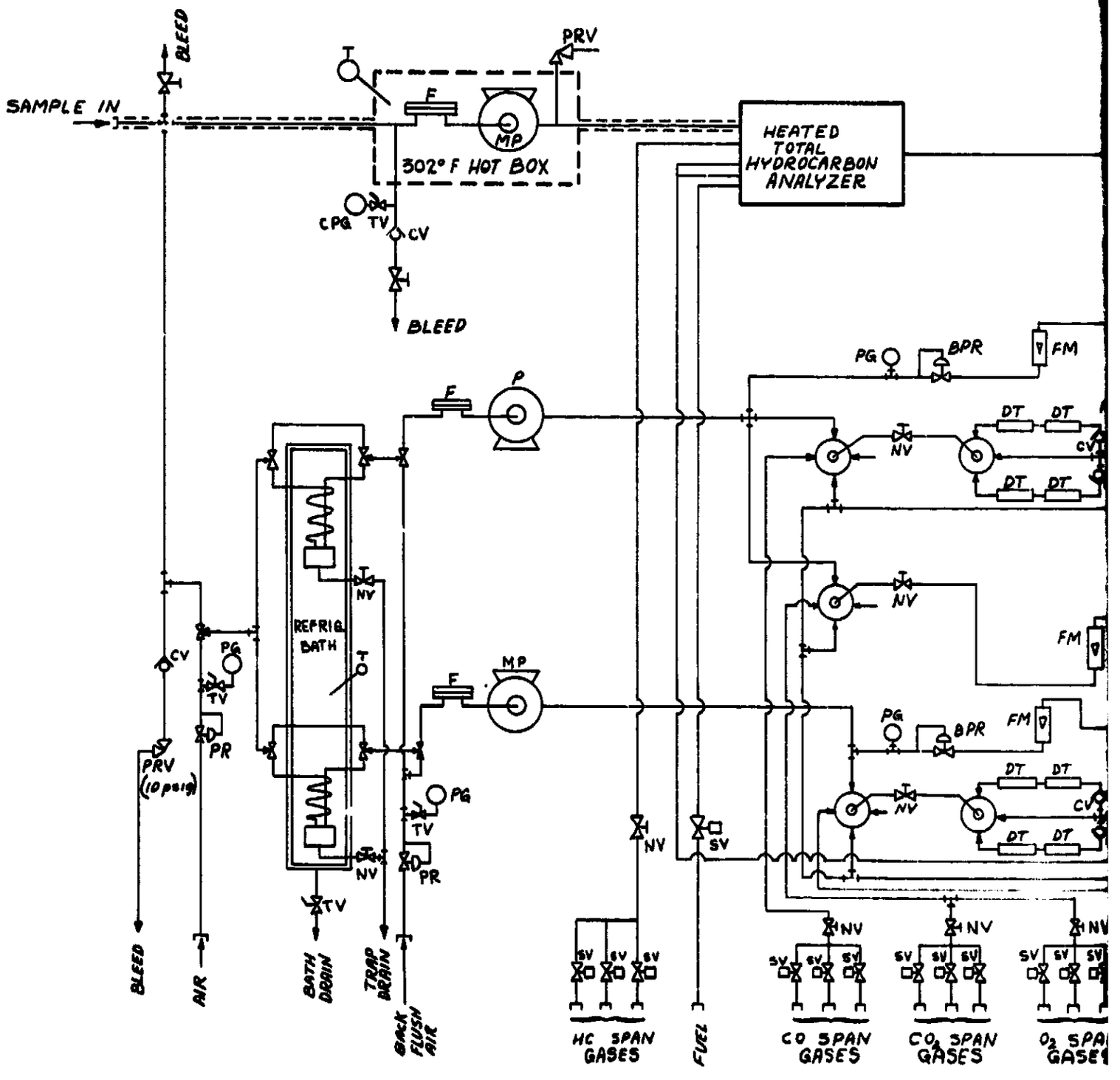

Figure 21. General Electric On-Line Exhaust Emission

FOLDOUT FRAME 2.

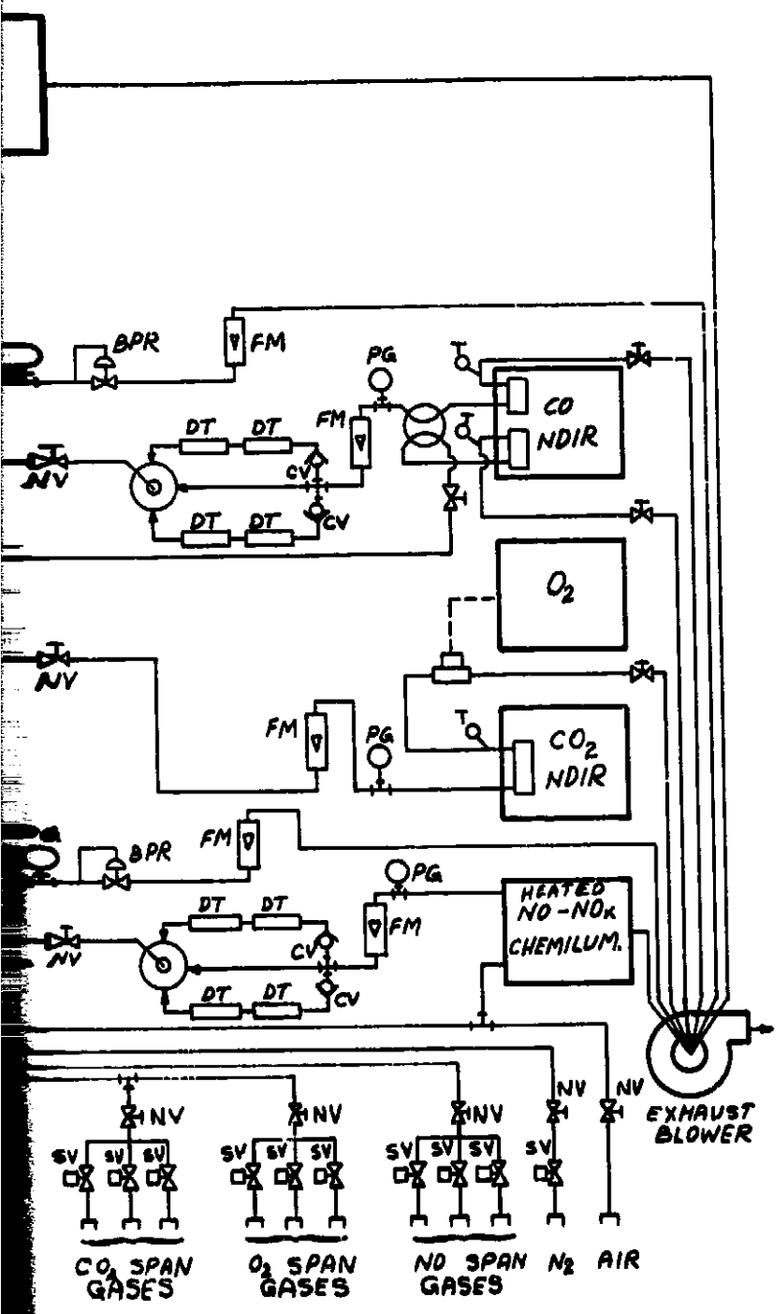

LEGEND

BPR	-	Back Pressure Regulator
CPG	-	Compound Pressure Gage
CV	-	Check Valve
DT	-	Dryer Tube
F	-	Filter
FM	-	Flowmeter
MP	-	High Temperature Metal Bellows Pump-Mounted in Inverted Position
NV	-	Needle Valve
P	-	Pump
PG	-	Pressure Gage
PR	-	Pressure Regulator
PRV	-	Pressure Relief Valve
SV	-	Solenoid Valve
T	-	Temperature Indicator
TV	-	Toggle Valve

ine Exhaust Emissions Measurement System Flow Diagram.

In addition, helium, argon, and other impurities were held to a minimum and were to be listed in the chemical analyses if over 10 ppm.

The zero on each NDIR instrument was set by using dry nitrogen which had been checked for the absence of H_2, CO, CO_2, and NO. All of the NDIR dual-cell instruments had three full-scale ranges per cell, which made a total of six scale ranges available. The CO_2 analyzer was a single-cell instrument having only three scale engine ranges available. The first range was the least sensitive, the second stage could be set up to three times the first range, and the third range could be set up to nine times the first range. The zero of the FID analyzer was set by using ultrapure breathing air.

Smoke emissions were measured using the standard General Electric filter stain method. With this method, a measured volume of sample gas is drawn through a filter paper. The smoke particulates filtered out of the sample gas leave a black stain on the white paper. The "blackness" of the spot is measured on a reflection densitometer. The densitometer is calibrated against absolute reflectance standards. Readings are converted to a sample flow flux of 0.0016 kg of exhaust gas per square cm of filter paper before computing to provide a smoke emission value in terms of SAE Smoke Number. The entire smoke measurement system is packaged into a portable console that also contains a pump, control valves, and flow metering devices. A flow diagram is shown in Figure 22. This smoke measurement technique is in conformance with SAE ARP 1179 (Reference 4).

Throughout this program, the combustor test data (except smoke emission data) were recorded by a digital data acquisition system. This apparatus scanned each of the measured parameters in sequence, controlling the position of pressure scanning valves when required, converted the amplified DC signal of the measurement to digital form, and recorded the value on a perforated paper tape suitable for input to a time-sharing computer through a teletype terminal. During each scan, the overall voltage accuracy was checked against a precision potentiometer that had been calibrated in the standards laboratory. The digital voltmeter and low level amplifier were of sufficient quality that voltages were accurate to 0.02 percent of full scale in the 0 to 10 millivolt range.

All connections between data sensors and readout instrumentation, and all programming of the sequencing and control circuitry, were accomplished through interchangeable program boards. The test setup included its own prewired, preprogrammed front panel for rapid changeover from one circuit configuration to the next. A schematic of the data acquisition installation setup is shown in Figure 23.

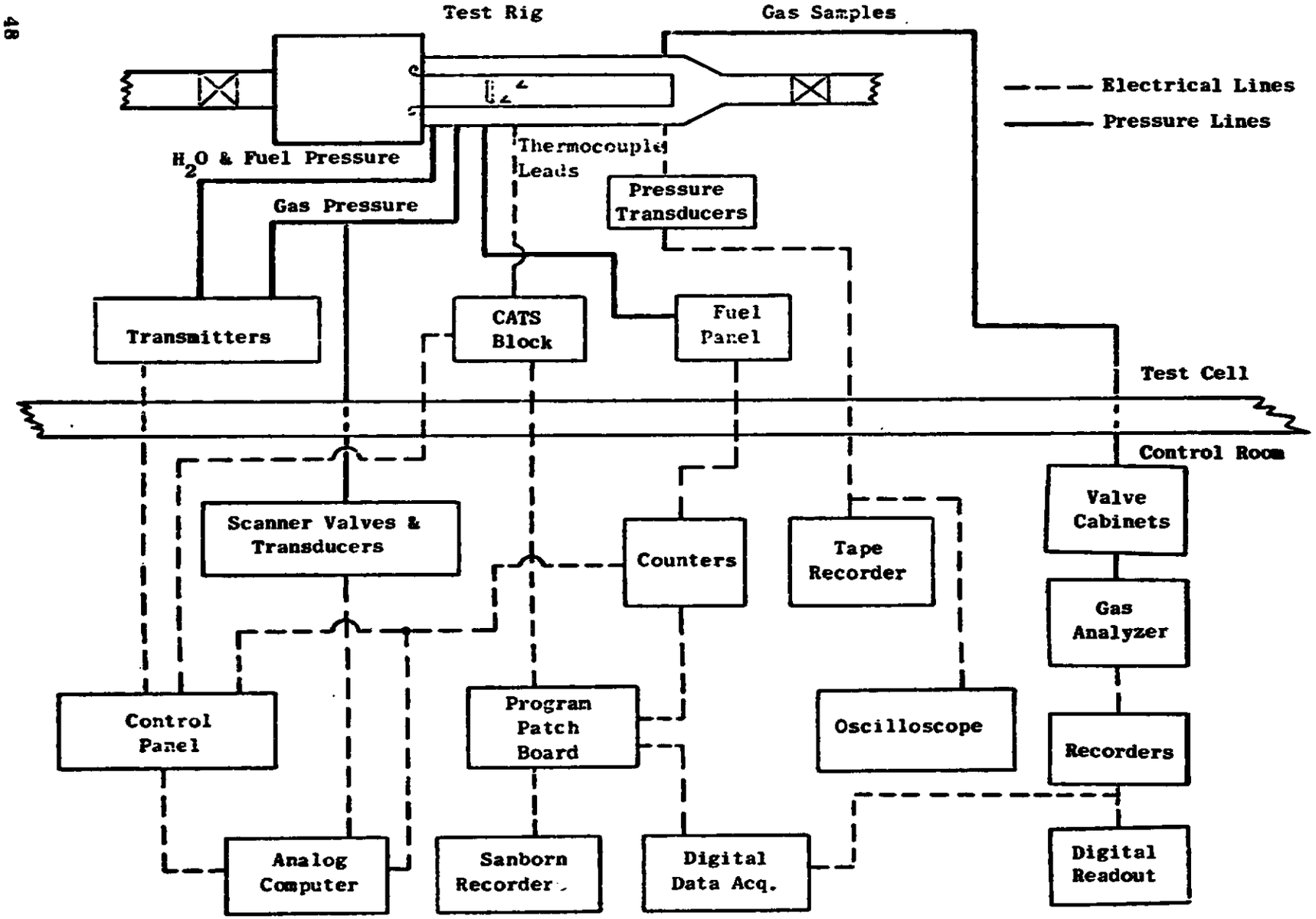

Figure 22. Test Cell Data Acquisition Schematic.

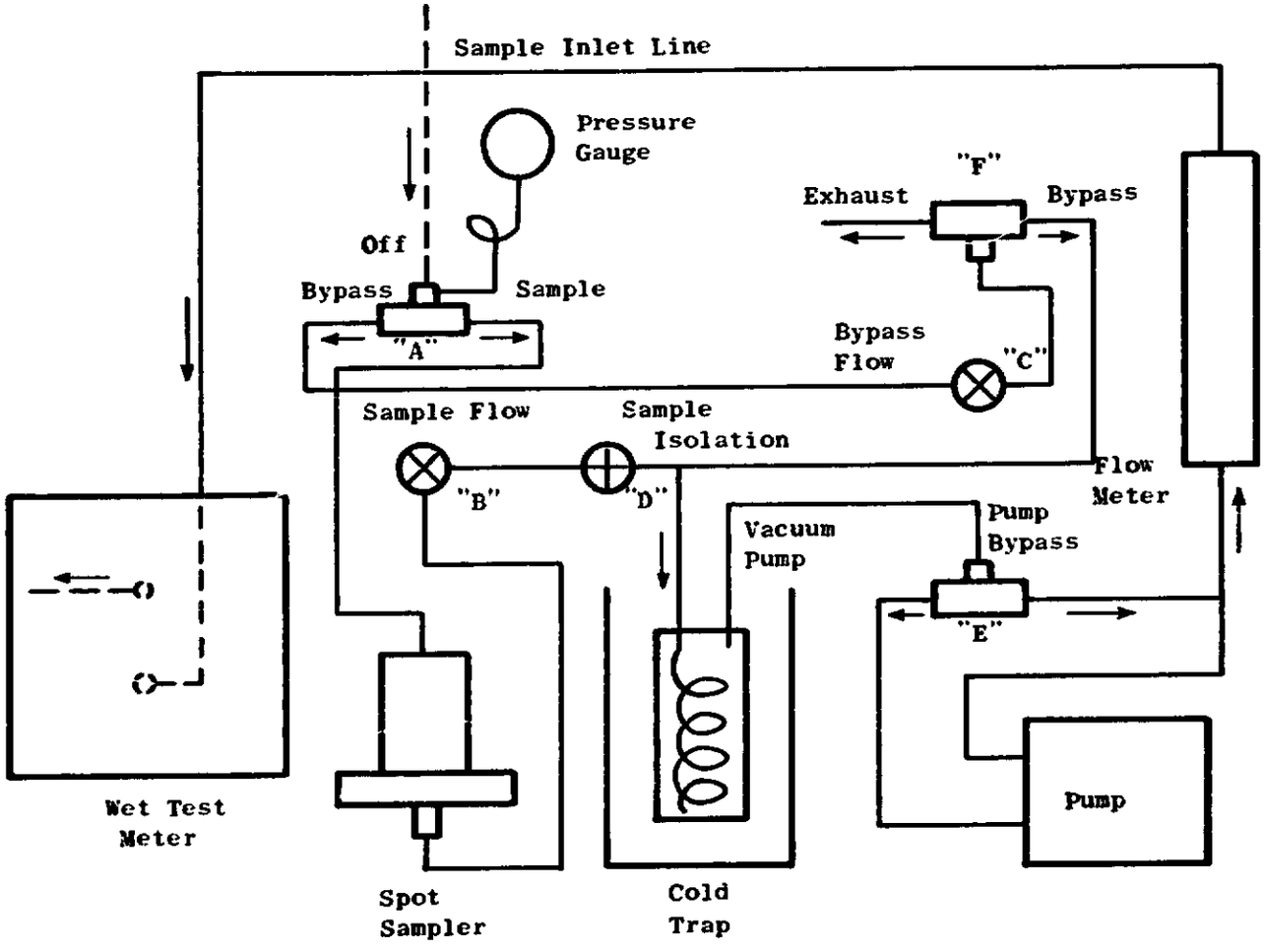

Figure 23. General Electric Smoke Measurement System Flow Diagram.

5.0 EXPERIMENTAL PROCEDURES

5.1 Test Methods

The methods described below are typical of those used in this program. Variations occurred from configuration to configuration as techniques were improved or test emphasis shifted. When these variations affected the test results, they are noted where the results are reported.

Preliminary procedures prior to each test included a "pressure check" in which the blast gate was closed and sufficient unheated air was admitted to the test rig to pressurize it. All pressure measurements were then recorded and examined. With little flow, the pressure throughout the test rig was known to be essentially uniform, so that any pressure measurement deviating from the others indicated an instrumentation error, which was corrected before proceeding.

In each test, the airflow, temperature, and pressure were established prior to introducing fuel to the test rig. The pilot fuel flow was always established and ignited before the main stage fuel was admitted. Changes in fuel flow required changes in blast gate position to maintain burner inlet pressure at specified values. When changing air conditions, the main stage fuel was usually turned off.

5.1.1 Ignition Tests

All duct burner ignition tests were performed at the air temperature and reference velocity of the "altitude relight" operating condition (Table III). Most tests were performed at a pressure slightly lower than the 142 kPa of the altitude relight condition to relieve the necessity of manipulating the blast gate when ignition occurred.

To conduct the test, the airflow and temperature were established with the blast gate open. Then the spark igniter was turned on and the pilot fuel flow increased slowly until ignition occurred. Ignition was detected by displaying pilot fuel flow, injection pressure drop, and several pilot liner surface temperatures as a function of time on a multichannel strip-chart recorder. Ignition appeared as an abrupt increase in liner temperature. When ignition occurred, the igniter was turned off, the fuel flow was held constant, and an instrument reading was taken with a manifolded gas sample as described below. This reading documented the fuel/air ratio and temperature rise at ignition.

5.1.2 Atmospheric Pressure Performance Tests

For some configurations, combustion performance and emissions were measured at air temperature and reference velocity corresponding to the supersonic cruise operating condition (Table III), but with the exhaust

system blast gate left open, so that the duct burner pressure was essentially atmospheric. The reasons for using this expedient test method were: test conditions could be established more rapidly, since the blast gate need not be adjusted when the exhaust gas temperature was changed; and resonance, when encountered, was not as destructive as at high pressure. Atmospheric test data were used to evaluate the relative effects of changes in burner fuel/air ratio and fuel staging on performance parameters, in order to select operating conditions for subsequent evaluation at full pressure.

The test condition was set by establishing air temperature and flow at predetermined values. The airflow was determined from an a priori estimate of the duct burner pressure drop. The pilot fuel flow was ignited and set at the desired value; then one or both of the main stage fuel flows were set, as required. The exhaust gas sampling rake was back-purged with air during adjustment of the test conditions to avoid loading the sample system with unburned fuel.

When all test flows were stabilized, the exhaust rake assembly was moved to a position where the left rake (aft looking forward) was 140 mm from the left sector endwall and the right rake was 254 mm from the wall, and all sample valves were turned off. All flows, temperatures, and pressures were then recorded, including the total pressure measured by the rakes, and the dynamic pressures. The gas sample valves were then manipulated to manifold all elements of one or both rakes together, and the resulting gas sample was directed through the analyzers. When the analyzers stabilized, the gas analysis parameters were recorded.

5.1.3 Full Pressure Performance Tests

Tests at full pressure were performed in a manner similar to that of the atmospheric pressure tests, except that the exhaust system blast gate was adjusted to provide the specified duct burner inlet total pressure. For some test points, gas samples were drawn from several or all of the rake elements simultaneously and manifolded together for a single analysis. For selected test points, the sample from each rake element was analyzed individually to provide information on the gas composition profiles in the exhaust stream. The rakes were traversed between analyses so that the sampled points formed a pattern across the exhaust stream. The sampling patterns are described below. In each case, the rake total pressure measurements were made before beginning the analysis, with the rakes in a single position.

For the points in which the samples were individually analyzed, a smoke sample was also drawn from all elements of one rake, manifolded, located 254 mm from the left endwall of the sector (aft looking forward).

5.1.4 Gas Sample Survey Patterns

The patterns in which individual and manifolded samples were drawn from the duct burner exhaust stream changed from time to time during the program as better test techniques evolved. The various patterns used are indicated schematically in Figure 24. The exact location of each sample element may be obtained from the rake stop diagram shown previously, Figure 19. The specific pattern used for each data reading is given in the test summary table in Section 6.0.

5.2 Emissions Data Reduction Procedure

The voltage responses of the CO, CO_2, HC, and NO_x analyzers were recorded at each traverse position of a test condition by the test cell digital data acquisition system. These data were then transmitted directly to an on-line data reduction computer for calculation of the exhaust emission concentrations, emission indices, combustion efficiency, and fuel/air ratio of the gas sample at each traverse position. The equations used for these calculations were basically those contained in ARP 1256 (Reference 5).

Before the various emission parameters were calculated, the concentrations of CO, CO_2, HC, and NO_x were determined from the gas sample measurements. The true concentrations of these constituents, however, were not necessarily those measured by the analyzers, due to the removal of some of the water from the various samples before analysis. Samples for the CO and CO_2 analyzers were measured "semi-dry"; that is, the sample was passed through a 273 K ice bath in which the water content of the sample was reduced to about 3.9 g water/kg air (or 0.00602 moles/mole). The samples for the HC and NO_x analyzers were measured "wet", with no water removed before analysis. A step-by-step discussion of the emissions calculation procedures used for all the data reduction is presented below.

At the beginning of each test, each of the four gas analyzers was calibrated over three overlapping concentration ranges, using gas mixtures of known composition. For each range of each instrument, the millivolt response of the instrument to a given concentration of its particular gas was characterized by a calibration equation, the coefficients of which were evaluated by a least-squares fit of the calibration data. During most of the program, the calibration equations were of the form:

$$\text{Concentration} = A_1 \times (\text{Millivolts} - A_0)^{A_2} \qquad (1a)$$

Twelve sets of values of the coefficients A_0, A_1, and A_2 were derived, representing three ranges for each of four instruments. Note that when $A_2 = 1$, this equation is linear. The responses of the CO and CO_2 analyzers, in particular, were nonlinear at high concentrations, so that appropriate values of $A_2 \neq 1$ were required to accurately represent the instrument calibrations. Part way through the program, an alternate calibration equation

Pattern 1

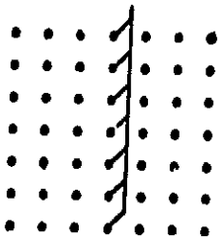

Pattern 2

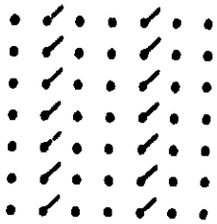

Pattern 3

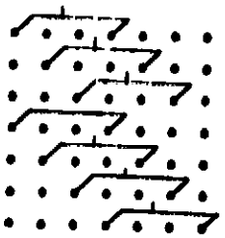

Pattern 4

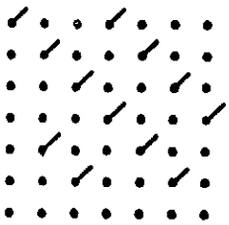

Pattern 5

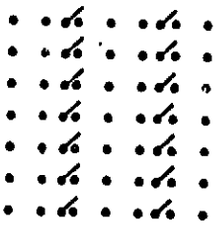

Pattern 6

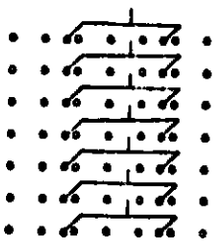

Pattern 7

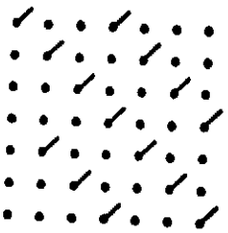

Pattern 8

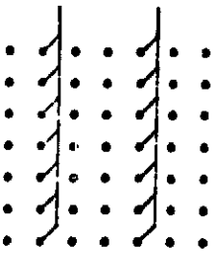

Pattern 9

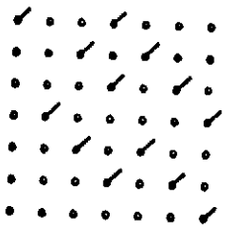

Pattern 10

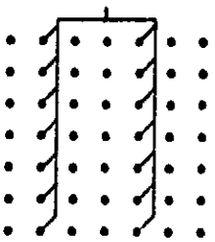

Pattern 11

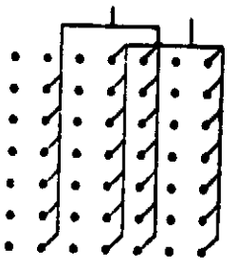

Pattern 12

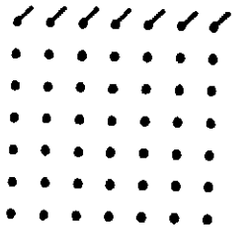

Pattern 13

Figure 24. Gas Sampling Survey Patterns.

was adopted, which could be fitted more closely to the calibration data for high concentrations of CO and CO_2. The alternate form of the calibration equation, used for Configurations 9, 11, and 12 was:

$$\text{Concentration} = \frac{\text{Millivolts} - A_0}{A_1 + A_2\ (\text{Millivolts} - A_0)} \qquad (1b)$$

Note that this equation is also linear when $A_2 = 0$, so that the change of calibration equations had little effect on lean mixtures with low contaminant levels.

The concentrations of CO and CO_2, calculated from Equations 1, were then corrected for the removal of water (both from the products of combustion and the inlet humidity) before the samples reached the various analyzers. To correct for the water removed, two parameters were defined:

$$K_d = \frac{100}{100 + \frac{1.00602n}{2}\left(\frac{CO}{10^4} + CO_2\right)} \qquad (2)$$

and

$$K_w = K_d \frac{200 - y\ (1 + n/2)}{200 - y + \frac{K_d\ yn}{2}\left(1 - \frac{1.00602\ CO}{10^6}\right)} \qquad (3)$$

where the CO and CO_2 concentrations are the measured (semi-dry) concentrations (PPM and percent, respectively), y represents the humidity content of the inlet air (percent by volume), and n is the fuel hydrogen-to-carbon atom ratio. Then,

$$(CO)_{wet} = 1.00602 \times Kw \times (CO)_{measured\ (semi\text{-}dry)} \qquad (4)$$

$$(CO_2)_{wet} = 1.00602 \times Kw \times (CO_2)_{measured\ (semi\text{-}dry)} \qquad (5)$$

$$(HC)_{wet} = (HC)_{measured} \qquad (6)$$

$$(NO_x)_{wet} = (NO_x)_{measured} \qquad (7)$$

Once all measured concentrations were converted to wet concentrations from Equations 4 through 7, the respective emission indices, sample fuel/air ratio, and combustion efficiency were calculated from the following equations (all concentrations refer to wet concentrations):

$$EI_{CO} = \frac{2.801\ (CO)}{(12.01 + 1.008\ n)\left(\frac{CO}{10^4} + CO_2 + \frac{HC}{10^4}\right)} \tag{8}$$

$$EI_{HC} = \frac{0.100\ (HC)}{\left(\frac{CO}{10^4} + CO_2 + \frac{HC}{10^4}\right)} \tag{9}$$

$$EI_{NO_x} = \frac{4.601\ (NO_x)}{(12.01 + 1.008\ n)\left(\frac{CO}{10^4} + CO_2 + \frac{HC}{10^4}\right)} \tag{10}$$

$$f_s = \left(\frac{12.01 + 1.008\ n}{28.966}\right)\left[\frac{\frac{CO}{10^4} + CO_2 + \frac{HC}{10^4}}{100 - \frac{CO}{10^4}\left(\frac{1}{2} + \frac{n}{4}\right) - CO_2\left(\frac{n}{4}\right)}\right] \tag{11}$$

$$\eta = \left(1 - 0.2334\ \frac{EI_{CO}}{10^3} - \frac{EI_{HC}}{10^3}\right) \times 100 \tag{12}$$

where the constant 0.2334 is the ratio of the heating value of CO to that of fuel.

Since JP-5 fuel was used throughout these tests, a typical value for n (fuel hydrogen-to-carbon atom ratio) of 1.92 was used.

These detailed equations (8 through 12) were used to calculate the emission indices, gas sample fuel/air ratio, and combustion efficiency at each sample location of a test condition. The overall average emission indices, sample fuel/air ratio, and combustion efficiency for the test condition was then determined by weighing the level determined at each traverse position, using the following equations:

$$f_{s_{avg}} = \frac{\sum_{i=1}^{J} f_{s_i}}{J} \tag{13}$$

$$EI_{X_{avg}} = \frac{\sum_{i=1}^{j} f_{s_i} \; EI_{X_i}}{\sum_{i=1}^{j} f_{s_i}} \qquad (14)$$

$$\eta_{avg} = (1 - .0002334\ EI_{CO,\ avg} - .001\ EI_{HC,\ avg}) \times 100 \qquad (15)$$

where the subscript i denotes the value of the quantity at each of the j traverse positions, and the subscript X is used to denote CO, HC, or NO_X. The quantities defined in Equations 13 through 15 were then designated as the average values for the specific test condition.

The average burner exit total pressure was similarly determined from values measured at each rake element:

$$P_{T_{avg}} = \frac{\sum_{i=1}^{j} P_{T_i}}{j} \qquad (16)$$

Burner inlet total pressure and temperature were measured by rakes located in the inlet duct. The individual pressure measurements were averaged by Equation 16 and the temperature measurements by:

$$T_{avg} = \frac{\sum_{i=1}^{j} T_i}{j} \qquad (17)$$

Reference velocity was computed as the one-dimensional velocity of the heated duct burner inlet airflow through the effective area of the empty test duct (0.0823 m^2).

The burner exit temperature was computed from inlet temperature and pressure, average fuel/air ratio, and combustion efficiency, using standard thermodynamic calculation procedures for dissociated combustion products.

5.3 Effects of Test Air Humidity on Measured NO_x Emissions

The test air humidity was measured on Reading 113 and all subsequent readings. On earlier readings, the dew point meter was not available, so the air was assumed to have a humidity of 3.57 g water per kg dry air.

The emissions for Reading 113 were calculated using both the measured and the assumed values of air humidity in the formula for including the water removed in the ice trap ahead of the CO and CO_2 analyzers (Equation 3). The assumed humidity produced a mean sample fuel/air ratio of 0.02259 and a NO_x emission index of 1.09, as reported in Table VIII. The measured humidity was 7.31 g/kg, which produced a mean sample fuel/air ratio of 0.02246 and a NO_x emission index of 1.10.

The test air humidity was, in general, different from the humidity of the air that the engine would ingest in flight. The humidity difference might be expected to influence the NO_x emission of the burner by reason of its influence on the rate of generation of NO_x in the flame. A correction is frequently applied to main combustor NO_x data to adjust the measured value to the value expected at standard takeoff humidity conditions (Reference 1):

$$(EI_{NO_x})_{Std} = (EI_{NO_x})_{Meas} \quad \exp\left(\frac{H - 6.29}{53.19}\right) \tag{18}$$

The highest measured humidity was that of Reading 113, 7.31 g/kg, which would have produced a correction factor of 1.019 by Equation 18. A similar correction derived for the dry air encountered at high altitude would have been 1.147 for this test air humidity level. The lowest test air humidity measured in subsequent tests was 0.59 g/kg, which would have produced a takeoff correction factor of 0.898. Since these corrections were not large, and since they could not be uniformly applied because the dew point meter was unavailable during the first part of the program, the data reported here have not been extrapolated to standard atmospheric humidity.

6.0 TEST RESULTS

A summary of the test program is presented in Table V. The information presented includes the data readings taken on each duct burner test configuration, the flight conditions simulated (see Table III), the types of measurements made, the exit survey pattern (from Figure 24) where applicable, and comments pertinent to interpretation of the data.

In the paragraphs that follow, the results of the emissions measurements for each configuration are presented along with a brief narration of the test events. Subsequently, the measured ignition characteristics, the measured exhaust smoke levels, and the fluid dynamic performance characteristics are presented.

6.1 Pollutant Emissions

Exhaust gas sampling for emissions determination was done by two different methods: point sample surveys and manifolded samples. In the point sample survey method, up to 14 gas samples were drawn from individual rake elements distributed across the stream, and the results of the individual sample analyses were averaged to determine overall performance. In the manifolded sample method, samples from some or all of the rake elements were analyzed together. The latter method was faster, as the number of gas analyses required for each reading was less; but the accuracy of the measurement is not regarded as highly, because the averaging across the exit stream profile was a function of the flow coefficients of individual sampling elements, which were not well controlled.

The overall emissions performance of all configurations, as measured by the point sample survey method, is presented in Tables VI, VII, and VIII for the sea level takeoff, transonic climb, and supersonic cruise flight conditions, respectively. In these tables, PT6 and TT6 are the total pressure and temperature measured by rakes located 60 mm from the duct inlet, as described previously. DP/P is (PT6-PT148)/PT6, where PT148 is the exit rake total pressure (1480 mm from the duct inlet). The "F/A UNDER LINER" values are the ratios of the indicated measured fuel flows to that part of the measured airflow exclusive of the main stage liner cooling air. The fraction of the total airflow by the main stage liners was estimated from the nominal effective flow area of the liners and the pressure drop measured for each configuration. The FTOT values are overall fuel/air ratios measured by the flowmeters (not including endwall liner air) and the gas sample analyses. TT148 was calculated from the sample analyses, as explained before.

A smoke sample was drawn from the duct burner exit survey rakes during each reading in which performance was measured by the point sample survey method, and these samples showed very low smoke emission levels for all configurations. Only two of the smoke samples indicated SAE smoke numbers

Table V. Test Summary.

Reading	Configuration	Simulated Flight Condition	Measurement Type	Survey Pattern	Comments
			Test Run 1		May 17, 1976
2	1	TS Climb	Dry Rdg.	---	
3	1	Alt. Relight	Dry Rdg.	---	
4	1	Alt. Relight	Ignition	1	Ignition fuel flow
5	1	Alt. Relight	Pressure Perf.	1	Nominal fuel flow
6	1	TS Climb	Pressure Perf.	1	
7	1	TS Climb	Pressure Perf.	2	Verification
8	1	TS Climb	Pressure Perf.	1	Lower secondary spraybar plugging evident
9	1	TS Climb	Pressure Perf.	1	
10	1	TS Climb	Pressure Perf.	3	Rake damage found after test
			Test Run 2		May 27, 1976
11	1	SLTO	Dry Rdg.	---	
12	1	SLTO	Pressure Perf.	---	Pilot only - no samples taken
13	1	SLTO	Pressure Perf.	4	Reduced pressure and flow forced by pilot nozzle plugging
14	1	SLTO	Pressure Perf.	5	Lower secondary spray bar plugging evident
15	1	SS Cruise	Pressure Perf.	6	Rake traverse mechanism jammed
16	1	SS Cruise	Pressure Perf.	6	
17	1	SS Cruise	Pressure Perf.	7	Resonance damage found after test
			Test Run 3		June 17, 1976
18	2	Alt. Relight	Dry Rdg.	---	
19	2	Alt. Relight	Ignition	4	
20	2	SLTO	Pressure Perf.	4	
21	2	SLTO	Pressure Perf.	8	Audible resonance. Severe damage found after test.
22	2	Alt. Relight	Dry Rdg.	---	Posttest dry reading
			Test Run 4		July 22, 1976
23	3	SLTO	Open-End	---	
24	3	SLTO	Open-End	---	Slight resonance. Minimum stable pilot fuel. No fire in upper system
25	3	SLTO	Open-End	---	Loud resonance
26	3	SLTO	Open-End	---	Loud resonance
27	3	SLTO	Open-End	---	Moderately noisy
28	3	SLTO	Open-End	---	
			Test Run 5		July 23, 1976
29	4	SLTO	Open-End	---	
30	4	SLTO	Open-End	---	Quiet rumble. Flickering yellow flame in main stage. No fire in upper flameholders
31	4	SLTO	Open-End	---	Moderately loud resonance. Long yellow flames, fire spreads to top at exit
32	4	SLTO	Open-End	---	Moderately quiet resonance
33	4	SLTO	Open-End	---	Loud resonance
34	4	SLTO	Open-End	---	Intermittent resonance

Table V. Test Summary (Continued).

Reading	Configuration	Simulated Flight Condition	Measurement Type	Survey Pattern	Comments
			Test Run 6		July 29, 1976
35	4	Alt. Relight	Dry Rdg.	---	
36	4	Alt. Relight	Dry Rdg.	---	P_{T148} void. Rake purge air on
37	4	Alt. Relight	Ignition	9	
38	4	SLTO	Dry Rdg.	---	
40	4	SLTO	Atmospheric Perf.	9	Incomplete - burner blew out
41	4	SLTO	Atmospheric Perf.	---	Unstable - no samples. Low frequency chugging
42	4	SS Cruise	Dry Rdg.	---	
43	4	SS Cruise	Atmospheric Perf.	9	HC measurement invalid. Analyzer loaded
44	4	SS Cruise	Atmospheric Perf.	9	HC measurement invalid. Analyzer loaded
45	4	SS Cruise	Atmospheric Perf.	9	
46	4	SS Cruise	Atmospheric Perf.	9	
47	4	SS Cruise	Atmospheric Perf.	9	
48	4	SS Cruise	Atmospheric Perf.	9	
49	4	SS Cruise	Atmospheric Perf.	---	Audible resonance - no samples taken
50	4	SS Cruise	Atmospheric Perf.	9	
51	4	SS Cruise	Atmospheric Perf.	9	Intermittent audible resonance
52	4	SS Cruise	Pressure Perf.	9	
53	4	SS Cruise	Pressure Perf.	8	
54	4	SLTO	Pressure Perf.	8	
			Test Run 7		August 6, 1976
55	5	SS Cruise	Dry Rdg.	---	
57	5	SS Cruise	Atmospheric Perf.	9	
58	5	SS Cruise	Atmospheric Perf.	9	
59	5	SS Cruise	Atmospheric Perf.	9	
60	5	SS Cruise	Atmospheric Perf.	9	Spraybar air off
61	5	SS Cruise	Atmospheric Perf.	9	Spraybar air on
62	5	SS Cruise	Atmospheric Perf.	9	Spraybar air on
63	5	SS Cruise	Atmospheric Perf.	9	Spraybar air off
64	5	SS Cruise	Atmospheric Perf.	9	Spraybar air on
65	5	SS Cruise	Atmospheric Perf.	9	Spraybar air on
66	5	SS Cruise	Atmospheric Perf.	9	Spraybar air on
67	5	SS Cruise	Atmospheric Perf.	9	Spraybar air on
68	5	SS Cruise	Atmospheric Perf.	9	Spraybar air on
69	5	SS Cruise	Atmospheric Perf.	9	Spraybar air on
70	5	SS Cruise	Atmospheric Perf.	9	Spraybar air on
71	5	SS Cruise	Pressure Perf.	8	Spraybar air on
72	5	SS Cruise	Pressure Perf.	8	Spraybar air on
73	5	SS Cruise	Pressure Perf.	8	Spraybar air on
74	5	SLTO	Pressure Perf.	8	Spraybar air on. Resonance damage to pilot found after test

Table V. Test Summary (Continued).

Reading	Configuration	Simulated Flight Condition	Measurement Type	Survey Pattern	Comments
			Test Run 8		September 23, 1976
75	6	SLTO	Open-End	---	Only one cup lit
76	6	SLTO	Open-End	---	All cups lit, but center cup unstable
77	6	SLTO	Open-End	---	
78	6	SLTO	Open-End	---	No visible burning in main stage
79	6	SLTO	Open-End	---	Flickering flame in main stage
80	6	SLTO	Open-End	---	Good flame but loud
81	6	SLTO	Open-End	---	Good flame, intermittent noise
82	6	SLTO	Open-End	---	Good flame, steady loud noise
83	6	SLTO	Open-End	---	
			Test Run 9		September 23, 1976
84	8	SLTO	Open-End	---	No visible flame in main stage
85	8	SLTO	Open-End	---	Main stage lit. Pilot fuel increased to reduce noise
86	8	SLTO	Open-End	---	Burning quietly. Less pilot fuel extinguishes main stage
87	8	SLTO	Open-End	---	
88	8	SLTO	Open-End	---	Pilot fuel increased to reduce noise
89	8	SLTO	Open-End	---	Good flame. Quiet
90	8	SLTO	Open-End	---	
			Test Run 10		September 24, 1976
91	6	Alt. Relight	Ignition	9	
92	6	SS Cruise	Dry Rdg.	---	
93	6	SS Cruise	Atmospheric Perf.	9	
94	6	SS Cruise	Atmospheric Perf.	9	
95	6	SS Cruise	Atmospheric Perf.	9	
96	6	SS Cruise	Atmospheric Perf.	9	
97	6	SS Cruise	Atmospheric Perf.	9	
98	6	SS Cruise	Atmospheric Perf.	9	Occasional audible resonance
99	6	SS Cruise	Atmospheric Perf.	9	
100	6	SS Cruise	Atmospheric Perf.	9	
101	6	SS Cruise	Atmospheric Perf.	9	
102	6	SS Cruise	Atmospheric Perf.	9	
103	6	SS Cruise	Dry Rdg.	---	
104	6	SS Cruise	Pressure Perf.	9	
105	6	SS Cruise	Pressure Perf.	8	NO_x measurements questionable - leaking sample pump
106	6	SS Cruise	Pressure Perf.	8	
107	6	SS Cruise	Pressure Perf.	10	
108	6	SS Cruise			
			Test Run 11		September 24, 1976
109	8	SS Cruise	Atmospheric Perf.	9	
110	8	SS Cruise	Atmospheric Perf.	9	
111	8	SS Cruise	Pressure Perf.	8	
112	8	SS Cruise	Pressure Perf.	8	
113	8	SS Cruise	Pressure Perf.	8	

Table V. Test Summary (Continued).

Reading	Configuration	Simulated Flight Condition	Measurement Type	Survey Pattern	Comments
			Test Run 12		November 3, 1976
115	7	Alt. Relight	Ignition	11	
116	7	SS Cruise	Dry Rdg.	---	
117	7	SS Cruise	Pressure Perf.	11	
118	7	SS Cruise	Pressure Perf.	11	
119	7	SS Cruise	Pressure Perf.	11	
120	7	SS Cruise	Pressure Perf.	11	
121	7	SS Cruise	Pressure Perf.	11	
122	7	SS Cruise	Pressure Perf.	11	
123	7	SS Cruise	Pressure Perf.	8	
124	7	SS Cruise	Pressure Perf.	11	
125	7	SS Cruise	Pressure Perf.	11	
126	7	SS Cruise	Pressure Perf.	11	
127	7	SS Cruise	Pressure Perf.	8	
			Test Run 13		November 3, 1976
128	10	SS Cruise	Pressure Perf.	11	
129	10	SS Cruise	Pressure Perf.	11	
130	10	SS Cruise	Pressure Perf.	8	
131	10	SS Cruise	Pressure Perf.	11	
132	10	SS Cruise	Pressure Perf.	11	
134	10	SS Cruise	Pressure Perf.	11	
135	10	SS Cruise	Pressure Perf.	11	
136	10	SS Cruise	Pressure Perf.	11	
137	10	SS Cruise	Pressure Perf.	8	
138	7	SS Cruise	Pressure Perf.	11	Lower reference velocity
139	7	SS Cruise	Pressure Perf.	11	Lower reference velocity
140	7	SS Cruise	Pressure Perf.	11	Lower reference velocity
141	7	SS Cruise	Pressure Perf.	11	Lower reference velocity
142	7	SS Cruise	Pressure Perf.	11	Lower reference velocity
143	7	SS Cruise	Pressure Perf.	11	Lower reference velocity
144	7	SS Cruise	Pressure Perf.	11	Higher reference velocity
145	7	SS Cruise	Pressure Perf.	11	Higher reference velocity
146	10	SS Cruise	Pressure Perf.	12	Higher reference velocity
			Test Run 14		November 8, 1976
148	10	TS Climb	Pressure Perf.	11	
149	10	TS Climb	Pressure Perf.	11	HC analyzer off scale
150	10	TS Climb	Pressure Perf.	11	HC analyzer off scale
151	10	TS Climb	Pressure Perf.	11	
152	10	TS Climb	Pressure Perf.	11	
153	10	TS Climb	Pressure Perf.	11	
154	10	TS Climb	Pressure Perf.	8	
155	10	SLTO	Dry Rdg.	---	
156	10	SLTO	Pressure Perf.	11	
157	10	SLTO	Pressure Perf.	8	Survey with pilot fuel only
158	10	SLTO	Pressure Perf.	11	
159	10	SLTO	Pressure Perf.	11	

Table V. Test Summary (Continued).

Reading	Configuration	Simulated Flight Condition	Measurement Type	Survey Pattern	Comments
			Test Run 14 (Continued)		
[illegible]	10	SLTO	Pressure Perf.	11	Resonance prohibits higher fuel flows
[illegible]	10	SLTO	Pressure Perf.	11	
[illegible]	10	SLTO	Pressure Perf.	8	Lower reference velocity
[illegible]	10	SLTO	Pressure Perf.	11	Lower reference velocity. Resonance at higher fuel flows
[illegible]	10	SLTO	Pressure Perf.	11	Lower reference velocity
[illegible]	10	SLTO	Pressure Perf.	13	
			Test Run 15		November 11, 1976
[illegible]	9	SS Cruise	Pressure Perf.	11	
[illegible]	9	SS Cruise	Pressure Perf.	8	
[illegible]	9	SS Cruise	Pressure Perf.	11	
[illegible]	9	SS Cruise	Pressure Perf.	8	
[illegible]	9	SS Cruise	Pressure Perf.	11	
[illegible]	9	SS Cruise	Pressure Perf.	11	
[illegible]	9	SS Cruise	Pressure Perf.	11	
[illegible]	9	SS Cruise	Pressure Perf.	8	
[illegible]	9	SS Cruise	Pressure Perf.	11	
			Test Run 16		January 24-25, 1977
[illegible]	11	SS Cruise	Dry Rdg.	---	
[illegible]	11	SS Cruise	Pressure Perf.	11	
[illegible]	11	SS Cruise	Pressure Perf.	11	
[illegible]	11	SS Cruise	Pressure Perf.	11	
[illegible]	11	SS Cruise	Pressure Perf.	11	
[illegible]	11	SS Cruise	Pressure Perf.	11	
[illegible]	11	SS Cruise	Pressure Perf.	11	
[illegible]	11	SS Cruise	Pressure Perf.	11	
[illegible]	11	SS Cruise	Pressure Perf.	11	
[illegible]	11	SS Cruise	Pressure Perf.	11	
[illegible]	11	SS Cruise	Pressure Perf.	8	CO analyzer off scale on elements 2 and 9
[illegible]	11	SS Cruise	Pressure Perf.	11	HC analyzer off scale
[illegible]	11	SS Cruise	Pressure Perf.	11	Resonance prohibits higher fuel flows
[illegible]	11	SS Cruise	Pressure Perf.	11	Lower reference velocity
[illegible]	11	SS Cruise	Pressure Perf.	11	Lower reference velocity
[illegible]	11	SS Cruise	Pressure Perf.	11	Higher reference velocity
[illegible]	11	SS Cruise	Pressure Perf.	11	Higher reference velocity
[illegible]	11	TS Climb	Dry Rdg.	---	
[illegible]	11	TS Climb	Pressure Perf.	11	
[illegible]	11	TS Climb	Pressure Perf.	11	HC analyzer off scale
[illegible]	11	TS Climb	Pressure Perf.	11	HC analyzer off scale
[illegible]	11	TS Climb	Pressure Perf.	11	HC analyzer off scale
[illegible]	11	TS Climb	Pressure Perf.	8	
[illegible]	11	TS Climb	Dry Rdg.	---	
[illegible]	11	SLTO	Pressure Perf.	11	

Table V. Test Summary (Concluded).

Reading	Configuration	Simulated Flight Condition	Measurement Type	Survey Pattern	Comments
			Test Run 16 (Continued)		
[illegible]	11	SLTO	Pressure Perf.	11	HC analyzer off scale
[illegible]	11	SLTO	Pressure Perf.	11	
[illegible]	11	Alt. Relight	Dry Rdg.	---	
[illegible]	11	Alt. Relight	Ignition	---	Fabric ashes caked on upper spraybars after test
			Test Run 17		February 25, 1977
[illegible]	12	SS Cruise	Dry Rdg.	---	
[illegible]	12	SS Cruise	Pressure Perf.	11	
[illegible]	12	SS Cruise	Pressure Perf.	8	
[illegible]	12	SS Cruise	Pressure Perf.	11	
[illegible]	12	SS Cruise	Pressure Perf.	11	
[illegible]	12	SS Cruise	Pressure Perf.	11	
[illegible]	12	SS Cruise	Pressure Perf.	11	
[illegible]	12	SS Cruise	Pressure Perf.	11	HC analyzer off scale
[illegible]	12	SS Cruise	Pressure Perf.	11	
[illegible]	12	SS Cruise	Pressure Perf.	8	HC analyzer off scale on elements 2, 4, and 8. Parts of splitter plate and lower flameholder burned away after test

Table VI. Data Summary, Point Sample Surveys at Full Pressure, Sea Level Takeoff Operating Condition.

CON FIG	POG	PT6 KPA	TT6 K	V REF M/S	DP/P	F/A UNDER LINER PILOT	UPPER	LOWER	TOTAL	FTOT MET	FTOT SAMP	ETA PCT	TT148 K	EI, G/KG FUEL CO	HC	NOX
1	14	309.	455.	41.96	0.0661	0.0033	0.0237	0.0246	0.0520	0.0430	0.0507	97.36	1839.	110.14	0.66	2.70
2	21	303.	454.	41.64	0.0635	0.0032	0.	0.0453	0.0486	0.0402	0.0439	99.12	1786.	35.79	0.40	3.61
4	54	296.	455.	39.97	0.0544	0.0038	0.0159	0.0168	0.0374	0.0311	0.0345	87.93	1420.	130.87	90.16	4.43
6	74	385.	482.	44.70	0.0539	0.0044	0.0153	0.0162	0.0368	0.0304	0.0339	86.98	1412.	147.50	95.73	4.58
10	157	385.	455.	41.47	0.0797	0.0049	0.	0.	0.0049	0.0038	0.0041	98.74	608.	37.14	3.91	3.71
10	162	394.	456.	41.64	0.0999	0.0049	0.0177	0.0177	0.0403	0.0314	0.0370	97.59	1526.	24.20	18.48	1.06

Table VII. Data Summary, Point Sample Surveys at Full Pressure, Transonic Climb Operating Condition.

CON FIG	POG	PT6 KPA	TT6 K	V REF M/S	DP/P	F/A UNDER LINER PILOT	UPPER	LOWER	TOTAL	FTOT MET	FTOT SAMP	ETA PCT	TT148 K	EI, G/KG FUEL CO	HC	NOX
1	10	213.	443.	40.56	0.0648	0.0035	0.0231	0.0244	0.0522	0.0432	0.0423	95.62	1812.	173.35	3.32	2.88
10	154	211.	442.	41.47	0.1087	0.0047	0.0194	0.0193	0.0435	0.0339	0.0267	97.46	1587.	33.07	17.68	1.18
11	200	210.	445.	41.29	0.0503	0.0050	0.0173	0.0174	0.0396	0.0335	0.0346	89.12	1488.	123.02	80.10	1.08

Table VIII. Data Summary, Point Sample Surveys at Full Pressure, Supersonic Cruise Operating Condition.

CON FIG	PDG	PT6 KPA	TT6 K	V REF M/S	DP/P	F/A UNDER LINER PILOT	UPPER	LOWER	TOTAL	FTOT MFI	FTOT SAMP	ETA PCT	TT148 K	EI, G/KG FUEL CO	HC	NOX
1	15	262.	593.	48.47	0.0481	0.0034	0.0163	0.	0.0201	0.0166	0.0204	94.00	1164.	55.99	46.69	3.42
1	16	260.	593.	48.54	0.0473	0.0041	0.0154	0.	0.0197	0.0163	0.0195	96.23	1169.	50.00	26.07	2.85
4	53	265.	592.	46.41	0.0445	0.0038	0.	0.0162	0.0200	0.0166	0.0222	95.83	1172.	37.70	32.91	2.59
5	71	268.	598.	46.07	0.0448	0.0039	0.	0.0164	0.0202	0.0167	0.0212	91.84	1158.	52.96	69.24	3.53
5	72	264.	596.	47.11	0.0448	0.0044	0.	0.0157	0.0201	0.0166	0.0221	95.30	1174.	40.25	37.61	2.51
5	73	264.	598.	47.77	0.0474	0.0044	0.	0.0211	0.0256	0.0210	0.0268	97.78	1330.	39.96	12.85	4.83
6	107	261.	586.	47.01	0.0909	0.0055	0.0214	0.	0.0268	0.0209	0.0271	97.72	1313.	32.08	15.34	4.47
6	109	259.	585.	47.08	0.0902	0.0055	0.0158	0.	0.0212	0.0165	0.0201	96.47	1167.	37.85	27.68	1.83
7	123	261.	593.	47.50	0.0901	0.0049	0.	0.0162	0.0209	0.0163	0.0185	93.61	1155.	70.74	47.41	1.30
7	127	261.	592.	46.96	0.0900	0.0050	0.	0.0188	0.0238	0.0185	0.0191	96.37	1238.	52.91	23.90	2.12
8	111	260.	590.	47.46	0.0915	0.0055	0.0158	0.	0.0211	0.0164	0.0241	97.40	1176.	31.40	18.64	1.67
8	112	258.	594.	48.23	0.0938	0.0055	0.	0.0177	0.0231	0.0180	0.0228	96.81	1726.	39.34	22.76	1.39
8	113	254.	593.	47.69	0.0918	0.0049	0.	0.0188	0.0236	0.0184	0.0226	96.30	1234.	42.23	27.12	1.09
9	169	268.	592.	46.34	0.0810	0.0050	0.	0.0164	0.0212	0.0165	0.0134	92.46	1153.	70.88	58.81	1.40
9	171	267.	592.	46.39	0.0836	0.0050	0.	0.0186	0.0235	0.0183	0.0145	95.16	1225.	54.49	35.67	1.66
9	175	265.	592.	46.28	0.0875	0.0049	0.0153	0.0153	0.0352	0.0274	0.0228	98.12	1522.	19.24	14.51	1.46
10	130	260.	593.	47.07	0.0904	0.0050	0.0164	0.	0.0212	0.0165	0.0155	90.32	1140.	79.37	78.24	1.45
10	137	261.	593.	47.19	0.0924	0.0050	0.0138	0.0136	0.0324	0.0252	0.0202	97.12	1450.	24.22	23.12	1.19
11	199	259.	591.	48.55	0.0388	0.0050	0.	0.0149	0.0195	0.0165	0.0251	98.44	1130.	27.90	9.13	2.47
12	209	262.	591.	46.94	0.0454	0.0051	0.	0.0152	0.0203	0.0172	0.0219	97.78	1204.	26.91	15.95	2.31
12	216	261.	591.	47.10	0.0527	0.0051	0.0154	0.0151	0.0356	0.0301	0.0322	93.15	1551.	67.59	52.73	1.04

greater than 1.0. One of these was Reading 21, Configuration 2, tested at the sea level takeoff operating condition. The measured smoke number was 6.9. The other sample was Reading 74, Configuration 5, again at sea level takeoff. The smoke number was 5.7. Both of these values were well below the goal of 15.

6.1.1 Configuration 1

Configuration 1, being the first tested, endured more than its share of experimental difficulties. Rake damage was discovered after Reading 10. The two lower sampling tips on one rake and the three lower tips on the other were burned away, and three other tips were damaged. This water-cooled rake, which had been used in previous test programs, did not show any deficiencies in its pretest checkout. The rake was repaired and survived the remainder of the program undamaged. The fuel pressure in the lower main stage spraybars was abnormally high during all tests of Configuration 1. Visual checks indicated one or two spraybars not flowing, located in the corners of the sector. The problem was subsequently traced to a tight fit of in-line strainers used in the manifold pigtails, and was corrected by the use of tubing with thinner walls.

Pilot fuel nozzle clogging was also experienced. The test facility fuel system was unable to supply enough flow for full simulation of the sea level takeoff condition, so these points were tested with proportionally reduced air flow and pressure.

The rake actuation mechanisms failed during Reading 14. Readings 15 and 16 were taken with the rake fixed in one position.

Inspection after Reading 17 revealed substantial damage to the test configuration, presumably due to resonance. The flameholder gap springs were flattened, cracked, and nibbled. Half the lower spring was torn away and recovered from the test rig exhaust section. It appeared to have held flame awhile, then impacted a rake or quench bar. The lower main stage liner was distorted in the center near the flameholder. The center pilot fuel nozzle was missing its air shroud. The pilot burner was ripped along the cooling air metering holes of the second panel, upper and lower.

Emissions measurements made by the point sample survey method were shown previously in Tables VI through VIII. Measurements made with manifold samples are presented in Table IX. Data from this table, representing the transonic climb flight condition, are plotted in Figure 25. Only combustion efficiency is plotted rather than CO and HC emission indices. Efficiency is related to CO and HC by Equation 15. At this condition, the pilot efficiency was near 99%, and the pilot NO_x was less than 2 g/kg fuel. With the main stage operating near the estimated operating fuel/air ratio, efficiency fell to 94 or 95%, and NO_x increased to near 3 g/kg. At the sea level takeoff and supersonic cruise operating conditions, only isolated data points were taken.

Table IX. Data Summary, Configuration 1, Performance Measured from Manifolded Gas Samples.

RDG	PT6 KPA	TT6 K	V REF M/S	DP/P	F/A UNDER LINER PILOT	UPPER	LOWER	TOTAL	FTOT MET	FTOT SAMP	ETA PCT	TT4B K	EI, G/KG CO	HC	FUEL NOX
2	210.	444.	46.82	0.0410	0.	0.	0.	0.	0.			444.			
3	143.	365.	38.09	0.0409	0.	0.	0.	0.	0.			366.			
4	145.	360.	37.34	0.0442	0.0060	0.	0.	0.0060	0.0050	0.0065	98.08	366.	49.45	7.63	3.32
5	143.	368.	38.21	0.0408	0.0046	0.	0.	0.0046	0.0038	0.0047	97.68	523.	55.74	10.23	1.18
6	212.	438.	40.51	0.0397	0.0034	0.	0.	0.0034	0.0028	0.0034	98.90	552.	29.04	4.25	1.27
8	211.	444.	41.21	0.0619	0.0034	0.0186	0.0196	0.0425	0.0352	0.0444	94.69	1591.	150.20	18.22	2.91
9	213.	444.	40.55	0.0649	0.0034	0.0233	0.0256	0.0523	0.0433	0.0556	94.16	1797.	239.58	2.51	2.57
11	387.	451.	41.53	0.0358	0.	0.	0.	0.	0.			451.			
12	387.	432.	39.79		0.0035	0.	0.	0.0031	0.0026						
13	329.	455.	42.01	0.0593	0.0034	0.0185	0.0196	0.0421	0.0348	0.0413	97.25	1620.	53.59	14.97	3.31
17	261.	592.	48.52	0.0406	0.0038	0.	0.	0.0033	0.0027	0.0027	68.84	667.	64.96	295.45	6.35

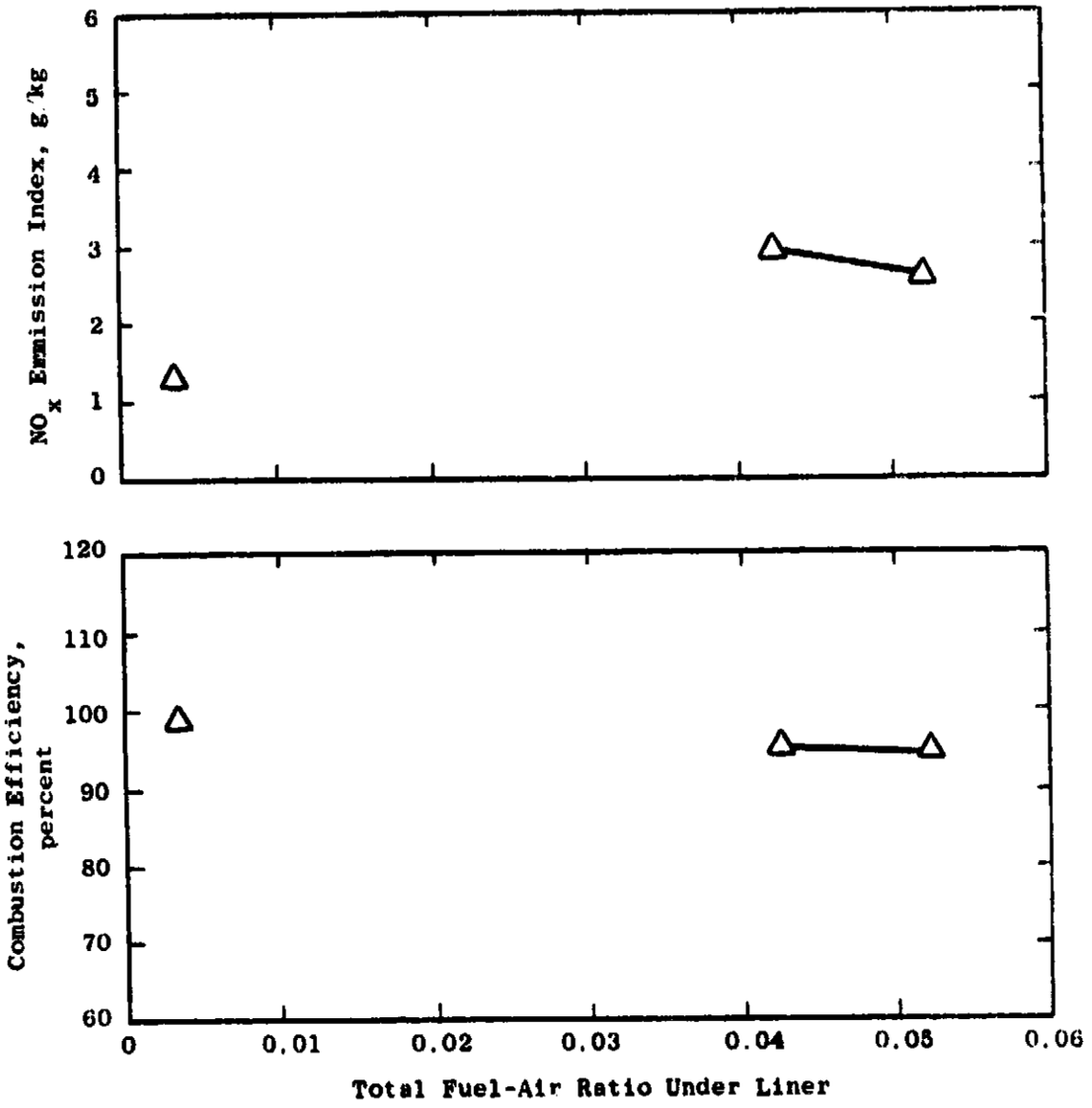

Figure 25. Configuration 1 Performance, Transonic Climb Condition, T = 438-444 K, P = 213 kPa.

Profiles measured at the transonic climb condition are shown in Figure 26. The fuel distribution was not uniform, due perhaps to the spraybar clogging problem. Profiles measured at the sea level takeoff condition are shown in Figure 27. This survey was incomplete, but the edge of a rich streak near the lower liner is evident, and the local NO_x emission index is above 2.0 throughout the stream.

Profiles measured at the supersonic cruise condition are shown in Figures 28 and 29. These two test points differ primarily by the pilot fuel flow. Since the cruise condition requires a low fuel/air ratio, only the upper main stage flameholders were fueled. Some fuel is seen to have migrated, poorly burned, to the lower half of the duct. High local NO_x is associated with this lean, inefficient region.

6.1.2 Configuration 2

Configuration 2 was tested at the altitude relight and the sea level conditions. At the design fuel/air ratio of the latter condition, the duct burner emitted audible resonance, and a high dynamic pressure level was observed at a point 137 mm from the duct burner exit. The main stage fuel flow was immediately reduced 20%, at which point the dynamic pressure decreased to a level judged acceptably low, and the resonance audibly subsided. After an exhaust survey was performed, the main stage fuel flow was turned off, then reestablished from alternate injectors located 200 mm farther upstream. Audible resonance was again apparent, and after a minute or so at this condition, the duct burner blew out and could not be relighted.

Subsequent disassembly and examination disclosed severe damage to the pilot dome and liner. The air shrouds were missing from all five pilot fuel nozzles, and all swirlers had broken loose. Fuel evidently had been released and ignited ahead of the dome, as one swirler was badly burned and a large hole was burned in the dome. The pilot liners were burned, broken, and buckled downstream from this area. Vibration damage was sustained by the flameholders, the second-stage cooling liners, the pilot cowl, and other test rig parts.

The point sample survey reading was included in Table VI, and the remaining data are summarized in Table X. The combustion efficiency was quite high (99%). The measured duct burner exit profiles are shown in Figure 30.

6.1.3 Configuration 3

Preliminary testing of Configuration 3 was performed with the outer pressure vessel, quench section, and sampling rakes removed in order to facilitate audio-visual observation. The purpose of this technique was to explore the operating limits of the duct burner imposed by resonance, under conditions where resonance would not be destructive when encountered. The conditions tested are shown in Table XI.

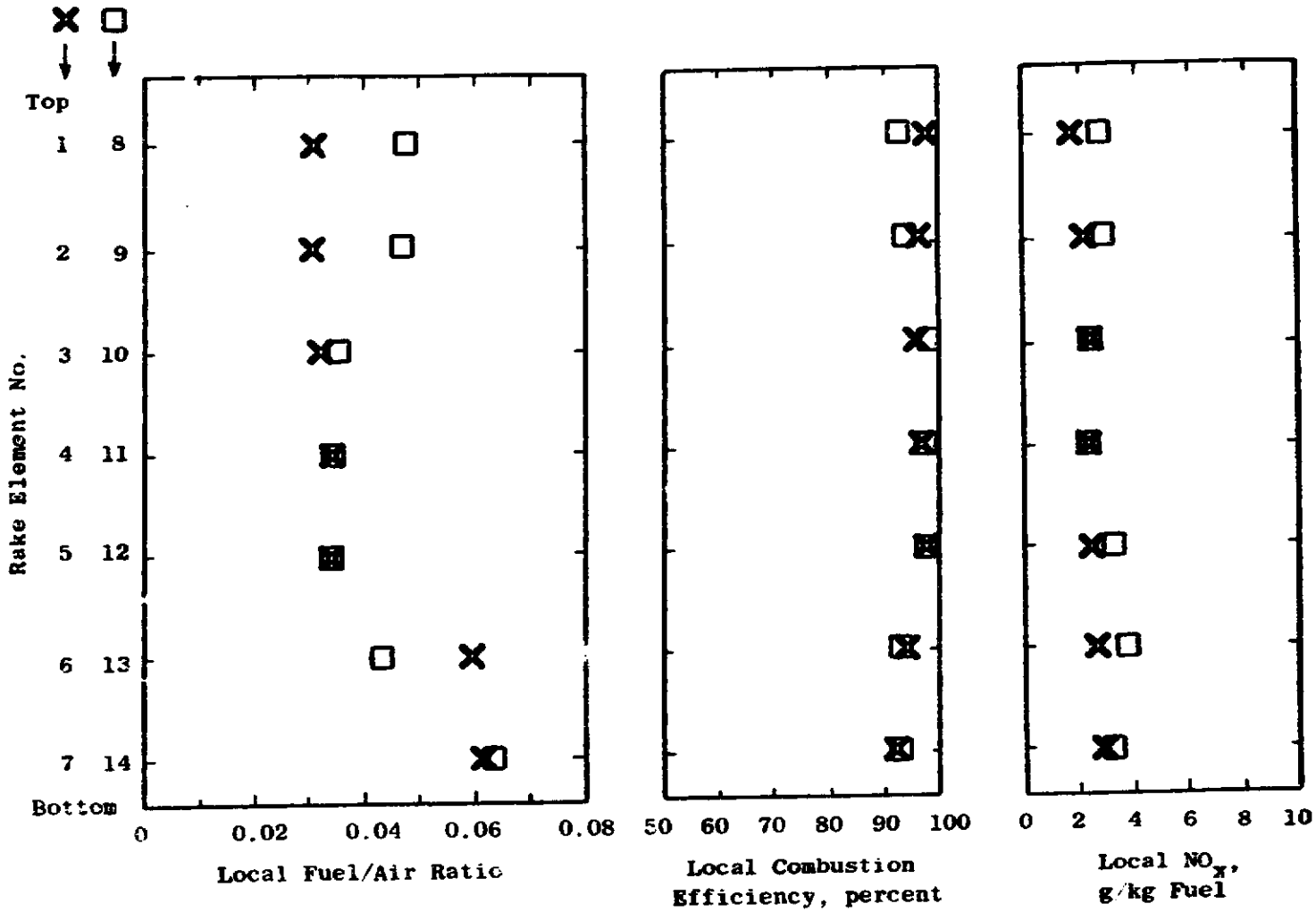

Figure 26. Duct Burner Exit Profiles, Configuration 1, Reading 10, Transonic Climb Condition, T = 443 K, P = 213 kPa, Metered Overall F/A = 0.0432.

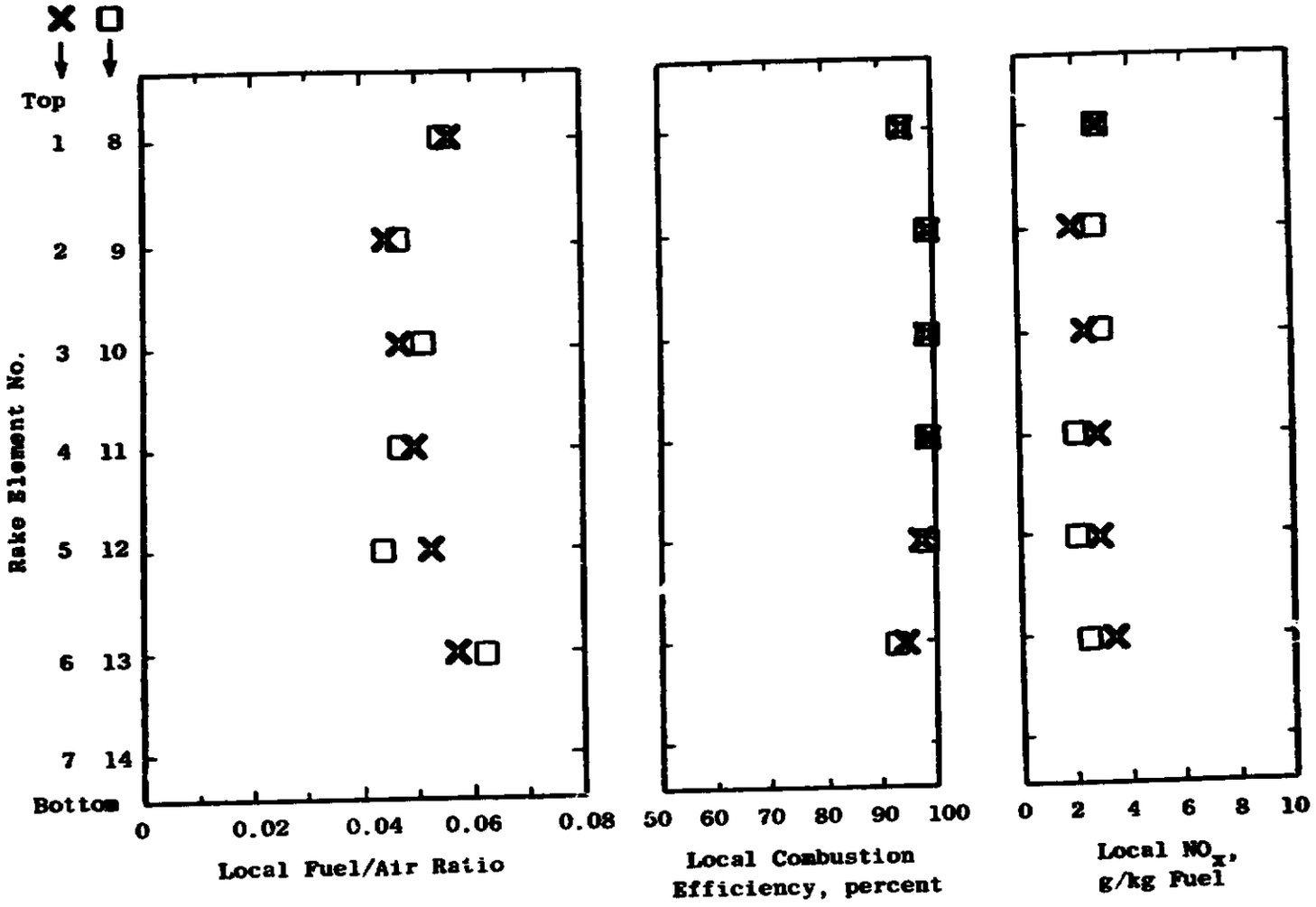

Figure 27. Duct Burner Exit Profiles, Configuration 1, Reading 14, Sea Level Takeoff Condition, T = 455 K, P = 309 kPa, Metered Overall F/A = 0.0430.

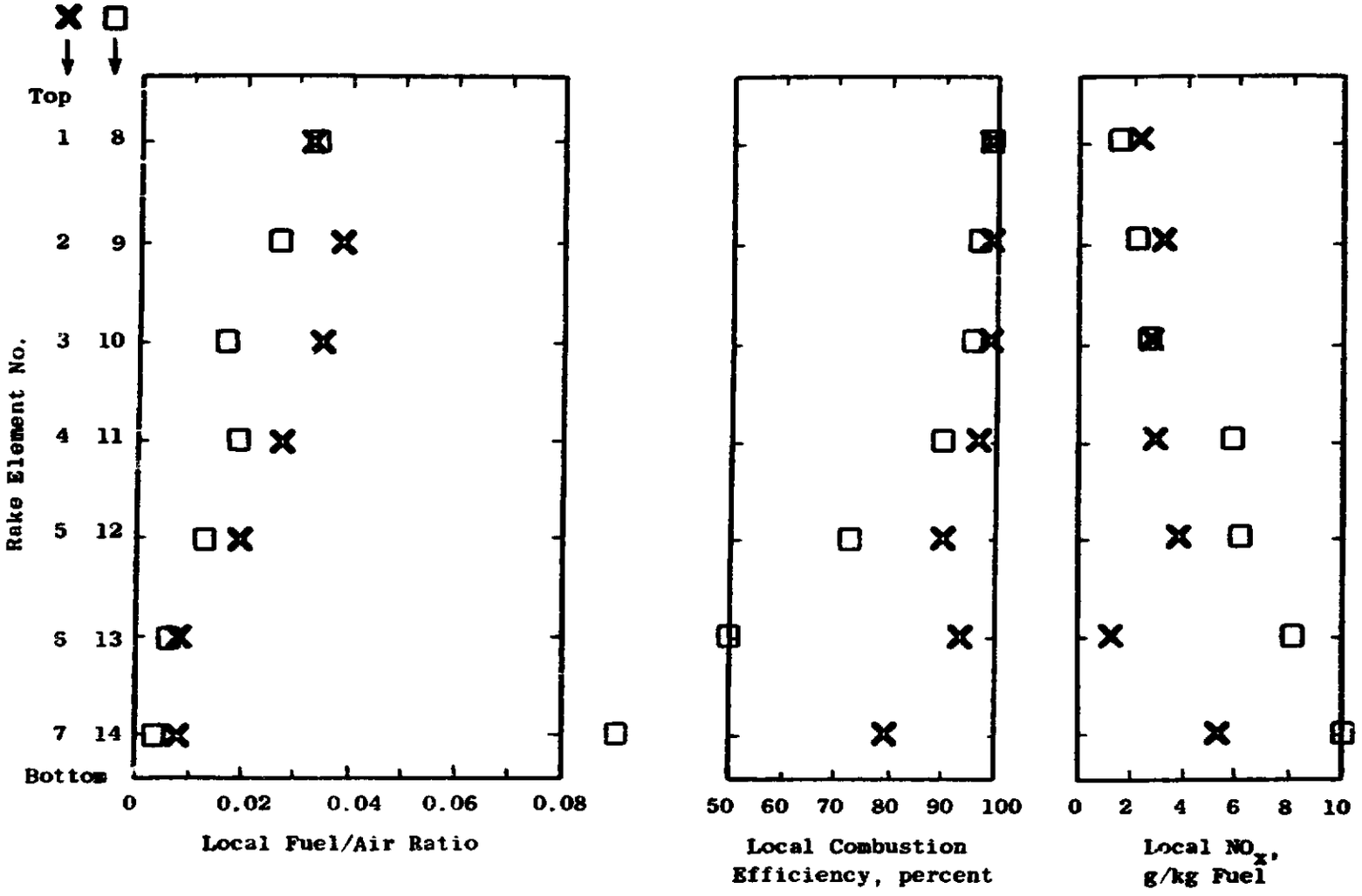

Figure 28. Duct Burner Exit Profiles, Configuration 1, Reading 15, Supersonic Cruise Condition, T = 593 K, P = 262 kPa, Metered Overall F/A = 0.0166.

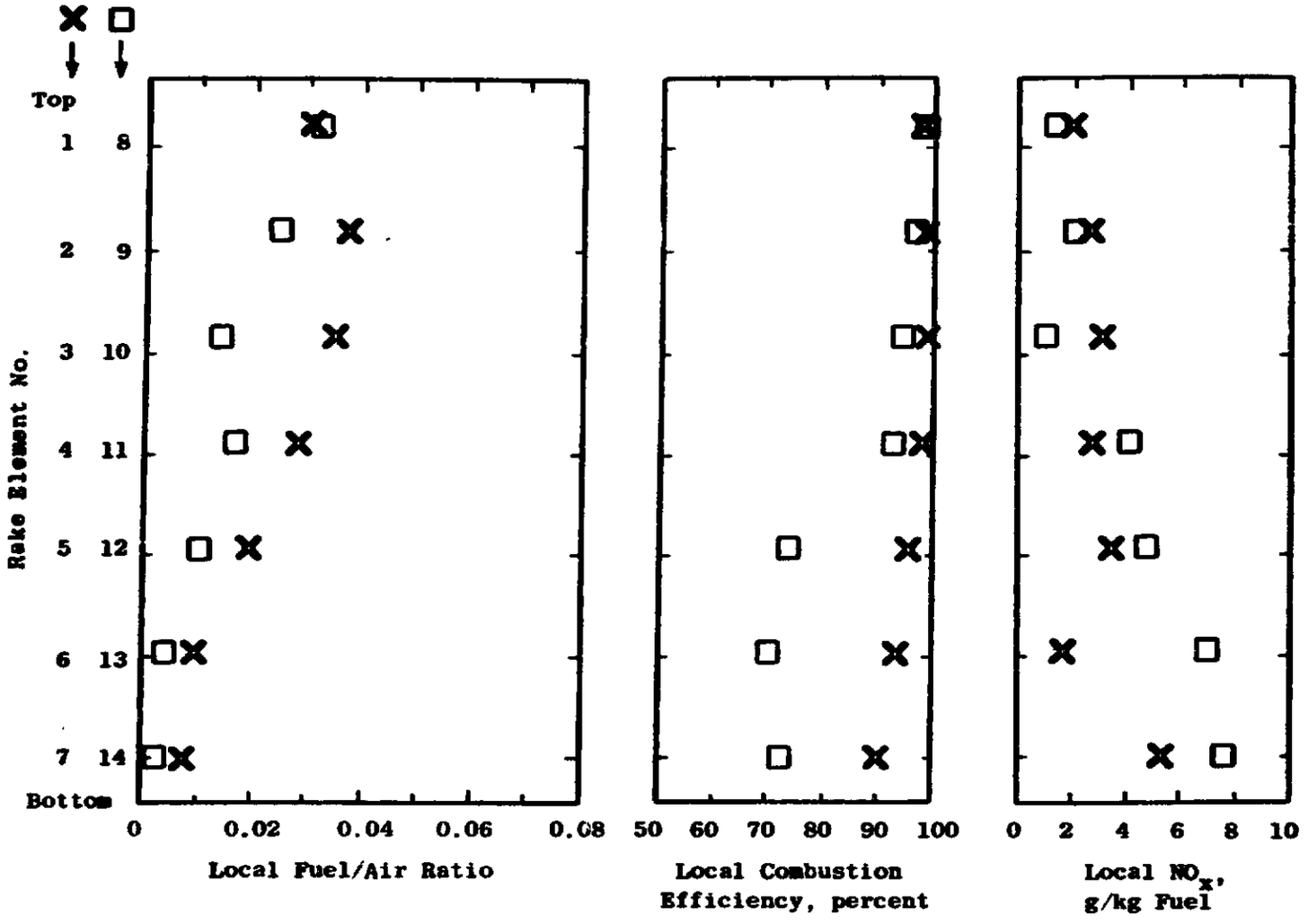

Figure 29. Duct Burner Exit Profiles, Configuration 1, Reading 16, Supersonic Cruise Condition, T = 593 K, P = 260 kPa, Metered Overall F/A = 0.0163.

Table X. Data Summary, Configuration 2, Performance Measured from Manifolded Gas Samples.

RDG	PT6 KPA	TT6 K	V REF M/S	DP/P	F/A UNDER LINER PILOT	UPPER	LOWER	TOTAL	FTOT WET	FTOT SAMP	ETA PCT	TT148 K	EI, G/KG CO	HC	FUEL NOx
18	143.	370.	37.47	0.0566	0.	0.	0.	0.	0.			370.			
19	143.	371.	37.33	0.0501	0.0048	0.	0.	0.0047	0.0039	0.0034	94.77	527.	90.98	31.13	4.75
20	384.	454.	41.20	0.0413	0.0033	0.	0.	0.0033	0.0027	0.0026	99.42	564.	16.78	1.92	3.35
22	143.	371.	38.69	0.0492	0.	0.	0.	0.	0.			371.			

Table XI. Data Summary, Configuration 3, Performance Measured from Manifolded Gas Samples.

RDG	PT6 KPA	TT6 K	V REF M/S	DP/P	F/A UNDER LINER PILOT	UPPER	LOWER	TOTAL	FTOT WET	FTOT SAMP	ETA PCT	TT148 K	EI, G/KG CO	HC	FUEL NOx
23	106.	453.	41.86	0.0513	0.	0.	0.	0.	0.			453.			
24	106.	454.	41.81	0.0592	0.0046	0.0136	0.0140	0.0321	0.0267						
25	108.	453.	40.97	0.0771	0.0048	0.0183	0.0190	0.0429	0.0356						
26	108.	453.	41.16	0.0720	0.0043	0.0183	0.0195	0.0429	0.0356						
27	107.	453.	41.39	0.0670	0.0038	0.	0.0191	0.0230	0.0191						
28	106.	453.	42.52	0.0591	0.0032	0.	0.0190	0.0223	0.0185						

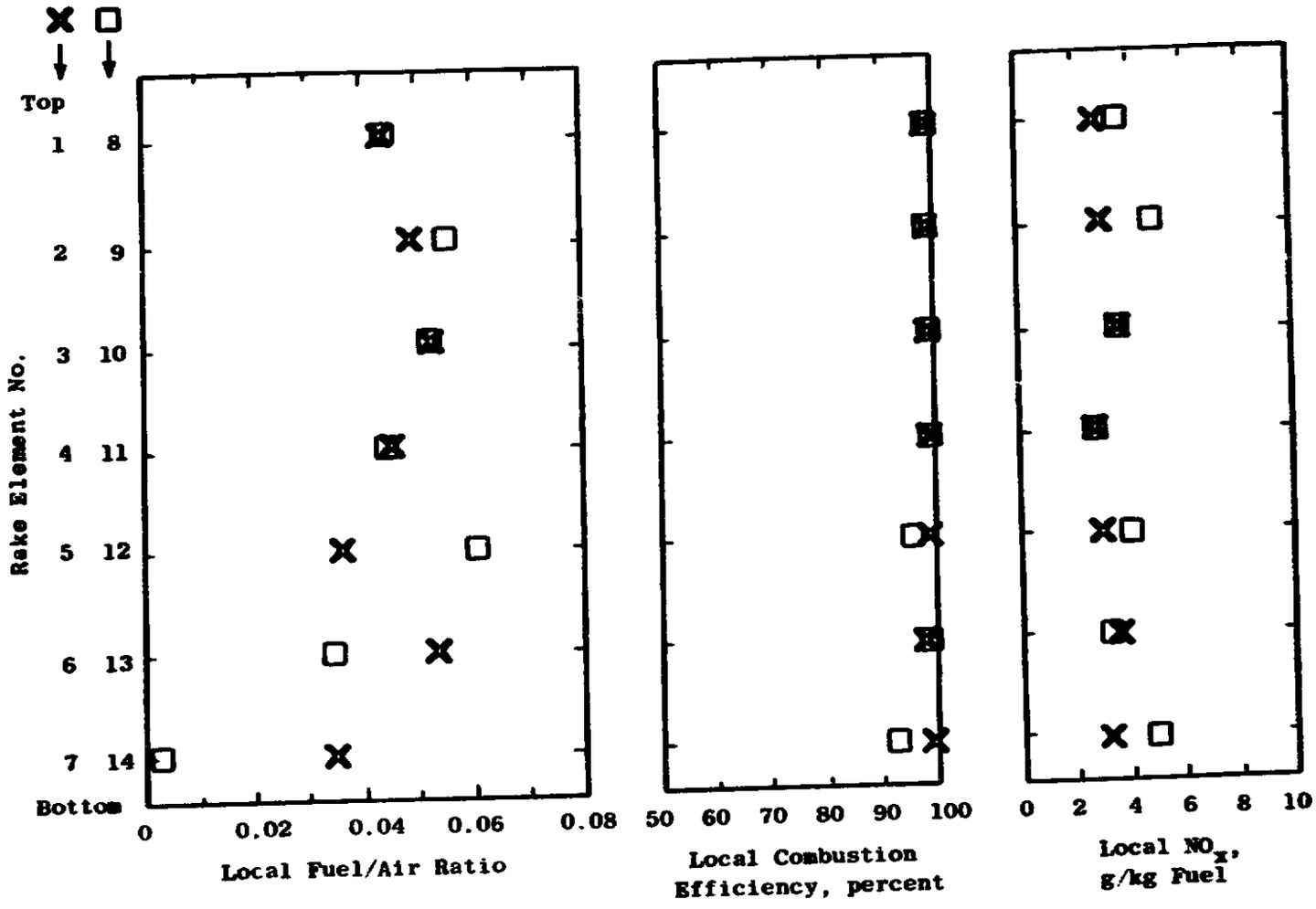

Figure 30. Duct Burner Exit Profiles, Configuration 2, Reading 21, Sea Level Takeoff Condition, T = 454 K, P = 383 kPa, Metered Overall F/A = 0.0402.

Severe resonance was apparent at fuel/air ratios less than originally estimated for the sea level takeoff operating condition. Although the number of dynamic pressure pickups had been increased for this test, instrument malfunctions prevented full documentation of the resonance levels observed. Testing of Configuration 3 was terminated at this point in favor of Configuration 4, in hopes that reduced resonance would result from use of the alternate sector endwall liners that were installed for Configuration 4. Configurations 3 and 4 were expected to have identical emissions performance.

The emissions performance of Configuration 3 was not measured.

6.1.4 Configurations 4 and 5

Like Configuration 3, Configuration 4 was first tested without the outer pressure vessel, quench section, and sampling rakes, at the conditions indicated in Table XII as Readings 29 through 34. The new endwall liners were audibly judged to quiet the burner somewhat, but dynamic pressure measurements did not substantiate this judgement.

Additional tests of Configuration 4 at atmospheric pressure were performed with the rakes and quench bars installed. At the supersonic cruise inlet temperature, emissions measurements were made over a range of total fuel/air ratios at two different pilot fuel flows: with only the lower secondary passage carbureted, and with both passages carbureted equally. These data are included in Table XII and are plotted in Figure 31. Although the emissions performance seemed to improve with increasing fuel-air ratio, the duct burner could not be tested at fuel/air ratios higher than shown because of dangerous resonance amplitudes.

Based on these data, a pilot fuel flow 20% higher than normal was selected for testing Configuration 4 at the full-pressure supersonic cruise condition, with only the lower main stage flameholders carbureted. The results are included in Table VIII, shown previously, and the measured profiles are shown in Figure 32. The low combustion efficiency (96%) seemed to be due mainly to the uncarbureted upper flameholder region. Lean and inefficient regions, which also had high NO_x emission index, were observed in the upper half of the tunnel.

At the sea level takeoff temperature, few data were obtained because a low frequency (1 to 2 Hz) flow oscillation was encountered at atmospheric pressure which repeatedly blew out the burner. At full pressure, the maximum fuel/air ratio that could be set without excessive 300 Hz resonance was 0.036 (under the liner) with both passages fueled. This was considerably below the originally estimated operating fuel/air ratio of 0.050. The profiles measured for Configuration 4 at this condition are shown in Figure 33. The upper main stage fuel burned poorly with high local NO_x emissions.

Configuration 5 was derived from Configuration 4 by replacing the standard splash plate spraybars with spraybars using air jets to atomize

Table XII. Data Summary, Configuration 4, Performance Measured from Manifolded Gas Samples.

RDG	PT6 KPA	TT6 K	V REF M/S	DP/P	F/A UNDER LINER PILOT	UPPER	LOWER	TOTAL	FTOT MET	FTOT SAMP	ETA PCT	TT16B K	EI, G/KG CO	HC	FUEL NOX
29	105.	458.	42.01	0.0526	0.0039	0.	0.	0.0040	0.0033						
30	106.	454.	42.50	0.0559	0.0038	0.0130	0.0136	0.0308	0.0256						
31	107.	453.	40.80	0.0651	0.0040	0.0183	0.0173	0.0405	0.0336						
32	108.	452.	39.76	0.0779	0.0036	0.0221	0.0237	0.0502	0.0417						
33	109.	451.	39.37	0.0806	0.0042	0.0222	0.0235	0.0507	0.0421						
34	107.	451.	40.47	0.0672	0.0039	0.	0.0232	0.0267	0.0222						
35	105.	366.	38.95	0.0458	0.	0.	0.	0.	0.						
36	105.	364.	37.61		0.	0.	0.	0.	0.						
37	106.	369.	37.84	0.0484	0.0073	0.	0.	0.0072	0.0060	0.0073	96.91	609.	68.48	14.91	1.14
38	105.	453.	41.86	0.0452	0.	0.	0.	0.	0.						
40	106.	454.	41.32	0.0446	0.0039	0.	0.	0.0037	0.0031	0.0042	93.97	575.	114.63	33.55	1.29
41	107.	458.	42.15		0.0041	0.0127	0.0136	0.0303	0.0252						
42	106.	594.	48.35	0.0462	0.	0.	0.	0.	0.						
43	106.	592.	48.27	0.0461	0.0029	0.	0.	0.0029	0.0024	0.0044	78.77		61.92	197.97	1.29
44	106.	590.	48.34	0.0496	0.0038	0.	0.	0.0037	0.0031	0.0047	90.90	702.	16.32	87.18	3.96
45	107.	589.	48.43	0.0504	0.0038	0.	0.0115	0.0148	0.0123	0.0138	69.88	916.	149.00	264.43	4.31
46	107.	589.	48.20	0.0512	0.0031	0.	0.0130	0.0160	0.0133	0.0142	73.26	940.	113.31	279.91	4.35
47	107.	588.	47.89	0.0539	0.0030	0.	0.0165	0.0191	0.0159	0.0179	76.38	1039.	113.30	260.77	3.98
48	107.	592.	47.42	0.0524	0.0039	0.	0.0163	0.0197	0.0164	0.0191	86.58	1113.	96.78	111.53	1.35
49	109.	591.	45.52	0.0601	0.0039	0.	0.0217	0.0254	0.0211						
50	108.	590.	46.66	0.0548	0.0038	0.0138	0.0132	0.0313	0.0260	0.0227	77.44	1299.	162.56	187.67	2.30
51	109.	591.	45.67	0.0540	0.0037	0.0151	0.0161	0.0355	0.0295	0.0315	80.10	1409.	269.68	135.74	4.56
52	266.	592.	46.[illegible]	0.0385	0.0039	0.	0.	0.0037	0.0031	0.0044	96.19	712.	3.42	37.34	3.57

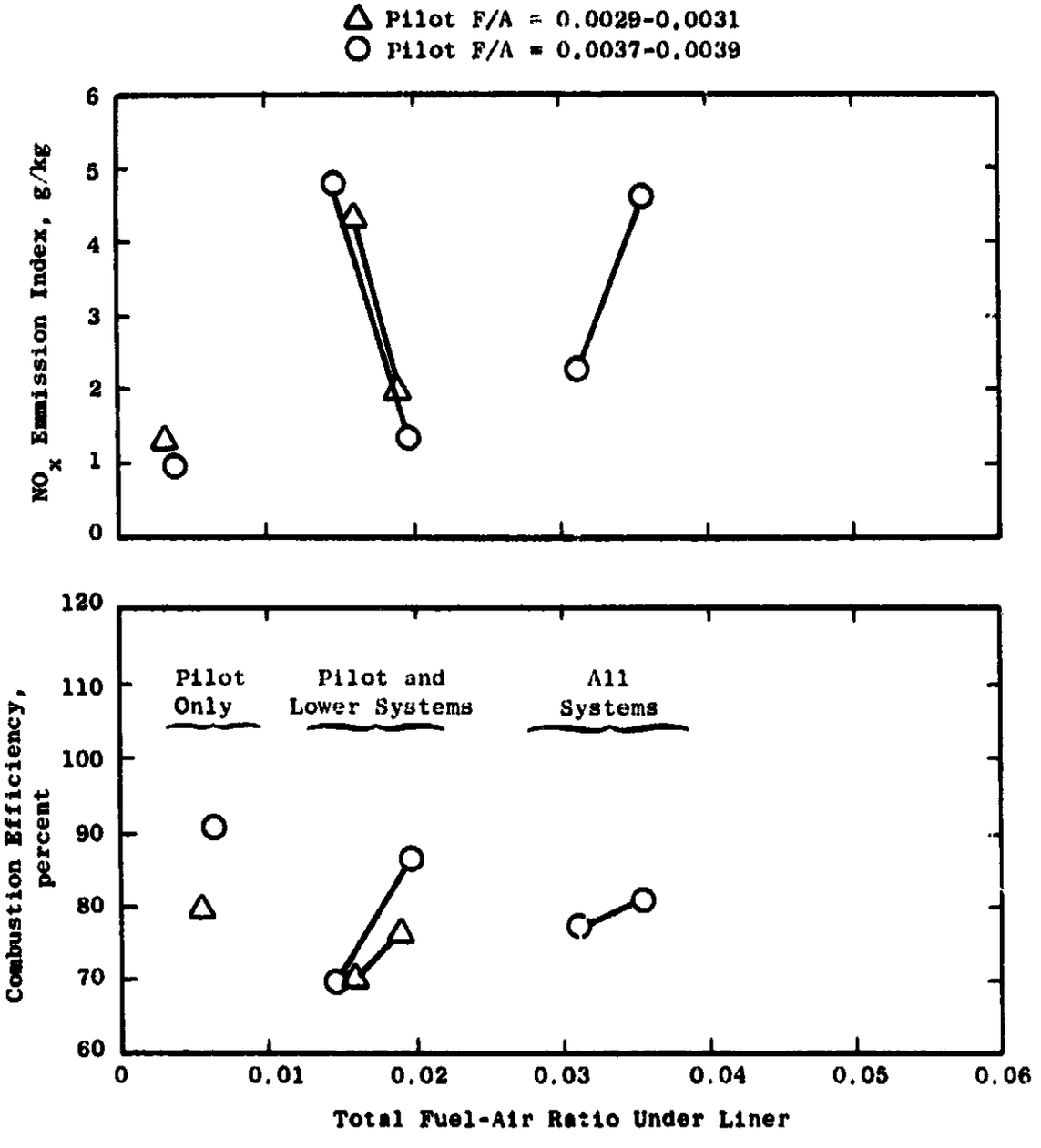

Figure 31. Configuration 4 Performance, Supersonic Cruise Condition, T = 588-592 K, P = 106-109 kPa.

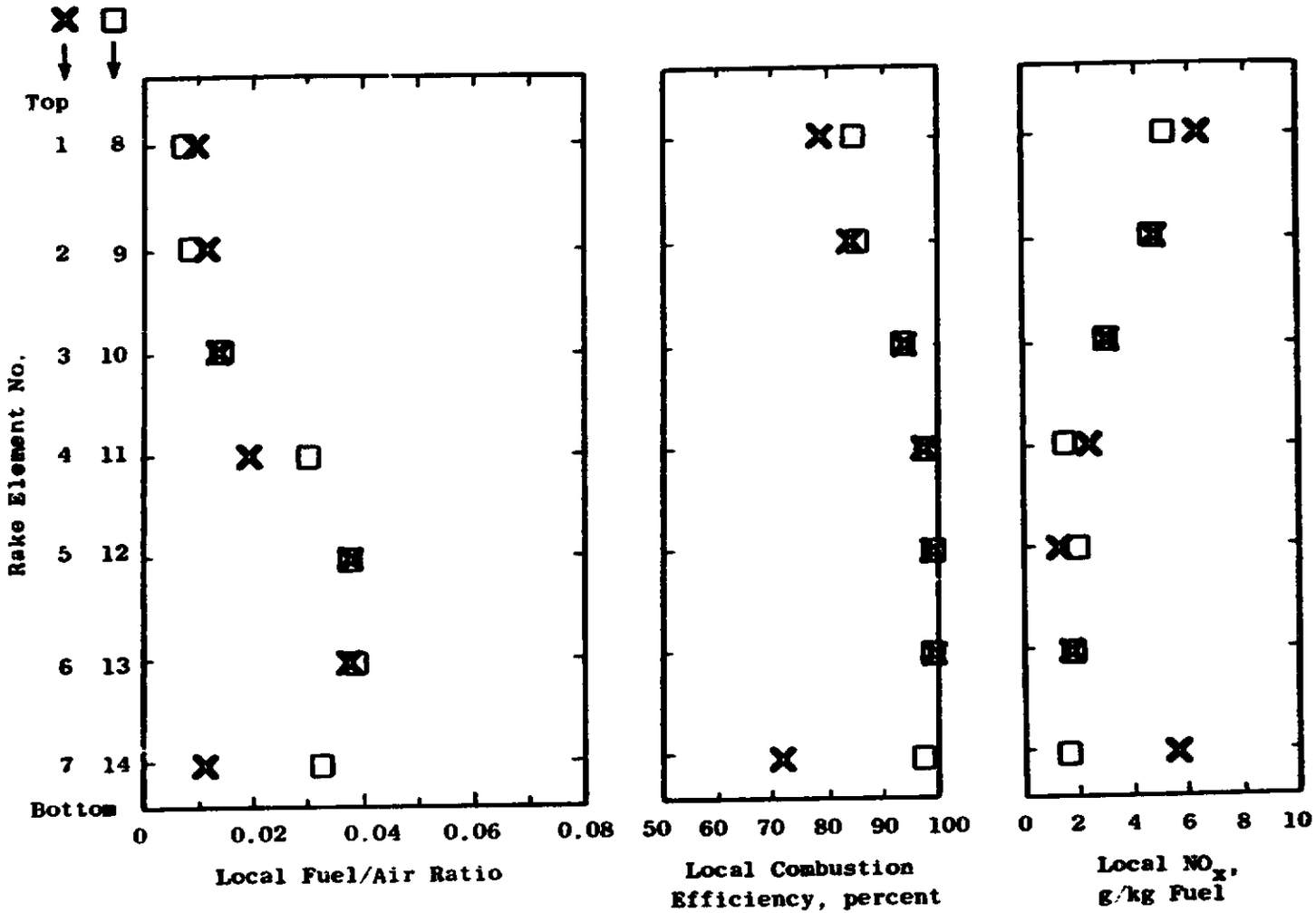

Figure 32. Duct Burner Exit Profiles, Configuration 4, Reading 53, Supersonic Cruise Condition, T = 592 K, P = 265 kPa, Metered Overall F/A = 0.0166.

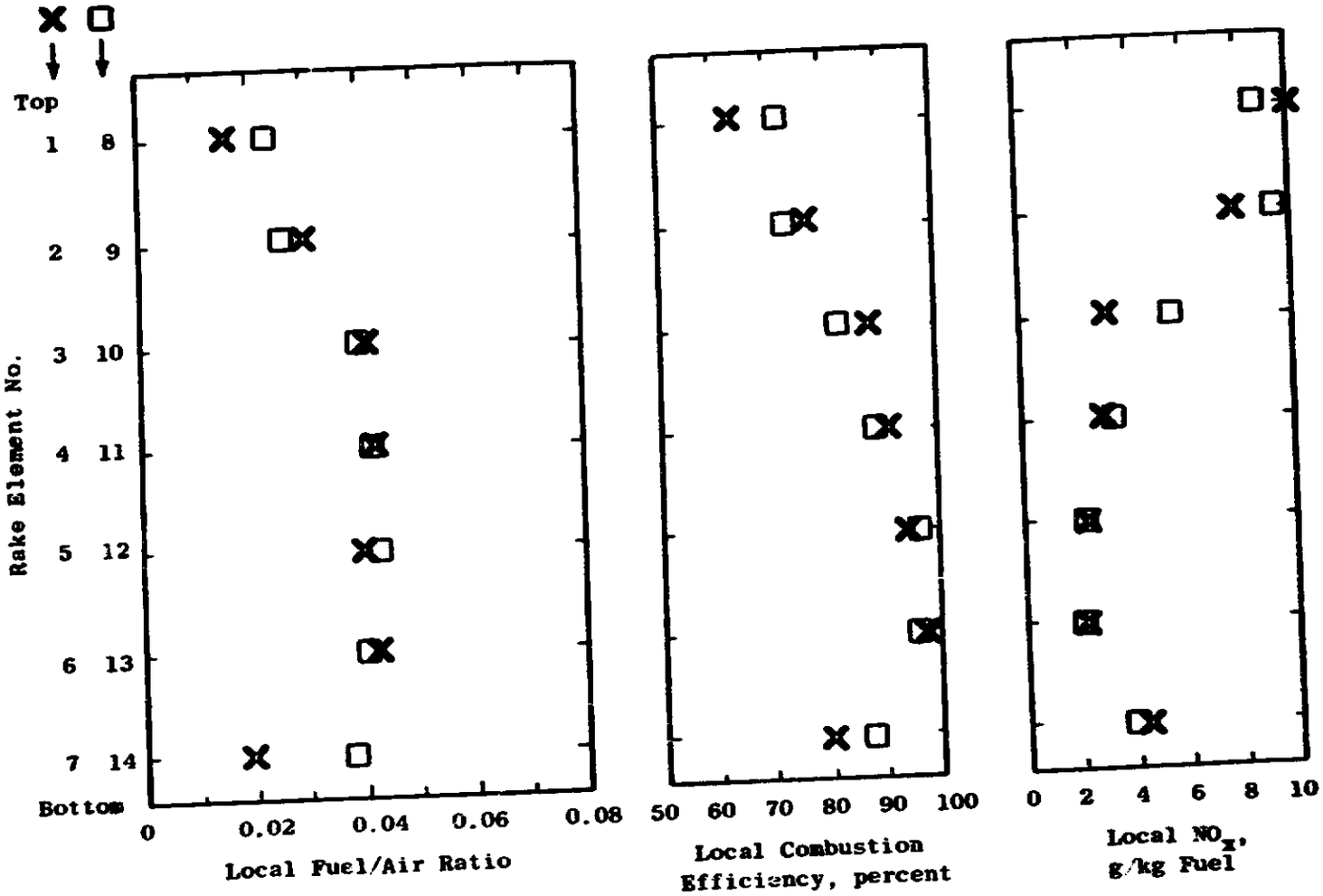

Figure 33. Duct Burner Exit Profiles, Configuration 4, Reading 54, Sea Level Takeoff Condition, T = 455 K, P = 386 kPa, Metered Overall F/A = 0.0311.

the fuel. Preliminary testing was performed at atmospheric pressure and the supersonic cruise air temperatures. The results are shown in Table XIII and plotted in Figure 34. Emissions were measured by manifolded samples using three pilot fuel flows and a variety of main stage fuel and atomizing air configurations. In general, the results compare closely with those of Configuration 4.

Three fuel flow combinations were selected for evaluation of Configuration 5 at full-pressure supersonic cruise conditions, using single-point sample surveys. In all combinations, only the lower main stage flameholders were carbureted, and the atomizing air was on. The first two combinations used the nominal total fuel/air ratio (0.020) and different pilot fuel flows. The third combination used a higher total fuel/air ratio (0.025). The results are included in Table VIII, and the profiles are plotted in Figures 35, 36, and 37. The highest efficiency and the highest NO_x level were produced by the higher fuel/air ratio. At the lower fuel/air ratio, the fuel that migrated into the upper flameholder region was poorly burned. High local NO_x concentrations were found in these lean, inefficient regions. A lean streak containing high HC concentration was present next to the lower liner in all surveys.

At the sea level takeoff condition, the maximum safely-attainable fuel/air ratio for Configuration 5 was 0.036 under the liner, about the same as for Configuration 4. The results of these point-sample survey measurements are included in Table VI, and the profiles are plotted in Figure 38. The upper main stage fuel was poorly burned. In Configuration 5, the upper flameholders were located 150 mm downstream from the lower flameholders, so that combustion length was shorter, and much more pilot liner film air was injected next to the upper flameholders.

Posttest inspection showed damage to be limited to one ripped pilot liner cooling slot, broken tack welds on two pilot swirlers, and a broken film slot on one sector endwall liner.

6.1.5 Configurations 6 through 10

Tests of Configurations 6 through 10 are reported together, as these configurations shared the same basic pilot and flameholder designs.

Preliminary testing of Configurations 6 and 8 was performed with the outer pressure shell, quench section, and sampling rakes removed and the air temperature adjusted to the sea level takeoff value. This testing was done to explore the fuel/air ratio ranges over which the augmentor could be operated without excessive resonance. The conditions tested are listed as Readings 75 through 90 in Tables XIV and XV. Neither configuration could be operated at the originally estimated sea level takeoff fuel/air ratio.

The emissions performance of Configurations 6 and 8 was measured only at the supersonic cruise operating condition, mostly at atmospheric pressure

Table XIII. Data Summary, Configuration 5, Performance Measured from Manifolded Gas Samples.

RDG	PT6 KPA	TT6 K	V REF M/S	DP/P	F/A UNDER LINER PILOT	UPPER	LOWER	TOTAL	FTOT MET	FTOT SAMP	ETA PCT	TT48 K	EI, G/KG FUEL CO	HC	NOX
55	106.	591.	47.05	0.0420	0.	0.	0.	0.	0.						
57	106.	591.	46.80	0.0418	0.0030	0.	0.	0.0031	0.0026	0.0031	98.78		33.93	6.28	0.87
58	107.	590.	46.87	0.0419	0.0039	0.	0.	0.0038	0.0031	0.0038	99.32	713.	19.42	2.78	1.32
59	107.	591.	46.14	0.0417	0.0049	0.	0.	0.0045	0.0037	0.0047	99.29	735.	24.04	1.47	2.39
60	107.	592.	46.47	0.0453	0.0037	0.	0.0120	0.0157	0.0130	0.0172	80.43	983.	161.19	158.77	4.35
61	108.	592.	45.92	0.0522	0.0038	0.	0.0121	0.0157	0.0130	0.0153	76.80	968.	127.82	202.20	5.51
62	109.	591.	45.86	0.0537	0.0037	0.	0.0169	0.0206	0.0170	0.0230	93.39	1153.	81.57	77.79	2.99
63	108.	593.	46.34	0.0494	0.0042	0.	0.0170	0.0207	0.0171	0.0230	91.94	1167.	90.76	59.42	2.73
64	108.	591.	46.03	0.0533	0.0038	0.	0.0176	0.0206	0.0170	0.0218	85.69	1124.	91.42	123.79	3.31
65	109.	592.	46.04	0.0546	0.0046	0.	0.0164	0.0206	0.0170	0.0227	93.00	1168.	72.82	53.91	2.58
66	109.	593.	45.09	0.0546	0.0046	0.	0.0220	0.0263	0.0217	0.0271	96.54	1339.	81.36	15.57	2.41
67	109.	584.	45.60	0.0570	0.0042	0.	0.0220	0.0257	0.0212	0.0271	94.50	1302.	100.38	31.59	2.59
68	109.	598.	46.59	0.0558	0.0045	0.0134	0.0137	0.0321	0.0265	0.0263	78.96	1330.	219.44	159.22	4.99
69	110.	589.	45.84	0.0577	0.0046	0.0164	0.0155	0.0372	0.0307	0.0335	81.46	1449.	274.31	121.38	4.38
70	111.	590.	45.54	0.0624	0.0044	0.0176	0.0190	0.0419	0.0346	0.0432	87.67	1609.	223.18	71.25	2.75

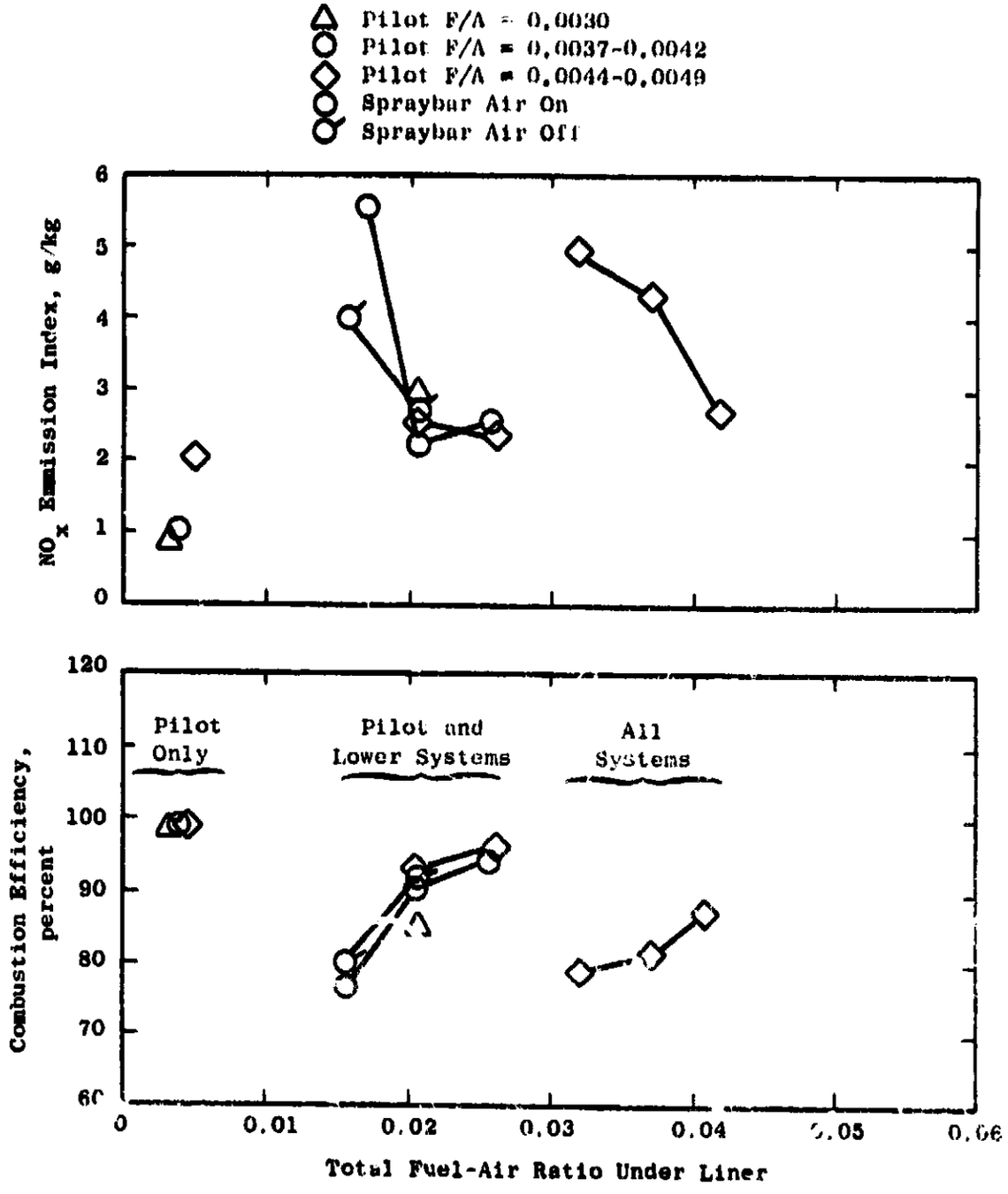

Figure 34. Configuration 5 Performance, Supersonic Cruise Condition, T = 584-593 K, P = 106-111 kPa.

C-2

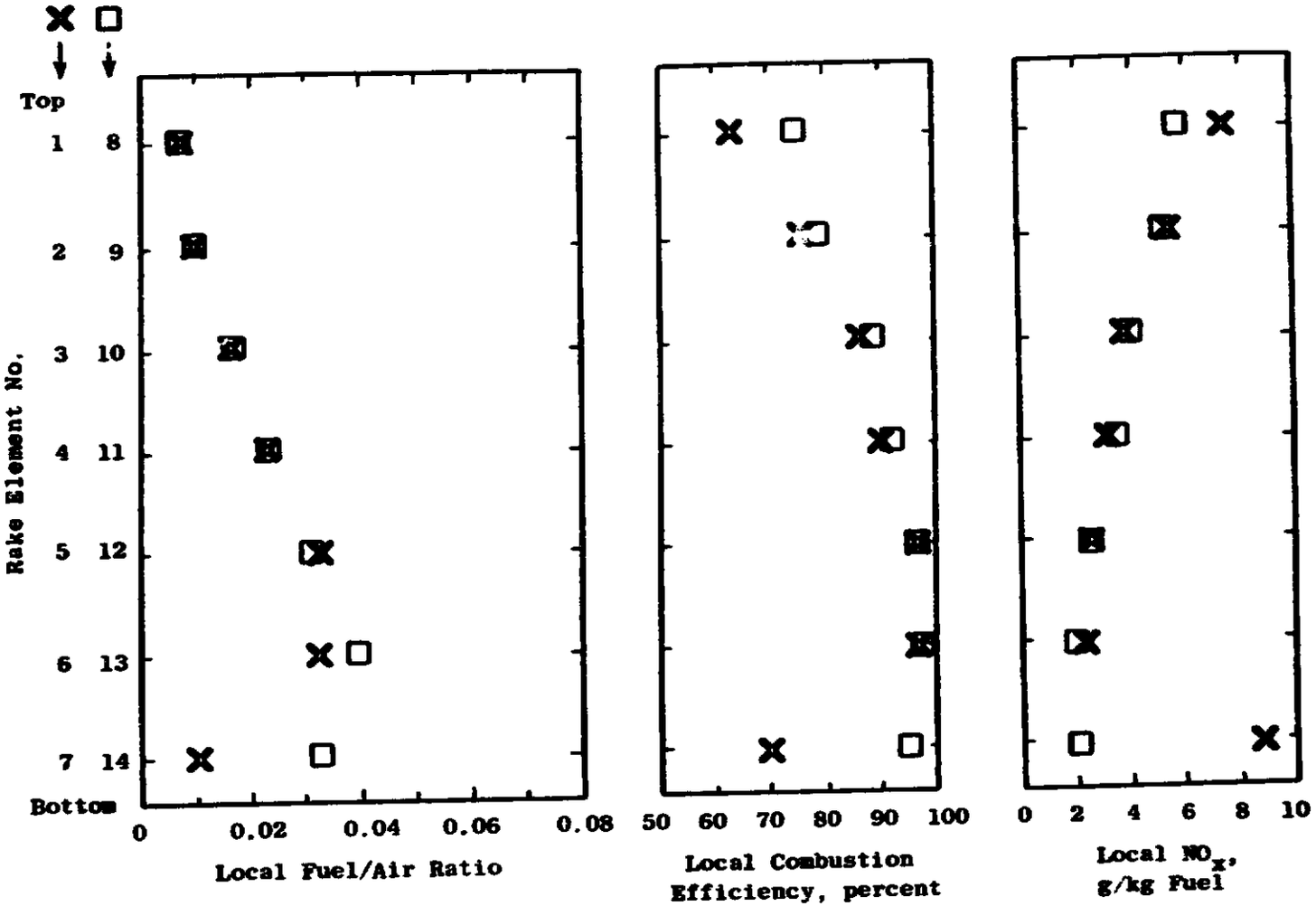

Figure 35. Duct Burner Exit Profiles, Configuration 5, Reading 71, Supersonic Cruise Condition, T = 598 K, P = 268 kPa, Metered Overall F/A = 0.0167.

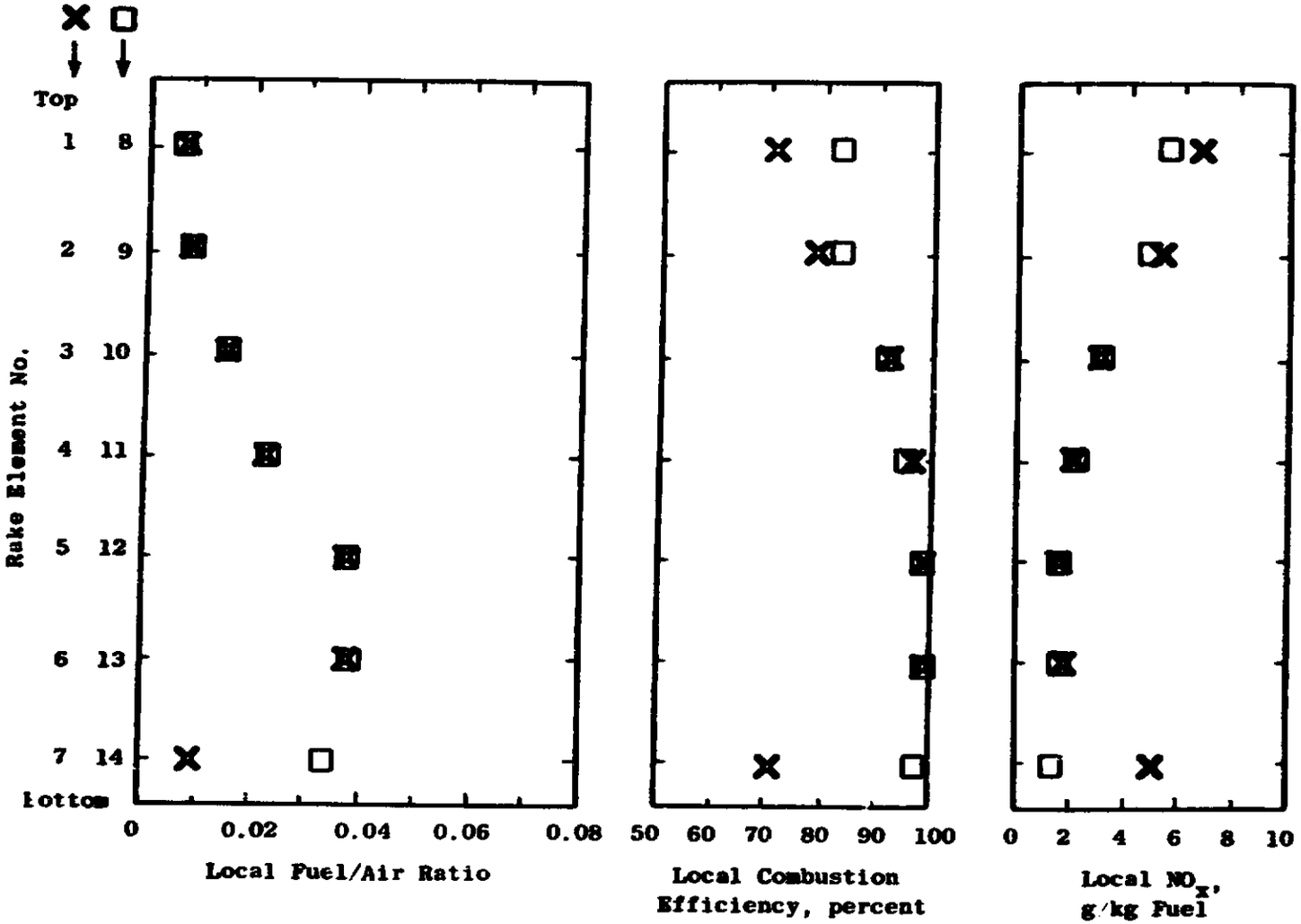

Figure 36. Duct Burner Exit Profiles, Configuration 5, Reading 72, Supersonic Cruise Condition, T = 596 K, P = 264 kPa, Metered Overall F A = 0.0166.

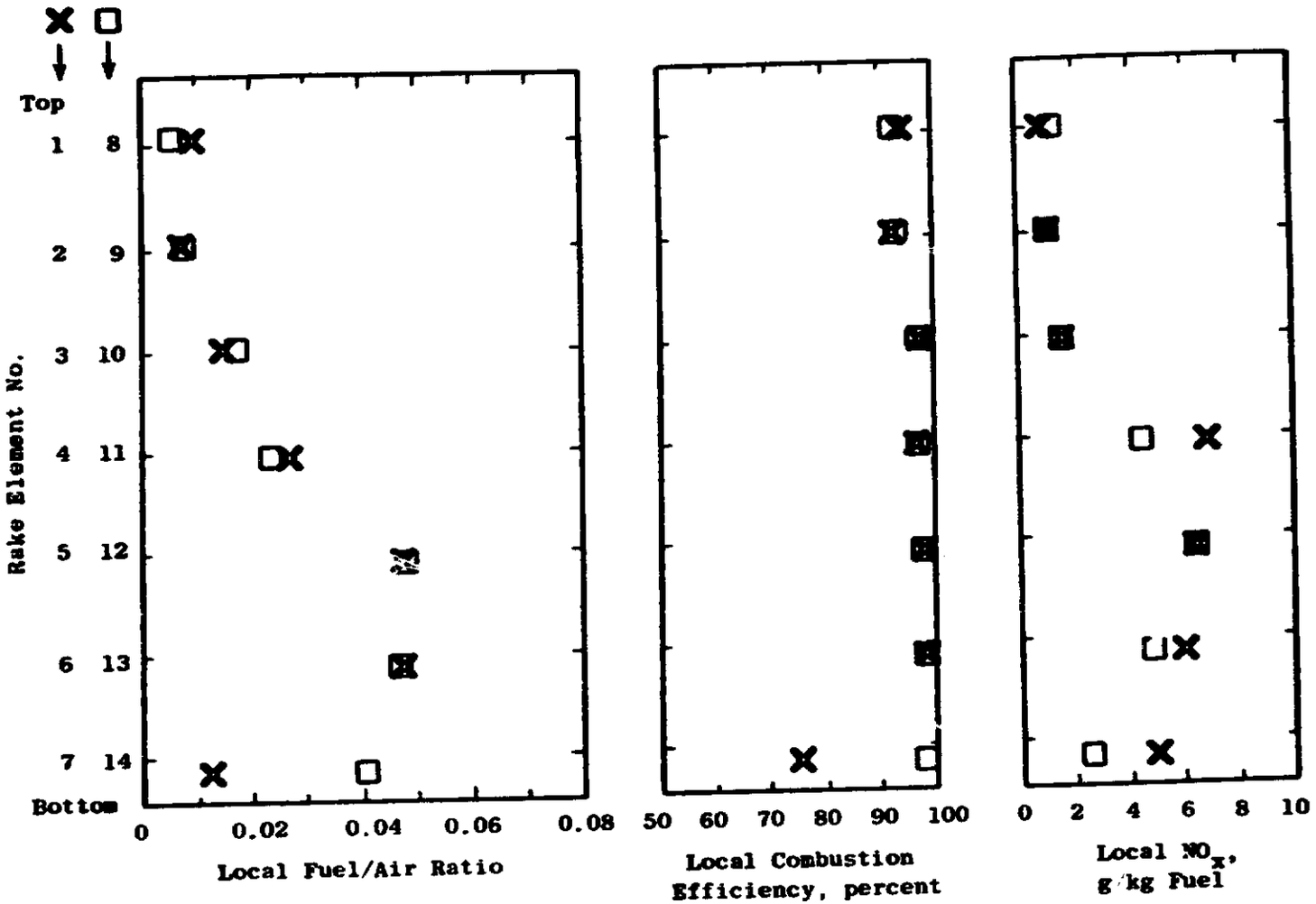

Figure 37. Duct Burner Exit Profiles, Configuration 5, Reading 73, Supersonic Cruise Condition, T = 598 K, P = 264 kPa, Metered Overall F/A = 0.0210.

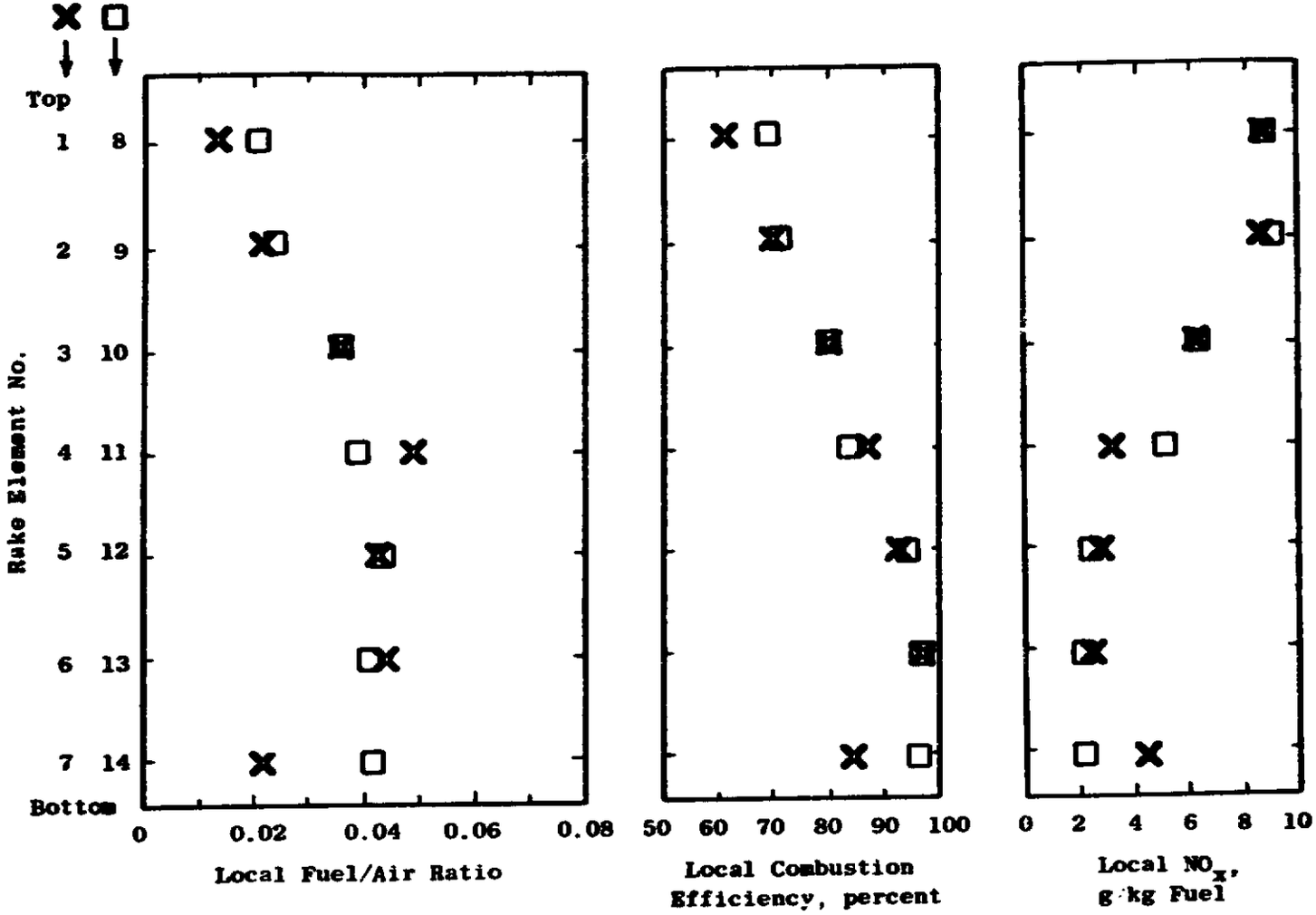

Figure 38. Duct Burner Exit Profiles, Configuration 5, Reading 74, Sea Level Takeoff Condition, T = 482 K, P = 385 kPa, Metered Overall F A = 0.0304.

Table XIV. Data Summary, Configuration 6, Performance Measured from Manifolded Gas Samples.

RDG	PT6 KPA	TT6 K	V REF M/S	DP/P	F/A UNDER LINER PILOT	UPPER	LOWER	TOTAL	FTOT MET	FTOT SAMP	ETA PCT	TT148 K	EI, G/KG CO	HC	FUEL NOX
75	109.	452.	40.16	0.0818	0.	0.	0.	0.	0.			452.			
76	109.	451.	40.21	0.0867	0.0034	0.	0.	0.0033	0.0026						
77	110.	451.	40.04	0.0897	0.0041	0.	0.	0.0041	0.0032						
78	110.	450.	40.06	0.0900	0.0046	0.	0.	0.0046	0.0036						
79	110.	451.	41.29	0.0963	0.0040	0.0125	0.	0.0162	0.0126						
80	111.	450.	40.94	0.0990	0.0040	0.0177	0.	0.0216	0.0168						
81	112.	450.	40.64	0.1104	0.0040	0.0226	0.	0.0267	0.0208						
82	112.	450.	40.66	0.1103	0.0039	0.0169	0.0167	0.0376	0.0293						
83	112.	450.	40.39	0.1121	0.0046	0.0222	0.	0.0268	0.0209						
92	111.	368.	35.79	0.0249	0.0066	0.	0.	0.0064	0.0050	0.0060	89.38	554.	160.77	58.55	0.51
93	111.	591.	45.75	0.0774	0.	0.	0.	0.	0.			591.			
94	112.	588.	44.51	0.0774	0.0056	0.	0.	0.0054	0.0042	0.0051	98.28	752.	44.56	6.33	2.59
95	112.	588.	46.18	0.0776	0.0067	0.	0.	0.0065	0.0051	0.0061	98.38	785.	55.51	3.29	3.39
96	112.	587.	44.74	0.0768	0.0044	0.	0.	0.0042	0.0033	0.0034	98.23	717.	51.04	5.83	2.39
97	113.	594.	45.79	0.0849	0.0057	0.0110	0.	0.0162	0.0126	0.0165	86.80	1005.	129.13	131.82	1.03
98	114.	595.	45.86	0.0848	0.0058	0.0158	0.	0.0212	0.0165	0.0222	97.06	1182.	60.68	15.28	1.37
99	114.	595.	45.73	0.0852	0.0068	0.0151	0.	0.0214	0.0167	0.0221	97.33	1187.	58.86	12.94	1.13
100	114.	595.	45.94	0.0863	0.0046	0.0171	0.	0.0213	0.0166	0.0220	95.34	1173.	74.51	29.20	0.93
101	114.	595.	45.36	0.0868	0.0057	0.0218	0.	0.0272	0.0212	0.0289	98.57	1340.	47.74	3.16	2.39
102	115.	593.	45.25	0.0882	0.0056	0.0269	0.	0.0324	0.0252	0.0352	96.07	1439.	164.01	1.94	3.55
103	124.	593.	41.81	0.0730	0.0055	0.0140	0.0137	0.0330	0.0257	0.0323	98.21	1472.	36.13	9.44	3.99
104	258.	593.	47.59	0.0827	0.	0.	0.	0.	0.			593.			
105	260.	597.	47.92	0.0833	0.0056	0.	0.	0.0054	0.0042	0.0052	99.33	763.	21.67	1.55	6.89
106	260.	589.	46.90	0.0880	0.0056	0.0160	0.	0.0213	0.0166	0.0218	96.50	1176.	31.65	27.61	1.58

Table XV. Data Summary, Configuration 8, Performance Measured from Manifolded Gas Samples.

RDG	PT6 KPA	TT6 K	V REF M/S	DP/P	F/A UNDER LINER PILOT	UPPER	LOWER	TOTAL	FTOT MET	FTOT SAMP	ETA PCT	TT148 K	EI, G/KG CO	HC	FUEL NOX
84	110.	451.	41.25	0.0955	0.0041	0.0122	0.	0.0161	0.0125						
85	111.	450.	40.48	0.1056	0.0047	0.0169	0.	0.0214	0.0167						
86	112.	450.	40.51	0.1094	0.0049	0.0143	0.0138	0.0331	0.0258						
87	113.	450.	39.93	0.1168	0.0051	0.0157	0.0159	0.0366	0.0285						
88	114.	450.	39.80	0.1238	0.0062	0.0172	0.0173	0.0407	0.0317						
89	112.	450.	40.61	0.1139	0.0057	0.0209	0.	0.0266	0.0207						
90	113.	450.	40.59	0.1189	0.0057	0.0262	0.	0.0318	0.0248						
109	112.	591.	45.89	0.0863	0.0057	0.0163	0.	0.0217	0.0169	0.0253	96.94	1189.	61.40	15.27	1.13
110	113.	592.	45.66	0.0871	0.0054	0.0220	0.	0.0272	0.0212	0.0324	98.15	1333.	64.45	3.53	3.26

with manifolded samples. The data are listed in Tables XIV and XV and plotted in Figures 39 and 40. With only the upper main stage flameholders carbureted, the efficiency peaked at a total fuel/air ratio under the liner of about 0.02%, but the NO_x increased rapidly with fuel/air ratios above 0.021. The large difference in main stage fuel premixing length between Configurations 6 and 8 had a relatively small effect on performance.

Performance measurements made by the point sample survey method at full pressure for Configurations 6 and 8 are included in Table VIII, and the profiles are plotted in Figures 41 through 45. Some tests were made with only the upper main stage flameholders carbureted, and some were made with only the lower flameholders carbureted. At fuel/air ratios near nominal for the supersonic cruise condition, these configurations provided NO_x and CO emissions closely approaching the program goals. Fuel migrating into the uncarbureted side of the duct was burned more efficiently than in Configurations 4 and 5. The high HC levels were due primarily to a lean, inefficient streak adjacent to the liner on the carbureted side.

Configurations 7 and 10 were subjected to extensive parametric variation at full pressure, with emissions performance measured by manifolded samples. The data are listed in Tables XVI and XVII. Figure 46 illustrates the minor effect of pilot fuel/air ratio on the performance of Configuration 7 at supersonic cruise. Figure 47 shows the performance of Configuration 10 at supersonic cruise. The NO_x level is comparable to Configuration 8 (Figure 40), but the efficiency is lower.

Figure 48 shows the effect of reference velocity on Configuration 7 at supersonic cruise. NO_x improves and efficiency falls with increasing velocity. The data at 47 m/s are the same as Figure 46 and do not correlate perfectly with the combustion efficiencies measured at other velocities. The efficiencies of Configuration 10 (Figure 47) correlate better.

Figure 49 shows the performance of Configuration 10 at the transonic climb condition, and Figure 50 shows the performance at sea level takeoff at two reference velocities. Both NO_x and efficiency are lower than at the higher temperature supersonic cruise condition.

Configuration 9 was tested only at supersonic cruise. Measurements made with manifolded samples are listed in Table XVIII and plotted in Figure 51. The performance is comparable to the liquid-fueled configurations, although the rate of increase of NO_x with fuel/air ratio is somewhat less. Configuration 9 seemed to be less prone to resonance than others with liquid fuel injection.

Point sample surveys at the burner exit stream were performed on Configurations 7, 9, and 10 at selected operating conditions. These data are included in Tables VI, VII, and VIII. The measured profiles are plotted in Figures 52 through 61. The local fuel/air ratios shown for Readings 103, 137, 154, 169, 171, and 175 have been corrected upward to compensate for a leak that admitted air to the sample system. The data generally showed that with only one main stage flameholder fueled, the fuel that penetrated

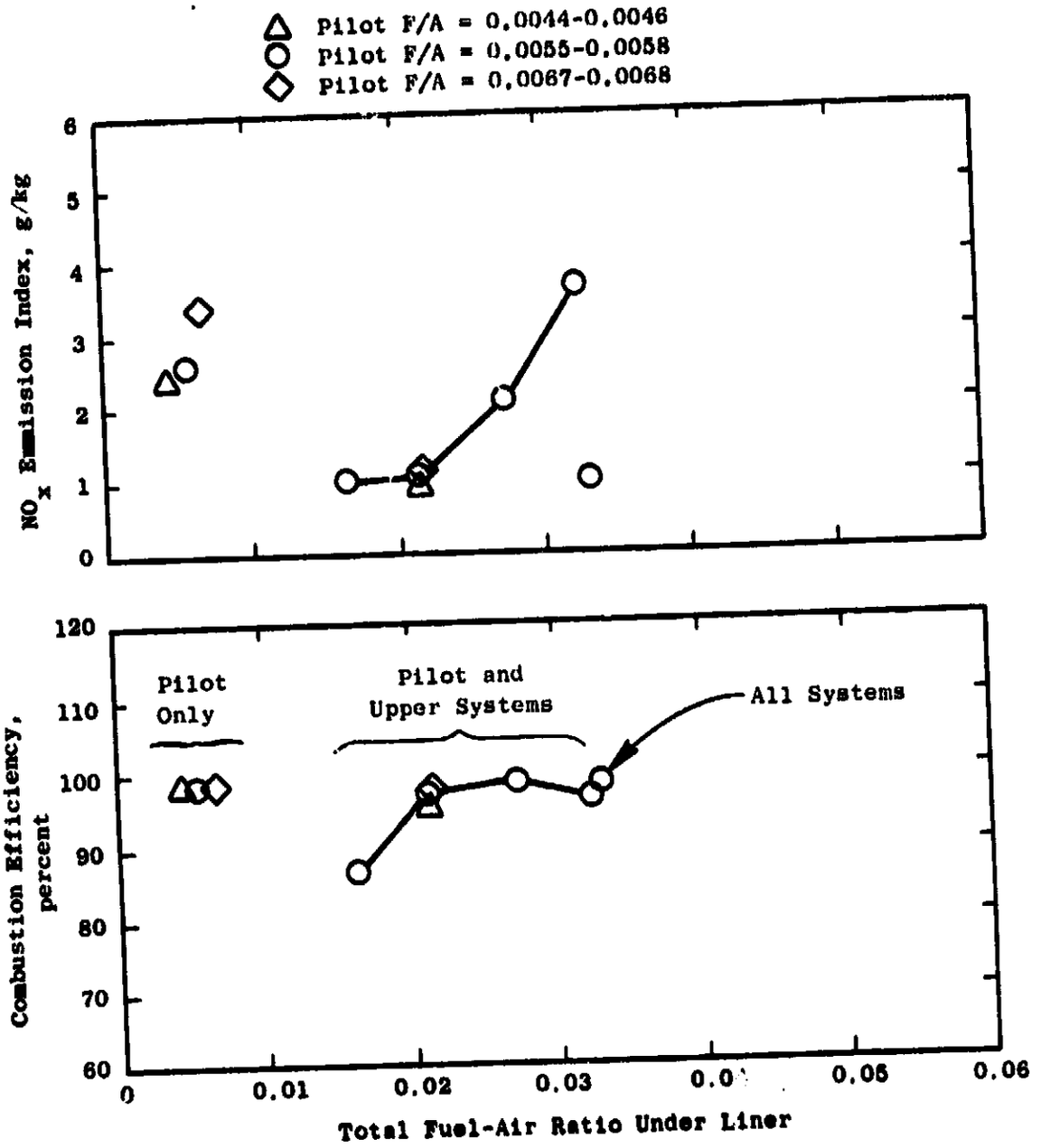

Figure 39. Configuration 6 Performance, Supersonic Cruise Condition, T = 587-595 K, P = 112-124 kPa.

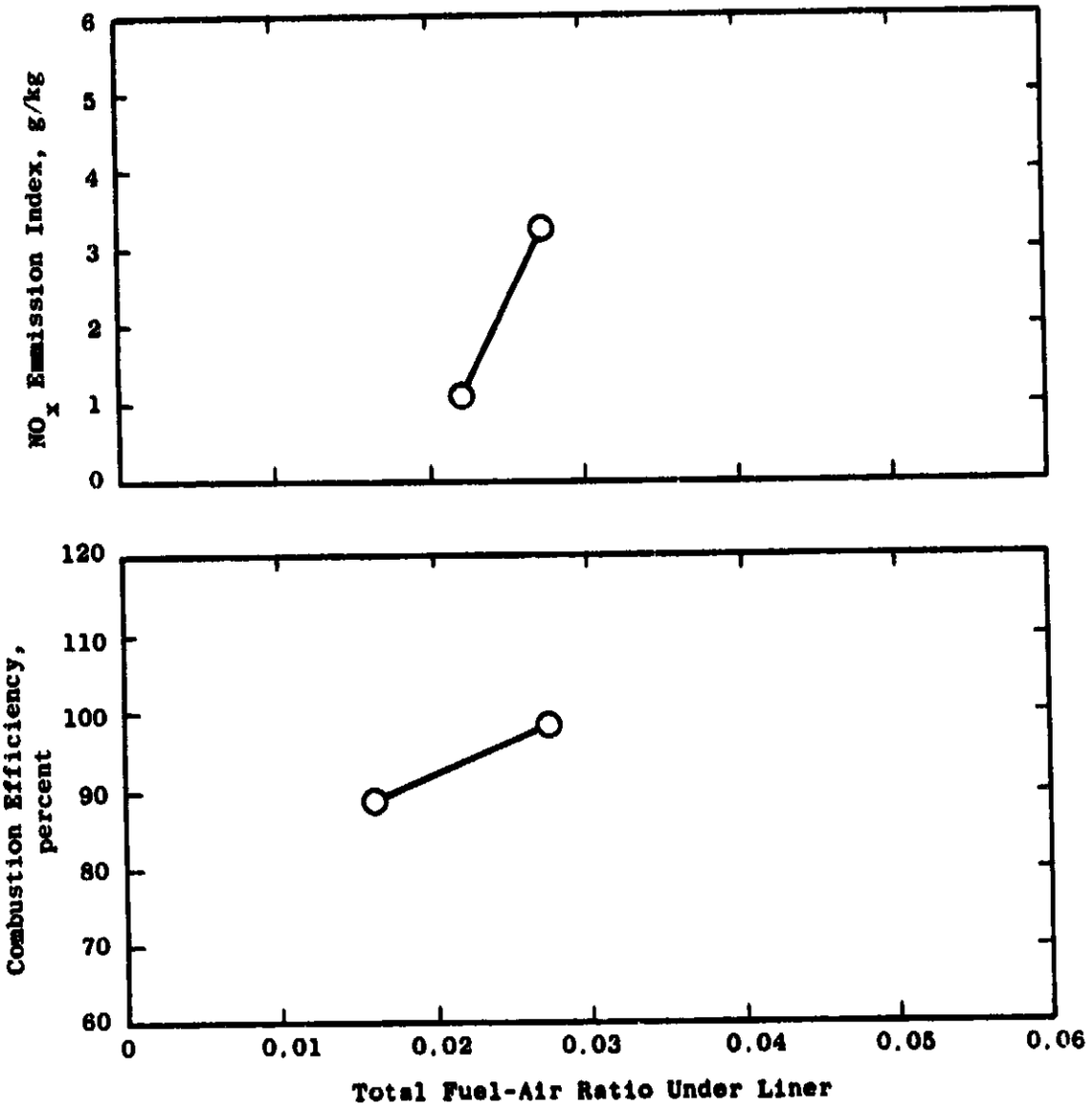

Figure 40. Configuration 8 Performance, Supersonic Cruise Condition, T = 591-592 K, P = 112-113 kPa.

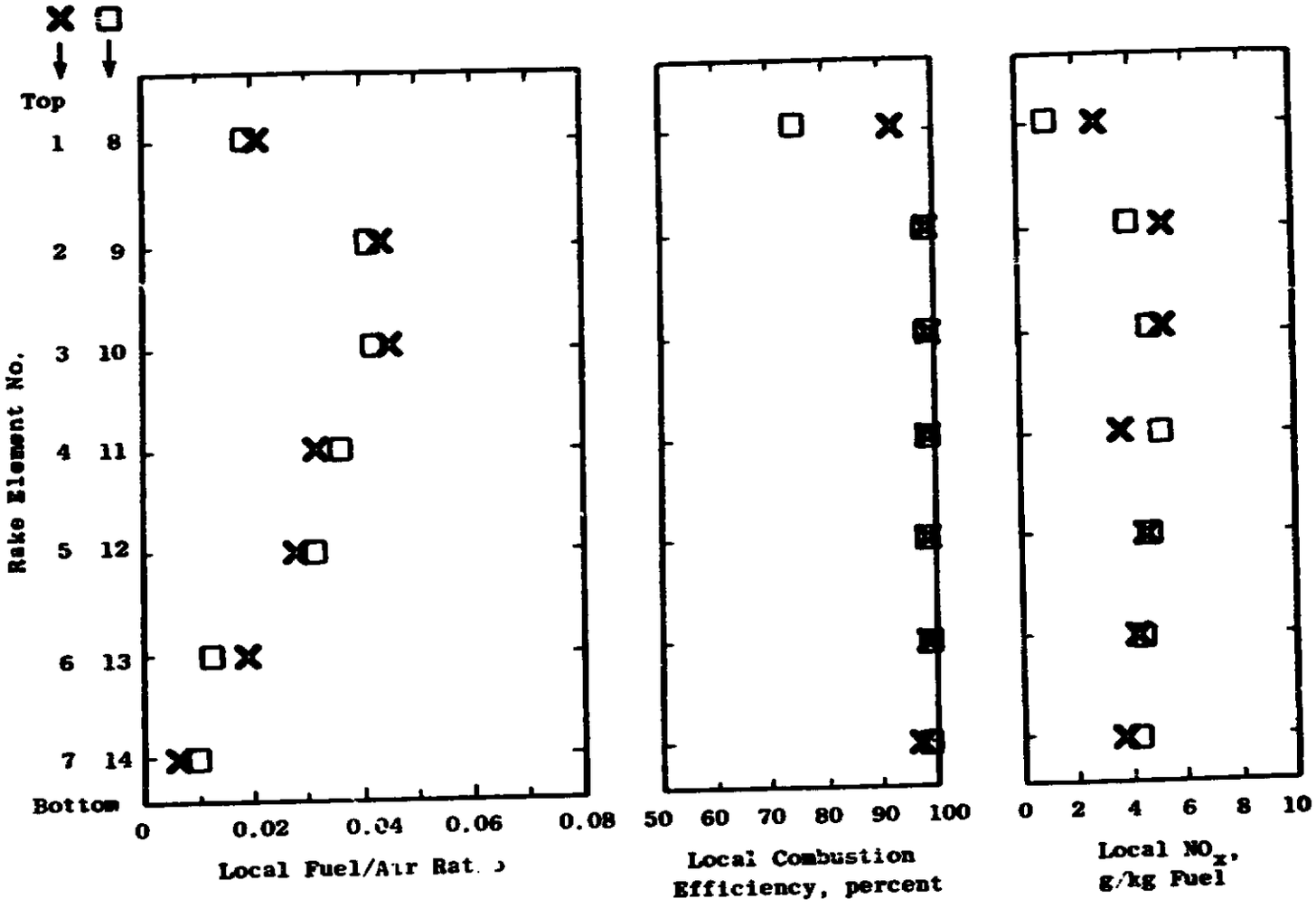

Figure 41. Duct Burner Exit Profiles, Configuration 6, Reading 107, Supersonic Cruise Condition, T = 584 K, P = 261 kPa, Metered Overall F/A = 0.0209.

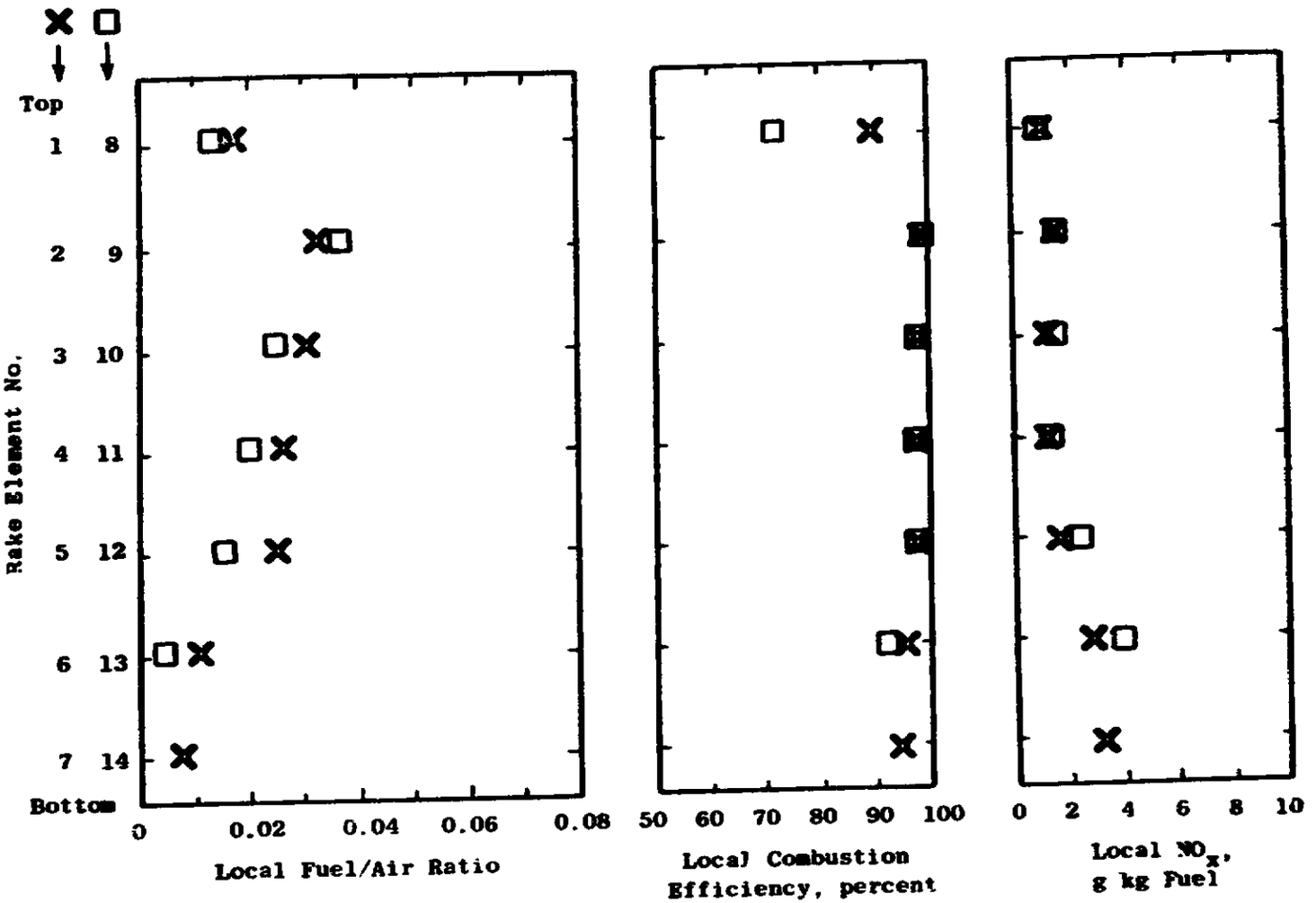

Figure 42. Duct Burner Exit Profiles, Configuration 6, Reading 108, Supersonic Cruise Condition, T = 585 K, P = 259 kPa, Metered Overall F A = 0.0165.

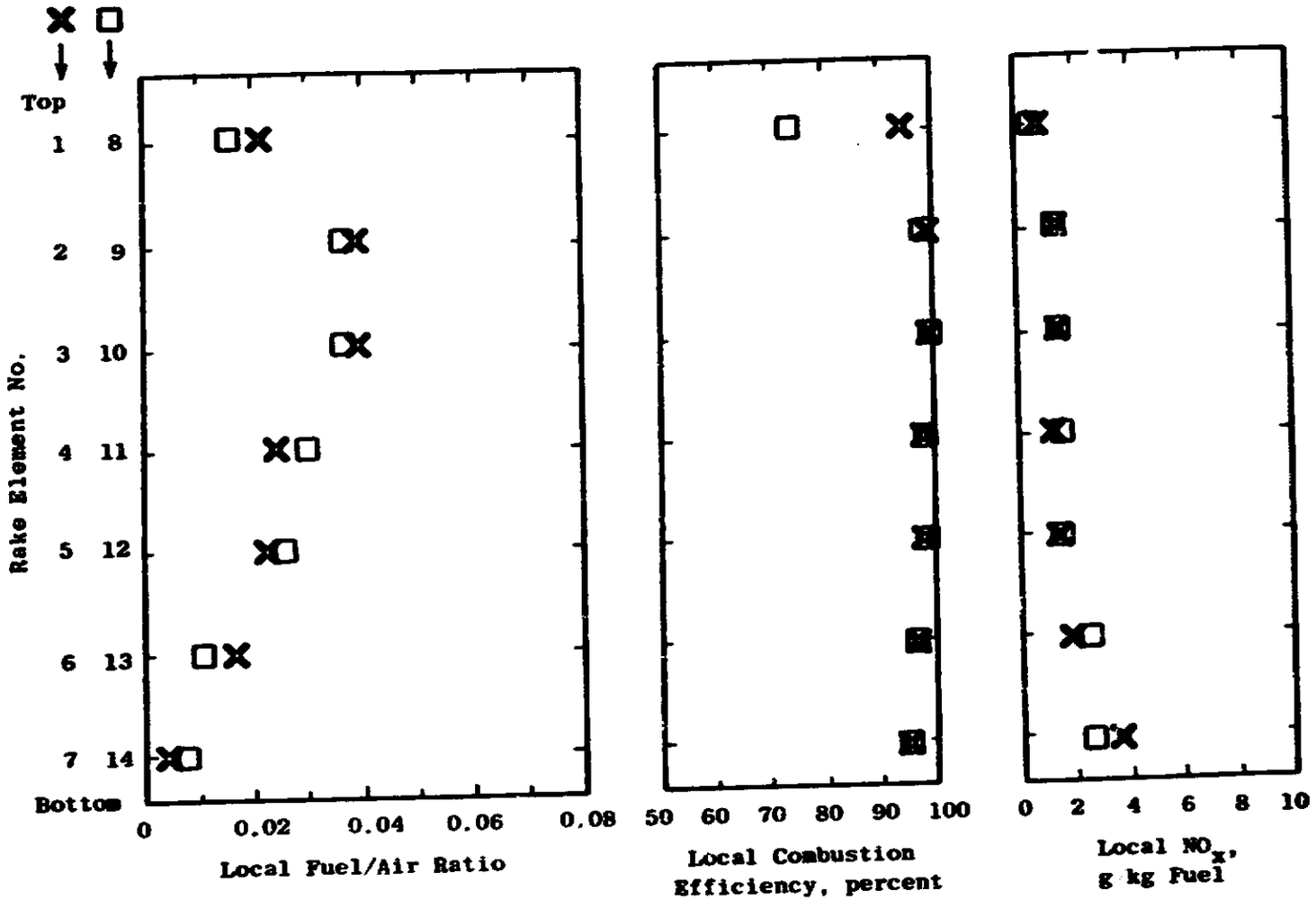

Figure 43. Duct Burner Exit Profiles, Configuration 8, Reading 111, Supersonic Cruise Condition, T = 590 K, P = 260 kPa, Metered Overall F/A = 0.0164.

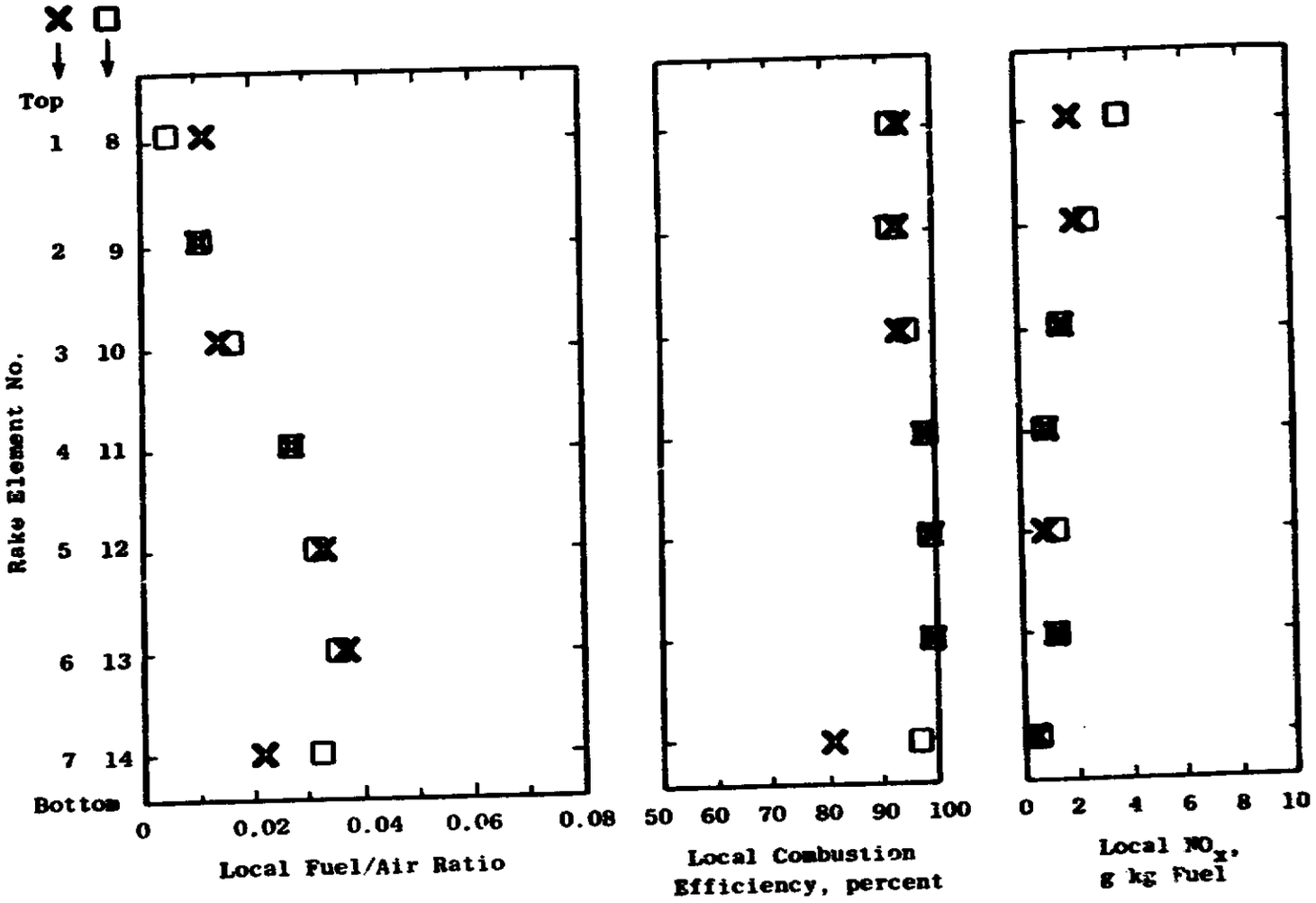

Figure 44. Duct Burner Exit Profiles, Configuration 8, Reading 112, Supersonic Cruise Condition, T = 594 K, P = 258 kPa, Metered Overall F A = 0.0180.

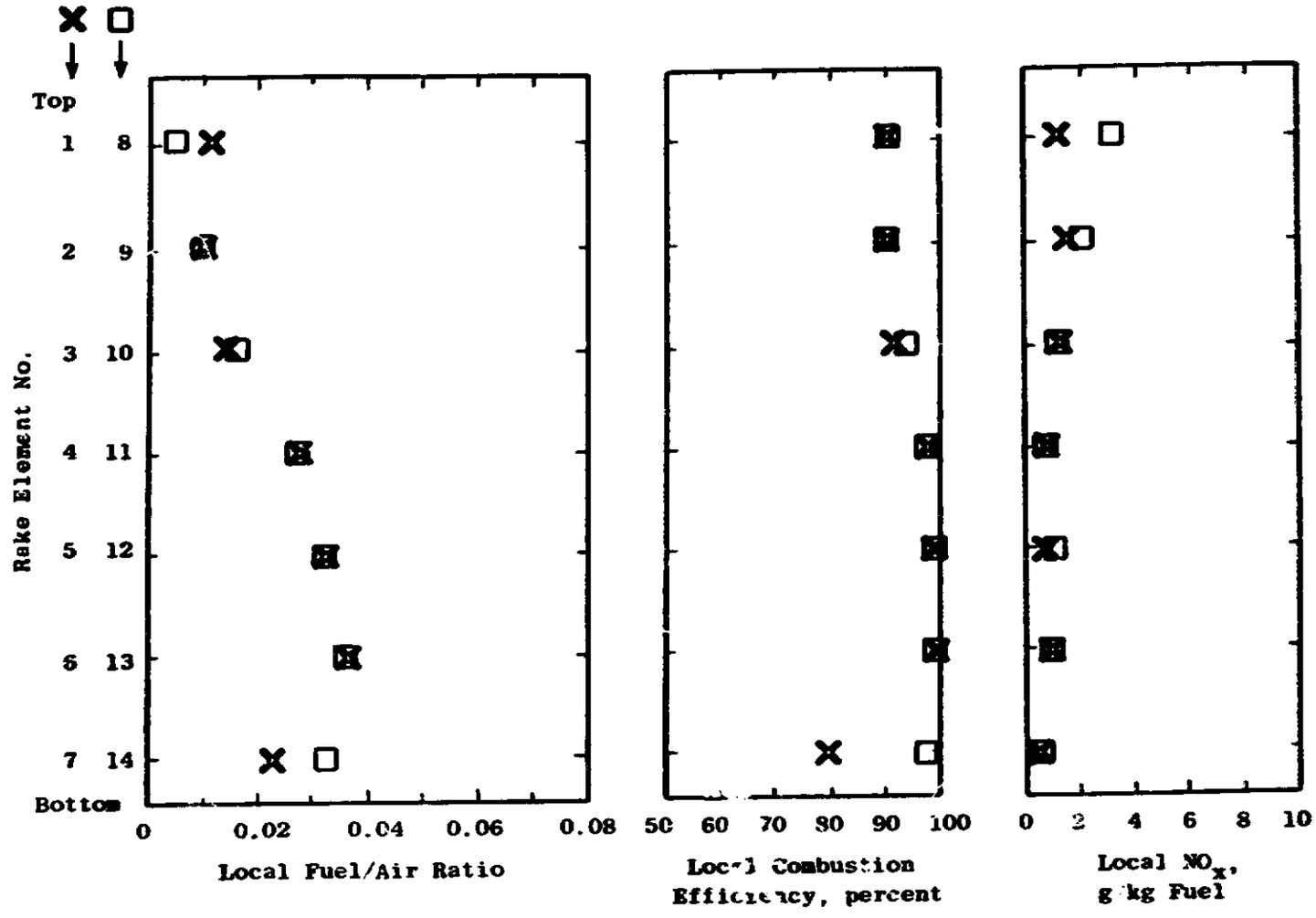

Figure 45. Duct Burner Exit Profiles, Configuration 8, Reading 113, Supersonic Cruise Condition, T = 593 K, P = 254 kPa, Metered Overall F/A = 0.0184.

Table XVI. Data Summary, Configuration 7, Performance Measured from Manifolded Gas Samples.

RDG	PT6 KPA	TT6 K	V REF M/S	DP/P	F/A UNDER LINER PILOT	UPPER	LOWER	TOTAL	FTOT MET	FTOT SAMP	FTA PCT	TT148 K	EI, G/KG CO	HC	FUEL- NOX
115	115.	375.	37.53	0.1084	0.0045	0.	0.	0.0044	0.0034	0.0026	78.72	489.	157.02	175.17	3.93
116	265.	598.	46.82	0.0790	0.	0.	0.	0.	0.			598.			
117	264.	602.	47.18	0.0795	0.0022	0.	0.	0.0022	0.0017	0.0017	99.18	670.	10.26	5.85	5.78
118	261.	592.	47.20	0.0850	0.0037	0.	0.	0.0036	0.0028	0.0029	99.11	703.	29.59	2.06	6.20
119	261.	594.	47.33	0.0838	0.0049	0.	0.	0.0049	0.0038	0.0042	98.93	744.	41.45	1.07	4.55
120	262.	595.	47.21	0.0897	0.0022	0.	0.0189	0.0212	0.0165	0.0182	93.81	1162.	68.30	45.95	1.11
121	261.	593.	47.09	0.0886	0.0037	0.	0.0176	0.0212	0.0165	0.0179	93.44	1158.	74.98	48.11	1.20
122	261.	592.	47.45	0.0898	0.0049	0.	0.0162	0.0211	0.0164	0.0178	92.98	1151.	80.58	51.35	1.29
124	261.	591.	46.99	0.0904	0.0050	0.	0.0188	0.0238	0.0185	0.0202	95.75	1232.	62.66	27.92	1.87
125	261.	593.	47.08	0.0893	0.0037	0.	0.0200	0.0236	0.0184	0.0203	96.29	1235.	57.87	23.57	1.84
126	261.	592.	47.00	0.0904	0.0023	0.	0.0214	0.0238	0.0185	0.0206	96.71	1241.	52.05	20.78	2.19
138	259.	594.	35.64	0.0466	0.0050	0.	0.0135	0.0186	0.0145	0.0150	88.98	1073.	94.26	88.25	1.42
139	260.	595.	35.58	0.0467	0.0051	0.	0.0160	0.0212	0.0165	0.0172	92.40	1153.	76.39	58.20	1.59
140	260.	595.	36.08	0.0482	0.0051	0.	0.0212	0.0263	0.0205	0.0214	97.93	1313.	35.40	12.46	3.12
141	260.	595.	35.27	0.0458	0.0051	0.	0.0254	0.0306	0.0238	0.0260	99.28	1425.	22.61	1.93	7.56
142	260.	597.	23.24	0.0182	0.0052	0.	0.0133	0.0189	0.0147	0.0150	91.54	1095.	77.91	55.43	1.83
143	260.	595.	23.32	0.0193	0.0052	0.	0.0167	0.0221	0.0172	0.0180	95.59	1195.	51.32	32.14	2.27
144	261.	592.	58.98	0.1483	0.0050	0.	0.0162	0.0212	0.0165	0.0175	88.59	1128.	104.56	89.58	0.94
145	261.	591.	58.98	0.1537	0.0049	0.	0.0210	0.0259	0.0202	0.0219	93.84	1273.	79.63	42.99	1.53

Table XVII. Data Summary, Configuration 10, Performance Measured from Manifolded Gas Samples.

RDG	PT6 KPA	TT6 K	V REF M/S	DP/P	F/A UNDER LINER PILOT	UPPER	LOWER	TOTAL	FTOT MET	FTOT SAMP	ETA PCT	TT148 K	EI, G/KG CO	HC	FUE. NOX
128	260.	592.	47.30	0.0879	0.0049	0.0111	0.	0.0161	0.0125	0.0156	78.54	960.	127.97	186.59	1.09
129	260.	592.	47.48	0.0898	0.0049	0.0162	0.	0.0211	0.0164	0.0212	89.29	1130.	88.41	86.44	1.22
131	261.	592.	47.24	0.0911	0.0050	0.0211	0.	0.0259	0.0202	0.0285	97.15	1298.	49.35	16.97	2.89
132	261.	592.	47.13	0.0926	0.0050	0.0253	0.	0.0300	0.0234	0.0329	98.78	1409.	39.39	7.99	7.37
134	260.	592.	47.17	0.0899	0.0050	0.0139	0.0107	0.0266	0.0207	0.0245	90.88	1269.	90.53	77.39	3.34
135	261.	593.	46.83	0.0920	0.0050	0.0128	0.0128	0.0307	0.0239	0.0292	96.18	1402.	50.58	26.37	1.01
136	260.	592.	47.03	0.0930	0.0050	0.0139	0.0137	0.0325	0.0253	0.0306	97.49	1455.	34.64	17.01	1.17
146	261.	592.	59.08	0.1596	0.0050	0.0160	0.0141	0.0349	0.0272	0.0329	97.80	1515.	34.56	13.93	1.03
148	212.	444.	41.16	0.0847	0.0050	0.	0.	0.0049	0.0038	0.0046	98.32	599.	62.30	9.22	2.81
149	209.	443.	42.04	0.0921	0.0048	0.0098	0.0096	0.0244	0.0190	0.0173	67.99	936.	264.39	258.37	3.45
150	203.	442.	43.39	0.1048	0.0048	0.0119	0.0121	0.0289	0.0225	0.0245	74.73	1070.	292.72	184.37	3.24
151	220.	442.	38.91	0.0860	0.0048	0.0149	0.0150	0.0347	0.0270	0.0332	87.20	1294.	140.73	95.19	2.32
152	213.	440.	40.51	0.1009	0.0048	0.0172	0.0173	0.0394	0.0307	0.0301	93.90	1456.	85.43	41.11	0.80
153	212.	441.	41.07	0.1068	0.0047	0.0195	0.0195	0.0438	0.0341	0.0299	97.53	1592.	52.29	12.52	1.56
155	385.	462.	42.27	0.0778	0.	0.	0.	0.	0.			462.			
156	385.	456.	41.62	0.0796	0.0049	0.	0.	0.0049	0.0038	0.0041	99.10	609.	20.07	4.32	3.99
158	382.	456.	40.67	0.0898	0.0050	0.0106	0.0106	0.0262	0.0204	0.0204	75.04	1032.	219.83	198.29	3.45
159	385.	456.	41.68	0.0898	0.0048	0.0126	0.0127	0.0302	0.0235	0.0264	84.10	1183.	136.27	127.17	3.38
160	385.	456.	41.76	0.0952	0.0049	0.0151	0.0150	0.0352	0.0274	0.0338	92.25	1360.	64.30	62.52	3.59
161	385.	456.	41.71	0.0997	0.0049	0.0178	0.0177	0.0403	0.0314	0.0385	97.70	1529.	27.04	16.67	1.32
163	384.	457.	31.35	0.0513	0.0049	0.0128	0.0126	0.0304	0.0237	0.0287	88.72	1225.	80.44	94.33	3.56
164	385.	457.	31.31	0.0525	0.0049	0.0152	0.0151	0.0353	0.0275	0.0351	95.72	1397.	40.11	33.42	3.37
165	386.	456.	31.13	0.0522	0.0049	0.0151	0.0151	0.0352	0.0274	0.0213	91.28	1353.	68.60	71.22	1.15

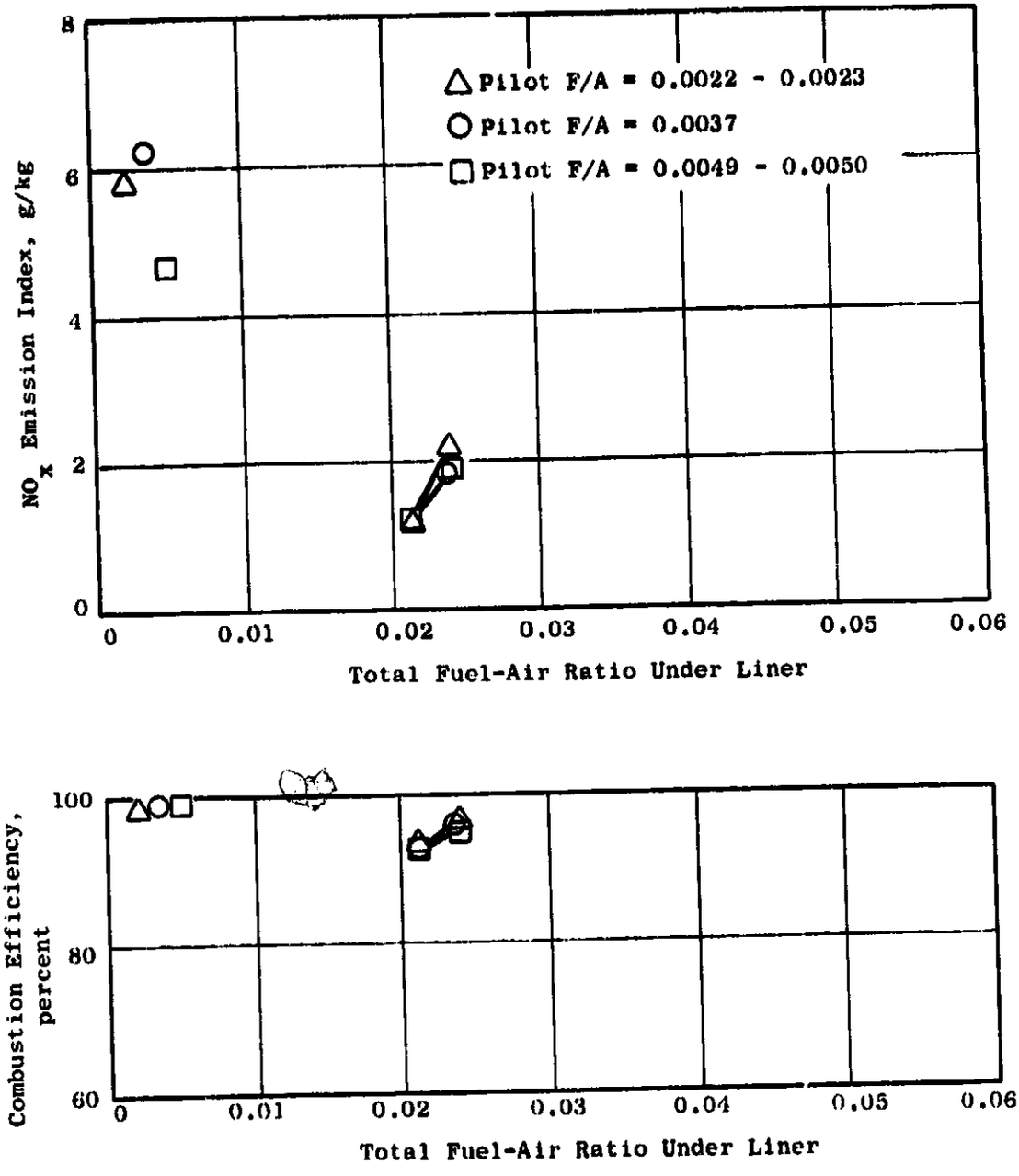

Figure 46. Configuration 7 Performance, Supersonic Cruise Condition, T = 591-602 K, P = 261-264 kPa, V_{ref} = 46.8-47.5 m/s.

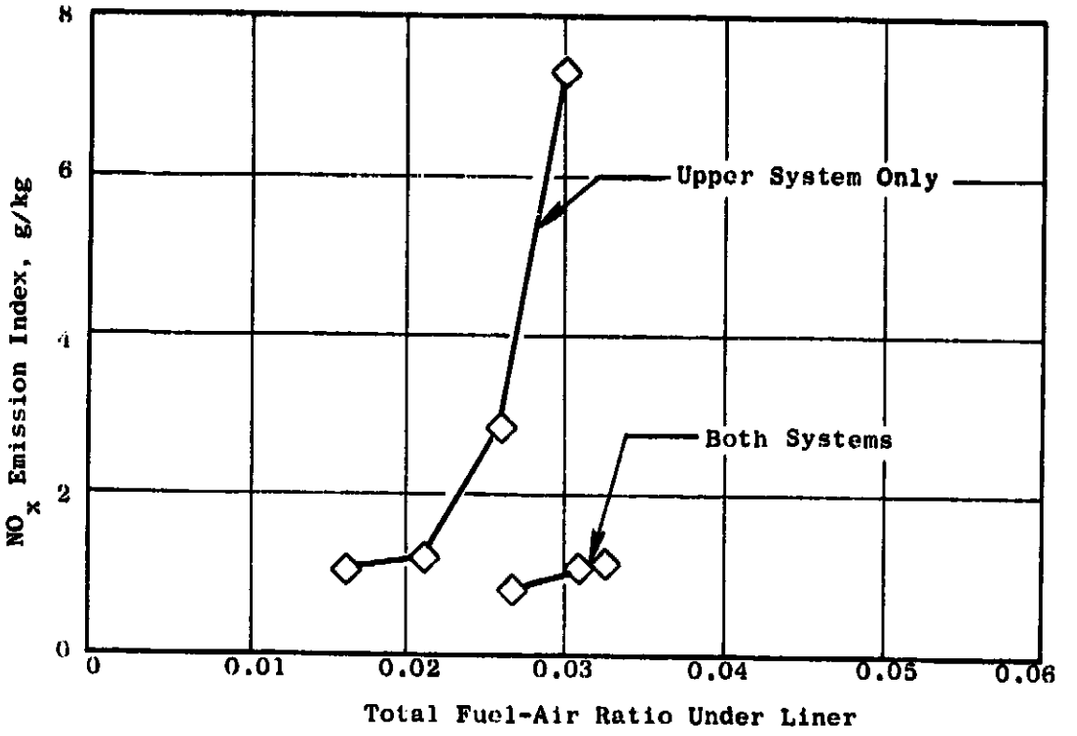

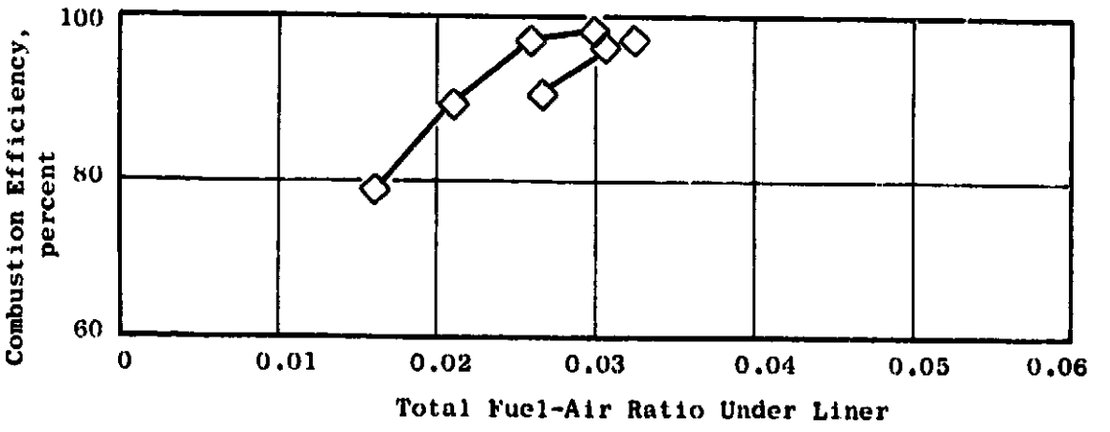

Figure 47. Configuration 10 Performance, Supersonic Cruise Condition, T = 592-593 K, P = 260-261 kPa, V_{ref} = 46.8-47.5 m/s.

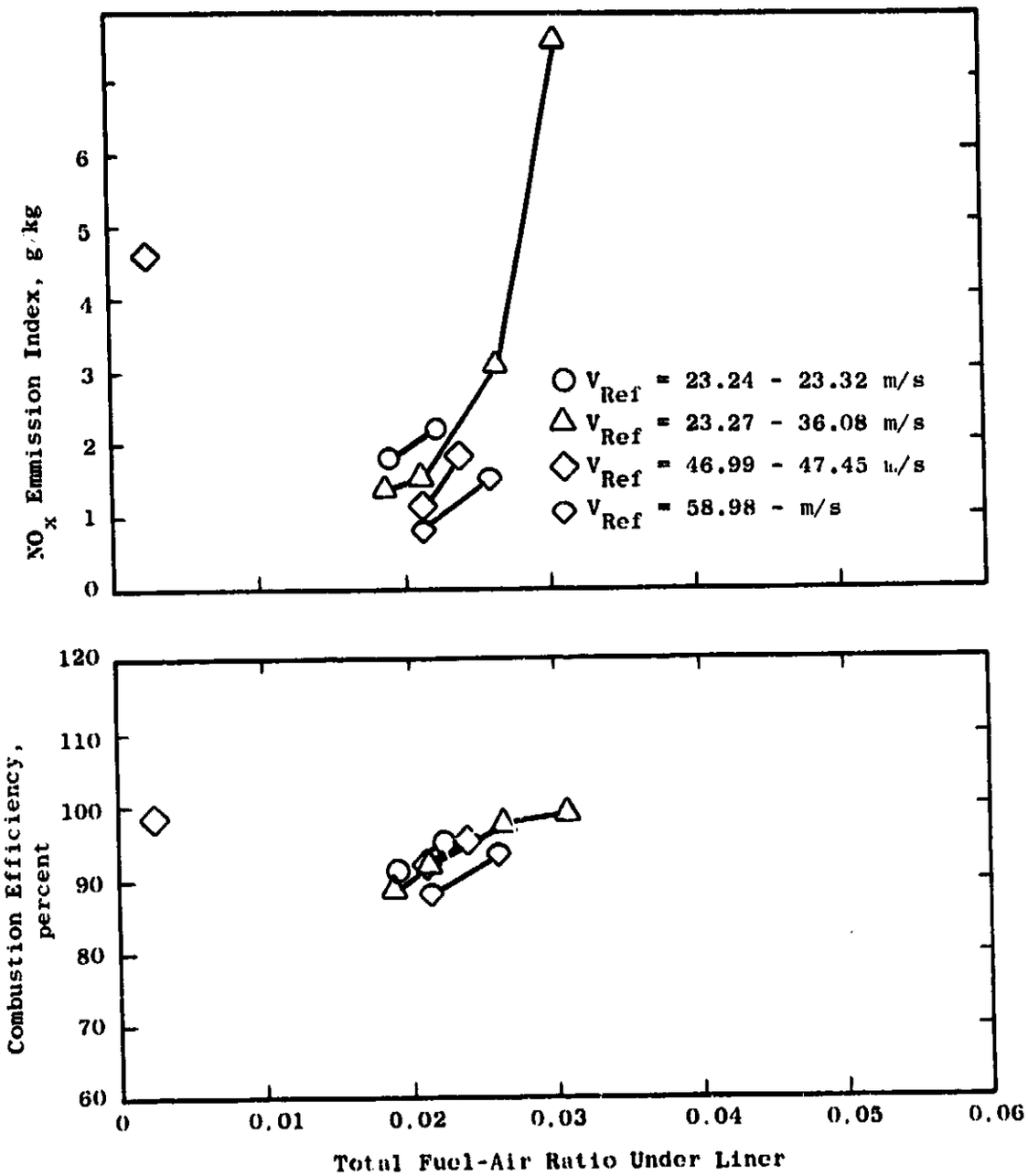

Figure 48. Configuration 7 Performance, Supersonic Cruise Condition, T = 591-597 K, P = 259-261 kPa, Pilot F/A = 0.0049-0.0052.

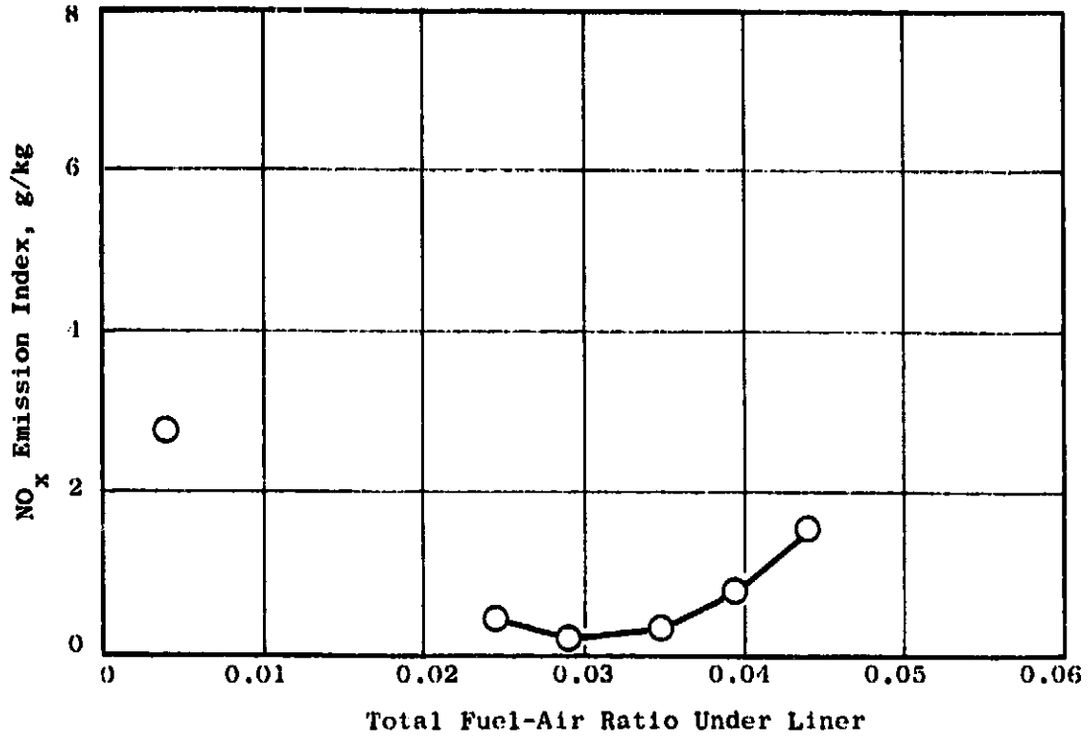

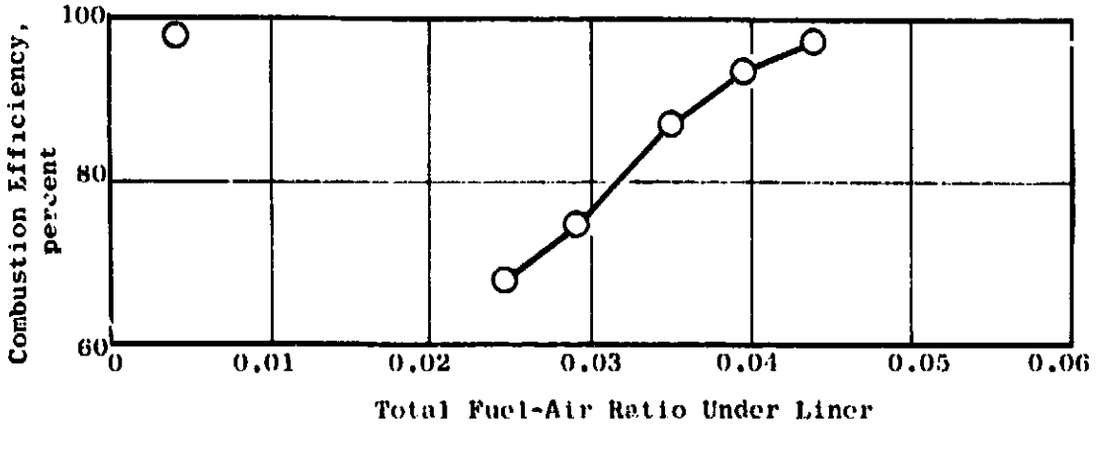

Figure 49. Configuration 10 Performance, Transonic Climb Condition, T = 440-444 k, P = 203-220 kPa, V_{ref} = 38.9-43.4 m/s, Pilot F/A = 0.0047-0.0050.

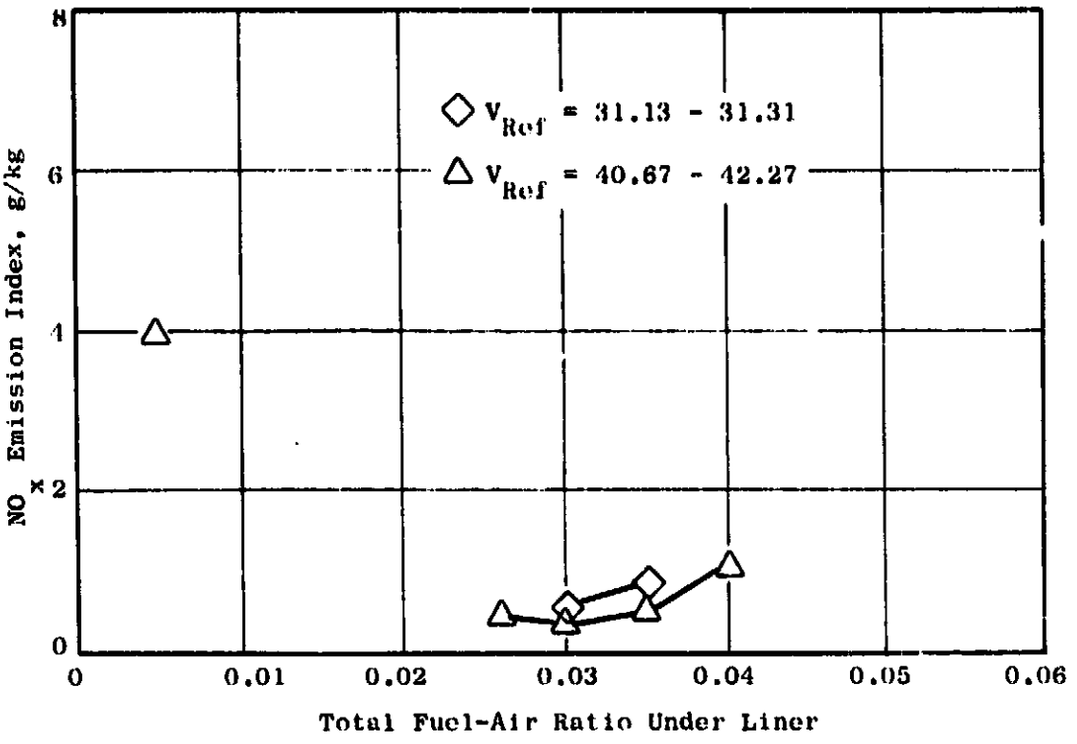

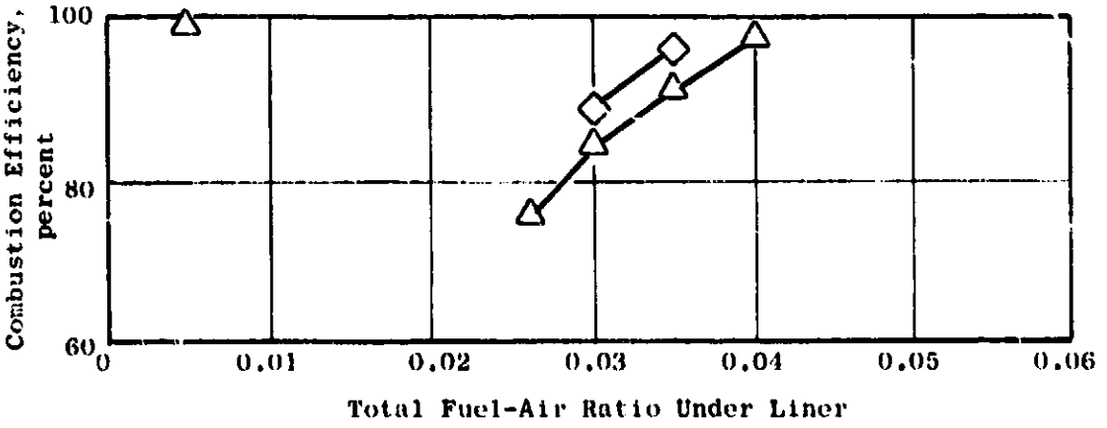

Figure 50. Configuration 10 Performance, Sea Level Takeoff Condition, T = 456-457 K, P = 382-386 kPa, Pilot F/A = 0.0048-0.0050.

Table XVIII. Data Summary, Configuration 9, Performance Measured from Manifolded Gas Samples.

RDG	PT6 KPA	TT6 K	V REF M/S	DP/P	F/A UNDER LINER PILOT	UPPER	LOWER	TOTAL	FTOT MET	FTOT SAMP	ETA PCT	TT48 K	EI, G/KG CO	HC	FUE NOX
168	267.	593.	46.65	0.0803	0.0049	0.	0.0164	0.0213	0.0166	0.0161	90.30	1141.	89.88	26.05	1.62
170	266.	593.	46.65	0.0830	0.0050	0.	0.0182	0.0232	0.0181	0.0175	93.70	1208.	68.51	47.31	1.57
172	267.	591.	46.48	0.0840	0.0049	0.	0.0216	0.0265	0.0206	0.0200	95.84	1298.	52.19	29.43	2.03
173	266.	592.	46.89	0.0867	0.0049	0.0127	0.0127	0.0302	0.0235	0.0251	95.94	1386.	46.31	29.75	1.93
174	267.	591.	46.37	0.0880	0.0050	0.0153	0.0153	0.0354	0.0276	0.0292	97.74	1522.	23.55	17.12	1.42
176	266.	592.	46.52	0.0912	0.0050	0.0177	0.0177	0.0402	0.0313	0.0336	98.74	1639.	20.00	7.97	1.35

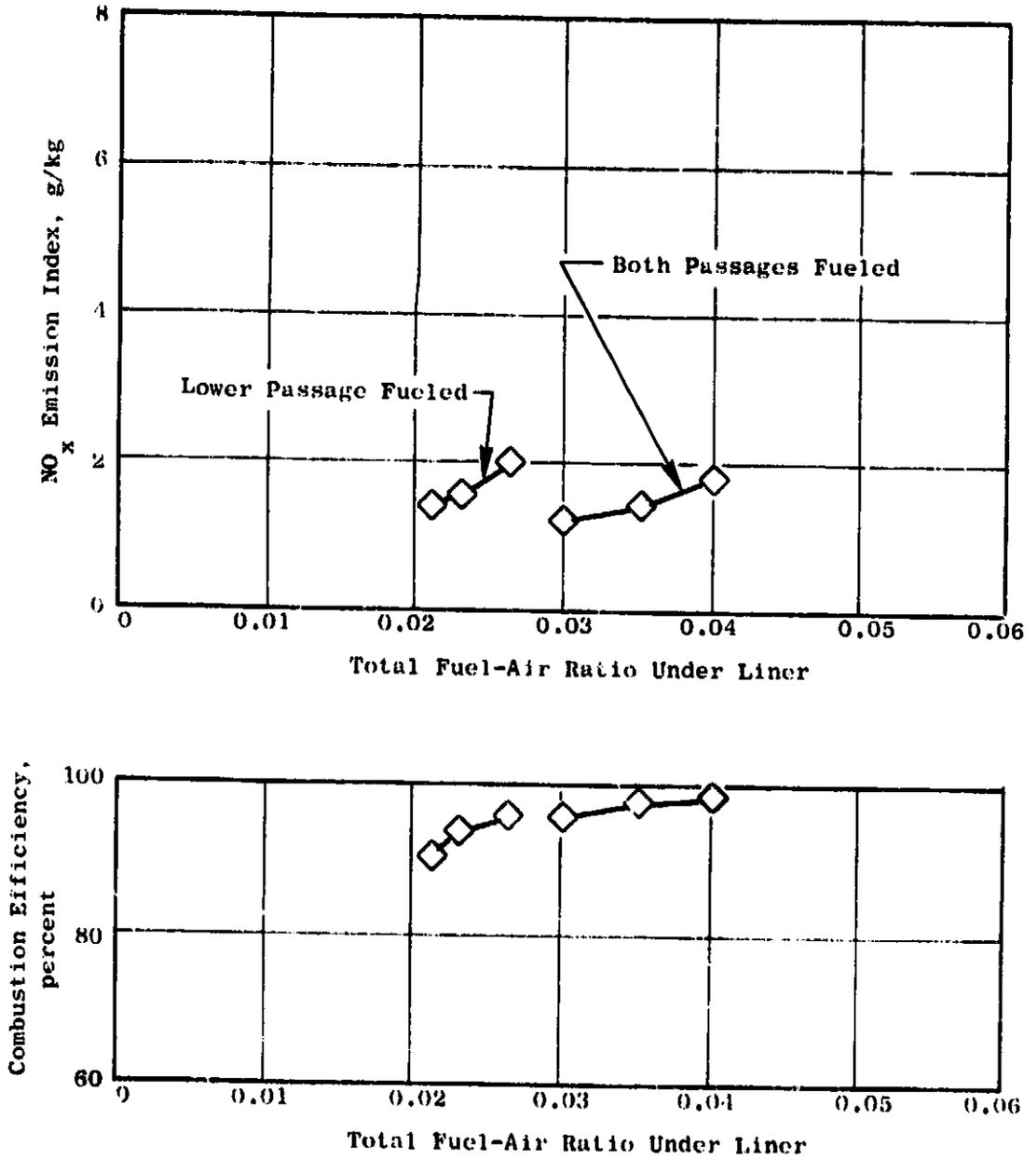

Figure 51. Configuration 9 Performance, Supersonic Cruise Condition, T = 591-593 K, P = 266-267 kPa, V_{ref} = 46.4-46.9 m/s, Pilot F/A = 0.0049-0.0050.

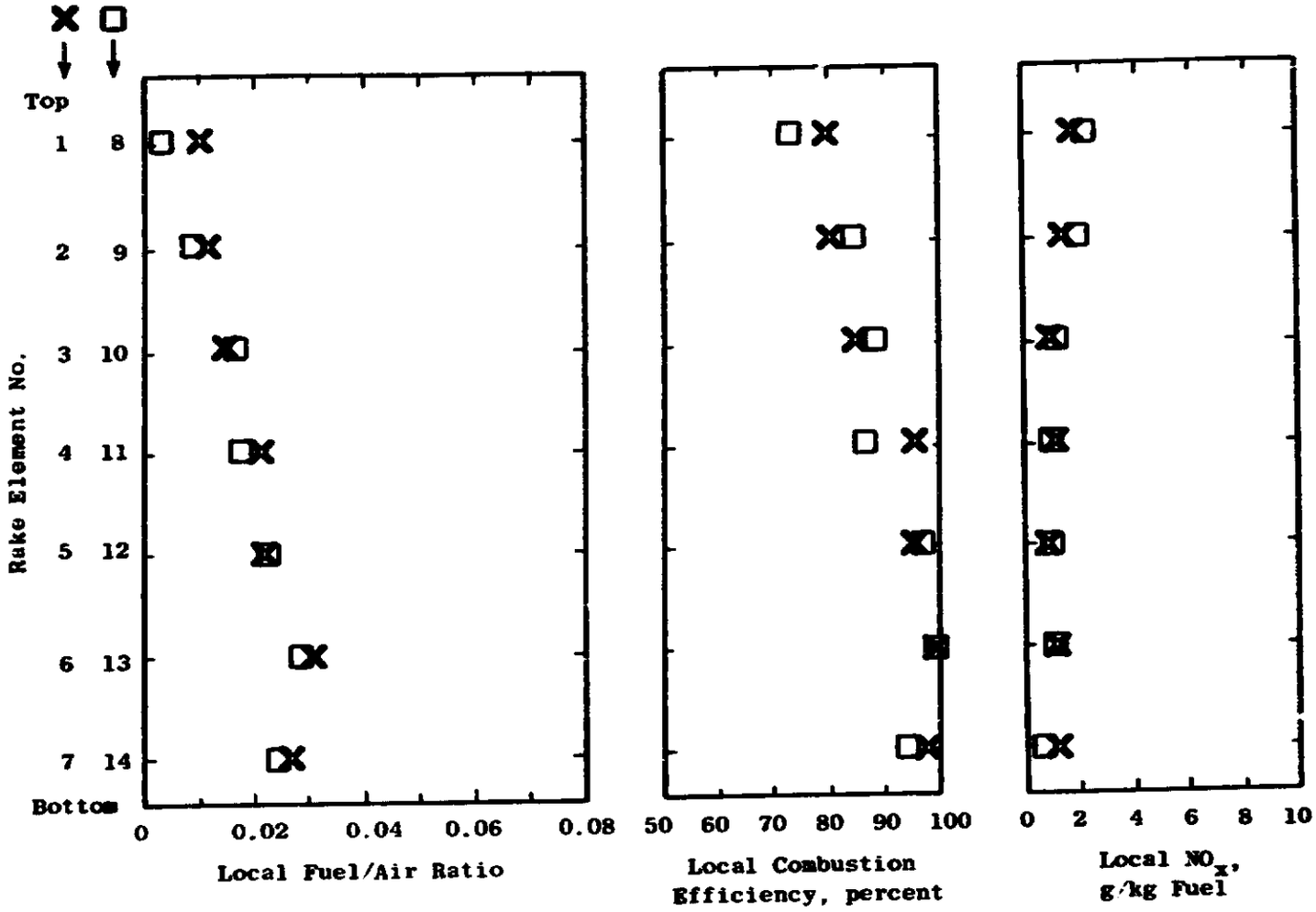

Figure 52. Duct Burner Exit Profiles, Configuration 7, Reading 123, Supersonic Cruise Condition, T = 593 K, P = 261 kPa, Metered Overall F/A = 0.0163.

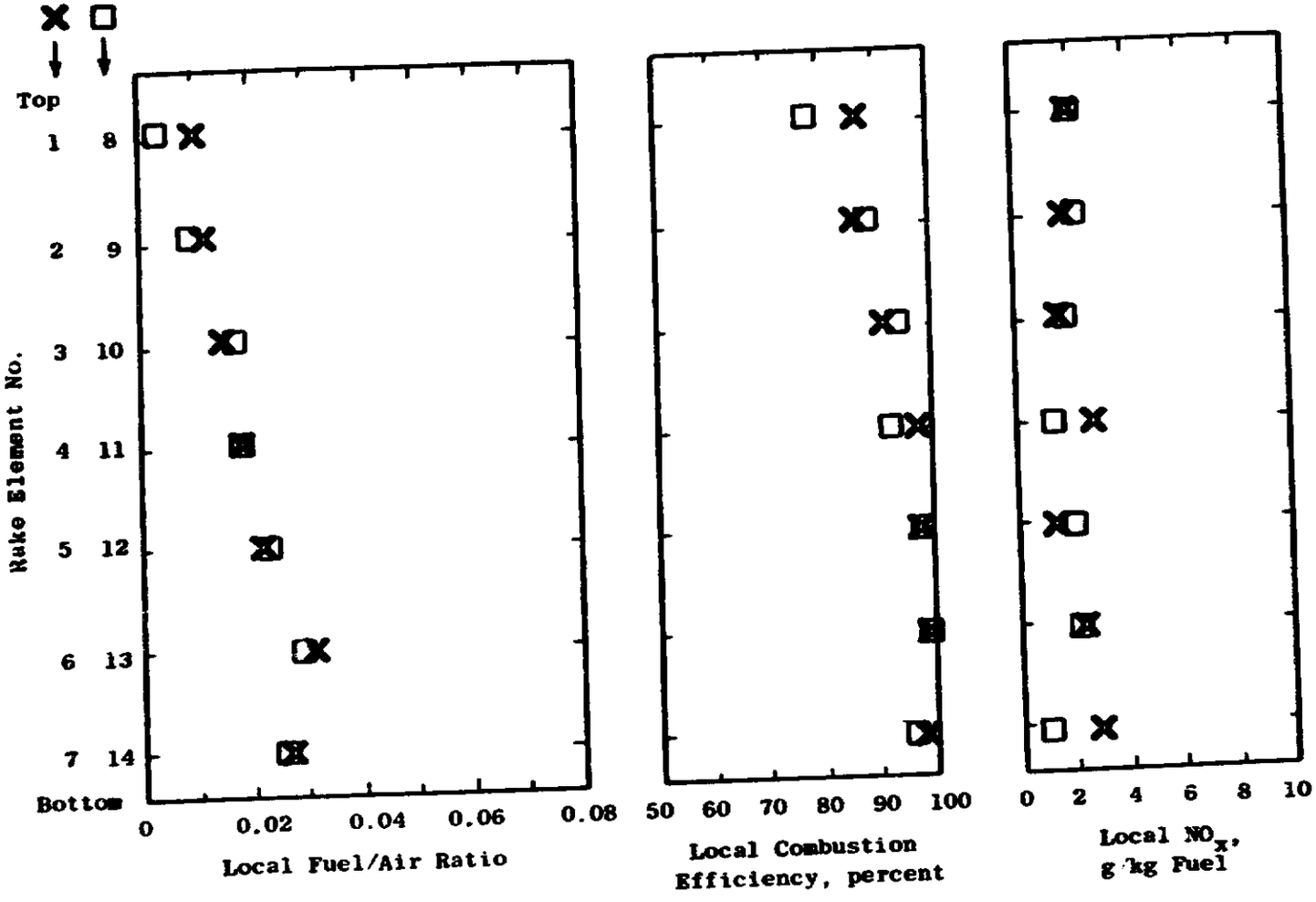

Figure 53. Duct Burner Exit Profiles, Configuration 7, Reading 127, Supersonic Cruise Condition, T = 592 K, P = 261 kPa, Metered Overall F/A = 0.0185.

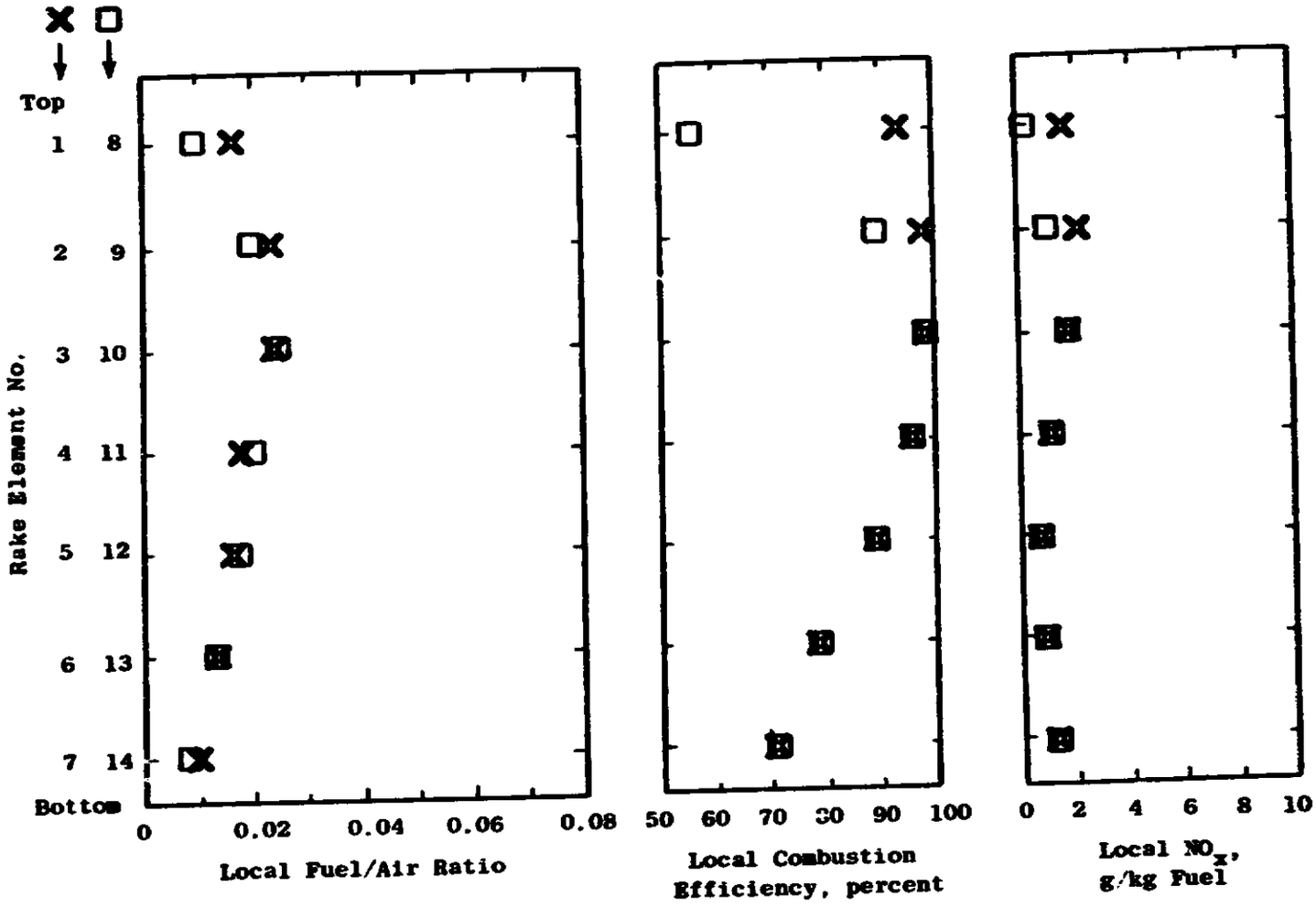

Figure 54. Duct Burner Exit Profiles, Configuration 10, Reading 130, Supersonic Cruise Condition, T = 593 K, P = 260 kPa, Metered Overall F/A = 0.0165.

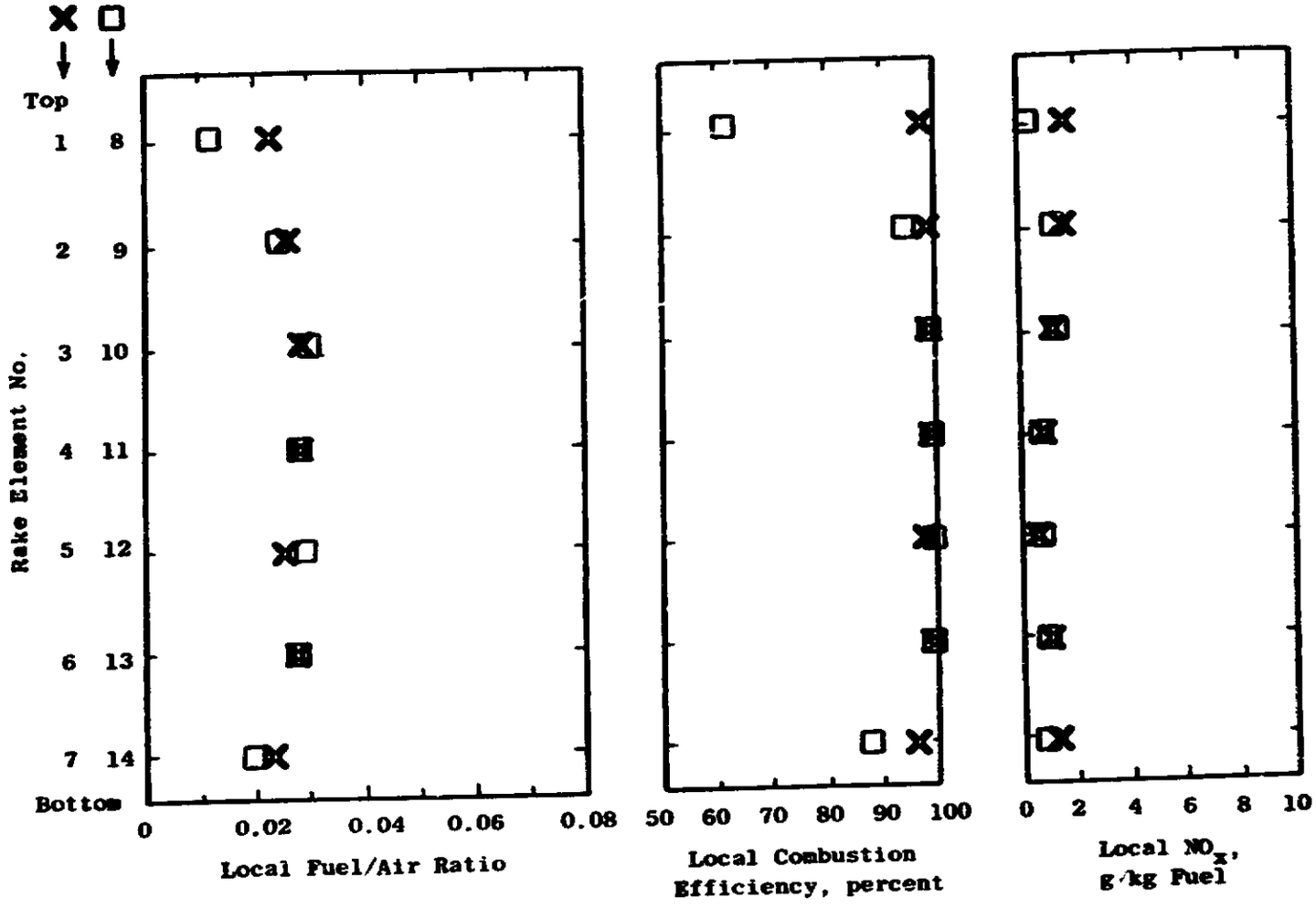

Figure 55. Duct Burner Exit Profiles, Configuration 10, Reading 137, Supersonic Cruise Condition, T = 593 K, P = 261 kPa, Metered Overall F/A = 0.0252.

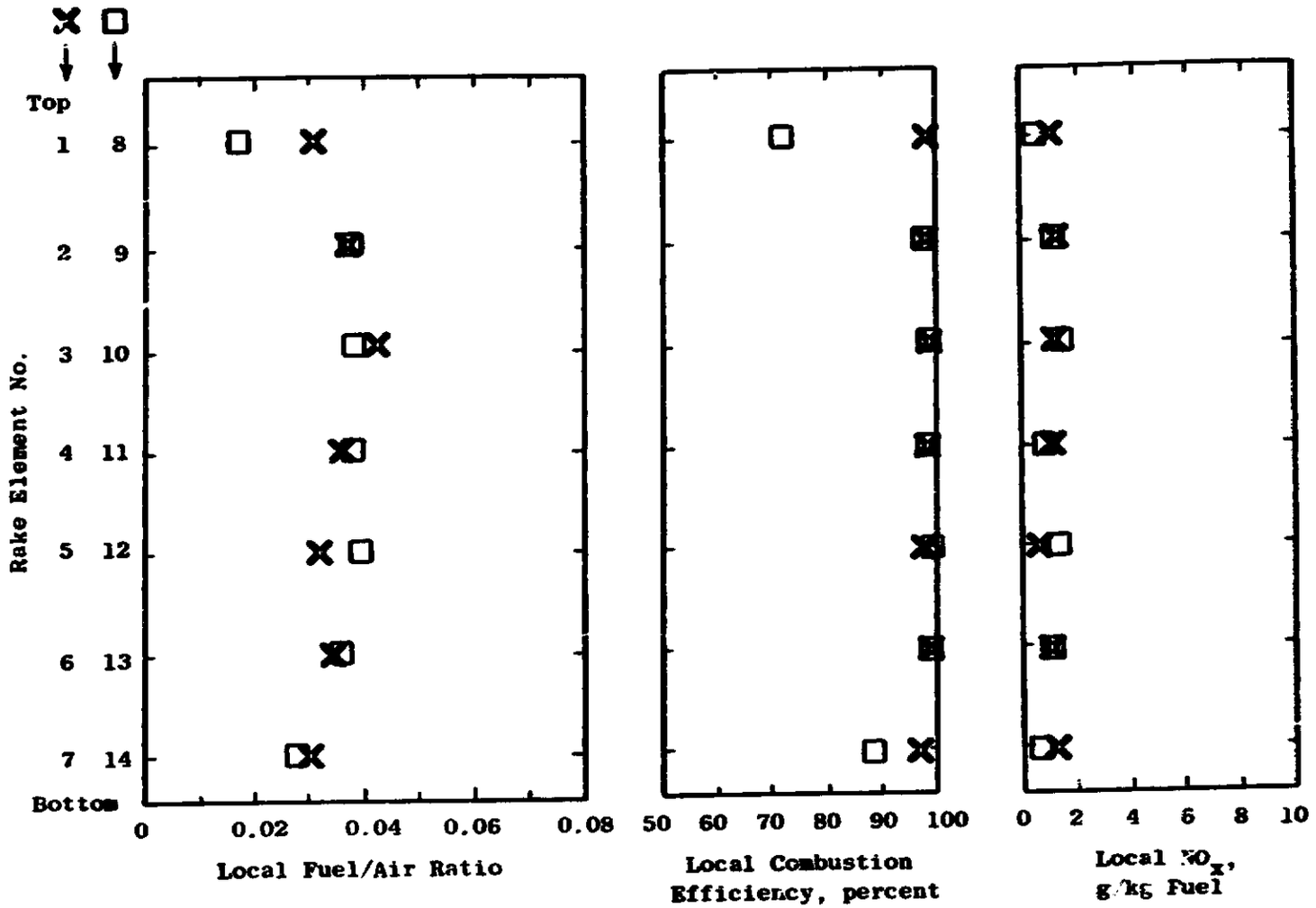

Figure 56. Duct Burner Exit Profiles, Configuration 10, Reading 154, Transonic Climb Condition, T = 442 K, P = 211 kPa, Metered Overall F/A = 0.0339.

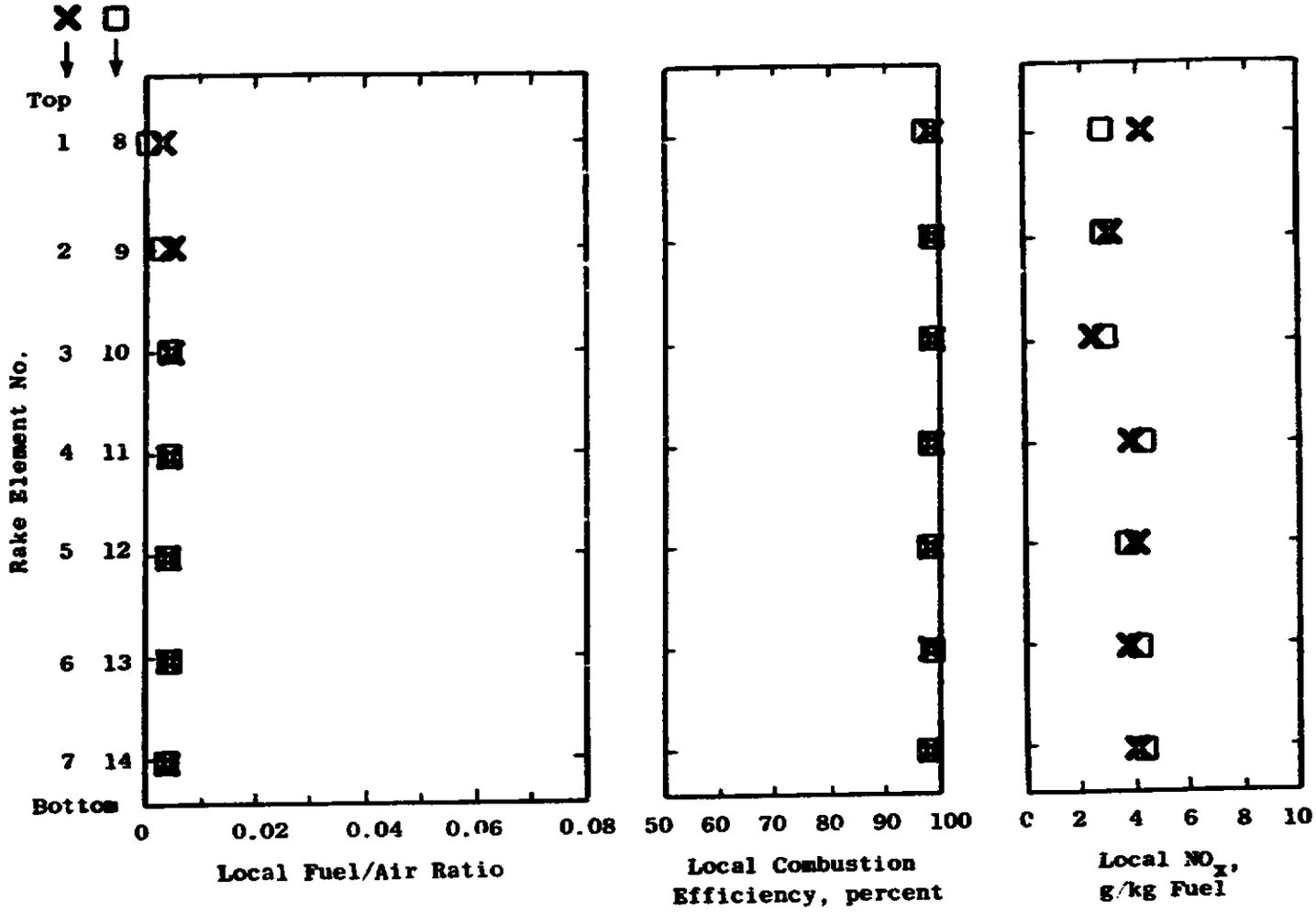

Figure 57. Duct Burner Exit Profiles, Configuration 10, Reading 157, Sea Level Takeoff Condition, T = 433 K, P = 385 kPa, Metered Overall F/A = 0.0038.

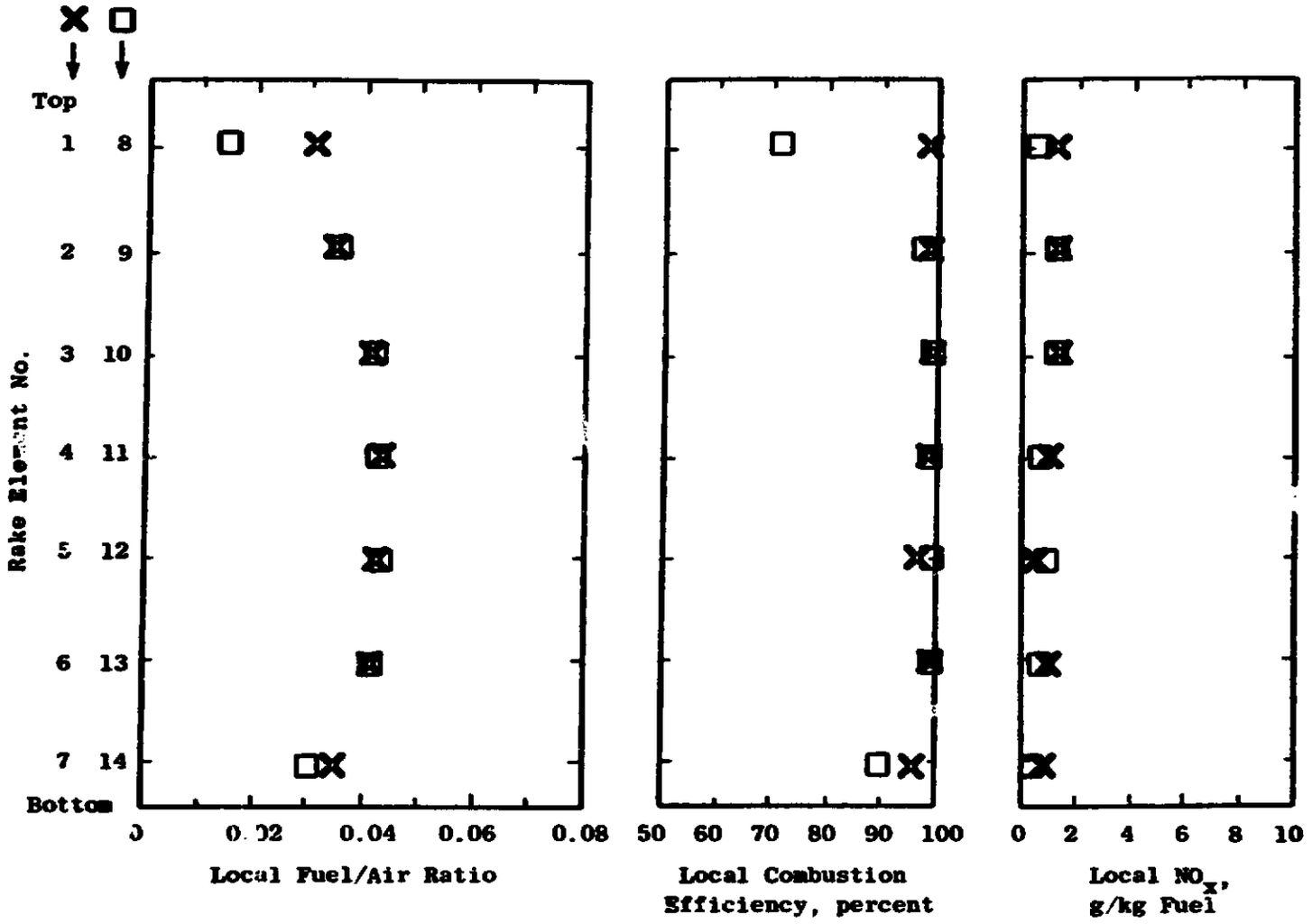

Figure 58. Duct Burner Exit Profiles, Configuration 10, Reading 162, Sea Level Takeoff Condition, T = 456 K, P = 384 kPa, Metered Overall F/A = 0.0314.

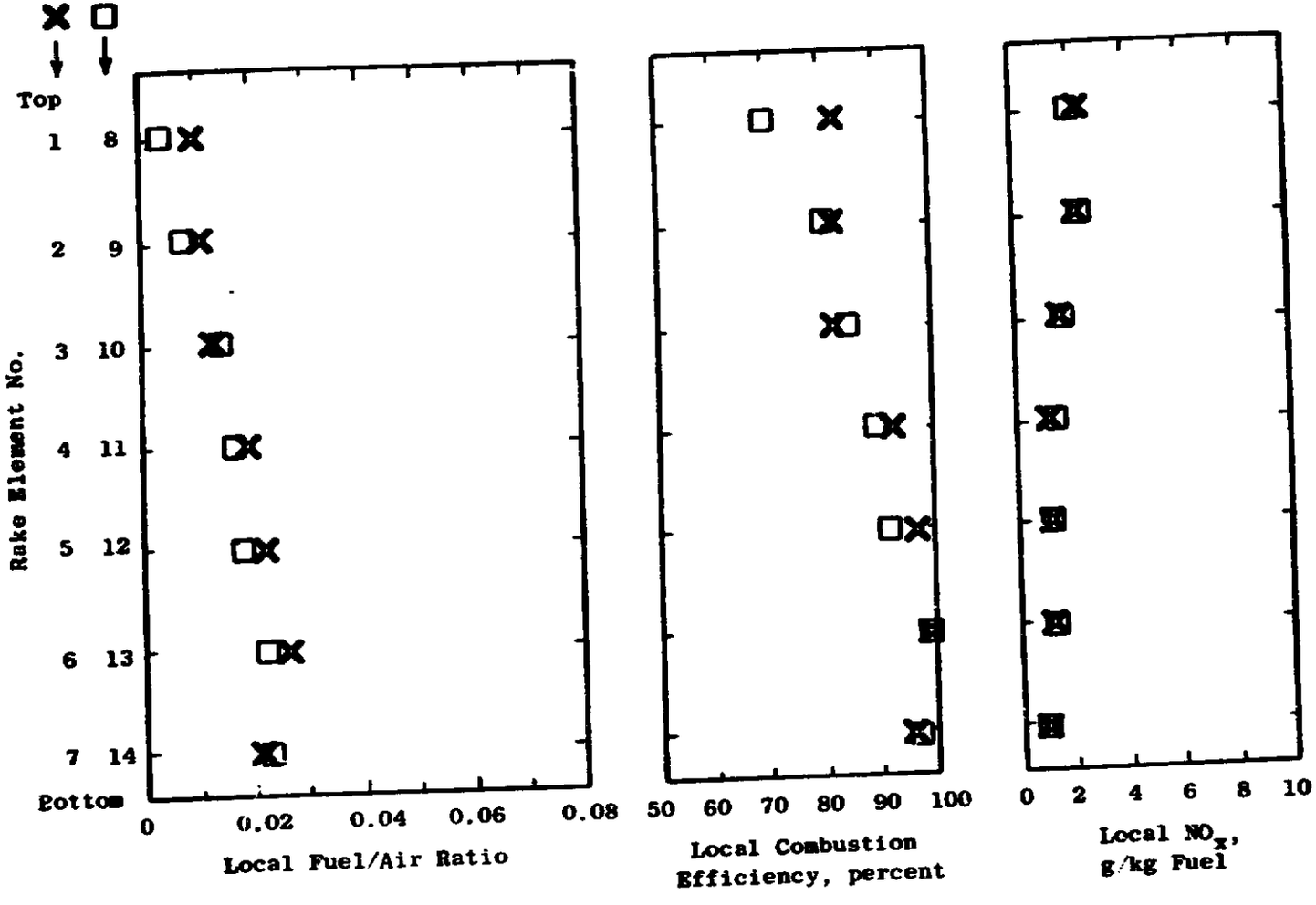

Figure 59. Duct Burner Exit Profiles, Configuration 9, Reading 169, Supersonic Cruise Condition, T = 592 K, P = 268 kPa, Metered Overall F/A = 0.0165.

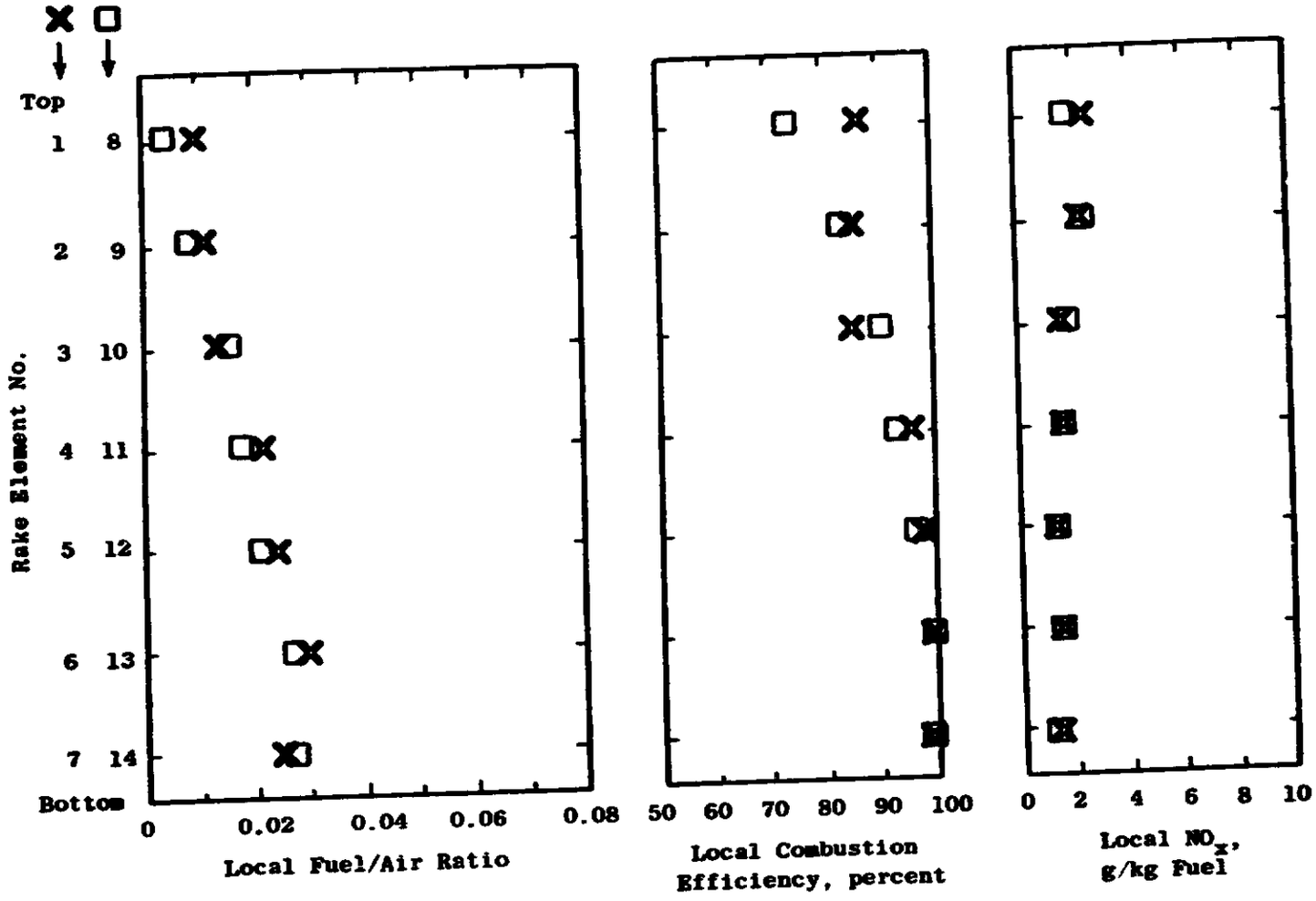

Figure 60. Duct Burner Exit Profiles, Configuration 9, Reading 171, Supersonic Cruise Condition, T = 592 K, P = 267 kPa, Metered Overall F/A = 0.0183.

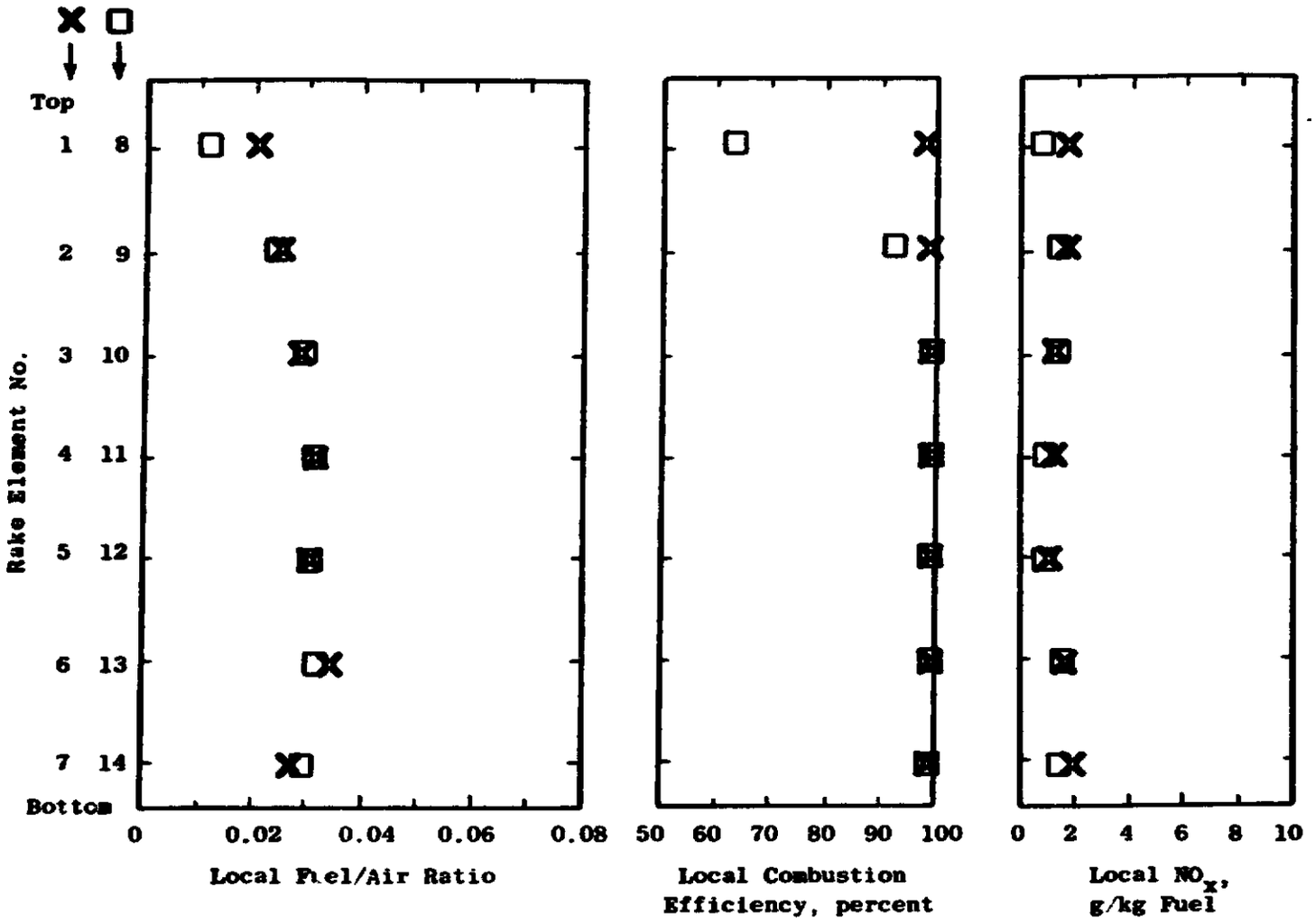

Figure 61. Duct Burner Exit Profiles, Configuration 9, Reading 175, Supersonic Cruise Condition, T = 592 K, P = 268 kPa, Metered Overall F/A = 0.0274.

to the opposite side burned less efficiently than with Configurations 6 and 8. With both flameholders fueled and the fuel/air ratio high enough for effective flame propagation, the local combustion efficiency was generally satisfactory except adjacent to the liners.

Reading 137 was taken on Configuration 10 at the supersonic cruise operating condition with both main stage flameholders carbureted equally. Figure 55 shows lean regions containing raw fuel next to the liners, even the upper liner where the small circumferential flameholder was located to assist flame spreading. When the outer four samples were disregarded, Reading 137 produced a combustion efficiency of 99.15% with CO, HC, and NO_x emission indices of 8.43, 6.54, and 1.17, respectively. The lean, inefficient region next to the upper liner could be seen in a survey made with pilot fuel only (Reading 157, Figure 57) suggesting that the cause was air intrusion downstream from the flameholders, rather than maldistribution of the main stage fuel approaching the flameholders. To determine the extent of this streak, a survey was made in Reading 165 using only the upper sampling element of each rake. The results, shown in Figure 62, indicated that the streak was confined to the upper left corner (aft looking forward) of the surveyed region of the burner exit.

Posttest inspection revealed the test hardware to be in excellent condition. The pilot liner showed evidence of a hot streak on the upper centerline opposite the igniter, but was undamaged. Some pilot nozzle flow coefficients had deteriorated as much as 28%, so that the pilot was probably operating somewhat lean in the center. Thus, the exact cause of the concentrated nature of the streak of inefficiency remains unidentified.

6.1.6 Configurations 11 and 12

Configuration 11 was tested at full pressure at all operating conditions. Emissions performance measurements made with manifolded samples are listed in Table XIX and plotted in Figures 63, 64, and 65.

Figure 63 shows the performance of Configuration 11 at the supersonic cruise operating condition, as a function of fuel distribution. Little effect of pilot fuel/air ratio was found at the nominal total fuel/air ratio, so a high pilot fuel/air ratio was selected for further testing. With only the lower main stage flameholders carbureted, the combustion efficiency appeared high and varied little with fuel/air ratios. The NO_x was much higher than measured with previous configurations at comparable fuel/air ratios, and increased steeply with fuel/air ratio. With both flameholders carbureted, NO_x was improved, but efficiency was low.

The effect of reference velocity at the supersonic cruise condition is shown in Figure 64. The intermediate velocity data are the same as Figure 63, and the other data were acquired later. A downward efficiency shift appears to have occurred in the interim. The high reference velocity produced less NO_x.

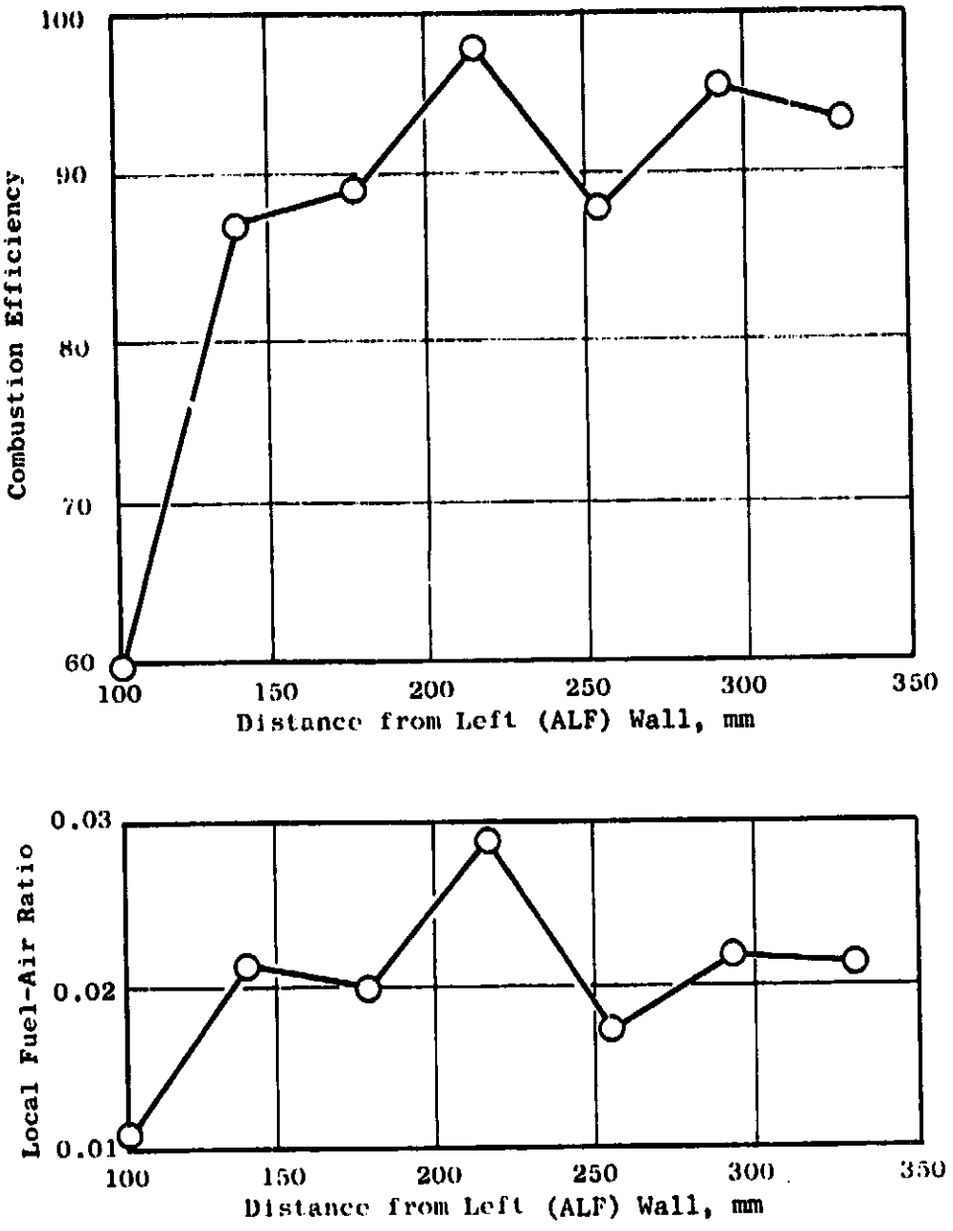

Figure 62. Duct Burner Exit Profiles, 10 mm from Upper Liner, Configuration 10, Reading 165, Sea Level Takeoff Condition, T = 456 K, P = 386 kPa, Metered Overall F/A = 0.0274.

Table XIX. Data Summary, Configuration 11, Performance Measured from Manifolded Gas Samples.

RDG	PT6 KPA	TT6 K	V REF M/S	DP/P	F/A UNDER LINER PILOT	UPPER	LOWER	TOTAL	FTOT MET	FTOT SAMP	ETA PCT	TT14B K	EI, G/KG CO	HC	FUE- NOX
177	277.	599.	45.31	0.0305	0.	0.	0.	0.	0.			589.			
178	276.	594.	44.57	0.0285	0.0031	0.	0.	0.0034	0.0029	0.0043	99.68	708.	9.02	1.12	5.24
179	275.	592.	45.43	0.0320	0.0040	0.	0.	0.0041	0.0035	0.0054	99.70	733.	10.03	1.70	5.18
180	276.	591.	45.59	0.0278	0.0049	0.	0.	0.0051	0.0043	0.0066	99.70	760.	11.00	1.40	5.30
181	274.	592.	45.95	0.0372	0.0048	0.	0.0148	0.0194	0.0164	0.0247	98.89	1186.	19.75	6.46	3.87
182	275.	593.	45.74	0.0342	0.0040	0.	0.0158	0.0194	0.0164	0.0240	98.56	1185.	22.14	9.27	4.35
183	274.	593.	45.72	0.0351	0.0030	0.	0.0169	0.0196	0.0166	0.0243	97.19	1182.	31.35	20.76	3.82
184	262.	592.	48.20	0.0396	0.0059	0.	0.0137	0.0194	0.0164	0.0239	98.82	1185.	20.66	7.72	3.85
185	260.	591.	48.13	0.0396	0.0050	0.	0.0177	0.0224	0.0189	0.0275	99.19	1269.	22.70	7.77	6.22
186	258.	591.	48.52	0.0427	0.0050	0.	0.0208	0.0254	0.0215	0.0309	98.84	1347.	46.11	7.85	9.64
187	258.	592.	47.39	0.0373	0.0050	0.	0.0122	0.0170	0.0144	0.0209	97.65	1114.	29.59	16.58	2.53
189	259.	592.	48.11	0.0403	0.0050	0.0123	0.0127	0.0298	0.0252	0.0266	84.02	1339.	94.49	137.71	1.38
190	259.	591.	47.56	0.0427	0.0051	0.0148	0.0150	0.0348	0.0294	0.0346	89.71	1501.	76.20	85.12	1.99
191	259.	593.	36.90	0.0186	0.0050	0.	0.0146	0.0196	0.0166	0.0229	96.65	1181.	27.08	27.19	4.26
192	262.	594.	35.76	0.0123	0.0051	0.	0.0120	0.0173	0.0146	0.0197	94.73	1106.	46.86	61.75	2.27
193	260.	592.	60.69	0.0682	0.0049	0.	0.0146	0.0194	0.0164	0.0227	97.25	1178.	35.84	19.13	1.54
194	261.	592.	60.21	0.0651	0.0050	0.	0.0118	0.0168	0.0142	0.0197	94.28	1088.	62.23	42.53	1.29
195	165.	446.	53.25	0.0635	0.	0.	0.	0.	0.			446.			
196	209.	448.	42.12	0.0332	0.0050	0.	0.	0.0052	0.0044	0.0061	98.90	625.	22.86	5.73	2.33
197	209.	444.	41.26	0.0310	0.0051	0.0123	0.0124	0.0301	0.0254	0.0250	83.85	1222.	64.56	144.43	1.47
198	210.	444.	41.23	0.0472	0.0050	0.0148	0.0151	0.0349	0.0295	0.0315	85.90	1350.	103.76	116.77	1.53
199	209.	446.	41.30	0.0504	0.0052	0.0172	0.0173	0.0398	0.0336	0.0373	86.92	1469.	135.39	99.23	1.82
201	392.	454.	42.39	0.0318	0.	0.	0.	0.	0.			454.			
202	383.	454.	41.60	0.0322	0.0050	0.	0.	0.0051	0.0043	0.0060	97.27	626.	11.58	24.59	3.32
203	383.	454.	41.61	0.0393	0.0050	0.0121	0.0124	0.0295	0.0249	0.0229	82.77	1208.	57.12	158.97	1.52
204	383.	453.	42.27	0.0479	0.0049	0.0145	0.0147	0.0341	0.0288	0.0282	85.11	1330.	79.83	130.24	1.83
205	112.	366.	36.47	0.0374	0.	0.	0.	0.	0.			367.			
206	112.	367.	36.14	0.0391	0.0059	0.	0.	0.0063	0.0053	0.0083	87.74	562.	61.22	108.33	1.25

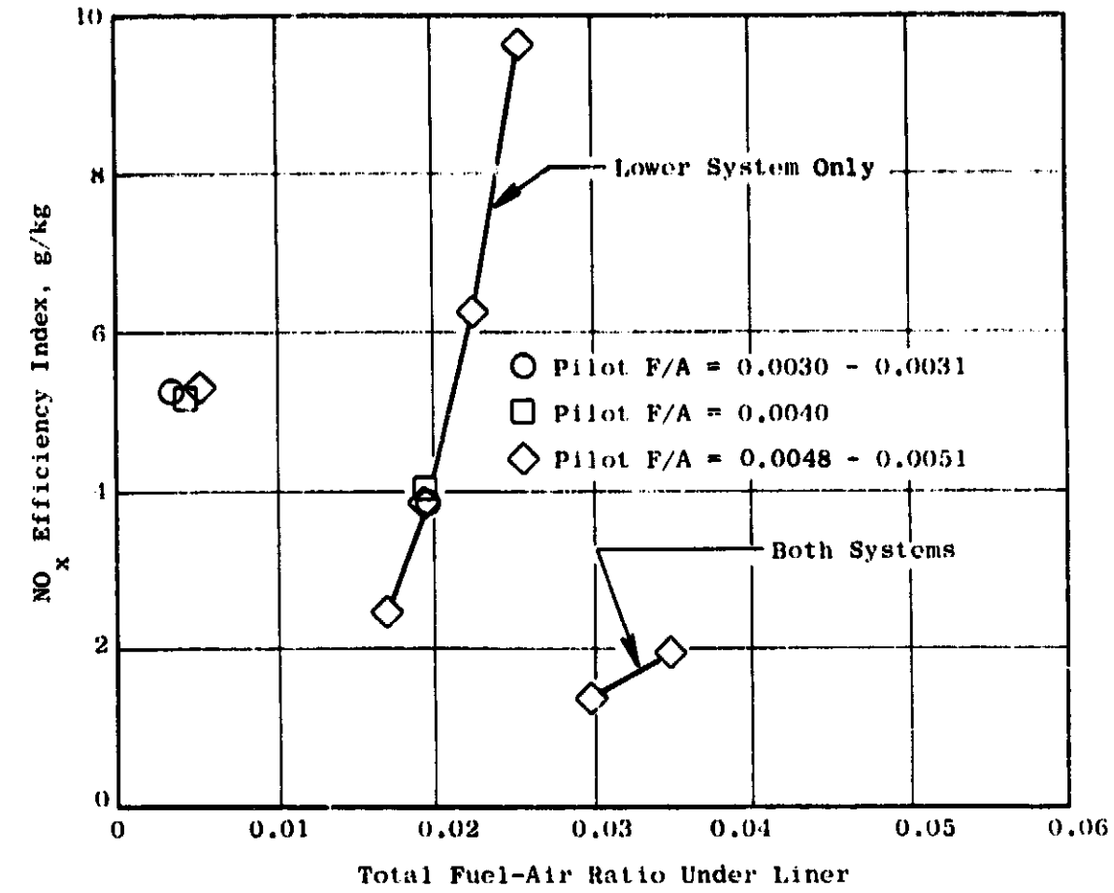

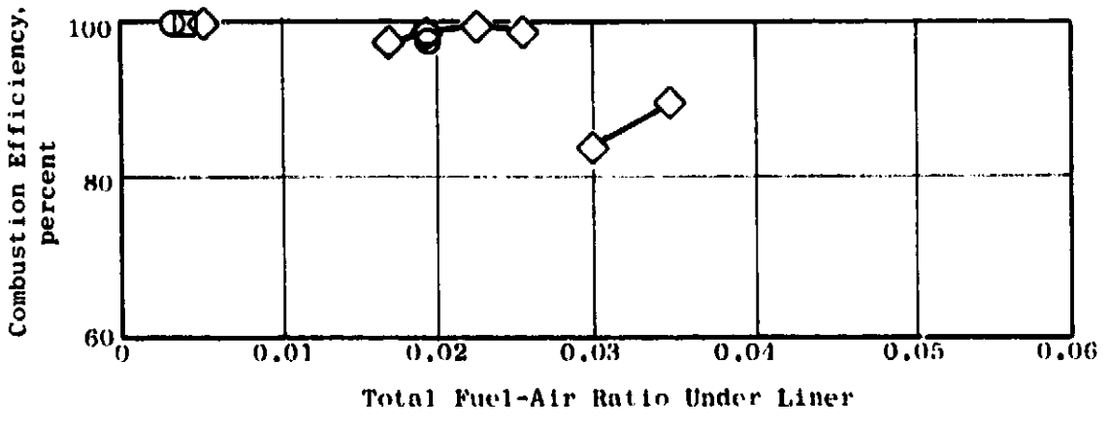

Figure 63. Configuration 11 Peformance, Supersonic Cruise Condition, T = 591-594 K, P = 258-276 kPa, V_{ref} 44.6-48.5 m/s.

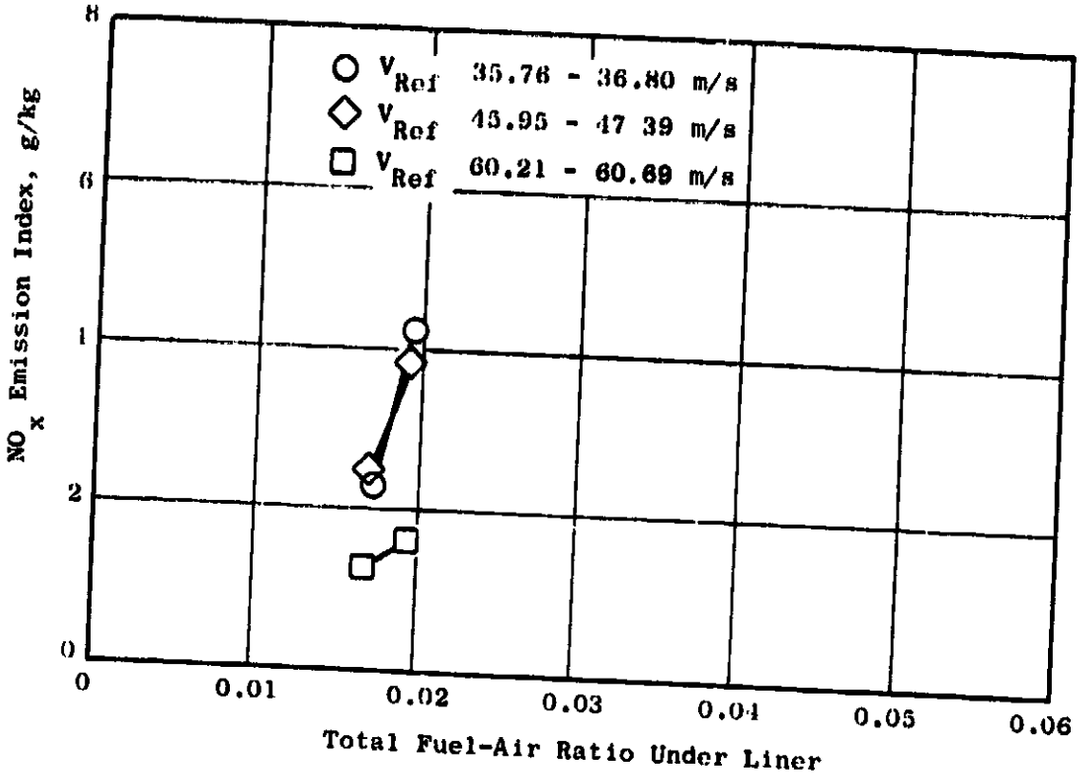

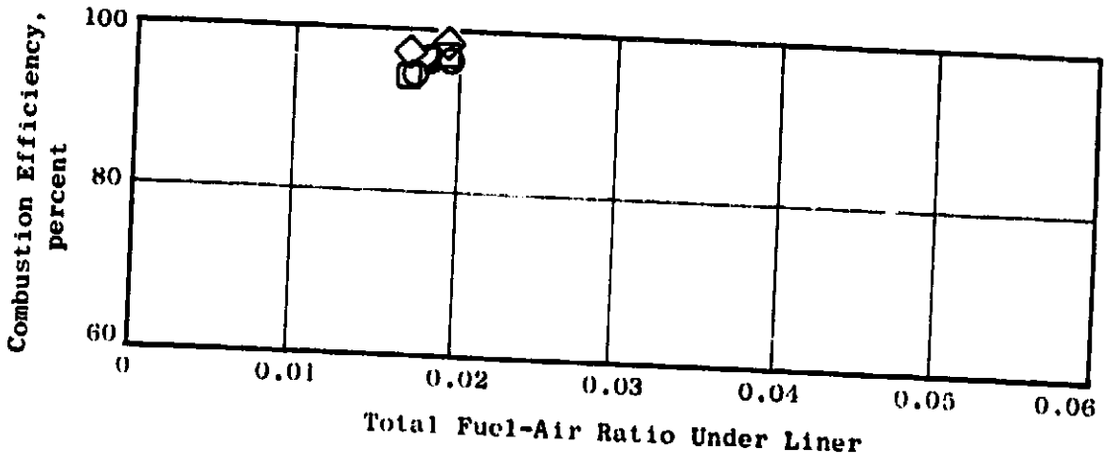

Figure 64. Configuration 11 Performance, Supersonic Cruise Condition, T = 592-594 K, P = 258-274 kPa, Pilot F/A = 0.0048-0.0051.

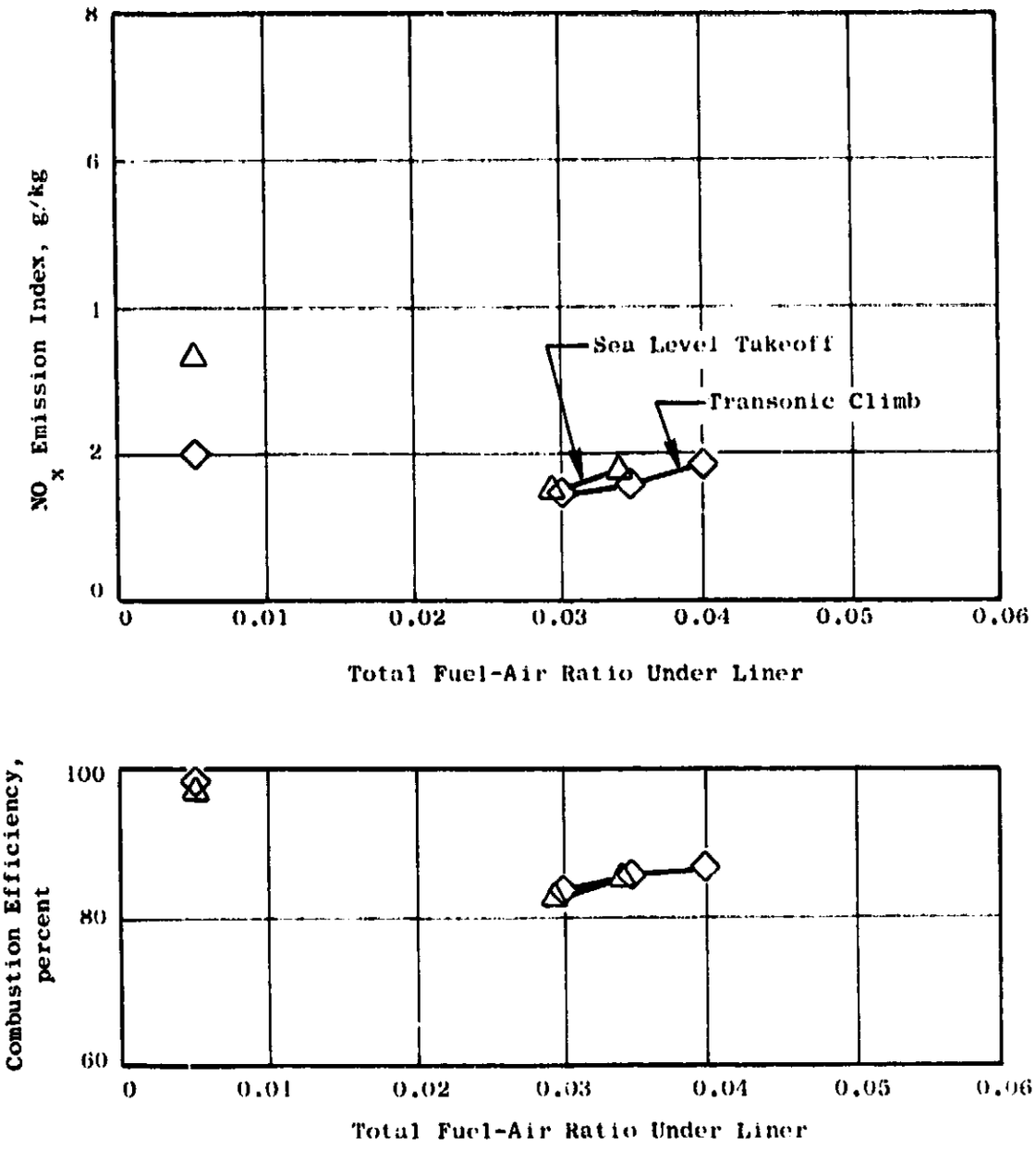

Figure 65. Configuration 11 Performance, Transonic Climb Condition, T = 444-448 K, P = 209-210 kPa, and Sea Level Takeoff Condition, T = 453-454 K, P = 383 kPa, Pilot F/A = 0.0049-0.0052.

Measurements made at the transonic climb and sea level takeoff conditions are shown in Figure 65. Combustion efficiency was poor at both conditions, and at the higher pressure, very high NO_x was measured at low fuel/air ratios. Resonance did not permit testing at total fuel/air ratios higher than 0.04.

Point sample surveys were made at two conditions. These data are included in Tables VII and VIII, and the profiles are shown in Figures 66 and 67. At the supersonic cruise condition, the point sample survey confirmed the manifolded samples, except that from two of the sample elements located 34mm from the upper liner on the uncarbureted side, the instrument responded to an apparently very rich CO streak. Since no sign of this streak was seen in nearby sample points or in manifolded samples before or after this point survey, nor in subsequent testing of Configuration 12, these two sample results cannot be considered typical of this configuration and were, therefore, omitted from the calculated averages. At the transonic climb condition, the fuel distribution on the upper flameholders was nonuniform, and the combustion efficiency was low in that area.

Configuration 12 was tested at the supersonic cruise operating condition only. The emissions performance, measured with manifolded samples, agreed closely with that of Configuration 11. These measurements are listed in Table XX and plotted in Figure 68.

Point sample surveys were made with two fuel/air ratios. These data are included in Table VIII. At the nominal cruise fuel/air ratio, with only the lower flameholders carbureted, the very heavy CO streak observed in the unfueled side of Configuration 11 was absent, as shown by the profiles in Figure 69. A raw fuel streak next to the lower liner, which the splitter plate was intended to correct, was still present. With both flameholders carbureted, combustion was inefficient in the upper part of the duct, as shown in Figure 70.

Posttest inspection revealed that most of the splitter plate had burned away, together with part of the lower circumferential flameholder from the center to within 75mm of the left wall (aft looking forward). The center radial spoke flameholder was also burned away, and a hot streak was visible on the pilot cowl extending aft from the spark igniter. This was the only configuration that showed evidence of flameholding from the igniter. Configuration 12 did not carry flameholder temperature instrumentation.

6.2 Ignition Characteristics

Altitude ignition characteristics were measured only on those configurations which included changes to the pilot design. The ignition tests were made at the altitude relight operating condition, as described previously.

For Configurations 1 and 2, an attempt was made to regulate the duct burner pressure during the ignition test, using the blast gate. It was found that a step change in pressure occurred upon ignition, requiring

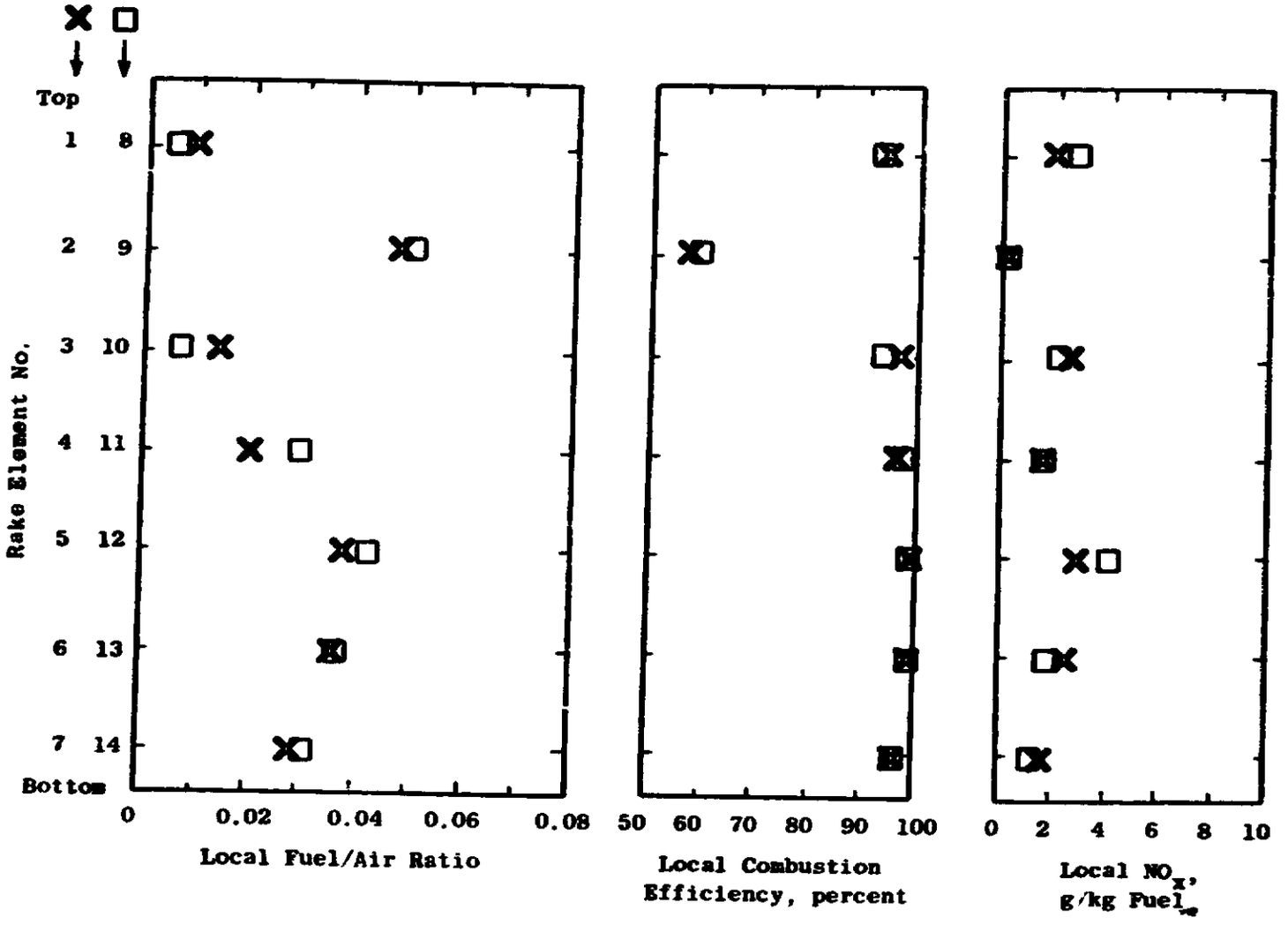

Figure 66. Duct Burner Exit Profiles, Configuration 11, Reading 188, Supersonic Cruise Condition, T = 591 K, P = 259 kPa, Metered Overall F/A = 0.0165.

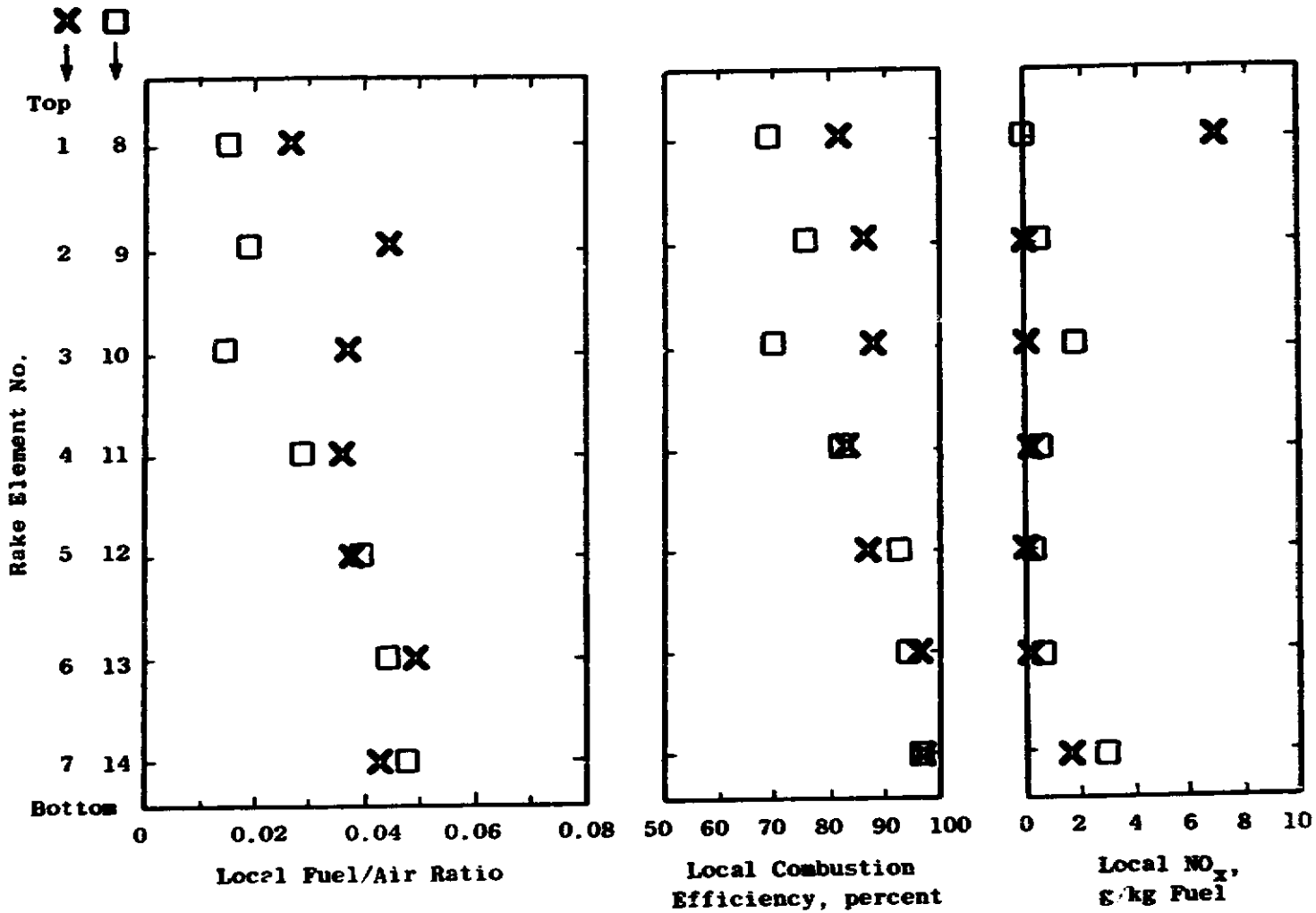

Figure 67. Duct Burner Exit Profiles, Configuration 11, Reading 200, Transonic Climb Condition, T = 445 K, P = 210 kPa, Metered Overall F/A = 0.0335.

Table XX. Data Summary, Configuration 12, Performance Measured from Manifolded Gas Samples.

RDG	PTA KPA	TT6 K	V REF M/S	DP/P	F/A UNDER LINER PILOT	UPPER	LOWER	TOTAL	FTOT MET	FTOT SAMP	FTA PCT	TT148 K	EI, G/KG FUEL CO	HC	NOX
207	264.	591.	46.55	0.0380	0.	0.	0.	0.	0.			591.			
208	262.	592.	47.09	0.0466	0.0051	0.	0.0182	0.0233	0.0197	0.0240	98.99	1293.	26.91	4.74	6.30
210	262.	592.	46.84	0.0450	0.0052	0.	0.0151	0.0203	0.0172	0.0208	98.42	1209.	22.83	10.48	3.77
211	263.	591.	47.48	0.0452	0.0050	0.	0.0118	0.0169	0.0143	0.0180	95.80	1100.	42.76	32.75	2.33
212	262.	593.	47.47	0.0434	0.0051	0.	0.0089	0.0141	0.0119	0.0156	85.93	978.	99.06	117.59	1.49
213	263.	592.	47.14	0.0395	0.0052	0.	0.	0.0051	0.0043	0.0059	99.61	763.	11.72	1.13	4.38
214	261.	593.	47.30	0.0475	0.0051	0.0129	0.0127	0.0306	0.0259	0.0250	83.43	1351.	111.10	139.78	0.93
215	261.	591.	47.36	0.0524	0.0051	0.0153	0.0150	0.0354	0.0299	0.0355	88.63	1501.	70.27	97.32	1.39

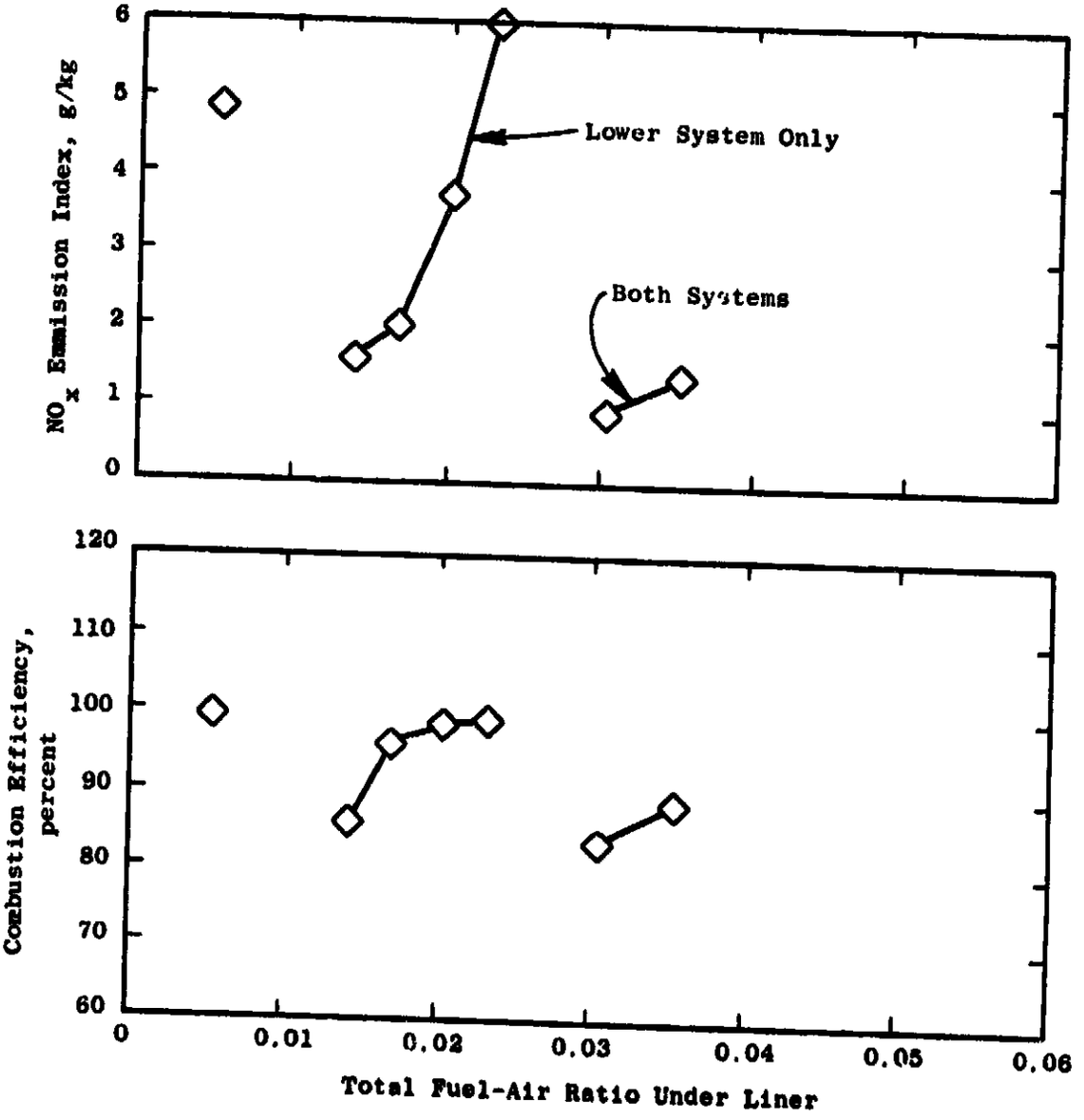

Figure 68. Configuration 12 Performance, Supersonic Cruise Condition, T = 591-593 K, P = 261-263 kPa.

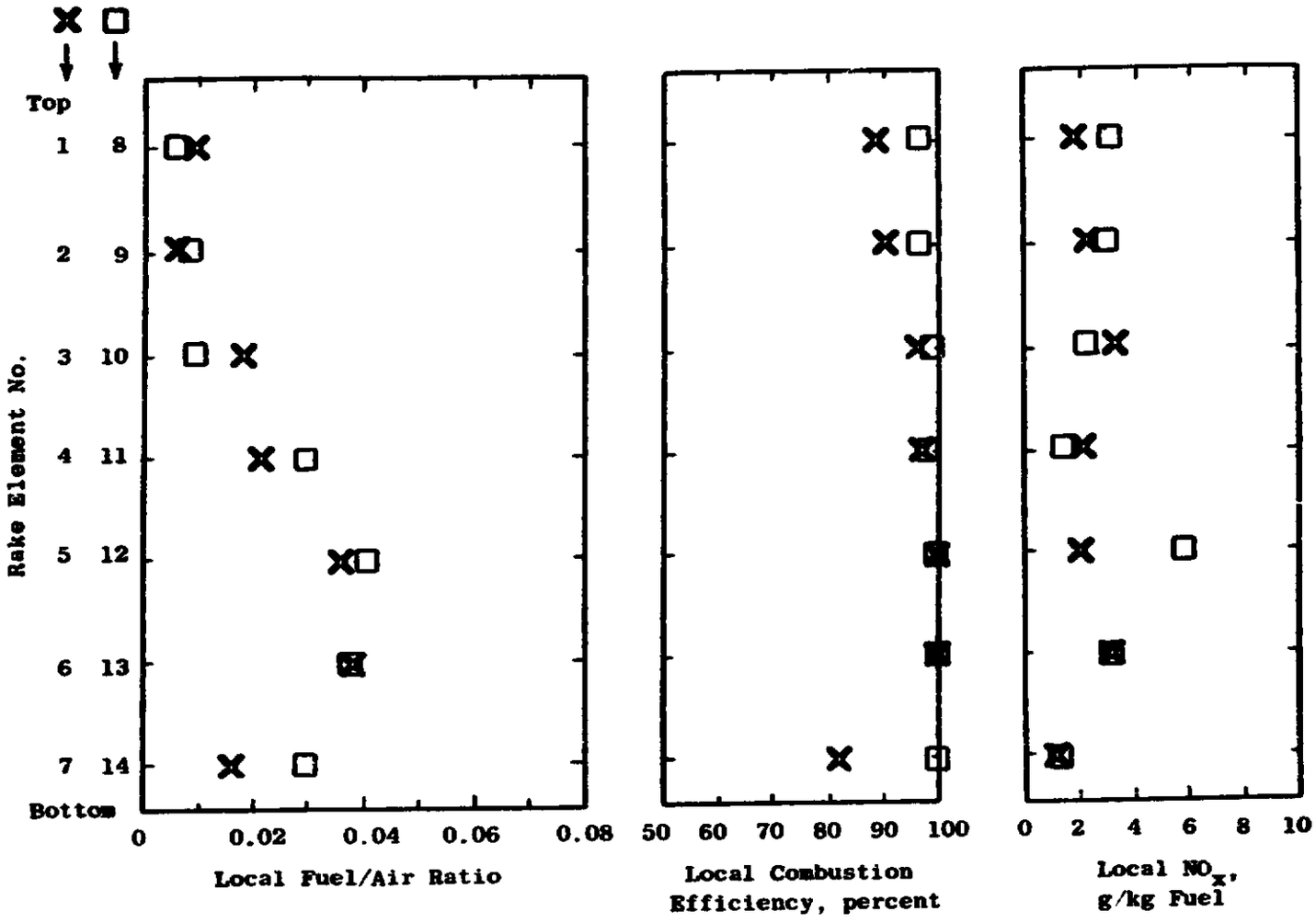

Figure 69. Duct Burner Exit Profiles, Configuration 12, Reading 209, Supersonic Cruise Condition, T = 591 K, P = 262 kPa, Metered Overall F/A = 0.0172.

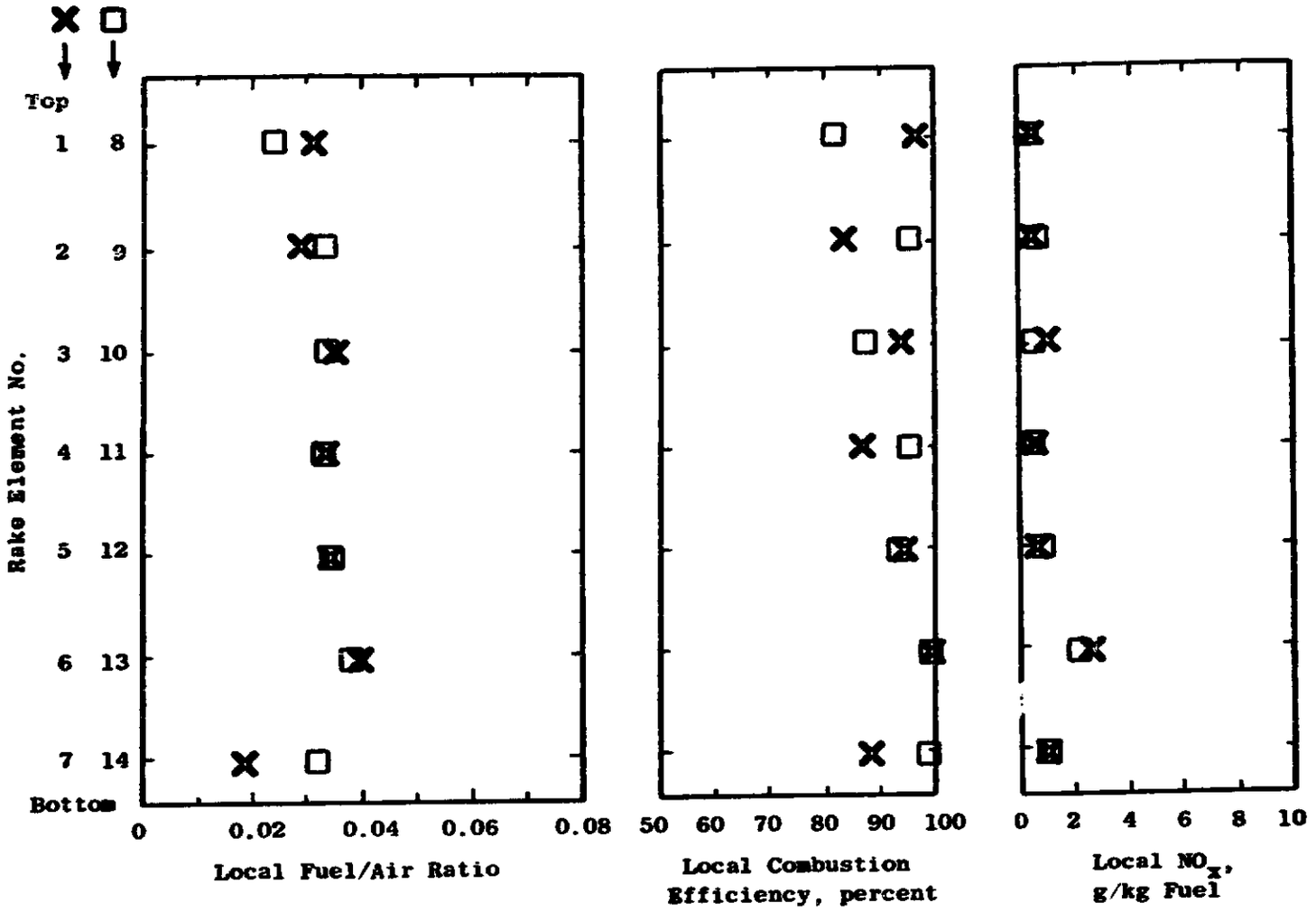

Figure 70. Duct Burner Exit Profiles, Configuration 12, Reading 216, Supersonic Cruise Condition, T = 591 K, P = 261 kPa, Metered Overall F/A = 0.0301.

further adjustment of the blast gate before the temperature rise could be measured. Since the pressure at the altitude relight condition is only slightly above atmospheric, it was decided to perform the remaining ignition tests with the blast gate open. The airflow was reduced to provide the correct reference velocity.

For each pilot design, ignition was accomplished at the nominal reference velocity using the spark igniter, although fuel flows somewhat higher than nominal were usually required. The minimum fuel/air ratios required for ignition, and the temperature rise calculated from manifolded gas samples, are listed in Table XXI.

6.3 Fluid Dynamic Performance

Measured duct burner performance parameters in addition to those related above included fan stream total pressure loss, fuel injector pressure drop, and dynamic pressure, frequency, and amplitude. The results of these measurements are summarized in this section.

6.3.1 Duct Burner Pressure Drop

Selected total pressure drop measurements made with only the pilot stage operating are summarized in Table XXII. Where they are available, measurements made at the supersonic cruise inlet conditions are presented as this was the primary design condition. The measured pressure drop includes the flameholder drag loss, fuel injector drag loss, and friction losses in the high velocity passages ahead of the flameholders. The data in Table XXII include losses associated with mixing of the uncarbureted main stage air with hot pilot discharge gas but do not include heat addition loss associated with the main stage combustion. Pressure loss data were also included in Tables VI through XX; these data include heat addition loss where appropriate.

Table XXII includes calculated values of reference velocity head (Q) and the ratio of total pressure drop to velocity head (DP/Q). Theoretically, DP/Q should be almost independent of reference velocity, so it is more useful than DP/P as a performance characterization parameter.

Configurations 6 and 7 (which are also characteristic of Configurations 8, 9, and 10) show higher pressure drop than other configurations because of the pilot snout extension, which required the main stage air to negotiate long, high velocity passages containing high-blockage fuel injectors. Without the snout extension, the dry pressure loss was typically 4% of the inlet total pressure at the nominal reference velocity, or 6 reference velocity heads.

Table XXI. Ignition Test Results.

Config.	Rdg	P_{T6} KPa	T_{T6} K	F/A Under Liner	Temp. Rise
1	4	145	360	.0060	206
2	19	143	371	.0047	156
4	37	106	369	.0072	240
6	92	111	368	.0064	186
7	115	115	375	.0044	114
11	206	112	367	.0063	195

Table XXII. Total Pressure Drop Data Summary, Pilot Stage Only at Supersonic Cruise Operating Condition.

CON FIG	RDG	PT6 KPA	TT6 K	V REF M/S	Q REF KPA	FTOT MET	DPT KPA	DP/P	DP/Q
1	17	261.	592.	48.52	1.806	0.0027	10.583	0.0406	5.862
2	20	384.	454.	41.20	2.503	0.0027	15.855	0.0413	6.335
4	52	266.	592.	46.23	1.673	0.0031	10.235	0.0385	6.117
5	58	107.	590.	46.07	0.668	0.0031	4.464	0.0419	6.682
5	59	107.	591.	46.14	0.669	0.0037	4.441	0.0417	6.637
6	105	260.	597.	47.92	1.742	0.0042	21.656	0.0833	12.432
7	117	264.	602.	47.18	1.704	0.0017	21.009	0.0795	12.332
7	118	261.	592.	47.20	1.713	0.0028	22.182	0.0850	12.947
7	119	261.	594.	47.33	1.715	0.0038	21.875	0.0838	12.757
11	178	276.	594.	44.57	1.612	0.0029	7.872	0.0285	4.883
11	179	275.	592.	45.43	1.671	0.0035	8.792	0.0320	5.262
11	180	276.	591.	45.59	1.691	0.0043	7.669	0.0278	4.536
12	213	263.	592.	47.14	1.720	0.0043	10.390	0.0395	6.042

6.3.2 Fuel Injection Pressure Drop

Fuel injection pressure drop was monitored for all three fuel systems. When liquid fuel was used, the parameter $W/\sqrt{\Delta P}$ was computed and compared with the value resulting from pretest injector flow checks. Theoretically, this parameter should remain constant. An increase from one reading to another was taken as evidence of a fuel line leak, and a decrease was taken as evidence of fuel injector clogging. No leaks were detected during the program. Several instances of injector clogging were encountered and have been related previously.

The measured values of the fuel injector pressure drop parameter are listed in Table XXIII.

6.3.3 Dynamic Pressure

All of the configurations tested in this program encountered resonance as fuel/air ratio was increased. To embark on major efforts to eliminate this resonance was beyond the scope of this program. In the earlier configurations tested, the resonance levels reached high amplitude levels that resulted in damage to the hardware. In subsequent tests, Configuration 3 through 12, fuel/air ratios were not increased beyond levels where resonance reached double amplitude levels in the range of 7 to 14 kPa. Practically all of these later data points, therefore, had amplitudes below 7 kPa, and many of the points below the maximum fuel/air ratio had no strong discrete frequencies present.

The resonance frequencies, when present, were in the range of 150 to 350 Hz and were axial modes. The radial modes and circumferential modes in the sector test rig would involve much higher frequencies. In a full annular duct burner, however, the circumferential mode would be closer to these axial mode frequencies. In a full annular duct burner, the circumferential mode would, therefore, be expected to occur coupled with the axial mode.

The measured frequency spectrum typical of the resonance encountered is illustrated in Figures 71 and 72 for Configuration 10. Figure 71 is at a fuel/air ratio of 0.0325 at supersonic cruise showing strong resonant peaks at 240 and 260 Hz. Other conditions may peak at only a single discrete frequency. Leaner conditions, such as a fuel/air ratio of 0.021 (Figure 72) showed considerably less activity in the resonant frequency range.

Specific development effort to introduce resonance suppression features into the design could be expected to provide designs with emissions performance similar to that documented here but without the presence of excessive resonance at the maximum fuel/air ratios of interest.

Table XXIII. Fuel Injection Pressure Data Summary, Values of Parameter WF/SQRT(DP), Kg/S*SQRT(PA).

RDG	FUEL MANIFOLD		
	PILOT	UPPER	LOWER
	CONFIGURATION 1		
4	0.1355E-04		
5	0.1338E-04		
6	0.1300E-04		
7	0.1303E-04		
8	0.1288E-04	0.1372E-03	0.1024E-03
9	0.1277E-04	0.1296E-03	0.1063E-03
10	0.1261E-04	0.1295E-03	0.1024E-03
12	0.1165E-04		
13	0.9661E-05	0.1211E-03	0.9777E-04
14	0.8960E-05		0.9784E-04
15	0.8073E-05		
16	0.8296E-05		
17	0.8618E-05		
	CONFIGURATION 2		
19	0.1903E-04		
20	0.1806E-04		
21	0.1812E-04		0.2690E-03
	CONFIGURATION 4		
29	0.2616E-04		
30	0.2582E-04	0.2171E-03	0.1983E-03
31	0.2499E-04	0.1663E-03	0.1670E-03
32	0.2499E-04	0.1664E-03	0.1476E-03
33	0.2483E-04	0.1965E-03	0.1568E-03
34	0.2426E-04		0.1453E-03
37	0.2348E-04		
40	0.2457E-04		
41	0.8199E-04	0.2183E-03	0.1977E-03
43	0.2271E-04		
44	0.2356E-04		
45	0.2445E-04		0.2016E-03
46	0.2352E-04		0.2108E-03
47	0.2328E-04		0.1904E-03
48	0.2425E-04		0.1865E-03
49	0.2388E-04		0.1911E-03
50	0.2506E-04	0.2188E-03	0.2799E-03
51	0.2370E-04	0.2117E-03	0.1917E-03
52	0.2199E-04		

Table XXIII. Fuel Injection Pressure Data Summary, Values of Parameter WF/SQRT(DP), Kg/S*SQRT(PA) (Continued).

ROG	FUEL MANIFOLD		
	PILOT	UPPER	LOWER
	CONFIGURATION 4		
53	0.2183E-04		0.1365E-03
54	0.2199E-04	0.1351E-03	0.1321E-03
	CONFIGURATION 5		
57	0.2306E-04		
58	0.2394E-04		
59	0.2407E-04		
60	0.2119E-04		0.2005E-03
61	0.2228E-04		0.2258E-03
62	0.2078E-04		0.1837E-03
63	0.2361E-04		0.1886E-03
64	0.2047E-04		0.1803E-03
65	0.2311E-04		0.1943E-03
66	0.2235E-04		0.1589E-03
67	0.2450E-04		0.1540E-03
68	0.2269E-04	0.1957E-03	0.2491E-03
69	0.2289E-04	0.1813E-03	0.2031E-03
70	0.2194E-04	0.1749E-03	0.1679E-03
71	0.2150E-04		0.1366E-03
72	0.2145E-04		0.1370E-03
73	0.2149E-04		0.1352E-03
74	0.2155E-04	0.1309E-03	0.1354E-03
	CONFIGURATION 6		
75			
76	0.2750E-04		
77	0.2507E-04		
78	0.2437E-04		
79	0.2508E-04	0.2644E-03	
80	0.2467E-04	0.1968E-03	
81	0.2420E-04	0.1776E-03	
82	0.2448E-04	0.1981E-03	0.1810E-03
83	0.2385E-04	0.1755E-03	
92	0.2286E-04		
94	0.2235E-04		
95	0.2318E-04		
96	0.2249E-04		
97	0.2225E-04	0.5280E-03	
98	0.2224E-04	0.2100E-03	

Table XXIII. Fuel Injection Pressure Data Summary, Values of Parameter WF/SQRT(DP), Kg/S*SQRT(PA) (Continued).

RDG	FUEL MANIFOLD		
	PILOT	UPPER	LOWER
	CONFIGURATION 6		
99	0.2226E-04	0.1864E-03	
100	0.2202E-04	0.1648E-03	
101	0.2198E-04	0.1735E-03	
102	0.2171E-04	0.1658E-03	
103	0.2193E-04	0.1818E-03	0.3705E-03
105	0.2122E-04		
106	0.2111E-04	0.1742E-03	
107	0.2103E-04	0.1468E-03	
108	0.2104E-04	0.1700E-03	
	CONFIGURATION 7		
115	0.2190E-04		
117	0.1987E-04		
118	0.1981E-04		
119	0.1975E-04		
120	0.1940E-04		0.1098E-03
121	0.1983E-04		0.1105E-03
122	0.1969E-04		0.1113E-03
123	0.2206E-04		0.1107E-03
124	0.1974E-04		0.1097E-03
125	0.1986E-04		0.1088E-03
126	0.1944E-04		0.1085E-03
127	0.2229E-04		0.1097E-03
138	0.1984E-04		0.1262E-03
139	0.1977E-04		0.1239E-03
140	0.2014E-04		0.1244E-03
141	0.1979E-04		0.1219E-03
142	0.1933E-04		0.1231E-03
143	0.1934E-04		0.1225E-03
144	0.1941E-04		0.1248E-03
145	0.1936E-04		0.1225E-03
	CONFIGURATION 8		
84	0.2382E-04	0.2883E-03	
85	0.2369E-04	0.1546E-03	
86	0.2375E-04	0.2091E-03	0.2308E-03
87	0.2410E-04	0.1886E-03	0.2219E-03
88	0.2401E-04	0.1745E-03	0.2017E-03
89	0.2382E-04	0.1508E-03	

Table XXIII. Fuel Injection Pressure Data Summary, Values of Parameter WF/SQRT(DP), Kg/S*SQRT(PA) (Continued).

RDG	FUEL MANIFOLD		
	PILOT	UPPER	LOWER
	CONFIGURATION 8		
90	0.2399E-04	0.1411E-03	
109	0.2190E-04	0.2034E-03	
110	0.2193E-04	0.1599E-03	
111	0.2098E-04	0.1426E-03	
112	0.2113E-04		0.1456E-03
113	0.2108E-04		0.1460E-03
	CONFIGURATION 9		
168	0.2140E-04		0.4204E-03
169	0.2138E-04		0.4175E-03
170	0.2109E-04		0.4116E-03
171	0.2108E-04		0.4091E-03
172	0.2112E-04		0.3933E-03
173	0.2113E-04	0.2987E-03	0.3693E-03
174	0.2107E-04	0.3061E-03	0.3642E-03
175	0.2104E-04	0.2991E-03	0.3532E-03
176	0.2104E-04	0.3101E-03	0.3474E-03
	CONFIGURATION 10		
128	0.1964E-04	0.1409E-03	
129	0.1959E-04	0.1263E-03	
130	0.2183E-04	0.1253E-03	
131	0.1963E-04	0.1292E-03	
132	0.1959E-04	0.1276E-03	
134	0.1958E-04	0.1328E-03	0.1285E-03
135	0.1960E-04	0.1288E-03	0.1265E-03
136	0.1953E-04	0.1276E-03	0.1258E-03
137	0.2190E-04	0.1270E-03	0.1258E-03
146	0.1972E-04	0.1354E-03	0.1261E-03
148	0.2251E-04		
149	0.2239E-04	0.1771E-03	0.1530E-03
150	0.2238E-04	0.1581E-03	0.1413E-03
151	0.2227E-04	0.1425E-03	0.1325E-03
152	0.2233E-04	0.1400E-03	0.1291E-03
153	0.2229E-04	0.1373E-03	0.1277E-03
154	0.2226E-04	0.1372E-03	0.1260E-03
156	0.2174E-04		
157	0.2169E-04		
158	0.2143E-04	0.1374E-03	0.1257E-03

Table XXIII. Fuel Injection Pressure Data Summary, Values of Parameter WF/SQRT(DP), Kg/S*SQRT(PA) (Continued).

ROG	FUEL MANIFOLD		
	PILOT	UPPER	LOWER
CONFIGURATION 10			
159	0.2142E-04	0.1359E-03	0.1254E-03
160	0.2130E-04	0.1338E-03	0.1245E-03
161	0.2136E-04	0.1332E-03	0.1248E-03
162	0.2129E-04	0.1328E-03	0.1256E-03
163	0.2135E-04	0.1356E-03	0.1271E-03
164	0.2133E-04	0.1340E-03	0.1266E-03
165	0.2127E-04	0.1339E-03	0.1259E-03
CONFIGURATION 11			
178	0.2366E-04		
179	0.2357E-04		
180	0.2326E-04		
181	0.2319E-04		0.1631E-03
182	0.2348E-04		0.1554E-03
183	0.2330E-04		0.1460E-03
184	0.2333E-04		0.1596E-03
185	0.2303E-04		0.1438E-03
186	0.2337E-04		0.1420E-03
187	0.2344E-04		0.1554E-03
188	0.2354E-04		0.1514E-03
189	0.2355E-04	0.1703E-03	0.1546E-03
190	0.2339E-04	0.1627E-03	0.1508E-03
191	0.2408E-04		0.1485E-03
192	0.2454E-04		0.1556E-03
193	0.2374E-04		0.1415E-03
194	0.2359E-04		0.1502E-03
196	0.2415E-04		
197	0.2370E-04	0.1665E-03	0.1495E-03
198	0.2432E-04	0.1666E-03	0.1476E-03
199	0.2424E-04	0.1491E-03	0.1399E-03
200	0.2357E-04	0.1483E-03	0.1405E-03
202	0.2417E-04		
203	0.2478E-04	0.1577E-03	0.1419E-03
204	0.2419E-04	0.1457E-03	0.1401E-03
206	0.2513E-04		
CONFIGURATION 12			
208	0.2205E-04		0.1343E-03
209	0.2210E-04		0.1408E-03

Table XXIII. Fuel Injection Pressure Data Summary, Values of Parameter WF/SQRT(DP), Kg/S*SQRT(PA) (Concluded).

RDG	FUEL MANIFOLD		
	PILOT	UPPER	LOWER
	CONFIGURATION 12		
210	0.2236E-04		0.1394E-03
211	0.2204E-04		0.1429E-03
212	0.2211E-04		0.1487E-03
213	0.2256E-04		
214	0.2220E-04	0.1632E-03	0.1430E-03
215	0.2232E-04	0.1715E-03	0.1382E-03
216	0.2216E-04	0.1707E-03	0.1385E-03

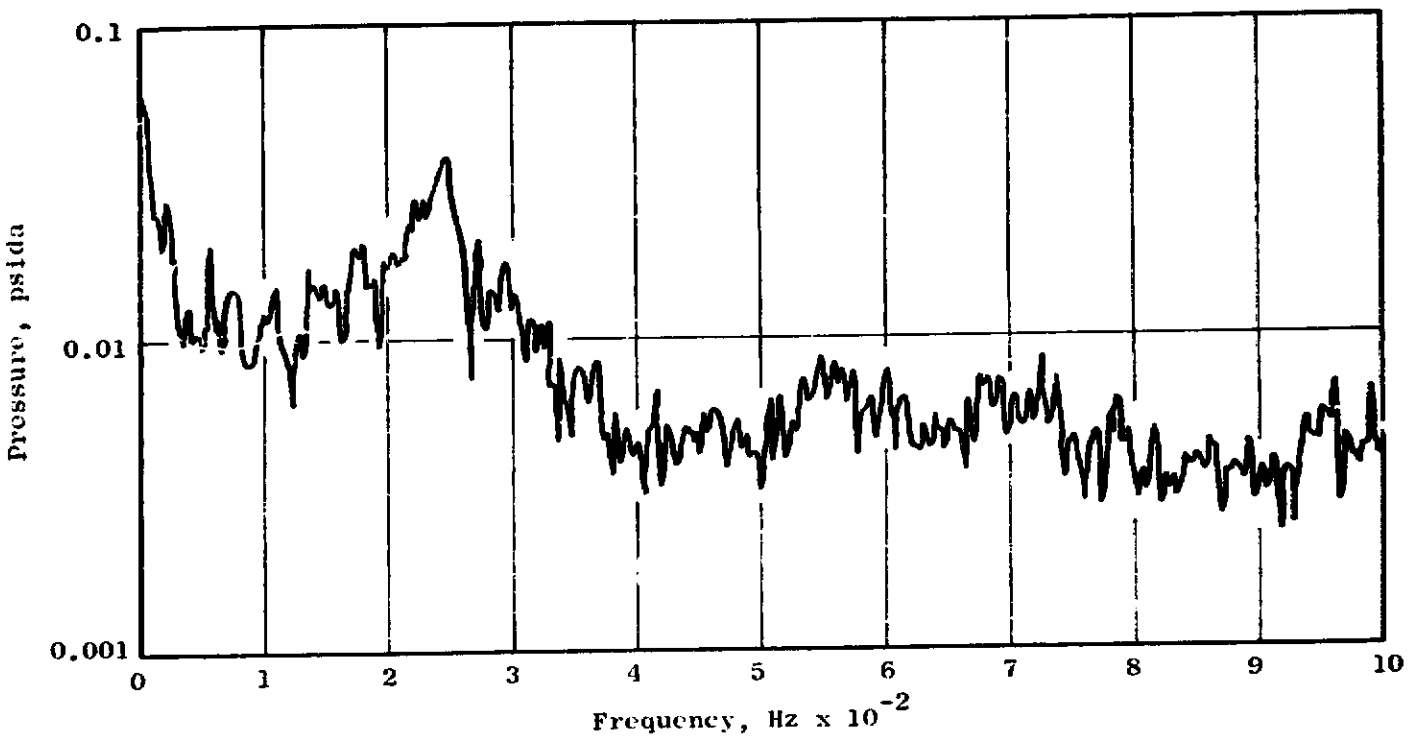

Figure 71. Dynamic Pressure Frequency Spectrum, Configuration 10, Reading 130, Supersonic Cruise Condition, Total F/A = 0.0212 Under Liner.

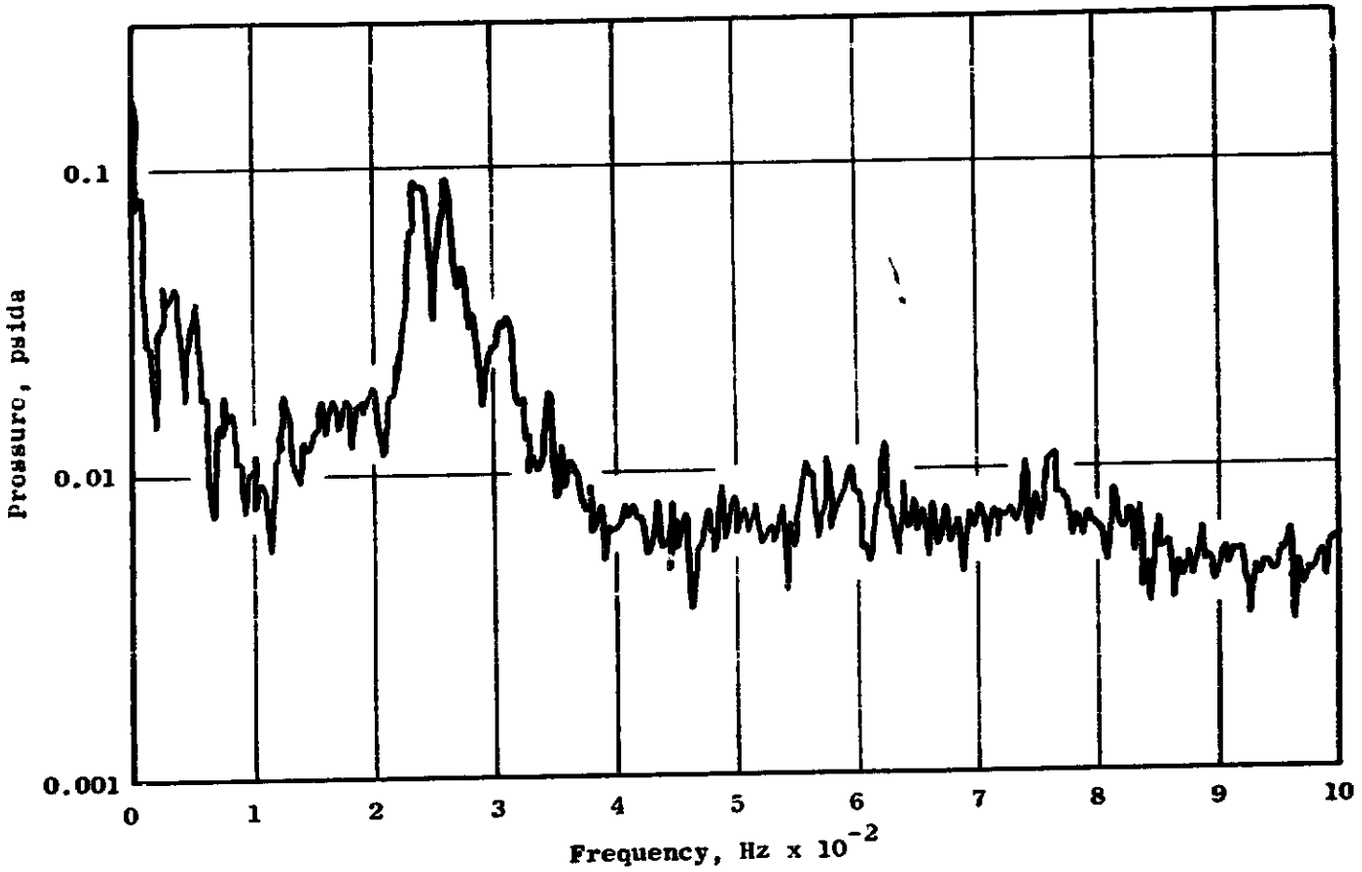

Figure 72. Dynamic Pressure Frequency Spectrum, Configuration 10, Reading 136, Supersonic Cruise Condition, Total F/A = 0.0325 Under Liner.

7.0 DISCUSSION OF RESULTS

7.1 Emission Levels Status

This experimental investigation has resulted in significant progress in the development of technology for obtaining the pollutant emission levels with duct burners. The first configuration tested in this program achieved a NO_x emission index of 3.4 and a combustion efficiency of 94% at the supersonic cruise conditions, compared with the target goals of 1.0 for NO_x emission index and 99% for combustion efficiency. The NO_x emission level for this configuration was near the level expected from previous duct burner experience. Because of the lean operating fuel/air ratio needed to achieve this NO_x level, the combustion efficiency was lower than for previous duct burners at their optimum fuel/air ratios. The configuration with the overall best emissions performance, Configuration 10, had a NO_x emission index of 1.2 and a combustion efficiency of 97% at the supersonic cruise inlet conditions at the optimum fuel/air ratio. Furthermore, it was possible to identify the major cause of the remaining combustion inefficiency and, from that knowledge, to suggest that ultimately even higher combustion efficiencies, near 99%, could be achieved. The NO_x emission index and combustion efficiency results for the best configuration, Configuration 10, are discussed below.

Figure 47 shows the emission trends with fuel/air ratio at the supersonic cruise inlet conditions. The data were calculated from gas samples in which 14 individual rake probes were manifolded together. The results show a trend of both increasing NO_x and increasing combustion efficiency with increasing fuel/air ratio. The leaner data were obtained with fuel feeding only the top half of the main stage flameholder array. The richer data were obtained with fuel feeding both the top and the bottom halves. Thus, two distinct curves exist. The richer curve results in the closest approach to the NASA goals. With only one half of the main stage airflow carbureted, quenching in the lean portion of the burner significantly limits the combustion efficiency that can be achieved. The emissions levels are very sensitive to fuel/air ratio, thus requiring a very narrow fuel/air design range for supersonic cruise.

Figure 50 shows the trends measured at takeoff conditions with this same test configuration. The NO_x levels and combustion efficiencies again increase with fuel/air ratio. Because of the lower inlet temperature, the NO_x levels do not rise to the level of 1.0 until a fuel/air ratio is provided that is higher than that associated with the supersonic cruise operating conditions.

Figure 49 presents the data obtained at the transonic climb conditions. The trend of increasing combustion efficiency with increasing fuel/air ratio is still strong. The rich end of the curve is of importance here since there is no NO_x requirement for this climb condition.

Figure 55, containing detailed traverse data from 14 individual probe locations, shows an additional important feature concerning the combustion efficiency. An appreciable portion of the measured inefficiency is due to the gas samples taken near the top and bottom liner walls. Quenching from the liner cooling air is believed to be responsible for these inefficient conditions. It is probable that future development work directed at this wall quenching problem could eliminate a considerable portion of this particular source of inefficiency. If the samples closest to the walls are omitted from a calculated average, as presented in Table XXIV, combustion efficiencies above 99% are calculated for all three flight conditions. Thus, insofar as the wall quenching can be reduced, the concept is potentially even closer to meeting the target goals than is suggested by Figures 47 through 50.

Further reduced NO_x levels may come from the use of an alternate pilot stage design, since a significant portion of the NO_x at supersonic cruise is believed to be generated in the pilot itself. This is illustrated in Figure 46, which shows the performance of Configuration 7 at the supersonic cruise conditions. The pilot alone produced values of NO_x emission index of 4.7 to 6.2. If the main stage fuel produced no NO_x, the pilot NO_x would be diluted to an emission index range of 0.6 to 1.1 at a total fuel/air ratio of 0.021. Since the actual measured NO_x at 0.021 fuel/air ratio was only about 1.1, relatively little additional NO_x was generated in the main stage at that fuel/air ratio.

In advanced supersonic transport preliminary design studies, the baseline engine generally operated with very little change in reference Mach number through the fan duct over the mission. However, the effects of reference Mach number at supersonic cruise were documented in this program. These results are presented in Figure 48. The effects were found to be moderate. As should be expected, both the NO_x level and the combustion efficiency increased with the increased residence time corresponding to lower reference Mach numbers.

7.2 Fuel/Air Modulation

Table XXIV summarizes the emissions levels achieved and compares the NASA goals with the calculated emissions performance at an optimum fuel/air ratio for each of the three flight conditions. These emissions levels were calculated from individual probe samples rather than from the manifolded samples used in Figures 47 through 50. The method involving individual probe sample calculations is considered to be the more accurate of the two methods. In addition to the values calculated from 14 individual samples from the two seven-element rakes, the emissions levels calculated from an average that omitted the four samples next to the top and bottom liners are also presented. The results at all flight conditions show a close approach to the NASA emissions goals, but each condition requires a narrow fuel/air ratio operating range.

Table XXIV. Comparison of Program Goals with Calculated Emissions at Optimum Fuel/Air Ratio for Each Flight Condition.

	Optimum Fuel/Air Ratio	EI, g/kg Fuel CO	HC	NO_x	Combustion Efficiency, %
Takeoff	0.0403	24.20	18.48	1.06	97.59
Program Goal				1.0	99.0
Acceleration	0.0435	33.07	17.68	1.18	97.46
Program Goal					99.0
Supersonic Cruise:					
One Side Carbureted	0.0209	70.74	47.41	1.30	93.61
Two Sides Carbureted	0.0324	24.22	23.12	1.19	97.12
Program Goal		30	2.5	1.0	99.0

Calculated Emissions with Samples near Liner Omitted

(Represents potential efficiency level if all wall quenching could be eliminated)

	Optimum Fuel/Air Ratio	EI, g/kg Fuel CO	HC	NO_x	Combustion Efficiency, %
Takeoff	0.0403	9.82	7.26	1.10	99.04
Acceleration	0.0435	19.98	4.33	1.23	99.10
Supersonic Cruise	0.0324	8.43	6.54	1.17	99.15

The optimum fuel/air ratio for each flight condition from an emissions standpoint is not necessarily the same fuel/air ratio desired for the aircraft mission. As a guide to a realistic fuel/air range that might be required, a single supersonic cruise aircraft mission with a specific study engine was selected in the original design effort as is described in Section 3.1. A very wide range of fuel/air ratios was required for this mission, from 0.01 at supersonic cruise to 0.024 at takeoff and acceleration Since the baseline engine was sized for noise requirements at takeoff, it generally had no need for fuel/air ratios higher than about 0.024. This wide range of required fuel/air ratios was very influential in establishing the development approaches investigated in this program.

The original duct burner concept involved some of the fan air bypassing the duct burner to permit the fuel/air ratios to be optimized. To achieve the optimum fuel/air ratio of 0.032 at the supersonic cruise condition, from an emissions standpoint, two-thirds of the fan air should bypass the duct burner. However, unfortunately, to achieve the desired takeoff and cruise thrust with two-thirds of the air bypassing the duct burner would require local duct burner fuel/air ratios 2.4 times as high, i.e., 0.077, which is above stoichiometric. If, instead, the quantity of duct burner airflow for takeoff is optimized first, perhaps 40% of the air should bypass the duct burners with some of this air reentering the duct burner through the cooling liners. Then some additional duct burner design features would be needed to accommodate the supersonic cruise operating condition. For supersonic cruise, carburetion of only one-half or less of the duct burner airflow by using only one side of the main stage is one approach for providing this needed staging. Unfortunately, this technique of carbureting only one-half of the duct burner was found to result in reduced combustion efficiency.

Two other techniques can also be considered. All advanced supersonic technology aircraft under recent study have four engines. If only two of these engines had their ductburners operating at supersonic cruise, this would permit the duct burners to operate at favorable fuel/air ratios from the standpoint of reduced emissions levels. However, this technique would result in a net increase in sfc. The thrust from one engine is not linear with fuel flow but increases approximately with the square root of the duct burner exhaust temperature. Therefore, engines operating at two different duct burner exhaust temperatures will require more total fuel for a given total thrust than if the two burners were operated at equal exhaust temperatures. A second possible staging technique, which has been evaluated for use in main combustors for emissions control at idle, involves sector burning in all of the engines. With sector burning, only a portion of the circumference is carbureted. Again, however, the thrust effectiveness of the carbureted sectors would suffer the same sfc disadvantages due to exhaust temperature nonuniformity as occurs when operating only two of the duct burners in the four engines. This effect is, of course, not objectionable in the case of main combustors at idle. In addition, combustion efficiency losses at the edges of the burning sectors due to quenching and some pressure loss due to airflow adjustment around the circumference would occur. Thus, while sector burning might achieve the desired range of fuel/air ratios to optimize

emissions, the resulting increase in sfc may be an even greater penalty than the combustion inefficiencies indicated for Configuration 10 at a fuel/air ratio near 0.020.

As discussed in Section 7.3, below, attempts to improve the combustion efficiency when only one half of the duct burner main stage is carbureted, by introducing axial stagger between the flameholders on the top and bottom of the pilot, did not result in satisfactory combustion efficiency when both the top and the bottom halves were carbureted.

7.3 Staggered Main Stage Flameholder Arrays

In order to minimize quenching from the uncarbureted side of the pilot stage, configurations with the uncarbureted main stage flameholder region staged axially downstream were investigated. It was hypothesized that this feature would permit the combustion process to progress further before the quenching effects began.

The effects of stagger for the sloped radial flameholders can be identified by comparing data from Configuration 6 with Configuration 4 data. At supersonic cruise conditions near 0.02 fuel/air ratio, the axially staggered version (Configuration 4) encountered lower combustion efficiencies and higher NO_x levels. The axial stagger also resulted in lower combustion efficiencies at higher fuel/air ratio operating conditions with both sides of the pilot stage carbureted.

For the circumferential flameholders, Configurations 11 and 12 can be compared with Configuration 1. The combustion efficiencies of Configurations 11 and 12 at 0.020 fuel/air ratio at supersonic cruise were measured at 98.4% and 98.8%, respectively, very close to the 99% goal and 4 to 5% higher than for Configuration 10. Eliminating the gas samples near the top and bottom liners containing the liner quenching effects from the calculated average, combustion efficiencies of 99.0% and 98.9% were calculated for these two configurations. Thus, these configurations avoided the quenching from the uncarbureted portion of the flameholder array which had limited the other configurations to well below 99% combustion efficiency at these partially carbureted lean conditions. While this technique was successful in improving combustion efficiencies at partially carbureted supersonic cruise conditions, at high fuel/air ratio conditions with both sides of the pilot stage carbureted, combustion efficiencies were lower than with the unstaggered configuration. The flame spreading from the lean upstream main stage flameholder region into the downstream region was apparently much inferior to that induced by the undiluted pilot gases. This effect occurred both with circumferential flameholders and with sloped radial flameholders.

7.4 Main Stage Fuel Injector Variations

Uniform fuel distribution is important for achieving minimum NO_x levels at a reasonable combustion efficiency. Thus, it is commonly assumed that

optimizing the fuel injection scheme will be an important variable in achieving low emissions levels in combustors and augmentors. However, the differences found in this investigation for various fuel injection techniques were surprisingly small. Some of these can be seen by referring to Table VIII, which contains a summary of point sample survey measurements from different configurations at the supersonic cruise operating condition.

The effect of axial location of the main stage fuel injectors is illustrated by comparing Configurations 6 and 8. Configuration 8, like Configuration 10, used injectors located well ahead of the flameholders, in the test rig inlet bellmouth. Configuration 6 used injectors located 390 mm farther downstream, closer to the flameholder. The combustion efficiency at a supersonic cruise fuel/air ratio of 0.020 was only slightly lowered, 96.5% versus 97.4% for Configuration 8. Two additional fuel injection techniques at the downstream axial station were also evaluated in Configuration 5. In place of the standard splash plate spraybars, the use of conventional afterburner injectors having simple orifices at a 45° angle to the airstream was one technique used in Configuration 5. A second technique involved the addition of an air blast atomizer to these orifices. At a supersonic cruise fuel/air ratio of 0.020, the air atomization decreased the NO_x emission index from 2.7 to 2.3 but simultaneously decreased the combustion efficiency from 91.9 to 90.4%. A comparison with splash plate fuel injectors in Configuration 4, using the data in Table VIII based on point sample surveys, showed essentially no difference between use of the splash plate and the air blast atomizing spraybars.

A test with vapor fuel, Configuration 9, was also conducted. This may represent the ultimate in atomization fineness and uniformity. The test results showed poorer results than with liquid fuel. At a supersonic cruise fuel/air ratio of 0.021, the combustion efficiency was lower (92.5% versus 93.6%) and the NO_x emission index was higher (1.4 versus 1.3) than those shown in Table XXII for Configuration 7, the most directly comparable configuration.

7.5 Main Stage Flameholder Type

Without the axial stagger, the circumferential type of flameholder, Configuration 1, demonstrated a slightly higher combustion efficiency at supersonic cruise than the sloped radial flameholders, but also a higher NO_x level. Some hypotheses that may help explain these effects are discussed below.

There are two mechanisms that may be responsible for the effects on NO_x. The longer time it takes to spread the flame through the carbureted stream in the circumferential configuration is one mechanism that may be responsible for the increased NO_x. There is more flameholding source length in the sloped configurations, and the gap between flameholders is only 37% of the distance between the pilot and the circumferential flameholder. The time period in which fuel is igniting and generating radicals may be the time of

maximum NO_x generation; this may result in more NO_x for the longer flame spreading time. A second possible explanation of the higher NO_x may be the reduced intensity of mixing. Imperfect fuel distribution will be slower to mix toward uniformity in less intense mixing; this may permit locally high fuel/air ratios, with their accompanying high NO_x generation rates, to exist for a longer time.

The combustion efficiency might be expected to be lower for the longer flame spreading time, but the quenching from the uncarbureted side of the pilot is the most important factor at supersonic cruise. The penetrating character and intense mixing of the airflow coming through the sloped flameholders results in more rapid quenching and, hence, lower combustion efficiency.

7.6 Prospects of Further Improvements in Future Development Work

The principle of achieving low NO_x emission levels by burning fuel in a lean premixed condition in piloted duct burner designs has been demonstrated. The levels achieved closely approach the target levels for NO_x at supersonic cruise. The combustion efficiency levels, while quite high, are below the 99% target. However, sources of the major portion of the combustion inefficiency have been identified. Because of this knowledge, it would be possible to direct future work at these specific causes with a relatively high probability of ultimate substantial improvement. This is not to suggest that major improvement should be expected from one or two tests of additional configurations. A substantial experimental development program is indicated to adequately demonstrate the desired and potential performance improvements. In addition to emissions reduction, development work on the resonance resistance of these configurations is also indicated. Previous development programs at General Electric on similar duct burner configurations in which the effects of resonance suppression liners were investigated have resulted in substantial increases in the resonance resistance of such configurations, including satisfactory operation up to stoichiometric fuel/air ratios. Such work was beyond the scope of this program.

For increasing combustion efficiency, initial work on minimizing the effects of liner wall quenching would be reasonably straightforward. The cooling liners used in the present investigation were already available and, in addition, were selected to be very conservative in design to minimize hardware risk in the test program and assure that any desired test condition could be investigated. Thus, optimization of this cooling liner design to minimize quenching is an obvious initial development direction. The possible achievable potential from this development work was indicated previously in Table XXIV. If these potential improvements were achieved, the combustion efficiency and NO_x targets for all three flight conditions - takeoff, transonic climb, supersonic cruise - could be met with a specific fuel/air operating range specified for each. While combustion efficiency targets would be met, Table XXIV suggests that the specific emission ingredients associated with the inefficiencies may involve HC emissions above the supersonic cruise target levels and CO emissions below the target levels. Some of

the HC emissions in the central portion of the stream may have mixed to that region from the inefficient liner regions. Thus, the development improvements that eliminate the liner quenching may also reduce the amount of HC present in the central portion of the stream, thus meeting the HC targets along with the combustion efficiency goals.

Simultaneous achievement of low emissions and the thrust modulation required for the supersonic cruise mission will require improved staging techniques. If specific fuel consumption can be compromised in order to achieve minimum emission levels at supersonic cruise, carburetion of only portions of the burner circumference or duct burning in only two of the four engines on the aircraft could provide the reduced average fuel/air ratio appropriate for the supersonic cruise thrust. If, on the other hand, specific fuel consumption is equally as important as emission levels, then further work on techniques for carbureting less of the total burner air without involving as much engine exit temperature nonuniformity would be appropriate. Treating the quenching from the uncarbureted side of the pilot is not as straightforward as treating the liner quenching. While previous work at General Electric has shown promise for maintaining high combustion efficiency using axial stagger of the flameholder array, the lean conditions required in this advanced supersonic technology duct burner to achieve low NO_x level greatly aggravated the problem of maintaining high combustion efficiency in the presence of fuel staging. The specific techniques of staggering the flameholder array tested in this investigation were not as successful as originally hoped. However, additional investigation of staggering techniques for achieving the desired fuel/air ratio operating range would be expected to yield improvements over the present performance status.

Further improvements in NO_x level may come from alternative pilot stage design characteristics, since a significant portion of the NO_x at supersonic cruise is believed to be generated in the pilot itself.

Aircraft engine applications utilizing these low emissions duct burners will need to schedule fuel flow and mission plans that allow the duct burners to operate within relatively narrow fuel/air ratio bands. Both the quantity of fan air bypassing the entire duct burner and the ratio of air between the inside and outside of the pilot stage will be selected to fit the specific fuel/air ratio range needs of particular advanced supersonic technology engine cycles and missions.

8.0 CONCLUSIONS

An experimental program was conducted to investigate techniques and develop technology to reduce the pollutant emissions levels of duct burner-type augmentors suitable for use on an advanced supersonic cruise aircraft. The experiments were performed using a 194 by 432 mm rectangular sector test rig with inlet air temperatures, pressures, and velocities fully representative of the engine fan stream at all important flight conditions.

Screening tests of 12 configurations identified a low emissions duct burner configuration. This low emissions duct burner exhibited emissions levels that were very sensitive to the fuel/air ratio, with NO_x and combustion efficiency increasing as fuel/air ratio increased. Much of the combustion inefficiency, which is made up of CO and HC emissions, was due to quenching near the liner walls. If this local inefficiency near the liner walls could be eliminated through future development work, combustion efficiencies would improve at optimum fuel/air ratios from the demonstrated levels near 97% to the target level of 99%. At these 99% efficiency conditions for the central part of the stream, NO_x emission index levels of 1.10 at takeoff and 1.17 at supersonic cruise were measured, closely approaching the program goal of 1.0.

To obtain the desired fuel/air ratio range over an advanced supersonic transport mission, the supersonic cruise fuel/air ratio should be leaner than that found for optimum emissions. At the desired leaner conditions, a combustion efficiency of 94% and a NO_x emission index of 1.3 were measured. Since attempts to maintain the optimum fuel/air ratio from an emissions standpoint by carbureting only a portion of the circumference result in specific fuel consumption increases, several of the screening tests included features selected specifically to investigate wide fuel/air ratio modulation techniques. However, additional development of configuration features would be required to closely approach the goals with one configuration at both the lean supersonic cruise conditions and the richer takeoff conditions.

Altitude relight characteristics and smoke emissions were both satisfactory. Smoke measurements on all configurations were well below the SAE smoke number goal of 15. For all configurations, the pilot stage ignited reliably at low temperature rise using a standard engine spark igniter.

REFERENCES

1. Gleason, CC, Rogers, DW, and Bahr, DW, "Experimental Clean Combustor Program Phase II Final Report," NASA CR-134971, 1976.

2. Bahr, DW and Gleason, CC, "Experimental Clean Combustor Program, Phase I Final Report," NASA CR-134737, 1975.

3. Anon., "Supplement to ASME Power Test Codes, Part 5 - Measurement of Quantity of Materials, Chapter 4 - Flow Measurement," ASME PTC 19.5,4 - 1959.

4. Anon.,"Aircraft Gas Turbine Engine Exhaust Smoke Measurement," SAE Aerospace Recommended Practice 1179.

5. Anon., "Procedure for the Continuous Sampling and Measurement of Gaseous Emissions from Aircraft Turbine Engines," SAE Aerospace Recommended Practice 1256, 1971.